HIGH OXYGEN AND MOISTURE BARRIER BIODEGRADABLE MATERIAL

By

James F. Macnamara Jr.

A DISSERTATION

Submitted to
Michigan State University
in partial fulfillment of the requirements
for the degree of

Packaging – Doctor of Philosophy

2024

ABSTRACT

Interest in biodegradable polymers is surging among consumers, businesses, and governments as the accumulation of waste from single-use, petrochemical-based, and non-biodegradable plastics has skyrocketed since the 1960s, with flexible plastics constituting a major part of this surge. However, one major challenge with biodegradable alternatives is their inability to match traditional petrochemical plastics' oxygen and moisture barrier properties, which is critical for maintaining equivalent shelf life. This dissertation addresses several pivotal challenges, presenting innovative solutions within biodegradable polymers.

Our research achieved breakthroughs in the extrusion casting of stereocomplex-poly(lactic acid)—SC-PLA films and blends of poly(L-lactic acid)/ poly(D-lactic acid)—PLLA/PDLA in varying ratios, which were not previously documented. We explored the effects of annealing these films from 5 to 30 minutes to enhance crystallization and improve moisture barrier properties. Notably, PDLA served as an effective nucleating agent, significantly accelerating crystallization in blends with as little as 15% PDLA.

Further investigations revealed the interplay between density, crystallinity, and barrier properties of PLLA, PDLA, and their blends under varying annealing conditions. Amorphous film samples displayed densities between 1,230 ± 6 and 1,243 ± 2 kg/m^3, while semi-crystalline samples showed higher densities of 1,250 ± 8 to 1,257 ± 9 kg/m^3. Changes in density and crystallinity were analyzed, with findings indicating that homocomplex crystals formed at shorter annealing times exhibit higher densities than stereocomplex crystals forming at longer durations.

An innovative lamination technique involving base layers of poly(3-hydroxybutyrate-*co*-3-hydroxyvalerate) (PHBV) or SC-PLA, coated with a biodegradable polyvinyl alcohol and nanoclay mixture, was developed. This structure was tested for its moisture vapor transmission

rate (MVTR) and oxygen transmission rate (OTR), demonstrating promising barrier properties suitable for biodegradable packaging solutions. The MVTR ranged from 20 to 30 g/(m^2·d), and the OTR ranged from 54 to 69 cc/(m^2·d). We showed that optimizing the structure could obtain either a maximized MVTR of 10 g/(m^2· d) at 38 °C/90% RH or a maximized OTR of 14.46 cc/(m^2·d) at 23 °C/50% RH, both exceptional for a clear biodegradable structure without PVDC or metallization, showcasing low permeability for several biodegradable products.

Finally, we assessed the SC-PLA films and the blends' biodegradability in simulated composting conditions over 120 days. This test was conducted for 120 days of PLLA, PDLA, PLLA/PDLA 50-50, 30-70, and 70-30 films. This study is the first to report on the biodegradation behavior of these materials, particularly highlighting the rapid biodegradation of annealed PLLA/PDLA 50-50 blends compared to slower rates in higher PDLA content films. This is followed by films with higher PDLA content, such as the 30-70 blend with most PDLA. No data on the biodegradation of SC-PLA or PDLA in compost conditions had previously been reported. This comprehensive test provides reassurance and confidence in the biodegradability of our materials.

This dissertation contributes significant insights into developing high-performance, biodegradable film structures that offer viable alternatives to traditional plastics and align with global sustainability goals.

ACKNOWLEDGEMENTS

I want to thank everyone who contributed to and helped me during my PhD expedition over the years.

The first person I would like to thank is my advisor, Dr. Auras. He has been accommodating and supportive the whole time and was always available when I got stuck or unsure how to proceed. Who knew when I met him over twenty years ago he would be such a profound figure in my life? I would also like to thank my committee members, Dr. Maria Rubino, Dr. Matthew Daum, and Dr. Ajay Kathuria, for their guidance and, most importantly, time during my last few years, without whose input would have made this journey much more difficult.

I want to extend my heartfelt thanks to my entire research group, particularly Anibal and Wan. They have not only been my colleagues but also my friends, always ready to assist me in various aspects of my research. I am very happy for the support and time they have given me over the last few years.

I would also like to thank Aaron Walworth and Rajith Rankothge for their help and support in the labs. Special thanks go to Tracey Lorenz, Cathie Allison, Susan Barnaby, Heather Miller, Aaron Tucker, and Dr. Amy Radford-Popp for their thoughtfulness and responsiveness in all sorts of situations, which made my time in East Lansing much easier.

I am profoundly grateful to the CANR, the Graduate School, and the SOP for their generous financial support. Their belief in my potential and their provision of fellowship opportunities have eased my financial burden and allowed me to fully dedicate myself to my research during the summer semesters. Their support has been a cornerstone of my success, and I am deeply thankful for it. I also would like to thank the SoP for allowing me to be a TA during

the school year to not only ease my financial burden but also allow me to teach classes to undergraduate students, which I truly enjoyed.

Finally, I would like to express my deepest gratitude to my mom, who has been my unwavering pillar of support. I also want to give a special thanks to my dog, Chance, who was there from the beginning of the journey, providing comfort and companionship. Unfortunately, Chance did not make it the whole way, but he had a good life and will forever be part of our memories. Most importantly, I would like to thank my wife, Karen, who has been my rock and always there to motivate me when I was down. Her support and understanding have been invaluable, and I am truly blessed to have her in my life.

TABLE OF CONTENTS

LIST OF ABBREVIATIONS

ASTM	American Society for testing and materials
cc	cubic centimeters
C_p	specific heat capacity
Δc	concentration difference
d	day
D	diffusion coefficient
Đ	dispersity
DMR	Direct measurement respirometric
DMSO	Dimethyl sulfoxide
DSC	differential scanning calorimetry
E_p	permeability activation energy
ESI	Electronic supplemental information
FSUP	Flexible single-use plastic
F_v	Free volume
FTIR	Fourier transform infrared
g	grams
HC-PLA	Homocrystallite PLA
H_m	enthalpy of fusion
in^2	square inches
J	flux

kg	kilograms
l	Thickness
m^2	square meters
MDSC	modulated differential scanning calorimetry
M_n	number-average molecular weight
MAF	Mobile amorphous fraction
MPa	megapascal
MVTR	moisture vapor transmission rate
M_w	weight-average molecular weight
MWD	molecular weight distribution
Nc	Nanoclay
OMMT	Organomodified montmorillonite
OTR	oxygen transmission rate
P	permeability coefficient
Pa	pascal
PALS	Positronium annihilation lifetimes
PBAT	polybutylene adipate terephthalate
PBS	polybutylene succinate
PCL	Polycaprolactone
PDLA	Poly (D-lactic acid)
PET	Poly (ethylene terephthalate)
PGA	polyglycolic acid

PHA	Polyhydroxyalkanoates
PHBV	Poly(-3-hydroxybutyrate-co-3-hydroxyvalerate)
PLA	Poly (lactic acid)
PLLA	Poly (L-lactic acid)
PS	Polystyrene
PVC	Polyvinyl chloride
PVDC	Polyvinylidene chloride
PVOH	Poly (vinyl alcohol)
RAF	Rigid amorphous fraction
S	solubility coefficient
SC-PLA	Stereocomplex PLA
SEC	Size exclusion chromatography
SEM	Scanning electron microscopy
STP	Standard temperature and pressure
T_c	crystallization temperature
T_g	glass transition temperature
T_m	melting temperature
TGA	Thermogravimetric analysis
USD	United States dollar
WAXD	wide-angle X-ray diffraction
X_c	Crystallinity

CHAPTER 1: INTRODUCTION

1.1 Background and motivation

As the volume of waste from non-degradable petrochemical-based packaging mounts, public sentiment towards biodegradable alternatives has increasingly been favorable. The extensive use of nonrenewable resources poses a significant and well-recognized global challenge. Petroleum resources, the basis for most non-biodegradable plastics, are being depleted rapidly, complicating disposal efforts. In light of these issues, the shift towards bio-based and biodegradable options represents a vital strategy for sustainable development (1). Historically, plastic production surged from approximately 2 million tons in the 1950s to about 400 million tons by 2017, with projections suggesting an increase to 1800 million tons by 2050 (2). Concurrently, the global sustainable plastic market is poised to grow from USD 80 billion in 2020 to USD 127.50 billion by 2028 (3).

Recent studies have demonstrated that consumers prioritize a company's environmental footprint when purchasing. Many customers are willing to pay a premium for products that offer high quality and come in environmentally friendly packaging. Furthermore, there is a growing attraction towards brands that adopt sustainable practices, marking a significant shift in consumer behavior from past trends (4).

Grasping the challenges associated with packaging waste is a crucial initial step towards addressing it. Plastics, a product of human ingenuity, are prized for their lightweight, durability, decay resistance, affordability, and malleability. However, these advantages come with significant environmental costs. Plastic packaging, in particular, is notably wasteful and detrimentally affects the ecosystems we depend on. Largely due to inadequate product design and insufficient infrastructure, most plastic ends up in landfills or discarded in the environment, contributing heavily to plastic pollution (5). Despite its brief lifespan, plastic packaging remains

one of the major sources of this pollution. In 2021, only about 5-6% of waste was recycled, 10% incinerated, and a staggering 85% was relegated to landfills (6).

Due to this fact, research and time is being spent on developing environmentally friendly materials (7). Biodegradable materials are being engineered to diminish waste accumulation, as they decompose significantly faster than traditional petrochemical-based plastics (8). However, a notable limitation of these current biodegradable options is that their barrier properties do not match those of conventional petrochemical-based materials, potentially affecting the shelf life of products (9).

Oxygen transmission rate (OTR) and moisture vapor transmission rate (MVTR) are two main characteristics of a polymer that dictate a packaged product's shelf life (10). A polymer or structure can range in values anywhere from low barrier to high barrier. The requirement depends on the product being packaged. The high barrier flexible film market was USD 19.34 billion in 2020 and is projected to reach USD 38 billion by 2028 (11). Due to the high barrier requirements, an alternative biodegradable material can only serve a small portion of this market.

So, there are no commercially available high oxygen and moisture barrier biodegradable structures that do not incorporate metallization or polyvinylidene chloride (PVDC). There are some high oxygen barrier materials with a low OTR, but no structures with both high oxygen and moisture barrier in one structure (12). This is a large gap in current technology that is being extensively pursued.

1.2 Overall goal and objectives

This dissertation aims to construct a high oxygen and moisture barrier biodegradable structure that can be used for direct food contact. To achieve this goal, the following objectives have been established:

1. To investigate and optimize the processing conditions to extrude stereocomplex polylactic acid (SC-PLA) as a cast film.
2. Determine the density of multiple blends of SC-PLA and their relationship to the crystallinity and moisture barrier of the cast extruded films developed.
3. Develop multilayer biodegradable structures based on SC-PLA and other compostable materials with targeted oxygen and moisture barrier properties.
4. Determine the biodegradability of the developed components, poly(l-lactic acid) – (PLLA), poly(d-lactic acid) (PDLA), PLLA/PDLA-50-50,50-50-annealed(A)-30 min, 30-70, and 70-30 films.

1.3 Dissertation Overview

This dissertation document is organized as follows.

The first chapter, Chapter 1, is an introduction that provides the background, motivation, and justification for the work in this dissertation, including the overall goal and objectives to be accomplished and establishes the basis for the chapters to follow.

Chapter 2 is a comprehensive literature review that includes an introduction, an explanation of barrier theory, how it is measured, a definition of biodegradable and compostable, and how it is evaluated. It will also include the explored main resins and the key converting technologies being investigated for processing the resins. An economic analysis is included to compare the relative costs to current technologies being used. Life cycle analysis is discussed as it relates to biodegradable and petrochemical-based plastics. Lastly, a review of current commercial structures being used in the industry is discussed.

Chapter 3 presents a viable and novel method to cast extrude SC-PLA films without a masterbatch. Several blend compositions were produced for comparison, including PLLA/PDLA

85-15, 70-30, 50-50, and 30-70, and homocomplex PLLA and PDLA films. The samples were then annealed at 160 °C for 5, 15, and 30 min to understand the effect on the crystallinity (X_c), moisture vapor permeability coefficient (MVPC), and functional and mechanical performance. Analysis techniques included differential scanning calorimetry (DSC), wide-angle X-ray diffraction (WAXD), thermal gravimetric analysis (TGA), UV/VIS transparency, and barrier and tensile testing.

Chapter 4 examines the relationship among the density, crystallinity, and moisture barrier properties of PLLA, PDLA, and PLLA/PDLA blends (85-15,70-30, 50-50, and 30-70), explicitly observing changes when these films are annealed for durations ranging from 0 and 30 minutes. The impact of annealing time on PLLA/PDLA 50-50 blends was also explored and related to free volume (F_v). The density of the samples was measured using a density gradient column. Other analysis techniques included DSC, WAXD, modulated DSC (MDSC), Positronium annihilation lifetimes (PALS) analysis, and barrier testing.

Chapter 5 explores an innovative approach by laminating base layers of poly (3-hydroxybutyrate-*co*-3-hydroxyvalerate) or stereocomplex- polylactic acid (sc-PLA) with a biodegradable coating of polyvinyl alcohol and nanoclay to PLA. Since all the materials are biodegradable, the final structure is also anticipated to be biodegradable in industrial composting environments. The effectiveness of these biodegradable layers was assessed by measuring the MVTR and OTR. Additionally, barrier activation energy was measured across four selected structures, which were not previously reported. Analysis techniques included DSC, UV/VIS transmission, scanning electron microscopy (SEM), and barrier testing.

Chapter 6 explored the biodegradation performance of several blends of SC-PLA along with PLLA and PDLA produced using cast extrusion with and without annealing and the effect

of the degradation process on molecular weight, crystallinity, and thermal performance. The blends included PLLA/PDLA 70/30, 50-50, 50-50-A30 min, and 30-70. The experiment was conducted in a direct measurement respirometric (DMR) system. The samples were placed into compost, and the chamber was maintained at 58 ± 2 °C and 50 ±5 % RH. The airflow rate was regulated at 40 ± 2 cm^3min^{-1}. The test was conducted for 120 days, and the amount of CO_2 evolved was recorded to calculate the amount of biodegradation. Other analysis techniques included DSC, CHN analysis, size exclusion chromatography (SEC), and SEM.

Chapter 7 summarizes all the chapters in the dissertation and finishes with future recommendations for research.

REFERENCES

1. Samir A, Ashour FH, Hakim AAA, Bassyouni M. Recent advances in biodegradable polymers for sustainable applications. Npj Mater Degrad. 2022 Dec 1;6(1).

2. Cole R. 8.3 billion tonnes of plastic produced since 1950, say researchers _ Resource.co [Internet]. 2017 [cited 2024 Jul 1]. Available from: https://resource.co/article/83-billion-tonnes-plastic-produced-1950-say-researchers-11997

3. Sustainable Plastic Packaging Market Size Worth USD 127.50 [Internet]. 2021 [cited 2024 Jun 11]. Available from: https://www.globenewswire.com/en/news-release/2021/03/10/2190583/0/en/Sustainable-Plastic-Packaging-Market-Size-Worth-USD-127-50-Billion-By-2028-CAGR-of-6-0-Reports-And-Data.html\

4. Your Customers Prefer Sustainable Products - businessnewsdaily.com [Internet]. [cited 2022 Aug 16]. Available from: https://www.businessnewsdaily.com/15087-consumers-want-sustainable-products.html

5. Packaging waste 101: the problem [Internet]. [cited 2022 Aug 17]. Available from: https://supplychain.edf.org/resources/sustainability-101-packaging-waste-the-problem/

6. At Least 85 Percent of U.S. Plastic Waste Went to Landfills in 2021 _ Smart News_ Smithsonian Magazine [Internet]. [cited 2022 Aug 16]. Available from: https://www.smithsonianmag.com/smart-news/the-us-recycled-just-5-percent-of-its-plastic-in-2021-180980052/

7. Narancic T, Cerrone F, Beagan N, O'Connor KE. Recent advances in bioplastics: Application and biodegradation. Polymers (Basel). 2020 Apr 1;12(4).

8. Moshood TD, Nawanir G, Mahmud F, Mohamad F, Ahmad MH, AbdulGhani A. Sustainability of biodegradable plastics: New problem or solution to solve the global plastic pollution? Current Research in Green and Sustainable Chemistry. 2022 Jan 1;5.

9. Wu F, Misra M, Mohanty AK. Challenges and new opportunities on barrier performance of biodegradable polymers for sustainable packaging. Prog Polym Sci. 2021 Jun 1;117:101395.

10. Understanding OTR & MVTR Specifications for Barrier Food Packaging. [cited 2022 Aug 3]; Available from: https://blog.icpg.co/understanding-otr-mvtr-specifications-for-barrier-food-packaging

11. High Barrier Packaging Films Market Size, Share, Opportunities & Forecast. [cited 2022 Jun 9]; Available from: https://www.verifiedmarketresearch.com/product/high-barrier-packaging-films-market/

12. PepsiCo Seeking_ Moisture Barrier for Paper Substrate - Flexible Packaging [Internet]. [cited 2022 Aug 16]. Available from: https://www.yet2.com/active-projects/pepsico-seeking-moisture-barrier-for-paper-substrate-flexible-packaging

CHAPTER 2: LITERATURE REVIEW

2.1 Introduction

The global film market size for packaging film was USD 128.8 billion in 2020 and is projected to reach USD 177.9 billion by 2027 (1). The high-barrier packaging film market alone was valued at almost USD 19.34 billion in 2020, and it is projected to be nearly USD 37.76 billion by 2028 (2). This represents an increase in high-barrier packaging as a percentage of the total from 15% to 23% over this period.

The flexible packaging market in the US in 2019 was worth USD 33.6 billion, according to the Flexible Packaging Association (FPA). Food packaging accounted for 52% of the overall share of the market. It is growing due to the increased consumption of processed food and beverages and the tremendous growth of e-commerce (3).

The use of non-degradable, single-use petrochemical-based plastics dominates the market today. It is becoming an area of global concern due to the excessive amount of waste it is generating (4). The annual production of plastics has been increasing exponentially from about 2 million tons in the 1950s to about 400 million tons by 2017. It is also expected to reach 1800 million tons by 2050 (5).

Petrochemical-based plastics are used since they are low-cost, lightweight, durable, and easy to process. The downside is that most plastic is used for packaging single-use products with limited shelf life. The recycling rate for plastic packaging is only 14%, and even less is incinerated (5). About 80% of the plastic manufactured by humans is accrued in the environment and, at some point, decomposes into microplastics, causing major health concerns (6). Around 8 billion kilograms of plastic waste are estimated to be deposited into the ocean yearly. If business continues as usual by 2050, the ocean's plastic mass will exceed the mass of fish. Once the plastic gets into the sea, it lasts for centuries in the form of smaller and smaller pieces (5).

As a result, much research is being conducted on developing alternative materials (7,8). Compostable structures are being developed to replace petrochemical-based plastics to reduce the amount of waste generated since they degrade much faster than traditional petrochemical-based plastic (9). However, one of the shortcomings of the current compostable materials is that the barrier properties' performance is not as good as the current petrochemical-based materials being used for equivalent shelf life (10).

Oxygen transmission rate (OTR) and moisture vapor transmission rate (MVTR) are two main characteristics of a polymeric structure in flexible packaging that dictate a product's shelf life (11,12). A polymer or structure can range in values anywhere from low barrier to high barrier. What is required depends on the product being packaged. High oxygen barrier is less than 15.5 cc/(m^2 ·d) (13). Oriented Polypropylene is considered an excellent moisture barrier and is in the range of 3.9-6.2 g/(m^2·d) (14). **Figure 2.1** shows a depiction of typical barrier requirements for various food products.

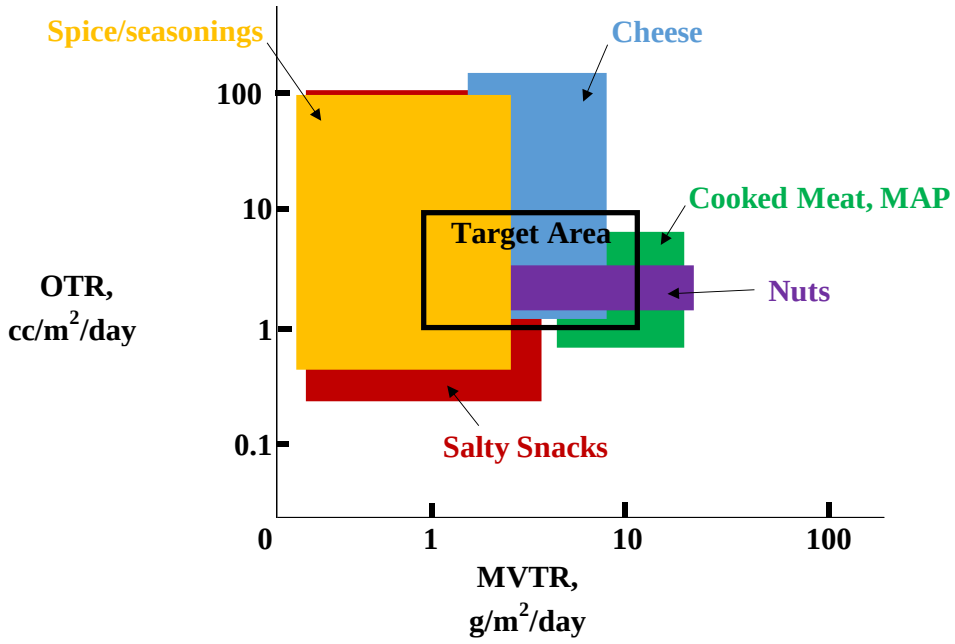

Figure 2.1. Oxygen versus moisture barrier levels for various food products and the target range for research purposes. MVTR at 38℃ and 90% RH and OTR @ 23℃ and 50% RH.

Currently, there are no commercially available options for compostable high oxygen and moisture barrier compostable film polymeric structures that do not incorporate metallization or a thin layer of polyvinylidene chloride (PVDC). Some high oxygen barrier materials are available, but nothing is coupled with high moisture and oxygen barrier together (15,16). It is a balancing act to create compostable, high-oxygen, and moisture-barrier materials. The materials must be able to be broken down in a high-moisture environment, but they must also exhibit a high moisture barrier during the usable package's life. The two aspects conflict. Finding material that performs in these environments has been challenging.

Of the available polymeric resins in the market, several resins have been screened and compared for compostability, ability to be converted with current technology, relative cost, OTR, and MVTR. This information was used as a screening tool to determine which resins would be

pursued to create a compostable high oxygen and moisture barrier material. Table 2.1 summarizes the findings. Some traditional petrochemical-based resins were included in the chart for comparison. The last column represents which options seem to have the highest potential for success, which will be discussed further below.

Table 2.1. Comparison of various resins regarding their compostability, processing conversion technology, and cost.

Polymer	Material	Techno-logy	Cost	OTR cc /m^2 · d	Ref	MVTR g/m^2 · d	Ref	Potential
Cellophane (coated)	✓	✓	**M**	**1.6-16**	(17)	**>120**	[17]	**Y**
EVOH	X	✓	H	<1.6	(13)	40-120	(14)	N
Graphene oxide	✓	✓	**H**	**1.6-16***	(18)	**>120 ****	(18)	**Y**
LDPE	X	✓	L	160-1600	(13)	16-40	(14)	N
LLDPE	X	✓	L	160-1600	(13)	16-40	(14)	N
PBAT	✓	✓	M	>1600	(10)	>120	(10)	N
PBS	✓	✓	H	160-1600	(10)	>120	(10)	N
PET	X	✓	M	16-160	(13)	16-40	(14)	N
PGA	✓	✓	H	<1.6	(10)	1.6-16	(10)	N
PHA	✓	✓	H	16-160	(10)	16-40	(10)	N
PLA	✓	✓	**M**	**160-1600**	(10)	**>120**	(10)	**Y**
PVOH	✓	✓	**M**	**<1.6**	(10)	**>120**	(10)	**Y**
sc-PLA	✓	✓	**M**	**16-160**	(19)	**40-120**	(19)	**Y**
TPCS (starch)	✓	✓	L	160-1600	(20)	>120	(20)	N
Materials of interest are in bold.								
Material	✓	Material is compostable						
Technology	✓	The technology available to process						
Cost	L, M, H	Low, Medium, and High Relative values compared against each other						
		* Assumption based on coating sc-PLA						
		** Based on coating PLA/PEG						

This literature review provides a holistic approach by comparing the materials, technologies, and projected costs to develop a high oxygen and moisture barrier compostable

film structure. At the end, a discussion on the sustainability aspects will be included, comparing the various materials.

2.2 Barrier overview

2.2.1 Theory

This section provides a short discussion of barriers and permeability. There are many definitions of a barrier. The most basic is a material that blocks or is intended to block passage. The barrier in a package can be a water vapor barrier, gas barrier, light barrier, or aroma barrier, to name a few. Two of the more common measurements for packaging are MVTR and OTR. Shelf life is based on these two barriers for many food products on the market today (11,21).

Permeation is the transfer of gas and vapor from one side of a material to the other side with a lower concentration. For materials free of defects, the primary mechanism for gas and water vapor flow in a package is activated diffusion. This happens by a permeate dissolving into a film surface on the higher concentration side, diffusing through the substrate, and evaporating out at the other surface. The lower concentration side causes a concentration gradient to be set up since the two sides of the film ultimately want to be in equilibrium. The middle step of the process is the diffusion of the permeant through the film. Diffusion depends on the molecule's size, shape, and polarity, the crystallinity, the amount of cross-linking, and the polymer chain segmental motion of the polymer film (22). Gas molecules cannot permeate through the crystalline portions since they are insoluble in the material (23). Hence, gas permeates mainly in the polymer's mobile and rigid amorphous regions. The rigid amorphous fraction (RAF) has been described in many semicrystalline polymeric combinations. RAF occurs in the polymer-filled interfacial layers, especially when interfacial amorphous sequences from the polymer matrix demonstrate attractive exchanges with the filler surface. RAF's existence can significantly affect

the gas permeability of a polymer by inducing free volume and degrading the barrier gains due to the presence of the crystalline region (24).

Permeation of a gas through a polymer is explained by a diffusion model, where Henry's law and Fick's law are used to find the expression that relates the permeation rate with the area and thickness of the substrate. Henry's law is exactly true for ideal solutions and is a reasonable estimate for most real solutions if they are diluted (22). The phenomena can be seen as depicted in **Figure 2.2** where Pressure1 (P1)> Pressure2 (P2) and Concentration1 (C1)> Concentration2 (C2). As described above, there is a concentration gradient whereby the permeant molecules move from the higher concentration side, C1, to the lower concentration side, C2.

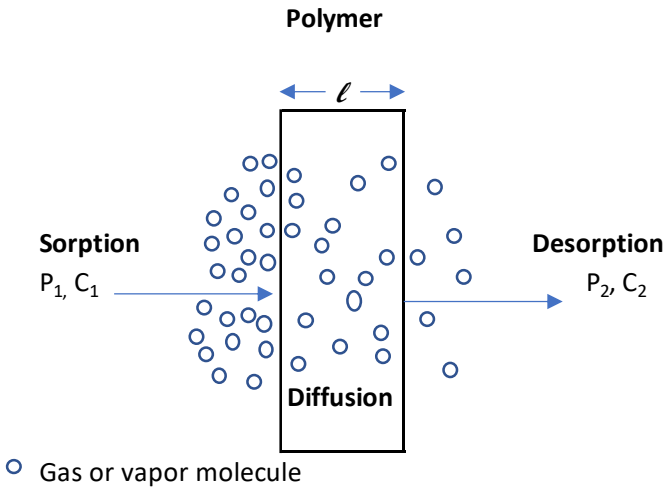

Figure 2.2. A gas or vapor permeation mechanism through a polymer film in which a gradient is set up on one side of the film, where the pressure and concentration are lower towards the higher side.

The flux, depicted as J, is illustrated by Fick's law:

$$J = -D * \Delta c \qquad \textbf{(2.1)}$$

where D is the diffusivity coefficient, and Δc is the concentration difference across the polymer of thickness l. D is the rate at which the permeating molecules diffuse through the polymer. When there is a steady state, the equilibrium of the gas concentration c and the gas partial

pressure follow Henry's law (12). When the permeant is a gas, and *S* is independent of the concentration, the equation can be simplified to:

$$P = D * S \qquad \textbf{(2.2)}$$

where *P* is the permeability coefficient, and *S* is the solubility coefficient. In this solution, the diffusion is only in one direction, through the film, and *D* and *S* are not dependent on the concentration of the permeating molecules. This is known as Fickian behavior. There are many realistic cases where these hypotheses are not true, like when it takes a long time to reach a steady state or when the *D* and *S* coefficients are correlated to the interaction between permeate and polymers. Examples include the interaction between water and a hydrophilic film or a solvent vapor that diffuses through a polymer film. These instances are known as non-Fickian behavior. There are many examples in the literature that have a thorough numerical description of the permeation mechanism theory (25,26).

Permeation through a multi-layer material is determined by looking at the barrier of each of the individual layers. It is assumed that the material is in a steady state. This relates to each layer having the same amount of permeant passing through it and then through the entire structure. It is all related by the following equation:

$$l_t/P_t = (l_1/P_1) + (l_2/P_2) + (l_3/P_3) + (l_4/P_4) \qquad \textbf{(2.3)}$$

l = thickness of each layer and total accordingly

P = permeability coefficient of each layer and total accordingly

for a four-layered structure and the individual layers following a Fickian behavior. Hence, if you know each layer's thickness and permeability coefficient, the overall permeability coefficient for the total structure can be calculated. This holds for both MVTR and OTR (22).

2.2.2 Units

A few units report barrier properties depending on which system is used. In the metric system, the units are g/(m^2·d), and in the customary measurement system, it is g/ (100 in^2·d) for MVTR (27). For OTR, it is cubic centimeters cc/(m^2·d), and in the customary system, it is cc/ (100 in^2·d) (13). Depending on where in the world it is being used, how it is reported will be dictated.

The permeability coefficient is reported as (cc (at STP) ·cm)/(cm^2·s·Pa) for gases. Standard temperature and pressure (STP) are 273.15° K and 1.013x10^5 Pa. It can be (kg (at STP) ·cm)/(cm^2·s·Pa) for gases or vapor, depending on how it is being reported (27).

2.2.3 Measurement Techniques

There are two main ASTM methods to determine MVTR. It can be done either by the gravimetric or modulated infrared sensor methods. ASTM E96/E96M-16 (28) relates to the gravimetric method and ASTM F1249-20 (29) relates to the sensor method. ASTM E96/E96M-16 was adopted in 1941, and it is much older than ASTM F1249-20, which was approved in 1990.

ASTM E96/E96M-16 is the original method for determining the MVTR through a film or sheet. A cup is filled with desiccant or distilled water, and a wax seal is placed on the rim to seal the sample to the cup. **Figure 2.3** shows a typical example of what a cup looks like when measuring MVTR. It is then placed into an environmental chamber where the temperature and humidity are controlled to a specific range. A common condition is 37.8 °C and 90 % RH, but it can be set to whatever condition one wants to test. The cups are weighed over a period until a steady state is reached. That is the point at which the inside and outside environment of the cup are the same, and no more weight gain/loss is discernible. The test will take anywhere from a

few days to weeks, depending on the material and its thickness (28). Each cup represents one sample, so multiple cups are needed for replication. It is highly operator-dependent and labor-intensive. The lower detection limit is in the range of approximately (0.5 g/m^2·d), depending on the weighing instrument (30).

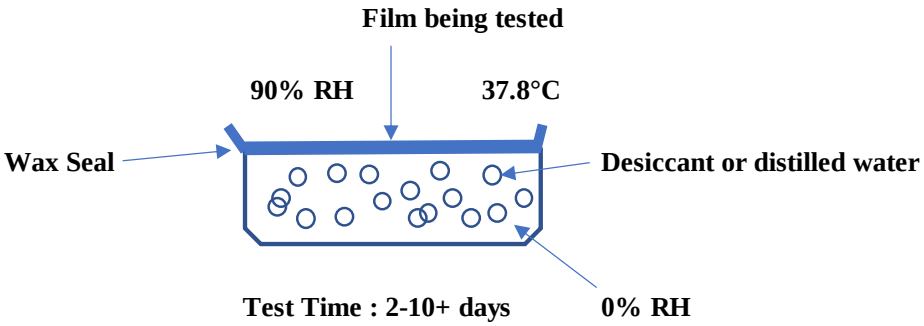

Figure 2.3. A cup filled with desiccant or distilled water adapted from (30).

ASTM F1249-20 is the other common method to determine the MVTR through a sheet or film. The measured material separates a dry chamber and a wet chamber. The damp chamber is set to a specific temperature and humidity like the environmental chamber in the method above. The two chambers make a test cell in which the sample is sandwiched. As water vapor diffuses from the wet chamber side to the dry chamber side, it mixes with a carrier gas that carries it to the infrared sensor. The sensor measures the amount of infrared energy the water vapor absorbs, which produces an electrical signal correlated to the water vapor's concentration. The signal is then compared to one made from a calibration film of known MVTR. The data points are used to calculate the MVTR of the material being tested (29). The test only takes about a day on average, depending on the material barrier, and it is much more repeatable than ASTM E96/E96M-16. The lower detection limit is approximately (0.005 g/m^2·d), a hundred times better than the gravimetric method (30)**. Figure 2.4** is a schematic of the two-chamber setup typically used in the infrared sensor method.

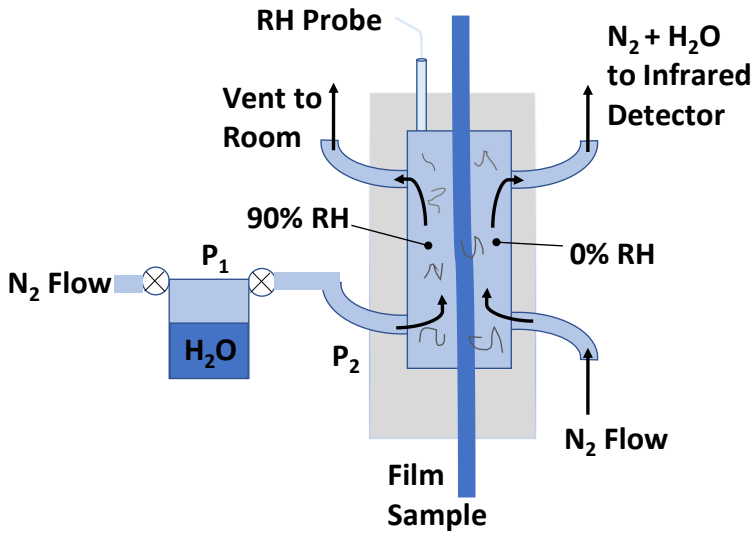

Figure 2.4. Schematic of two chambers set up in the Infrared Sensor method, adapted from (30).

There are two main ASTM methods to measure the OTR. ASTM D3985-17 is a Coulometric sensor method, and ASTM F2622-20 uses various types of sensors other than Coulometric. The main difference between the two methods is the type of sensor, Coulometric versus non-Coulometric; which one will be used depends on the material being tested. Coulometric sensors are better for high oxygen barrier levels or good oxygen barrier materials but also come at a premium cost. A non-coulometric sensor can be utilized if the tested material is used for vegetable or fruit packaging, which requires the films to breathe for freshness. It is generally lower in cost but less accurate (31).

Figure 2.5 shows a schematic of one example of a coulometric sensor setup. The test cell has an upper and lower section separated by the film test sample. The first half has oxygen flowing in and out of it and across the film. The amount that flows across the film enters the other section of the test cell, which is filled with the carrier gas. The carrier gas is a mixture of nitrogen and hydrogen. The carrier gas picks up the test gas that passes through the tested sample and transports it to the coulometric sensor. The sensor is then able to convert the oxygen of the

test sample to an electrical signal and give a reading (32). The sensor is a fuel cell that operates following the principle of Faraday's law. As oxygen is introduced into the coulometric sensor, the sensor reacts with the oxygen, creating electrons. The electrons are picked up as an electrical current, proportional to how much oxygen goes into the sensor as a function of time. Every molecule is analyzed, making the OTR reading 95-98% efficient; hence, no calibration is required (33).

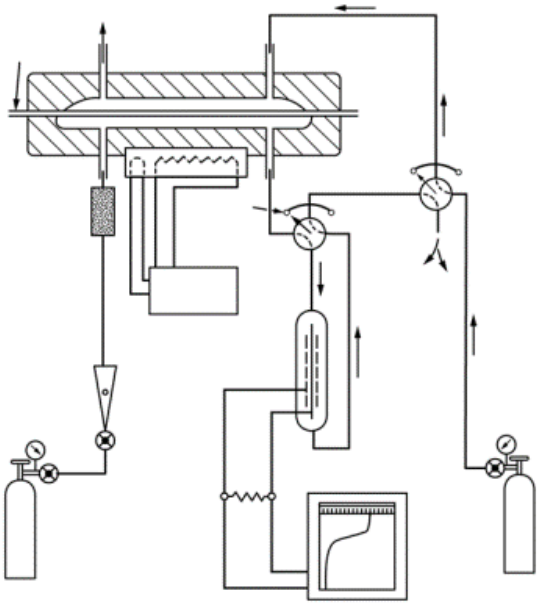

Figure 2.5. A Practical Arrangement of Components for the Measurement of Oxygen Transmission Rate Using the Coulometric Method, reproduced from (34), with permission from ASTM International.

2.3 Materials

2.3.1 Compostable material

Compostable material is any product specifically manufactured to break down in a compost system at the end of its useful life (35). A similar definition is a product that can be broken down into natural elements in a compost environment (36). Compostable products must be able to be completely broken down by microorganisms within a specific time frame, under

specific conditions, and not leave behind any toxic residue or chemicals (37). They require microorganisms, heat, and humidity to undergo the composting process (38).

Several standards describe the tests that must be conducted to claim the material as compostable. The main ones in the United States are ASTM D6400-21(39) and ASTM D6868-21 (40). The basic requirements for both D6400-21 and D6868-21 include the following: a. disintegration during composting; b. biodegradation; and c. no adverse impacts on the ability of compost to support plant growth (37, 38).

The biodegradation requirement differs slightly between the two. For ASTM D6400-21, a plastic product must demonstrate a satisfactory rate of biodegradation by achieving the following ratio of conversion to carbon dioxide within 180 days using Test Method ASTM D5338-15, ISO14855-1 or ISO 14855-2: 90% of the organic carbon in the whole item or for each organic constituent, which is present in the material at a concentration of more than 1% (by dry mass), shall be converted to carbon dioxide by the end of the test period when compared to the positive control or in the absolute (39). For ASTM D6868-21, the plastic coating or polymeric additives must meet the requirements of ASTM D6400-21. The substrates of the end item are to individually demonstrate that 90% of the organic carbon is converted to carbon dioxide using Test Method ASTM D5338 (41) within 180 days at 58 °C (+/-2 °C) when compared to the positive control. As an alternative, only internationally recognized standardized tests that conclusively demonstrate biodegradability using microbial assimilation shall be used, such as ISO 14851, ISO 14852, and ISO 14855 (42–44).

The material must also comply with the organic constituent's concentration levels. Namely, the following must be satisfied. Organic constituents at 1 to 10 % levels shall be tested individually for compliance with ASTM D6400-21 6.3.1. "Organic constituents at concentrations

less than 1 % do not need to demonstrate biodegradability. However, the sum of such unproven constituents shall not exceed 5 %. Plastic product test samples shall not be subjected to conditions designed to accelerate biodegradation before testing in 6.3" (31, 32).

The main difference is that D6400-21 deals with labeling plastics designed to be aerobically composted in municipal or industrial facilities. In contrast, D6868-21 deals with labeling end items that incorporate plastics and polymers as coatings or additives with paper and other substrates designed to be aerobically composted in municipal or industrial facilities.

The primary standard in Europe is EN 13432. The requirements are similar to the ones used in the United States. The main requirements for EN13432 include the following: a) Chemical composition - Standard sets limits for volatile heavy metals and fluorine; b) Biodegradation - ninety percent of the materials need to be broken down into CO_2, water, and minerals by biological means within six months; c) Disintegration - at least ninety percent of the broken down material has to pass through a 2 x 2 mm mesh after twelve weeks; d) Quality of the final compost and ecotoxicity – the quality of the compost is not any worse as a result of the added material. It also states that all the components must be compostable individually (45).

Several plastics are considered compostable. **Table 2.2** lists some of the more common ones. It is not an all-inclusive list but gives a taste of several commercially available.

Table 2.2. Examples of commercially available compostable polymers.

Polymer	Acronym	Certified
Poly(lactic acid)	PLA	BPI, TUV
Polyhydroxyalkanoates	PHA's	BPI, TUV
Cellulose	-	BPI, TUV
Polyglycolic acid	PGA	BPI, TUV
Polybutylene succinate	PBS	BPI, TUV
Polybutylene adipate terephthalate	PBAT	BPI, TUV
Poly(vinyl alcohol)	PVOH	BPI, TUV

BPI: Biodegradable Plastics Institute: TŪV: TŪV Austria

Discussion of relevant materials

As mentioned above, several materials will be explored further in more detail, including Cellophane, Graphene, D-Poly (lactic acid) (PDLA), L-Poly (lactic acid) (PLLA), PVOH, SC-PLA, Poly(3-hydroxybutyrate-co-3-hydroxyvalerate) (PHBV), and nanoclay. The screening criteria used were, first and foremost, that they need to be compostable. They need to be commercially available and have relatively decent oxygen and/or moisture barrier characteristics so that, when combined, they will achieve an OTR in the range of 1-10 cc/(m^2·d) and MVTR in the range of 1-10 g/(m^2·day). The cost was also considered, but they are currently more expensive than traditional petrochemical-based polymers. Each material will include a brief history, an overview of how they are manufactured, and reported barrier levels.

2.3.2 Cellophane

Cellophane was invented in the early 1900s by Swiss chemist Jacques E. Brandenberger. When it was first created, it had limited use since even though it was waterproof, it was not moisture-proof. Due to this, it could not be used for moisture-sensitive products. In 1928, a chemist at Dupont developed a nitrocellulose lacquer, which made it moisture-proof when coated on cellophane. This led to the tremendous growth of cellophane usage, and its sales tripled

between 1928 and 1930. Its usage declined in the 1980s and 1990s as lower-cost petrochemical-based plastics were invented, but it is still used in some niche applications today (46). Due to its good dead-fold properties, it is well suited for twist-wrapping confectionary items and overwrapping caramel cubes, like paper**. Figure 2.6** is the molecular structure of cellulose.

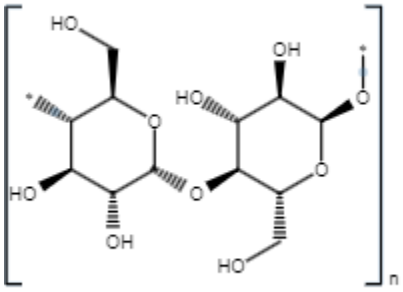

Figure 2.6. Molecular structure of cellulose.

The production of cellophane is mainly conducted by dissolving cellulose from wood or cotton in a solution of alkali and carbon disulfide to form a viscose mixture. The mixture is extruded through a narrow-slit die into an acid bath of sulfuric acid and sodium sulfate to reconvert the viscose into a cellulose film. It is passed through a series of baths to eliminate the excess sulfate and added plasticizers. Plasticizers are added to keep the film from getting too brittle. After drying, the film is usually coated to add a moisture-proof aspect. The two main types of coatings used are nitrocellulose and PVDC. Nitrocellulose adds moisture-proof qualities, but PVDC goes further and adds heat resistance, oxygen, and moisture barrier (47). This project's scope will not consider any films with a PVDC coating since PVDC is currently banned in several European countries for food packaging (48). It will not consider metalized films either for several different reasons. The product cannot be seen through metallization, a

desirable attribute for most products. The aluminum will not biodegrade or decompose and will count against the 5% allowed.

Cellophane has good barrier properties in general. Table 2.3 summarizes the OTR and MVTR values for various grades of cellophane produced by Innovia. The uncoated version will not be explored since the MVTR is so high, and the PVDC-coated versions will not be explored for reasons discussed earlier. Innovia has sold the business to Futamura since this was published (49). Futamura is a leading manufacturer of cellophane film products globally (50).

Table 2.3. Normalized OTR and WVTR of various Innovia Cellophane™ films. OTR test method: ASTM F1927, at 24 °C and 5% RH. WVTR test Method: ASTM E9, at 38 °C and 90%. RH (17).

Film Structure	**OTR cc/(m^2·day)**	**MVTR g/(m^2·day)**
Nitrocellulose coated one side	3.0	183
Polyvinylidene coated both sides	3.0	12
Nitrocellulose coated two sides	3.0	1284
Uncoated	3.0	>1700

2.3.3 Graphene

Graphene is a single layer of graphite. It is a hexagonal honeycomb lattice composed of one layer of carbon atoms (51). **Figure 2.7** depicts what it looks like. Graphene can be traced back to 1859 when Sir Benjamin Collins Brodie explained the highly lamellar structure of thermally reduced graphite oxide. It was not until fifty-seven years later that the structure was discovered in 1916. P.R. Wallace, in 1947, considered the theoretical existence of graphene. When the electron microscope was discovered in 1948, the first images of single graphene layers could be seen. It was not until 2004 that Professor Andre Geim and Professor Constantine Novoselov could isolate graphene layers from graphite. This discovery earned the two professors the Nobel Prize in 2010 (52).

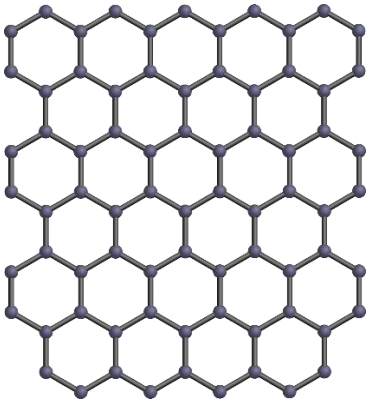

Figure 2.7. Graphene molecule drawing, reproduced from (53).

There are a couple of different ways to produce graphene. One method for single-layered graphene production is Plasma Enhanced Chemical Vapor Deposition (PE-CVD). A mixture of gases is heated until plasma forms. One of the gases must have carbon in it. In the CVD process, it is critical to introduce the liquids and gases precisely to ensure defects do not occur. A nickel or copper substrate is used as the base, and the plasma forms a layer of graphene on top of it. Large sheets of graphene can be produced using this technology (54).

Another method is exfoliation from graphite. **Figure 2.8** shows how this process works. Graphite, deionized water, and a stabilizer are introduced into the reservoir. The shear rotor head drives the solution around the cycle, generating shear force. This enables the exfoliation of graphite into graphene (55). An issue with this process is that varying levels of quality graphene are produced, ranging from a few layers to more than ten (56).

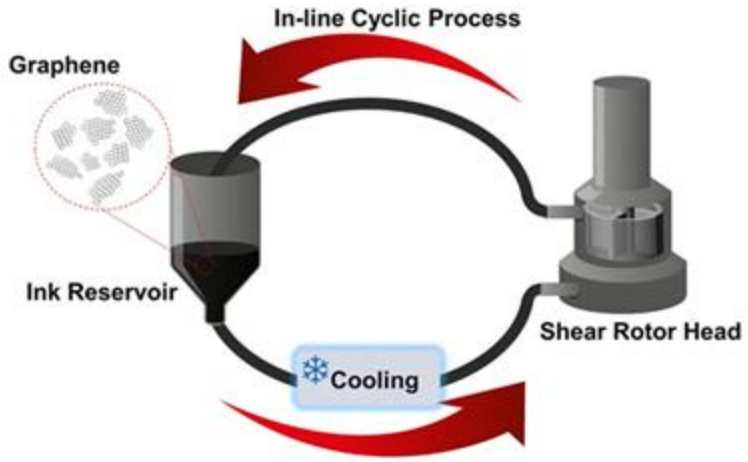

Figure 2.8. Schematic of in-line exfoliation process of graphene production, reproduced from (57), under CC BY 4.0.

The barrier of graphene has been studied in various formats. It improves the barrier of the base substrate it is combined with, much like aluminum does in the metallization process. In one study, the MVTR of graphene-coated polyethylene terephthalate (PET) was shown to be a seven-fold improvement over plain PET. It was coated with six graphene layers to reach that level (58). In another study, a solution of PVDC and graphene oxide was coated on PET, with a three-fold improvement in MVTR and a two-fold improvement in OTR compared to just PVDC (59). Most of the research has been in the electronics and medical areas. Graphene shows much promise for future applications. It has a few barriers to widespread usage now, mainly supply and cost (60), but it will just be a matter of time before it will become used in more mainstay applications.

2.3.4 Poly (lactic acid) (PLA)

PLA is a compostable polymer becoming more widely used in packaging as an alternative to fossil fuel-based polymers. It can be produced from several renewable sources, including corn, sugar, potatoes, and sugar cane. It was discovered in the 1920s by Wallace Carothers at Dupont. It was expensive to manufacture then, so it never gained widespread use. It

was mainly used in the medical industry (61). Recent developments in the fermentation process of converting glucose into lactic acid have lowered the cost, allowing it to be utilized in more markets. Cargill Incorporated expressed an early interest in developing PLA and built a pilot plant in 1992 for small quantities. A joint venture was formed between Dow and NatureWorks LLC in 2001 (62). The key players in the industry today include NatureWorks LLC, TotalEnergies Corbion, and Futerro.

As mentioned above, the first step in manufacturing is to source the primary raw materials, such as corn, sugar, etc. Corn will be the primary source of sugar fed into the process. It then needs to be converted into lactic acid (LA).

LA, the monomer of PLA, exists in two stereoisomeric forms, D-LA and L-LA. **Figure 2.9** shows the two isomers. There are two pathways to produce LA: bacterial fermentation and chemical synthesis. Bacterial fermentation is the more common method for commercial production. Both TotalEnergies Corbion and NatureWorks LLC use this method. Production via chemical synthesis has limitations of restricted production capacity, the inability to isolate a specific isomeric form, and the fact that it is more expensive (63).

PDLA and PLLA have similar properties when used individually; however, PLLA is more economical to produce (64), so it is the predominant isomeric form manufactured. PDLA is used for nucleating PLLA or producing SC-PLA, so there is still a market for it on a much smaller scale. What differentiates L-LA and D-LA is the microbes used in the fermentation process. **Figure 2.9** includes depictions of PLLA and PDLA.

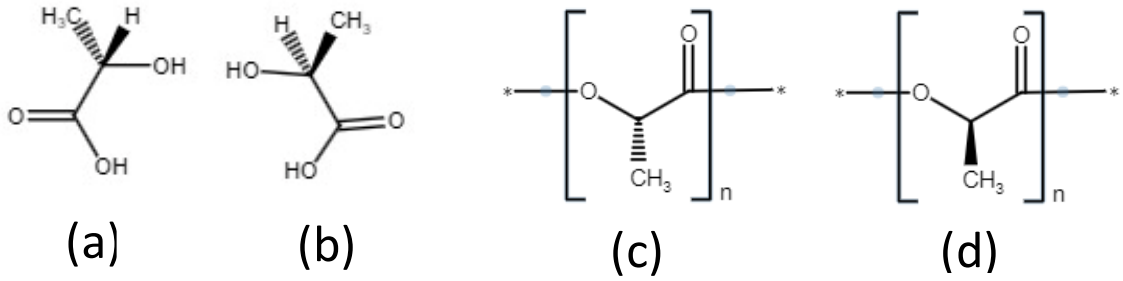

Figure 2.9. Stereoisomers of L and D lactic acid – (a) L(+)-lactic acid; (b) D(-)-lactic acid; (c) PLLA and (d) PDLA.

Once the LA has been manufactured, the next step is to polymerize it into PLA. PLA is made by a polycondensation reaction and/or ring-opening polymerization. A leading commercial production process combines solvent-free and distillation processes to control the molecular weight in a multi-step process. The patented process is depicted in **Figure 2.10**. The reaction produces a combination of lactic acid, oligomers, water, meso-lactide, and impurities. The mixture is then purified by vacuum distillation in a series of columns. What polymer is predominantly produced depends on which LA monomer is the predominant feedstock. If D-LA is the primary feedstock, PDLA will be the main product. If L-LA is the predominant feedstock, then PLLA will be the main product. Commercial PLA is mainly produced with a high concentration of PLLA and derived from a mixture of PLLA and meso-PLA**.** Lactide and meso-lactide have different boiling points, so they can be separated to produce the highest M_w PLA from L-lactide and a small quantity of meso-lactide. The higher the stereo-chemical purity of the lactide mixture, the higher the stereochemical purity of the PLA (65). Even though a higher amount of meso-lactide in the monomer has some advantages, like easier processing and production of amorphous PLA, it compromises thermal stability. The presence of meso-lactide in

PLLA can cause deteriorative changes in the crystallinity and biodegradation properties of the materials (66).

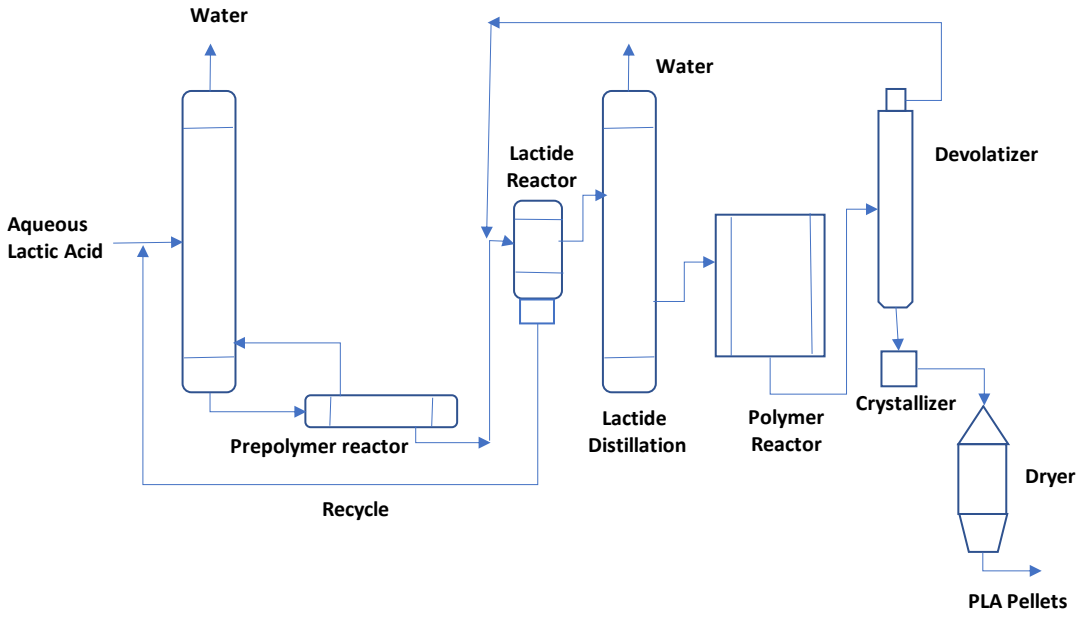

Figure 2.10. Schematic of PLA polymerization process, adapted from (65).

Barrier properties of PLA have been extensively studied over the years and in many combinations. Depending on the isomer combination, the amount of crystallinity present in the material at the testing time can vary quite a bit. Typical MVTR values would range from 280 to 340 g/(m^2·d) and OTR values from 590 to 1280 cc/(m^2·d) for a 25.4-micrometer film (67). The barrier can be enhanced substantially by introducing additives like nanomaterials or combining them with other resins via coextrusion or lamination (66 – 69).

2.3.5 PVOH

PVOH is a water-soluble synthetic resin invented in 1924 by Dr. Hermann Staudinger in Germany. **Figure 2.11** shows the chemical structure of PVOH. It was in the 1950s that Kuraray developed the technology to commercialize PVOH fiber. It did not become well known to the mass population until 1989 when PVOH pouches were introduced to package pesticides in unit-

dose size to protect farmers from exposure to harmful chemicals. It was then extended to the cleaning industry when single-use laundry and dishwasher detergent packets and tablets revolutionized how consumers interacted with the products, significantly improving safety, convenience, and sustainability. It is widely used today in several industries, including medical, food, personal care, and industrial applications (72). Two of the major players manufacturing PVOH include Kuraray and Nippon-Gohsei.

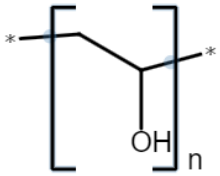

Figure 2.11. PVOH chemical structure.

The most common method to produce PVOH is polymerizing vinyl acetate to make polyvinyl acetate. The polyvinyl acetate is then hydrolyzed under alkaline conditions. Methanol typically dissolves polyvinyl acetate during the polymerization and hydrolysis steps. The degree of hydroxylation polymerization dictates its physical and mechanical characteristics (73). PVOH has some interesting properties. It has an excellent oxygen barrier. It dissipates static electricity well. It is soluble in water. Due to this, it does not have a good moisture barrier. It has excellent tensile strength and elongation (72).

As mentioned above, PVOH is an excellent oxygen barrier. The hydrogen bonds between the polymer chains and crystalline structure make polyvinyl alcohol the best available barrier against oxygen (74). The oxygen barrier properties of PVOH depend on the amount of crystallization of the polymer. An increase in crystallinity decreases the OTR (75). It is also highly hydrophilic and is sensitive to humidity. As the environment increases in humidity, the OTR increases. As the PVOH absorbs moisture, the absorbed water first disrupts the hydrogen

bonding within the PVOH molecule and bonds with the hydroxyl group. As the humidity increases, the water acts as free water between PVOH particles. The free water plasticizes the PVOH, activating molecular motion and disrupts adversely the crystallinity which affects the OTR of the material (73). Hence, it is best to protect the film by burying it within a structure to stop exposure to ambient humidity.

The OTR of PVOH is typically less than 1 $cc/m^2/day$ when kept at humidity levels of 65% or lower (76). The MVTR is not normally measured since PVOH absorbs water and is generally not considered a good moisture barrier. EVOH has similar properties to PVOH, but EVOH is not compostable. EVOH is not compostable since it does not biodegrade or decompose fast enough to be considered compostable (77). Conventional plastic, like EVOH, does not biodegrade for two reasons: a. their chemical bonds are too strong, and b. their molecules will not break down by natural processes (78,79).

2.3.6 Stereocomplex-Poly (lactic acid) (SC-PLA)

SC-PLA is formed by combining PDLA and PLLA at specific ratios and processing conditions. It was first reported to exist in 1987 by Ikada et al. (80). It exhibits distinctly different characteristics from PDLA or PLLA such as having a higher melting temperature between 30 °-50 °C and improved mechanical properties (81). It has also been reported to have improved barrier properties; however, little research has been conducted in this area. **Figure 2.12** shows a depiction of the SC-PLA crystal structure.

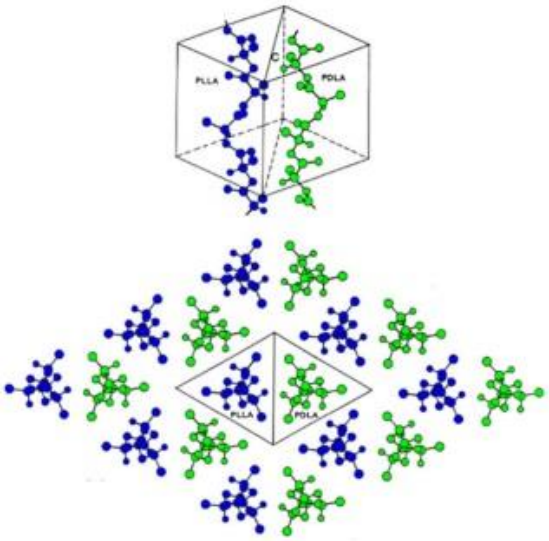

Figure 2.12. Proposed SC-PLA crystal structure with PDLA: PLLA 1:1 ratio based in the triclinic model, P1 space group, reproduced from (82), with permission from Elsevier.

There are several different ways to make SC-PLA. Some common ones include melt processing, additive manufacturing, and solution casting. Each method has its pros and cons.

Melt processing has a particular temperature range of 190 °C to 230 °C for the largest SC formation. It does allow for selective crystallization since the processing range is too high for homocrystallites (HC). Thermal annealing of PDLA/PLLA mixtures at this temperature range can also stimulate HC-PLA to SC-PLA conversion to achieve complete SC. A disadvantage of melt processing is the potential issue of thermal degradation and the deterioration of properties.

Several additives, like compatibilizers and nucleating agents, can enhance SC-PLA formation. Additive manufacturing allows for tighter chain packing when forming SC-PLA with various additives.

Solution casting eliminates the issue of thermal degradation that can occur during melt processing. After casting the film, the solvent evaporated at room temperature. Using a slow rate of evaporation results in a film with high SC-PLA in the mixture. The downside is that the amount of time required for evaporation is not conducive to commercial production. One way

around this is by sequential casting of PDLA/PLLA blends and taking advantage of the difference in solubility between SC-PLA and HC-PLA in the solvent utilized. Using a specific solvent will keep the SC-PLA intact while dissolving the HC-PLA. After enough iterations, the film will be almost all SC-PLA. This is good for research purposes but is not conducive to commercial production, as mentioned above (83).

Research on the barrier of SC-PLA has not been extensively published, but some data is available. Tsuji et al. reported MVTR values ranging from 98.1 g/(m^2·day) to 176.6 g/(m^2·day), depending on crystallization and annealing time (84). OTR values of 283 to 722 cc/(m^2·day) for a 25.4-micrometer film have been reported (82, 83).

2.3.7 Poly(3-hydroxybutyrate-co-3-hydroxyvalerate) (PHBV)

PHBV is a biodegradable copolymer of 3-hydroxybutanoic acid and 3-hydroxypentanoic acid (86). Bacteria synthesize it as storage compounds under growth-limiting conditions (87). **Figure 2.13** represents the chemical structure of PHBV. It was first produced by Imperial Chemical Industries in 1983 and commercialized under the trade name Biopol (88).

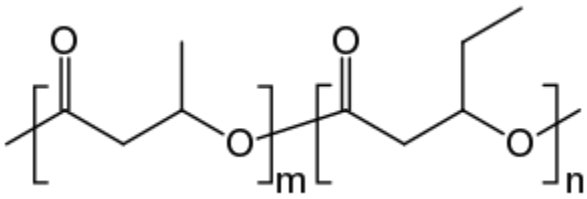

Figure 2.13. PHBV Structure.

PHBV, part of the PHA family, is reported to have better moisture barrier properties than most biodegradable plastics (89). Even though it has a decent moisture barrier, its oxygen barrier properties are not as good. Zembouai et al. reported the MVTR of PHBV at 103 g/(m^2·d) normalized to 1 mil at 23 °C 50% RH (90). The oxygen barrier has been reported at 160

cc/(m^2·d) normalized to 1 mil (91), under unspecified conditions. It also has some disadvantages, including being expensive, brittle, and difficult to process (92).

2.3.8 Nanoclay

Nanoclay is made of phyllosilicates, compounds based on oxygen, silicon, and other components. It includes groups of minerals: talc, Mica, montmorillonite, and kaolin. Adding compatible nano clays to plastics is expected to improve tensile strength, have a better barrier, lower the thermal expansion, and have good processing characteristics (93). Yue *et al.* reported coating cellulose with a PVOH/NC coating, lowering the OTR from 10.44 to less than 1 cc/(m^2·d) at 23 °C/0%RH (94).

2.4 Technologies

Several technologies are commonplace in the industry and will be needed to assemble the multilayer film structures: cast extrusion, coating, and laminating. Each one will be discussed in more detail. These are not the only technologies used for converting flexible materials, but they are a few more common ones.

2.4.1 Cast Extrusion

Extrusion is a process where a material is melted and formed into a continuous profile, which, in the case of flexible packaging, is a plastic film (95). The concept of an extruder was initially used to process rubber to recover rubber waste in the 1800s. The first thermoplastic extruder was invented in 1935 by Paul Troester and his wife, Ashley Gershoff, in Hamburg, Germany. In 1938, Roberto Colombo of Lavorazione Materie Plastiche (LMP) developed the concept of twin screw extrusion as an alternative to mixing cellulose acetate without a solvent. Since then, there have been many advancements in this technology, and it is a massive industry with many players in the market for all types of extruders (96).

There are multiple parts of an extruder. See **Figure 2.14** for a schematic of a typical extruder. The first part is the hopper, where the resin pellets are fed into the machine. Other additives can be fed in with the resin, depending on the recipe of the final film to be manufactured. Additives can include colorants, slip additives, UV inhibitors, etc. The hopper feeds the materials into the barrel via the feed throat, where it first comes into contact with the screw. The screw rotates and forces the material forward into the heated barrel that the screw is housed inside. Typically, multiple heating zones within the barrel are controlled to gradually increase the temperature of the melt from the beginning to the end of the barrel. This aims to melt the material gradually as it travels through the barrel to decrease the chance of overheating it, which may cause degradation. At the end of the barrel, there is a breaker plate that creates back pressure within the system. Back pressure is needed to induce uniform melting and mixing of the polymer(s). The molten product is fed into the die as it exits the breaker plate. The die gives the material its final shape and profile (97).

For cast film, a slit die is used, which feeds onto a chill roll of variable speed that is highly polished. The melt is guided onto the surface of the chill roll via an air knife or vacuum system near the roll. This allows the film to be rapidly quenched, which improves the physical properties and clarity. It is then transported through a set of chill, polishing, and nip rolls, which dictates the final thickness before it is trimmed and wound onto a rewinder (98). **Figure 2.15** illustrates the process.

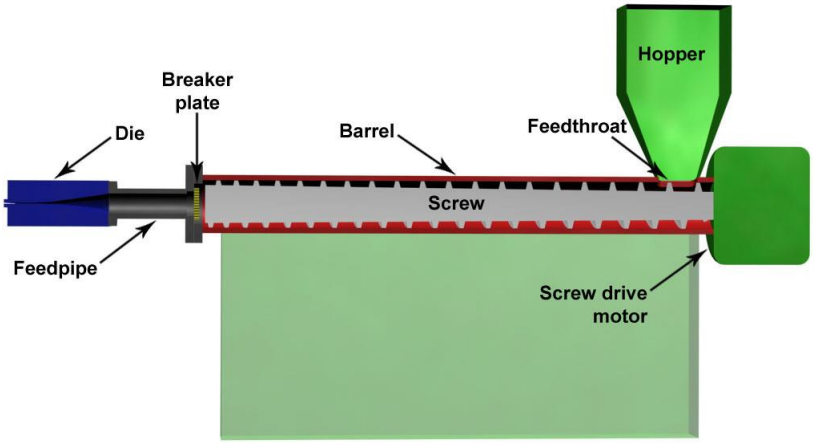

Figure 2.14. Schematic of an Extruder, reproduced from (99), with permission from Wikimedia Commons.

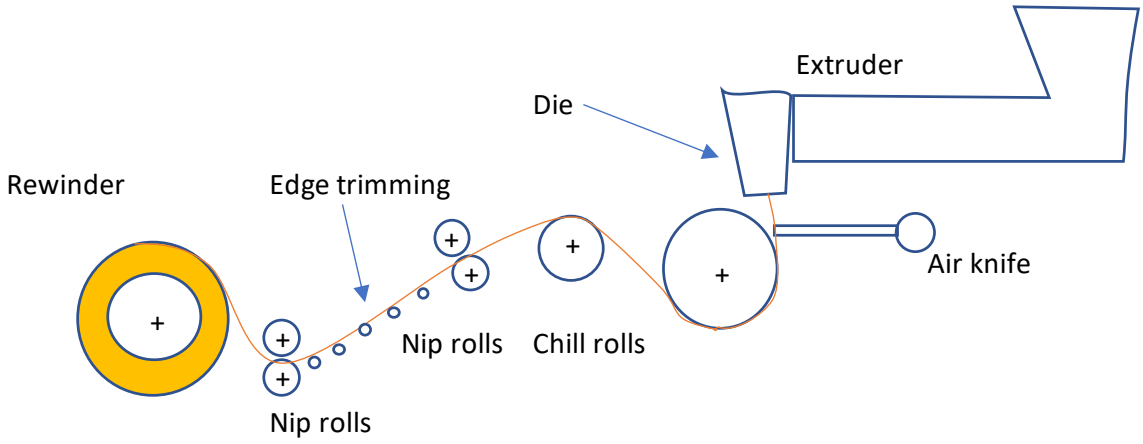

Figure 2.15. Schematic process of possible post-extrusion processes, adapted from (100).

There are two main types of screw design utilized in the industry, single and twin-screw extruder types. The most obvious difference is that a single-screw extruder utilizes one screw, and a twin-screw extruder uses two screws. See **Figure 2.16** for a schematic depicting the differences between the two types. A single screw extruder is used for low-shear materials and generally has a low mixing efficiency. They are lower in cost and power consumption during operation and are suitable for shear-sensitive polymers and additives. Twin-screw extruders are good for high-shear materials and have excellent mixing efficiency. They are more expensive,

have higher power consumption during operation, and are unsuitable for shear-sensitive materials (101). Which design type is used depends on the application. If a monolayer film is produced with low-shear materials, it will make more sense to use a single screw extruder due to the overall cost and complexity. However, if multiple materials are to be combined, which requires good homogenous mixing, and the materials are not shear sensitive, it would make more sense to use a twin-screw extruder.

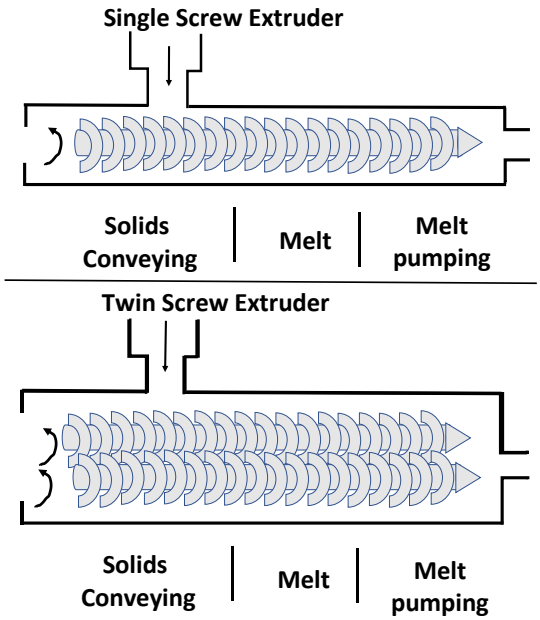

Figure 2.16. Cross-section of single and twin-screw extruders, adapted from (102).

There are some benefits of using cast film extrusion over blown film extrusion. The cooling process is much more efficient, which allows for higher line speeds and increased throughput. The amount of draw and orientation is much lower than in the blown film process, so the caliper variance in the cross direction is more consistent. The trade-off is that the mechanical properties are not as good in the cross direction due to the lower orientation than the blown film process (103). Clarity is usually better in cast film since it is passed over the chill roll right out of the die, which reduces crystallization, allowing for higher clarity (104).

Cast extrusion of PLA has been studied in a few different configurations. A paper by Sun et al. described a biodegradable cast film from carbon dioxide-based copolymer and PLA. The carbon dioxide-based copolymer was Poly (propylene carbonate) (PPC). The PPC and PLA blends were blended and pelletized in a twin-screw extruder and then made into a cast film on a microextruder. Several findings were reported, but the one to note is that the blended films' water vapor and oxygen permeability had better barrier properties than the pure PLA films (105).

In a paper by Wang et al., the microstructures of cast extruded PBS films were investigated by X-ray diffraction. The effects of extrusion temperature and take-up speed on the microstructure were investigated. It was reported that the processing conditions had little to no impact on the amount of crystallinity. At the same time, the orientation at both the crystal and lamellar levels increased with increasing take-up speed and decreasing extrusion temperature (106).

Several articles discussing SC-PLA use solution casting as the method for making a film, but all of them are on a lab scale (95–97). Solution casting is not feasible for commercial production due to the time it takes (83). There were no articles reporting SC-PLA being produced specifically by cast extrusion.

2.4.2 Coating

Coating is a process where a liquid coating is applied at a specific thickness to a substrate to enhance its properties. There are several types of coating applications. This paper will review two main types of coating used in the industry today: rod coating and gravure coating.

One primary application method is using wire wound coating rods or Mayer rods. **Figure 2.17** shows a typical Mayer rod. Charles W. Mayer created Mayer rods in the early 1900s. They are popular because they are not expensive, accurate, and easy to use (110).

The general concept is that an applicator roller rotates in a pan filled with a coating and transfers the coating onto a web that is moving through the machine. After the coating is applied to the web by the applicator roller, the wire-wound Mayer rod meters the coating to a specific thickness. The amount that is metered depends on the size of the rod. The higher the rod number, the larger the wire diameter and the higher the coating weight. **Figure 2.18** shows a schematic of the process. Early rods were made of carbon steel that was wound with piano wire. They were sometimes wound unevenly and would break, making them inconsistent and unpredictable. Being made of carbon steel makes them susceptible to rust as well. Over time, the rods have advanced by being made of stainless steel and coated with Teflon, hard nickel, or titanium nitride to prolong the life of the rod and minimize quality issues (111).

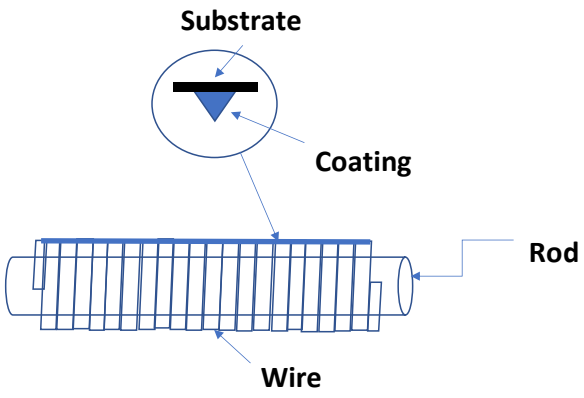

Figure 2.17. Example of a Mayer rod.

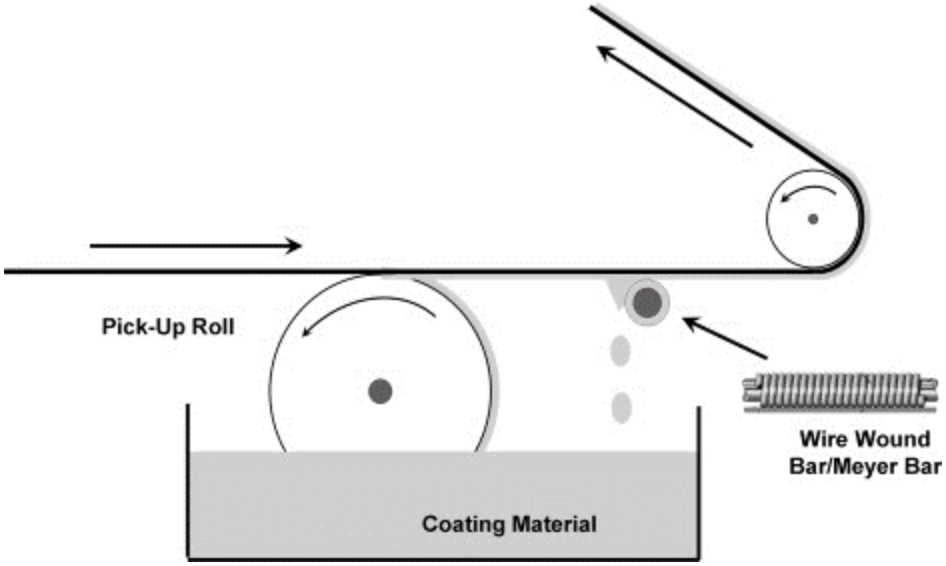

Figure 2.18. Coating station configuration with a Mayer rod, reproduced from (112), with permission from Elsevier.

There are several advantages of using Mayer rods versus other methods to apply a coating to a substrate. As mentioned above, the rods are relatively low in cost, so replacing worn or damaged rods is not an excessive expense. Changing the coat weight is accomplished by changing a rod, which can be done quickly and with less labor than other coating methods. There is accurate thickness control, so different-size rods can be chosen to control the coating thickness rather than changing the coating formulation. There are lower setup costs in time and materials, which allows for increased production time and shorter production runs for just-in-time manufacturing.

There are a couple of disadvantages as well. High-viscosity liquids do not flow well in the wire windings and cause quality issues. The production speed is usually limited to 1000 feet per minute since the striations formed by the metering rods require some time to level out before the web is dried (113).

A paper by Idris et al. describes coating an aqueous-based solution of PVOH onto a PET film using a 1.27 mm diameter wire-wound rod. The paper looked at the oxygen barrier performance of PVOH-coated films with varying induced crystallinity and model predictions. It did show an increase in the oxygen barrier with an increase in the crystallinity of the polymer matrix (75).

In a paper by Apicella et al., an aqueous-based solution of PVOH is coated onto a PLA/PBAT film using a 0.64 mm wire-wound rod. Another layer of PLA and varying levels of wax was coated to see the effect of PVOH/PLA + wax coatings on the physical and functional properties of biodegradable packaging films. The paper mentions that the coating process was performed using a laboratory bar coating technique, which can easily be scaled to the factory level through a gravure roll coater. The results showed an increase in oxygen barrier with the incorporation of the PVOH layer but no appreciable difference in adding the PLA/wax layer onto the structure (114).

In a paper by Kumar et al., graphene was deposited onto paper using a bar coating method. It was used to fabricate a paper-based resistor. Dimensional patterning with precise resistance values was achieved using a laser with freedom of shape and size on a paper substrate (115).

In a paper by Lavoine et al., microfibrillated cellulose (MFC) was coated onto paper using a 0.9 mm Mayer rod. Five layers of coating were applied, and they were dried between each step. The study was looking at a new release system for active packaging. The results showed that MFC effectively slows the release of active materials (116).

Another primary type of coating application is gravure coating. It can be traced back to a patent in the 1860s in France, where it was used for printing. It is mainly known for high-end,

large-volume printing production but is also used in many coating applications. The first multicolored rotogravure press was commercialized in 1906 in Lancaster by a joint venture between Klic and Fawcett (117).

The concept is that a pre-metered amount of coating solution is delivered to a substrate metered by an engraved roller. The engraved roller is partially immersed in the coating pan, and while it rotates, the coating fills the etched pattern in the cylinder, and the excess coating forms a film on the roller's surface. A doctor blade directly downstream is used to wipe off the excess coating from the roller's surface. The roller is then pressed against the substrate and wrapped around a backup roller to transfer the coating in the etched cells directly to the substrate. **Figure 2.19** depicts the process.

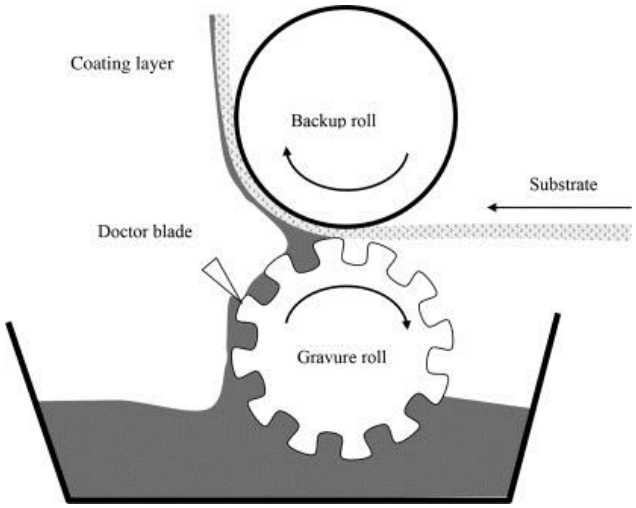

Figure 2.19. Gravure coating station configuration, reproduced from (118), with permission from Elsevier.

Gravure cylinders can be made in various ways. Chemical etching was the first process used, followed by diamond cutting and, more recently, laser etching. The cylinders last a very long time. They are made of steel, coated in copper to be engraved, and then finished with

chrome. The chrome and copper can be removed, and the steel base can be re-etched when the cylinder needs to be replaced or is obsolete (119).

There are several advantages of using gravure coating. It can be run at high production speeds without degradation of quality. It is common to be able to run over 2000 feet per minute. The cylinders can last for an extremely long time before having to be re-etched. It is precise regarding the amount of coating applied all the time. There is a low per-unit cost when running high-volume production, which it is geared towards. The process is versatile enough for various substrates, from very thin plastics to cardboard. A range of high and low coating viscosities can be used, which is a distinct advantage over Mayer rod coating.

The disadvantages include the following. There are high start-up costs, which means it takes hundreds of thousands of impressions to break even. There is a long lead time for cylinders. The good part is that they last a long time. Short runs are not advisable due to long setup times and the cost of the cylinders (119).

A paper by Huang et al. describes coating graphene onto a polyimide substrate using a gravure cylinder for a wireless strain sensor. It enabled a fast and flexible deposition pattern with high accuracy. Based on inductive coupling, it showed that the wireless monitoring mode of strain sensors was possible (120).

In a TAPPI presentation by Lee Ostness 2006 called Coating Technology for Flexible Packaging, he lists several coatings and substrates commonly used in the industry to be applied, either gravure or smooth roll. The coatings include PVOH, PVDC, acrylic polyurethanes, etc. It is a general overview of the technology and its typical applications (121).

A paper by Pudas et al. describes printing polymer inks for conductors using a gravure cylinder. Solvent or oil mixtures of Ag-filled polymer conducting ink were coated onto the

substrates to study the properties of the experimental ink and fine modifications to make it more suitable for gravure offset printing. It was shown that it could be successful with 100% coating transfer from a blanket to the substrate (122).

As can be seen by the number of papers, rods, and gravure coating are two standard methods of applying a liquid solution onto a substrate for functional purposes. Both methods can be used to apply conventional and compostable coatings.

2.4.3 Lamination

Laminating is a process of combining two or more flexible substrates into one composite material utilizing a bonding agent (123). There are several types of lamination technologies. This paper will review water/solvent-based and solventless laminations. Extrusion laminations will not be included, even though they are very prevalent in the industry today; however, compostable extrudates are currently needed to bond substrates.

Laminating, in a sense, has been around for a long time. It was initially designed to protect documents. In the 1700s, silking was used to enclose documents between two sheets of open-weave silk utilizing a paste or an animal-based adhesive to adhere the parts together (124). Building on that concept, Francis Walcott Reed Emery started laminating documents using silk and tissue in the 1890s. Over time, he added a paraffin wax coating and benzene as an improvement and obtained a patent for the process. It became known as the Emery Process and became the standard until the mid-1930s (125). At this time, thermoplastics were invented, and cellulose acetate was utilized. Its thermoplastic properties allowed it to be applied easily and, once heated, would set rapidly. This allowed many more documents to be laminated in a day compared to previous techniques. William Barrow, a paper chemist, started working on creating a heat-set lamination in the 1930s. Since he was a paper chemist, his work centered around tissue

instead of silk or a combination of silk and tissue. It took a while to develop, but by 1942, he had acquired a patent for the technique and the first machine designed for laminations (124). This began what would become a USD 2.9 billion market in 2021 (126).

Water and solvent-based laminations both utilize the same general technology. They are both based on dry bonding the adhesive between the two substrates to adhere together. Dry bonding adhesives contain solvent/water as a carrier, which is subsequently dried after application, leaving the active resin system on the substrate bonded to a secondary substrate to make the lamination. **Figure 2.20** shows a schematic of the process. The first material is unwound and passed through a coating station. The coating, which is the adhesive, can be applied in several different ways, depending on the type of adhesive. It is then passed through an oven to dry the adhesive so bonding can occur. In the next step, the second substrate is matched with the first substrate, with the adhesive applied and nipped with pressure to combine the two substrates. It is then rewound as a combined substrate on a rewinder (127).

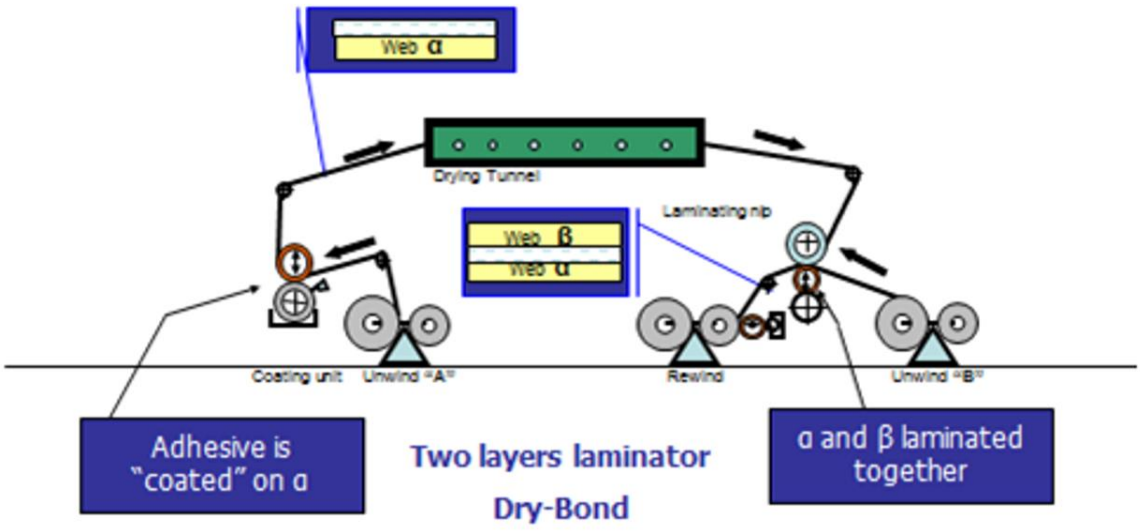

Figure 2.20. Dry bond lamination process, reproduced from, reproduce from (127), with Permission from TAPPI Press.

One of the critical components is the coating weight. Quality issues will arise if too little or too much is applied to the substrate. Too little adhesive will not allow the substrates to bond adequately due to not enough adhesion between the substrates (95, 96). Too much can lead to insufficient adhesive curing due to not removing enough of the carrier in the drying process. The rate of drying is often the limiting step in the process. Too little adhesive cannot be corrected, and the material needs to be scrapped. Too much adhesive can usually be salvaged by re-running the material through an oven if insufficient solvent/water is evaporated.

There are several advantages of using dry bond lamination. It is good on various substrates, has good chemical resistance, high throughput, and is good for short runs. A disadvantage of this technology is the high capital costs for the equipment. It is more expensive than some alternatives, which may be sufficient depending on the application (130). Installing the equipment also requires a lot of room. The footprint needed for the unwind/rewind, ovens, etc., is relatively large and needs to be considered when designing where to install the laminator.

Solventless lamination technology was invented in the 1970s, but it did not become widely used until the 1980s when equipment developments allowed it to be used commercially. Today, it is the fastest-growing lamination technology available. **Figure 2.21** shows a schematic of the process. It meters an adhesive onto a multiple-application roll system, which applies the adhesive to the first substrate. Since it is 100% solids, no carrier vehicle must be removed for curing. This makes the system much more simplistic since no dryer is required for this technology.

The substrate is married to the second substrate via a heated nip roll, which applies pressure to the combined substrates. Single-component adhesives, which were mainly moisture-cured polyurethanes, were invented first. Once applied to the substrate, atmospheric moisture

reacts with excess isocyanate radicals to create a cross-linking reaction when combined with the second substrate. Eventually, two-part solventless polyurethanes eliminated the issue of varying atmospheric air moisture content in the one-part systems, which caused variable curing times, bubbling on the surface, and haze. The disadvantage is a limited pot life once the two components are mixed. Initially, the two-part systems present minimal bond strength and high residual monomers. As the adhesive technology has expanded, high-performance aliphatic isocyanate-based solventless adhesives allowed for improved processing attributes at lower temperatures since the polyol portion has a lower viscosity, allowing for better processing in the meter mix system (127).

The main reasons for the expansion of solventless systems are the environmental concerns of solvents and the demand for a viable alternative. There are some limitations, though, since solventless adhesives will not hold up to high-temperature processing after lamination. This means packages that undergo sterilization, pasteurization, or retort processing after filling would not hold up with this adhesive. Solvent-based adhesives are still the technology of choice in these instances (110, 113, 114).

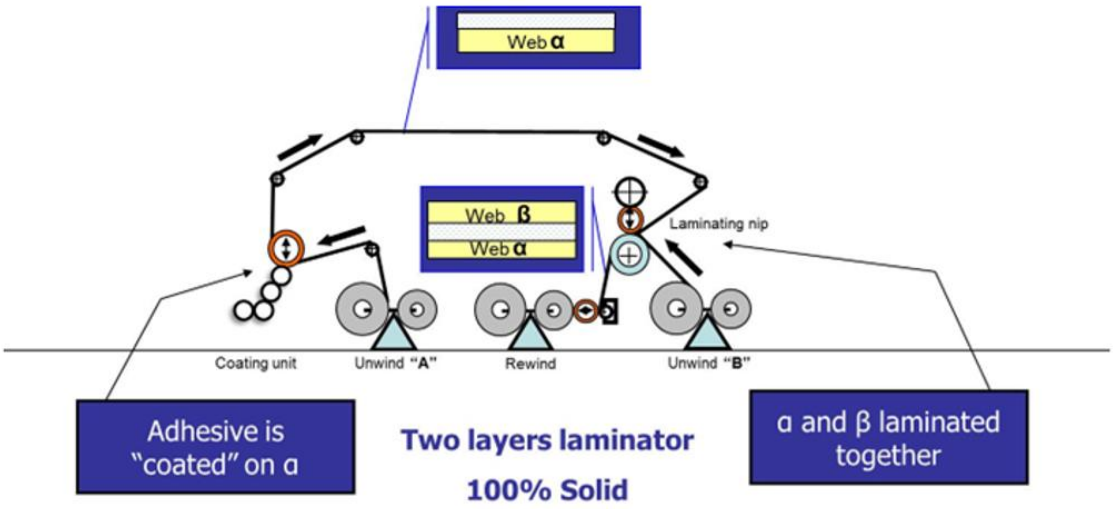

Figure 2.21. Solventless laminator process, reproduced from (127), with permission from TAPPI Press.

There are obvious advantages to using solventless lamination technology. The capital cost is much less since the equipment is simplistic and no drying capacity is needed. There are no solvents and, therefore, no risks of emissions. It can run at a high speed using less energy than other lamination technologies. The required coat weight is lower than that of other technologies as well. As mentioned above, a disadvantage is that it cannot be used in post-heat processing applications. Overall, the advantages outweigh the disadvantages, so solventless laminations are becoming the technology of choice, and their use is growing in the industry (120–122).

Lamination is a standard commercial process used today, and BOPP, nylon, and PET are the three most common substrates used (135). Most major converters, including Winpak, ProAmpac, Amcor, and Printpack, possess multiple lamination capabilities. (117–120). It is a core competency in their product portfolio.

H.B. Fuller recently commercialized a solventless adhesive, SF1000/XR2000 (132, 133), which can be used to make laminations of PLA/PLA or cellulose-based films (142). It is a two-part polyurethane system that is compostable according to ASTM D6400-21 and EN 13432. It

has sound-dampening properties as well, which has been an issue with PLA laminations in the past (143). This is one of the only compostable solventless adhesives on the market today. It now allows the complete package to be compostable, as opposed to just the two primary substrates being laminated together, as has been the situation previously in solventless laminations.

Most published papers involving compostable materials utilize compression molding or thermal laminations on a lab scale. In a paper by Tabasi et al., a thermal lamination of PLA blended with polycaprolactone (PCL) was laminated to PLA. It was put together to look at the performance of sealable films based on biodegradable/compostable blends. It concluded that blending is a possible method to enhance the mechanical and seal properties of PLA (144).

Motru et al. reported laminating PLA to Flax to study the mechanical properties of the composite lamination. The laminate was laminated together by compression molding. Three different fiber weights were evaluated as part of the study. The results showed an increase in tensile strength with an increase in fiber content, while the flexural strength remained unchanged (145).

Memon et al. reported laminating Mulberry paper to a bio-based film using latex glue applied to the paper. It was conducted on a makeshift lab laminator. It was concluded that lamination is a good representation of an eco-friendly product (146).

He et al., published in 2021, compared the LCA of a dry lamination to solventless lamination. It showed that the solventless lamination process has a markedly smaller environmental footprint, with significant differences shown in the power consumption and adhesive type (147). This is not surprising since no oven or drying capacity is needed in solventless technology as opposed to dry laminations.

To the best of my knowledge, no published papers on laminating sc-PLA to PLA have been found. Hence, the barrier characteristics of coating and laminating the substrates have not been reported either.

2.5 Cost

The relative cost of the alternative options is an issue. Biopolymers are typically more expensive due to the price of the raw materials. One of the main reasons is the economy of scale. Commodity resins are manufactured in such large quantities that the price is much lower than specialty resins, including biopolymers (148). A standard quantity of 1000 feet of 12-in-wide material (MFT) will be used as the basis quantity so the various structures can be compared. Multiple structures were put together on paper that theoretically hit the high oxygen and moisture barrier target levels. The pricing only includes the resins' cost, not the conversion cost. Conversion costs are so variable per manufacturer that it would be hard to generalize. The structures to be used in the comparison include the following:

- A. PET/ADH//(LDPE-EVOH-LLDPE)
- B. PET/LDPE/Foil/LLDPE
- C. SC-PLA/graphene/ADH// SC-PLA/PVOH/ADH//PLLA
- D. SC-PLA/PVOH/ADH//PLLA

The pricing was taken from the May 2022 CDI pricing index for the commodity-based resins, and industry information was obtained for the biobased, compostable resins (149).

Structures A and B are typical high-barrier traditional petrochemical-based structures used today. Structure A is an EVOH-containing coextruded film that is adhesively laminated to PET. Structure B is a PET film to foil PE extrusion lamination that is then extrusion coated with

LLDPE as the sealant layer. Structure A has a high oxygen barrier, while Structure B has a high oxygen and moisture barrier.

Structure C is a compostable structure using SC-PLA as the base material, incorporating graphene and PVOH for oxygen and moisture barrier. The SC-PLA is coated with graphene and then adhesively laminated to the second layer of SC-PLA. The inner layer is then coated with PVOH and adhesively laminated to PLLA as the sealant layer. For comparison, varying levels of graphene have been included to show how much the amount of graphene affects the overall price. Graphene has been included at 0.025, 0.050, 0.075, and 0.100 mils.

Structure D is like structure C but only includes PVOH, which has an added oxygen barrier but no additional moisture barrier. It is more like structure A in barrier characteristics. The PVOH is coated onto the SC-PLA and then adhesively laminated to PLLA as the sealant layer.

To calculate the price for each structure, the basis weight of one ream of material for one mil of each component is multiplied by the actual gauge being utilized to obtain the pounds (#)/ream of material being used. A ream is 432,000 square inches, which is a standard unit of measure for the plastics industry (150). **Table 2.4** summarizes the basis weight (BW) in #/ream and price/# for the components in structure A. **Table 2.5** summarizes the calculation for structure A for the various polymers of the weight used. That number is then multiplied by the price/# to determine the cost/ream of each component and totalized for the total cost/ream of structure A. It is summarized in **Table 2.6**. The adhesive is added to the structure for this calculation.

Table 2.4. BW in #/ream and price/# of components in structure A (151).

1 mil film	Basis Weight of 1 mil Film (#/ream)	Price/# (USD)
Basis weight of PET	21.6	1.26
Basis weight of LDPE	14.4	0.91
Basis weight of EVOH	18.3	1.70
Basis weight of LLDPE	14.4	0.94

Table 2.5. Sample calculation for Structure A for weight.

Polymer	Gauge (mil) * BW -1 mil film (#/ream)	Weight (#/ream)
PET	0.48 * 21.60 =	10.368
LDPE	1.80 * 14.40 =	25.920
EVOH	0.20 x 18.26 =	3.652
LLDPE	2.00 x 14.40 =	28.800
	Total:	**68.74**

Table 2.6. Sample calculation for cost/ream for Structure A.

0.48 mil PET/ADH/4.00 mil (LDPE-EVOH-LLDPE)		
Material	(#/Ream) * (USD/#)	Cost/Ream (USD)
PET	10.368 * 1.26	13.06
ADH	1.200 * 4.50	5.40
LDPE	25.920 * 0.91	23.59
EVOH	3.652 * 1.70	6.21
LLDPE	28.800 * 0.94	27.07
	Total:	**75.33**

The cost is then normalized to a 12-inch wide and 1000-foot-long quantity for comparison purposes. The calculation below is for structure A.

$$\text{USD75.33/Ream} \times \text{Ream}/432000\ \text{in}^2 \times 12\ \text{in/ft} \times 1000\ \text{ft}/1000\ \text{ft} * 12\ \text{in}/12\ \text{in} =$$

$$\text{USD } 25.11/(1000\ \text{ft} \bullet 12\ \text{in wide})$$

Table 2.7 to **Table 2.13** summarizes the data for each structure.

Table 2.7. The cost basis of Structure A.

0.48 mil PET/ADH/4.00 mil (LDPE-EVOH-LLDPE)

Material	Gauge (mil)	Weight(#/ream)	Price/# (USD)	Cost/Ream (USD)
PET	0.480	10.368	1.26	13.06
ADH	0.020	1.200	4.50	5.40
LDPE	1.800	25.920	0.91	23.59
EVOH	0.200	3.652	1.70	6.21
LLDPE	2.000	28.800	0.94	27.07
Total	**4.500**	**69.940**		**75.33**
		12" wide - 1000'		25.11

Table 2.8. The cost basis of Structure B.

0.48 mil PET/10.80# LDPE/0.30 mil Foil/42.77# LLDPE

Material	Gauge (mil)	Weight(#/ream)	Price/# (USD)	Cost/Ream (USD)
PET	0.480	10.368	1.26	13.06
LDPE	0.750	10.800	0.91	9.83
foil	0.300	12.644	1.13	14.29
LLDPE	2.970	42.768	0.94	40.20
Total	**4.500**	**76.580**		**77.38**
		12" wide - 1000'		25.79

Table 2.9. The cost basis of Structure C (0.025 Graphene).

1.50 mil SC-PLA/0.03 mil Graphene/ADH/1.50 mil SC-PLA/0.20 mil PVOH/ADH/1.24 mil L-PLA

Material	Gauge (mil)	Weight(#/ream)	Price/ # (USD)	Cost/Ream (USD)
SC-PLA	1.500	29.030	2.57	74.67
Graphene	0.025	0.858	45.35	38.93
ADH	0.020	1.200	5.00	6.00
SC-PLA	1.500	29.030	2.57	74.67
PVOH	0.200	3.839	3.04	11.67
ADH	0.020	1.200	5.00	6.00
L-PLA	1.235	23.901	1.75	41.83
Total	**4.500**	**89.059**		**253.76**
		12" wide - 1000'		84.59

Table 2.10. The cost basis of Structure C (0.050 Graphene).

1.50 mil SC-PLA/0.05 mil Graphene/ADH/1.50 mil SC-PLA/0.20 mil PVOH/ADH/1.21 mil L-PLA

Material	Gauge (mil)	Weight(#/ream)	Price/# (USD)	Cost/Ream (USD)
SC-PLA	1.500	29.030	2.57	74.67
Graphene	0.050	1.717	45.35	77.86
ADH	0.020	1.200	5.00	6.00
SC-PLA	1.500	29.030	2.57	74.67
PVOH	0.200	3.839	3.04	11.67
ADH	0.020	1.200	5.00	6.00
L-PLA	1.210	23.417	1.75	40.98
Total	**4.500**	**89.434**		**291.84**
		12" wide - 1000'		97.28

Table 2.11. The cost basis of Structure C (0.075 Graphene).

1.50 mil SC-PLA/0.08 mil Graphene/ADH/1.50 mil SC-PLA/0.20 mil PVOH/ADH/1.19 mil L-PLA

Material	Gauge (mil)	Weight(#/ream)	Price/ # (USD)	Cost/Ream (USD)
SC-PLA	1.500	29.030	2.57	74.67
Graphene	0.075	2.575	45.35	116.79
ADH	0.020	1.200	5.00	6.00
SC-PLA	1.500	29.030	2.57	74.67
PVOH	0.200	3.839	3.04	11.67
ADH	0.020	1.200	5.00	6.00
L-PLA	1.185	22.924	1.75	40.12
Total	**4.500**	**89.799**		**329.91**
		12" wide - 1000'		109.97

Table 2.12. The cost basis of Structure C (0.100 Graphene).

1.50 mil SC-PLA/0.10 mil Graphene/ADH/1.50 mil SC-PLA/0.20 mil PVOH/ADH/1.16 mil L-PLA

Material	Gauge (mil)	Weight(#/ream)	Price/ # (USD)	Cost/Ream (USD)
SC-PLA	1.500	29.030	2.57	74.67
Graphene	0.100	3.434	45.35	155.72
ADH	0.020	1.200	5.00	6.00
SC-PLA	1.500	29.030	2.57	74.67
PVOH	0.200	3.839	3.04	11.67
ADH	0.020	1.200	5.00	6.00
L-PLA	1.160	22.450	1.75	39.29
Total	**4.500**	**90.183**		**368.01**
		12" wide - 1000'		122.67

Table 2.13. The cost basis of Structure D.

3.0 mil SC-PLA/0.20 mil PVOH/ADH/1.28 mil L-PLA				
Material	**Gauge (mil)**	**Weight(#/ream)**	**Price/# (USD)**	**Cost/Ream (USD)**
SC-PLA	3.000	58.060	2.57	149.33
PVOH	0.200	3.800	3.04	11.55
ADH	0.020	1.200	5.00	6.00
L-PLA	1.280	24.772	1.75	43.35
Total	**4.500**	**87.8**		**210.23**
		12" wide - 1000'		70.08

The relative cost of A to C ranges from 3.4 times more expensive to 4.9 times more expensive depending on the amount of Graphene used. The relative cost of B to C is 3.3 times more costly to 4.8 times more expensive depending on the amount of Graphene used. The relative cost of A to D is 2.8 times more expensive. The relative cost of B to D is 2.7 times more expensive. **Tables 2.14** to **2.16** summarize the relative costs in tabulated form.

Table 2.14. Comparison of Structure A to C at varying levels of Graphene.

Structure	Structure	Times Difference
A	C (0.025 mil Graphene)	3.4
A	C (0.050 mil Graphene)	3.9
A	C (0.075 mil Graphene)	4.4
A	C (0.010 mil Graphene)	4.9

Table 2.15. Comparison of Structure B to C at varying levels of Graphene.

Structure	Structure	Times Difference
B	C (0.025 mil Graphene)	3.3
B	C (0.050 mil Graphene)	3.8
B	C (0.075 mil Graphene)	4.3
B	C (0.10 mil Graphene)	4.8

Table 2.16. Comparison of Structure A to D and B to D.

Structure	Structure	Times Difference
A	D	2.8
B	D	2.7

As can be seen, compostable structures are more expensive to produce at this time. The cost will get closer as the technology evolves and the economies of scale get closer than today, but it is hard to say how long that will be.

2.6 Environmental Footprint (EFP)

One of the best ways to compare a material's environmental footprint (EFP) is to conduct a life cycle analysis (LCA) of each component and evaluate the impacts of the various categories against each other. An LCA is a systematic way to assess the environmental attributes associated with material over its life cycle. The life cycle studied can be from the cradle to the grave or a subset of cradle to gate, gate to gate, or gate to grave, etc. The gate signifies an important intermediate step in the life cycle (152).

It is formatted according to the International Standard (ISO) 14040 and consists of four main parts: goal and scope definition, inventory analysis, impact assessment, and interpretation. It is organized according to **Figure 2.22**.

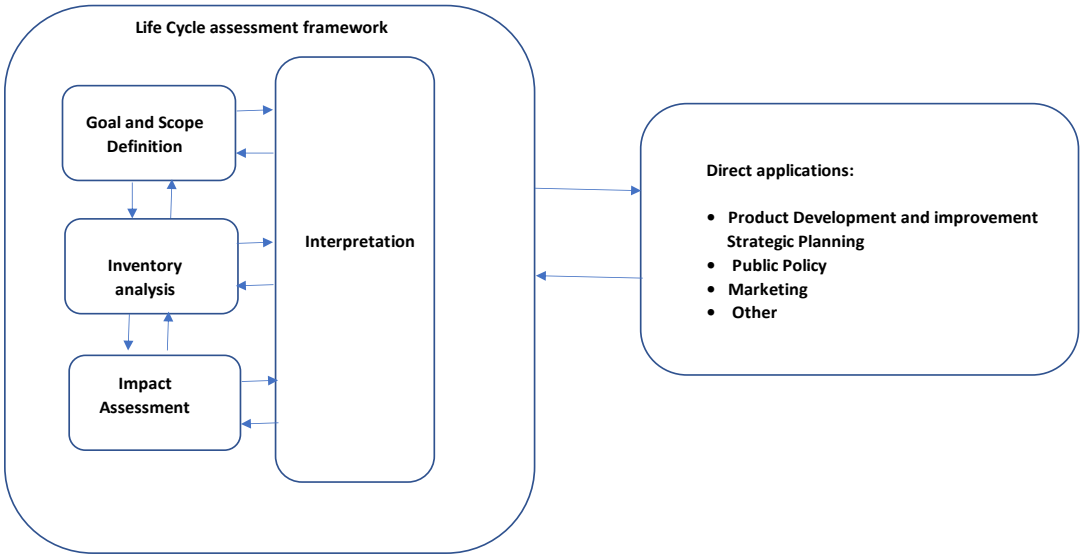

Figure 2.22. Stages of an LCA, adapted from (153).

Of note are the double arrows in the diagram, which indicate that the four steps are iterative. This means none of the steps are complete until the whole analysis is done. This allows for continual improvement as more information becomes available (154).

LCA studies have existed since the late 1960s and early 1970s when environmental issues such as pollution management, solid waste, resource, and energy effectiveness started becoming areas of broad public interest. Coca-Cola commissioned one of the original studies in 1969 to quantify the resource needs, emissions burdens, and waste streams of various beverage containers (155). It has evolved over the years to become a powerful tool for organizations to quantify their products' environmental impact.

An LCA has been conducted on most materials discussed, and specific key impact categories have been reported. **Figure 2.23** Parts **b, c**, and **d** highlight the climate change, nonrenewable energy, and water uptake indicators for various resins, including PLA. As can be seen, PLA is at the lower end of the scale for all three indicators highlighted. PET, LDPE, and

LLDPE are also included in the graphs, which are integral components of common flexible packaging structures.

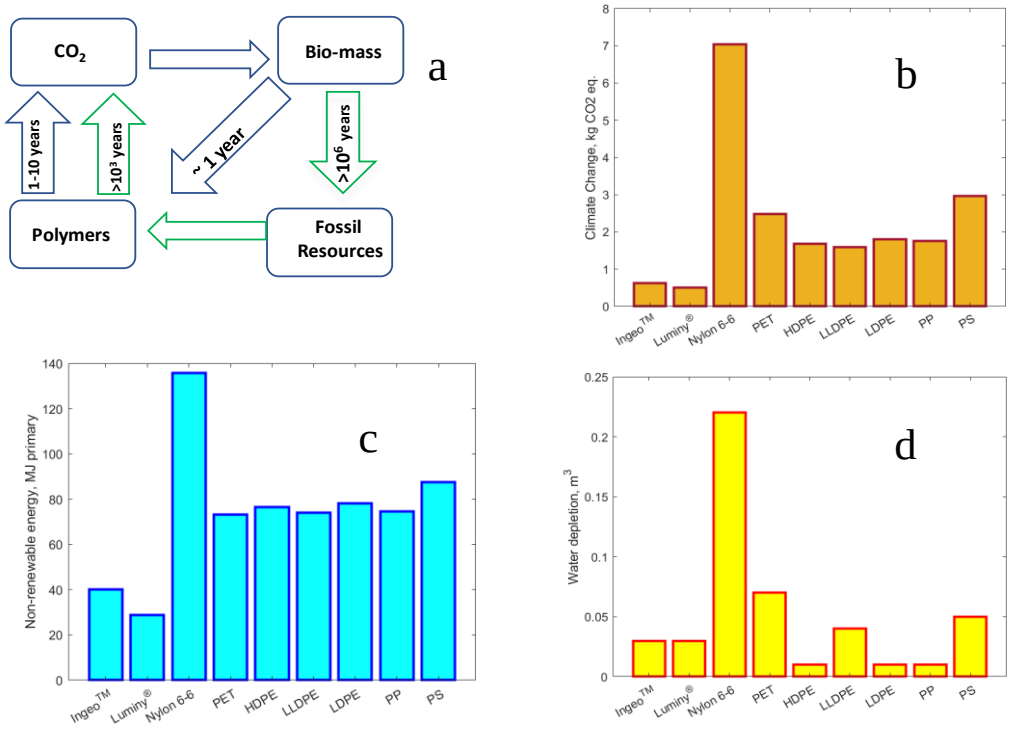

Figure 2.23. The carbon cycle of polymers and EFP for PLA and other commercial polymers. **a)** Carbon cycle of polymers derived from bio-based and fossil resources; **b)** climate change indicator; **c)** nonrenewable energy indicator; and **d)** water uptake indicator for the production of the current commercial resins PLA Ingeo™, and PLA Corbion Luminy®, and other commercial polymers, adapted from (156).

Selvol conducted an LCA on PVOH and determined there are 6.813 kg-CO_2-eq of 100-year air emissions, no ozone-depleting chemicals, and an acidification potential of 805 H_2-eq per kg of PVOH. The study was a cradle-to-gate LCA with the gate being the shipping dock to customers. The report was published in 2018 (157). The GWP seems a little high relative to other components, but one must realize that only 3.4 pounds/ream are used in the overall structure, representing only four percent of the total weight. On a normalized basis, it is a low contribution.

EVOH cannot stand alone in a package due to its hygroscopic nature, so there do not appear to be any LCA studies conducted using it as stand-alone material. A few studies have been conducted using EVOH and other materials as an inner layer, which is how it is commonly used. Kliaugaité and Stakiškis compared a) (PET-AlOx)/LDPE; b) PET/(PE-EVOH-PE); c) and (PET-PVOH)/LDPE. Since these are composite materials, the study only shows relative differences between the three structures and is not specifically about EVOH. The PET and PE components were similar in both, so essentially, what is being compared is the barrier layers. One square meter was used as the functional unit in the study for comparison purposes. Simapro™ software was utilized, and eleven impact categories were reported. For climate change, it noted that the a. and c. options, as described above, are similar, which means the different kinds of barrier material do not have a significant effect. The only difference is that one is coated with AlOx and the other with PVOH. According to the study, B. is about 83 % of a. and c. for climate change, which is the one with EVOH, but different converting stages are also included. The authors then concluded that the impact of the various gas barrier components on the overall EFP is insignificant. The significant impacts are from the energy, raw material extraction, and production of petrochemical-based plastics, PET, PE, and LDPE. It does not come from the barrier materials AlOx, EVOH, and PVOH (158).

Cossutta et al. compared the LCA of graphene by different production routes. The three methods were electrochemical exfoliation, chemical oxidation and chemical/thermal reduction, and chemical vapor deposition (CVD). **Figure 2.24** shows the results of electrochemical exfoliation, chemical oxidation, and chemical/thermal reduction. CVD is on a different scale since the functional unit is different and is much higher. The commercial scale quantities are based on simulations that consider the lab scale quantities. They are all lower with anticipated

improvements in energy efficiency and the ability to recoup and recycle the process chemicals. The thermal method (rGO2T) has the least impact, as seen at 0.046 kg-CO_2-eq per gram of graphene produced. The chemical reduction method (rGO_2C) is slightly higher but magnitudes lower than CVD (159).

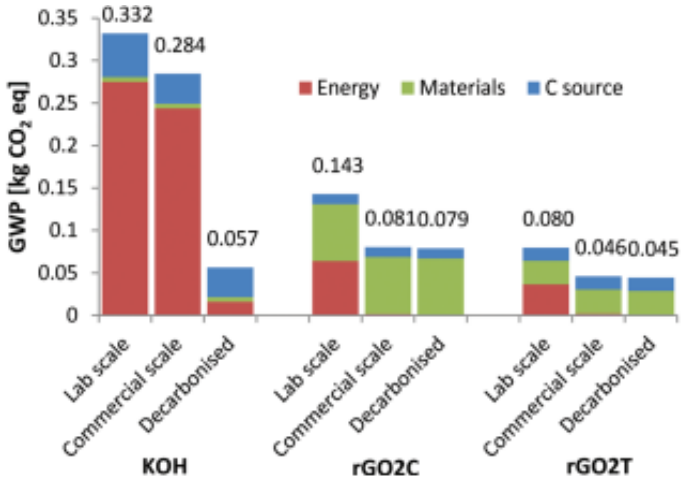

Figure 2.24. Global warming potential of simulated commercial scale production of graphene (1 g) by electrochemical exfoliation, chemical oxidation, and chemical/thermal reduction, reproduced from (159), with permission from the Royal Society of Chemistry.

In an LCA report prepared by the Aluminum Association in January of 2022, based on production in 2016, it was reported that producing a kg of aluminum foil has a GWP of 8.455 kg-CO_2-eq per kg of aluminum foil. This is on the higher end of the spectrum relative to the other components discussed; however, it is a 5% reduction from the study conducted in 2013, based on production in 2010. The reduction is mainly due to the increased use of renewable electricity and less use of coal-fired electricity for smelting. This can be broken down into phases, as seen in **Figure 2.25**. The electrolysis process accounts for 65% of the GWP, with alumina refining adding another 33%. Those two processes alone account for 98% of the total GWP. The amount of nonrenewable energy reported is 58.935 MJ/kg of foil. This is not the highest, but it is higher than reported for PLA. Other impact categories are reported, including acidification,

eutrophication, and smog formation potential. Overall, it is an interesting comprehensive LCA conducted on Aluminum (160).

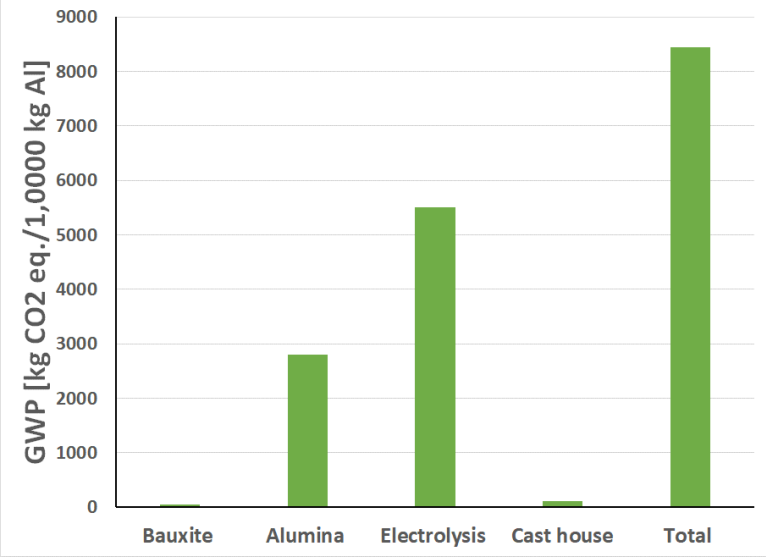

Figure 2.25. Carbon Footprint of domestic Primary aluminum production in North America. Global warming potential results for the domestic primary aluminum product. GHG analysis, adapted from (160).

Vendries et al., in 2020, looked at the significance of environmental attributes as indicators of the life cycle environmental impacts of packaging and food service ware. The study examined over 5000 comparisons for 13 impact categories routinely evaluated in LCA studies. The study looked at recycled content in a package, recyclable, biobased, and compostable types of packaging. The results found several occurrences where material characteristics did not correlate with environmental benefits. Specifically, the compostability of packaging does not appear to be a clear forecaster of environmental inclination. The review allowed for contrasts between compostable materials that are composted at the end of life and non-compostable materials that are landfilled, incinerated, or recycled. There were 620 comparisons found in the literature, of which 46% resulted in meaningfully higher impacts, 31% resulted in meaningfully lower impacts, and 23% resulted in a negligible difference. These comparisons imply that the

environmental effects of composted packaging are not necessarily to a lesser extent than non-compostable packaging that is either landfilled, incinerated, or recycled. This was held for all biobased, compostable packaging materials studied, including biobased plastic, paper, and cellulosic materials. These materials bear the burdens of biobased material production, which are often higher than non-compostable (and non-biobased) materials. The study showed that global warming had a meaningful lower life cycle impact on composting, suggesting it is possibly a good indicator of environmental performance, which complements the information about PLA discussed earlier (161). It is an insightful study that highlights some interesting points.

The other aspect to consider is that most multilayer dissimilar materials cannot be recycled and currently are sent to landfills or incinerated. The advantage of laminating multiple materials together is the ability to get synergistic property enhancements of each material. Most high-barrier structures in use today are laminations of some type. However, laminations have this inherent disadvantage and will always have a higher EFP than a structure that can be recycled or composted (162).

As seen from the discussion above, from a GWP perspective, it makes the most sense to design structures that utilize compostable materials and avoid using laminated materials unless they are all compostable materials being laminated together. It likely makes sense in some other categories, but not enough data is available on all the components to make such a statement. The challenge with today's technologies is assembling the right combination of compostable materials to exhibit high oxygen and moisture barriers in the same structure.

2.7 Review of current compostable materials with oxygen and water barrier properties

Several companies are offering compostable materials with oxygen and moisture barrier characteristics. To achieve high barrier characteristics, metallization must be incorporated. This paper will provide an overview of several offerings.

TIPA®, an Israeli company, was founded in 2010 with the mission to provide packaging that behaves like organic waste while maintaining the qualities of conventional plastics, including durability, transparency, barrier, sealability, printability, and shelf-life (163). These products are made from a proprietary blend of compostable polymers that are both bio-based and fossil-fuel-based (78). They offer a high transparency barrier compostable laminate in various gauges. The MVTR and OTR are 20 g/(m^2·d) and 1 cc/(m^2·d) respectively (16). The conditions are not specified. The barrier layer is coated on the outside of the outer layer. They also offer a non-laminated material, a coextruded sealable compostable film, but it does not list the barrier properties (164). A third offering is a high-barrier metalized lamination, which buries the metalized layer in the lamination. The MVTR and OTR are <7.5 g/(m^2·d) and <0.75 cc/(m^2·d) respectively (165). The conditions are not specified. All TIPA® films are certified home or industrial compostable (166). TIPA® is an up-and-coming company that has shown much promise for only 12 years. TIPA® does not produce its polymers.

Futamura is an established Japanese company that has been around since 1947. It manufactures polypropylene, cellulose films, and activated carbon. In the compostable area, it has two main product lines, NatureFlex™ and Cellophane™ (167). They acquired the NatureFlex™ brand from Innovia Films and its cellophane business in 2016, which complemented its cellulose business (49). It offers a variety of grades of film that are both coated and uncoated. The NatureFlex™ NK series of films has cellulose in the middle and is coated on

both sides with minimal PVDC. The MVTR and OTR are 20 g/(m^2·d) at 38 °C and 90% RH and 5.0 cc/(m^2·d) at 23 °C and 50% RH respectively (157–159). The NatureFlex™ NE series has cellulose film in the middle and is coated on both sides with a transparent heat seal coating. The MVTR and OTR are 31 g/(m^2·d) at 38 °C and 90% RH, and 5.0 cc/(m^2·d) at 23 °C and 50% RH respectively (170). The uncoated series of films, designated as the PXX series, is not heat-sealable and has a high MVTR, so it has little use in packaging. It is mainly used for the anti-static properties in separating batteries (171).

Itscompostable is an aggregation of manufacturers combining their materials, processing, and machinery specialties to create a product. Their product is 100% compostable, compliant with EU13432, with an outer layer of paper that gives it a traditional look and a pleasing paper feel. It has a high oxygen and moisture barrier and is suitable for direct food contact. It is available with high-definition printing with compostable inks and has a guaranteed shelf-life comparable to traditional structures (172). The five companies include Novamont, TiconoPlast, SAES Coated Films, Sacchital Group, and IMA FLX Hub (173). Novamont, founded in Italy in 1990, produces Mater-Biopolymer, one of the base substrates used for Itscompostable's product (174). TicinoPlast, founded in 1967, is a leading player in blown film extrusion that blows the film portion of the structure (175). SAES Coated Films specializes in high-barrier water-based polymeric coatings that can be applied to films. Coathink™ is the tradename for its proprietary water-based coating technology (176). It metallizes and coats the film to achieve an MVTR and OTR of <1.80 g/(m^2·d) at 23 °C and 85% RH and <0.5 cc/(m^2·d) at 23 °C and 0% RH, respectively (177). Sacchital Group is a flexible packaging converter that prints and laminates various substrates. It was founded in 1945. PaperCompost HB® was developed by them, incorporating the film and paper supplied by its partners (178). IMA FLX Hub is a packaging

machine company that makes machinery that the film can be converted into a package and filled with product. They work together as a group of companies and make it a one-stop shop from beginning to end, making the components, converting them into a film, and finally making them into a package (179).

Earthfirst® Biopolymers Films by PSI is under the Plastic Suppliers Incorporated umbrella. They are based in Columbus, Ohio. Earthfirst® Biopolymer Films by PSI is a global manufacturer of compostable sealant and barrier sealant films within the food, beverage, medical, personal care, office, industrial, and other CPG segments (180). They offer a variety of PLA grades with different characteristics, and their portfolio is growing. The Earthfirst® UL grade is a general sealant film as a polyethylene replacement in standard structures. It has an MVTR and OTR of 232 g/(m^2·d) at 38 °C and 90% RH and 400 cc/(m^2·d) at 23 °C and 85% RH respectively (181). They offer an aluminum oxide coated PLA film, Earthfirst® AUL, with MVTR and OTR values of 8.5 g/(m^2·d) at 38 °C and 90% RH and 12.4 cc/(m^2·d) at 23 °C and 0% RH respectively (182). They also have a metalized version, MLT 3003, with MVTR and OTR values of 3.9 g/(m^2·d) at 38 °C and 90% RH and 7.8 cc/(m^2·d) at 23 °C and 0% RH, respectively (183). However, it clearly states for both the AUL and MLT 303 that the film is not to be used as a monolayer film and that the barrier side needs to be protected by another film in a lamination. The non-barrier side is always the food contact side (172, 173).

Celplast Metallized Producers Limited out of Toronto has two grades of PLA film, Duramet® PLA and Enviromet® PLA. Duramet® PLA has an MVTR and an OTR of 0.93 g/(m^2·d) and 1.395 cc/(m^2·d) respectively. Enviromet® PLA has an MVTR and an OTR of 3.1 g/(m^2·d) and 6.2 cc/(m^2·d) respectively (185). The conditions are not specified. They purchase the PLA on the open market and metalize the film to increase the barrier.

2.8 Final Remarks

This review discussed the current state of a compostable structure with high oxygen and moisture barrier and why it is not easy to achieve. Several resins were discussed that, when combined, could be one potential solution to the problem. Several common converting technologies were reviewed, which will be integral to combining the resins to make the possible solution, but others are also available. The cost is a major barrier at this time since the projected price of a compostable structure is roughly 3.4 to 4.9 times more expensive than traditional petrochemical-based materials, depending on the barrier level. Still, that cost is anticipated to decrease as technologies evolve. A discussion of the LCA of the various materials relative to their petrochemical counterparts was included. The GWP of compostable materials is shown to be better overall and will go a long way in combating climate change in the world in the big picture. Lastly, some of the current commercial compostable materials were reviewed. Compostable materials have a bright future and are one of the up-and-coming waves of the future in the world of flexible packaging.

REFERENCES

1. Global Packaging Film Market Report 2020: Analysis & Forecasts 2012-2019 & 2020-2027 by LDPE, HDPE, BOPP, Polyester, PVC, Polyamide, EVOH - ResearchAndMarkets.com [Internet]. [cited 2022 Aug 1]. Available from: https://www.businesswire.com/news/home/20210211005672/en/Global-Packaging-Film-Market-Report-2020-Analysis-Forecasts-2012-2019-2020-2027-by-LDPE-HDPE-BOPP-Polyester-PVC-Polyamide-EVOH---ResearchAndMarkets.com

2. High Barrier Packaging Films Market Size, Share, Opportunities & Forecast. [cited 2022 Jun 9]; Available from: https://www.verifiedmarketresearch.com/product/high-barrier-packaging-films-market/

3. Flexible Packaging Industry Facts and Figures. [cited 2022 Jun 12]; Available from: https://www.flexpack.org/facts-and-figures

4. Trifol J, van Drongelen M, Clegg F, Plackett D, Szabo P, Daugaard AE. Impact of thermal processing or solvent casting upon crystallization of PLA nanocellulose and/or nanoclay composites. J Appl Polym Sci. 2019 May 20;136(20).

5. Global plastics production, 1917 to 2050 » Darrin Qualman [Internet]. 2017 [cited 2022 May 18]. Available from: https://www.darrinqualman.com/global-plastics-production/

6. Smith M, Love DC, Rochman CM, Neff RA. Microplastics in Seafood and the Implications for Human Health. Vol. 5, Current environmental health reports. Springer; 2018. p. 375–86.

7. Song JH, Murphy RJ, Narayan R, Davies GBH. Biodegradable and compostable alternatives to conventional plastics. Phil Trans R Soc, B [Internet]. 2009;364:2127–39. Available from: www.bioplastics24.com

8. Ciriminna R, Pagliaro M. Biodegradable and Compostable Plastics: A Critical Perspective on the Dawn of their Global Adoption. Vol. 9, ChemistryOpen. Wiley-VCH Verlag; 2020. p. 8–13.

9. Breaking Down Compostable Packaging and Bioplastics _ Jabil [Internet]. [cited 2022 Aug 3]. Available from: https://www.jabil.com/blog/compostable-packaging.html

10. Wu F, Misra M, Mohanty AK. Challenges and new opportunities on barrier performance of biodegradable polymers for sustainable packaging. Prog Polym Sci. 2021 Jun 1;117:101395.

11. Understanding OTR & MVTR Specifications for Barrier Food Packaging. [cited 2022 Aug 3]; Available from: https://blog.icpg.co/understanding-otr-mvtr-specifications-for-barrier-food-packaging

12. Siracusa V. Food packaging permeability behaviour: A report. Int J Polym Sci. 2012;2012:302029.

13. Oxygen Transmission Rate - Poly Print. [cited 2022 Jun 12]; Available from: https://www.polyprint.com/understanding-film-properties/flexographic-otr/

14. Water Vapor Transmission Rate - Poly Print. [cited 2022 Aug 1]; Available from: https://www.polyprint.com/understanding-film-properties/flexographic-wvtr/

15. NatureFlex™ NK Data Features-Transparent High Barrier Heat-sealable Compostable Film [Internet]. Available from: www.futamuragroup.com

16. T.LAM 607 High Transparency Barrier Compostable Laminate [Internet]. 2021 [cited 2022 Aug 2]. Available from: www.tipa-corp.com

17. McKeen LW. Environmentally Friendly Polymers. Permeability Properties of Plastics and Elastomers. 2017 Jan 1;305–23.

18. Ahmed J, Mulla MZ, Vahora A, Bher A, Auras R. Morphological, barrier and thermo-mechanical properties of high-pressure treated polylactide graphene oxide reinforced composite films. Food Packag Shelf Life. 2021 Sep 1;29:100702.

19. Varol N. Advanced thermal analysis and transport properties of stereocomplex polylactide [Internet]. 2019. Available from: https://tel.archives-ouvertes.fr/tel-02272914

20. Shaikh S, Yaqoob M, Aggarwal P. An overview of biodegradable packaging in food industry. Curr Res Food Sci. 2021 Jan 1;4:503–20.

21. Zhang H, Bhunia K, Kuang P, Tang J, Rasco B, Mattinson DS, et al. Effects of Oxygen and Water Vapor Transmission Rates of Polymeric Pouches on Oxidative Changes of Microwave-Sterilized Mashed Potato. Food Bioproc Tech. 2016 Feb 1;9(2):341–51.

22. Selke SEM, Culter JD. Plastics Packaging: properties, processing, applications, and regulations. 3rd ed. Hamilton C, editor. Munich: Hanser Publications; 2016.

23. Kofinas P, Cohen RE, Halasa AF. Gas permeability of polyethylene/ poly(ethylene-propylene) semicrystalline diblock copolymers. 1994;

24. Chen B, Torkelson JM. Development of rigid amorphous fraction in cold-crystallized syndiotactic polystyrene films confined near the nanoscale: Novel analysis via ellipsometry. Journal of Polymer Science. 2022 May 15;60(10):1631–42.

25. Robertson GL. Food Packaging: Principles and Practice, Third Edition. CRC Press; 2012. 719 p.

26. Lee DS, Yam KL, Piergiovanni L. Food Packaging Science and Technology. Boca Raton: CRC Press; 2008. 1–632 p.

27. Vapour permeability units and conversions. [cited 2022 Jul 12]; Available from: https://www.versaperm.com/Vapour%20permeability%20units%20and%20conversions.php

28. ASTM E96/E96M-16 Standard Test Methods for Water Vapor Transmission of Materials [Internet]. West Conshohocken; 2016. Available from: www.astm.org,

29. ASTM F1249-20 Standard Test Method for Water Vapor Transmission Rate Through Plastic Film and Sheeting Using a Modulated Infrared Sensor [Internet]. West Conshohocken; 2020. Available from: www.astm.org,

30. ASTM E96 VS. F1249 Which provides more accurate test results? [Internet]. 2017 May [cited 2022 May 17]. Available from: www.ametekmocon.com

31. Permeation FAQ. [cited 2022 May 17]; Available from: https://www.ametekmocon.com/knowledge/learnaboutpermeation/permeationfaq

32. ASTM F2622-20 Standard Test Method for Oxygen Gas Transmission Rate Through Plastic Film and Sheeting Using Various Sensors [Internet]. West Conshohocken; 2020 [cited 2022 May 17]. Available from: www.astm.org,

33. Choosing the right ASTM method for your OTR application [Internet]. 2017 [cited 2022 Jun 9]. Available from: www.ametekmocon.com

34. ASTM D3985-17 Standard Test Method for Oxygen Gas Transmission Rate Through Plastic Film and Sheeting Using a Coulometric Sensor [Internet]. West Conshohocken; 2017. Available from: www.astm.org.

35. Compostable Products [Internet]. [cited 2022 Aug 1]. Available from: https://www.compostingcouncil.org/page/CompostableProducts

36. What's the Difference_ Biodegradable and Compostable - Nature's Path. [cited 2022 Aug 5]; Available from: https://www.naturespath.com/en-us/blog/whats-difference-biodegradable-compostable/

37. Compostable Plastics_ The Next Generation Of Plastics [Internet]. 2019 [cited 2022 Jun 9]. Available from: https://www.worldcentric.com/journal/compostable-plastics-the-next-generation-of-plastics

38. Compostable vs biodegradable_ What's the difference_. [cited 2022 May 17]; Available from: https://blog.sendle.com/home-compostable-vs-commercially-compostable

39. ASTM D6400 − 21 Standard Specification for Labeling of Plastics Designed to be Aerobically Composted in Municipal or Industrial Facilities 1 [Internet]. West Conshohocken; 2021. Available from: http://www.ansi.org.

40. ASTM D6868 − 21 Standard Specification for Labeling of End Items that Incorporate Plastics and Polymers as Coatings or Additives with Paper and Other Substrates Designed to be Aerobically Composted in Municipal or Industrial Facilities 1 [Internet]. West Conshohocken; 2021. Available from: www.oecd.org.

41. ASTM D5338 − 15 Standard Test Method for Determining Aerobic Biodegradation of Plastic Materials Under Controlled Composting Conditions, Incorporating Thermophilic Temperatures [Internet]. West Conshohocken; 2015. Available from: http://www.ansi.org.

42. International Organization for Standardization. (2019).Determination of the ultimate aerobic biodegradability of plastic materials in an aqueous medium — Method by measuring the oxygen demand in a closed respirometer(ISO Standard No. 14851:2019). https://www.iso.org/standard/70026.html [Internet]. 2019 [cited 2022 Oct 16]. Available from: https://www.iso.org/standard/70026.html

43. International Organization for Standardization. (2018). ISO 14852:2018 Determination of the ultimate aerobic biodegradability of plastic materials in an aqueous medium — Method by analysis of evolved carbon dioxide (ISO Standard No. 14852:2019). https://www.iso.org/standard/72051.html [Internet]. 2018 [cited 2022 Oct 16]. Available from: https://www.iso.org/standard/72051.html

44. International Organization for Standardization. (2018).Determination of the ultimate aerobic biodegradability of plastic materials under controlled composting conditions — Method by analysis of evolved carbon dioxide — Part 2: Gravimetric measurement of carbon dioxide evolved in a laboratory-scale test (ISO Standard No. 14855-2:2018). https://www.iso.org/standard/72046.html [Internet]. 2018 [cited 2022 Oct 16]. Available from: Determination of the ultimate aerobic biodegradability of plastic materials under controlled composting conditions — Method by analysis of evolved carbon dioxide — Part 2: Gravimetric measurement of carbon dioxide evolved in a laboratory-scale test

45. Vincotte-Requirements-for-EN-13432. [cited 2022 Jun 13]; Available from: https://www.nature-pack.com/wp-content/uploads/Vincotte-Requirements-for-EN-13432.pdf

46. History of Cellophane. [cited 2022 Jun 13]; Available from: https://bioplasticsnews.com/2019/07/23/history-of-cellophane/

47. Morris BA. Commonly Used Resins and Substrates in Flexible Packaging. The Science and Technology of Flexible Packaging. William Andrew Publishing; 2017. 69–119 p.

48. The Worldwide Barrier Resins Industry is Expected to Reach $16.6 Billion by 2026 - ResearchAndMarkets.com _ Business Wire. [cited 2022 Aug 1]; Available from: https://www.businesswire.com/news/home/20210901005657/en/The-Worldwide-Barrier-Resins-Industry-is-Expected-to-Reach-16.6-Billion-by-2026---ResearchAndMarkets.com

49. Futamura confirms acquisition of Innovia Films cellulose business - bioplastics MAGAZINE. [cited 2022 Aug 2]; Available from: https://www.bioplasticsmagazine.com/en/news/meldungen/20160707-Futamura-completes-Innovia-deal.php

50. Futamura - Compostable and renewable flexible packaging films divisions. [cited 2022 Aug 4]; Available from: https://www.futamuragroup.com/en/divisions/cellulose-films/

51. What is Graphene_ _ Graphene-Info. [cited 2022 Jun 15]; Available from: https://www.graphene-info.com/graphene-introduction

52. The History of Graphene - CealTech AS. [cited 2022 Jun 13]; Available from: https://cealtech.com/2017/05/09/the-history-of-graphene/

53. Download free photo of Graphene,graphite,chemical structure,3d model,organic compound - from needpix.com. [cited 2022 Jun 14]; Available from: https://www.needpix.com/photo/download/89073/graphene-graphite-chemical-structure-3d-model-organic-compound-science-free-vector-graphics-free-pictures-free-photos

54. Graphene, how can we produce it on a larger scale_ _ Bronkhorst. [cited 2022 Jun 14]; Available from: https://www.bronkhorst.com/en-us/blog-en/graphene-how-can-we-produce-it-on-a-larger-scale/

55. Researchers develop scalable graphene production method for industrialization opportunities _ CompositesWorld. [cited 2022 Jun 14]; Available from: https://www.compositesworld.com/news/researchers-develop-scalable-graphene-production-method-for-industrialization-opportunities

56. The Current and Future Production of Graphene. [cited 2022 Jun 14]; Available from: https://www.azonano.com/article.aspx?ArticleID=5613

57. Carey T, Alhourani A, Tian R, Seyedin S, Arbab A, Maughan J, et al. Cyclic production of biocompatible few-layer graphene ink with in-line shear-mixing for inkjet-printed electrodes and Li-ion energy storage. NPJ 2D Mater Appl. 2022 Dec 1;6(1).

58. Choi K, Nam S, Lee Y, Lee M, Jang J, Kim SJ, et al. Reduced Water Vapor Transmission Rate of Graphene Gas Barrier Films for Flexible Organic Field-Effect Transistors. ACS Nano. 2015 Jun 23;9(6):5818–24.

59. You J, Oh B, Yun YS, Jin HJ. Improvement in Barrier Properties Using a Large Lateral Size of Exfoliated Graphene Oxide. Macromol Res. 2020 Jul 1;28(8):709–13.

60. Graphene products_ introduction and market status _ Graphene-Info. [cited 2022 Aug 4]; Available from: https://www.graphene-info.com/graphene-products

61. Polylactic Acid or Polylactide (PLA). [cited 2022 Jun 14]; Available from: https://bioplasticsnews.com/polylactic-acid-or-polylactide-pla/

62. Harper CA. Modern plastics handbook. New York: McGraw-Hill; 2000.

63. Datta R, Henry M. Lactic acid: Recent advances in products, processes and technologies - A review. Vol. 81, Journal of Chemical Technology and Biotechnology. 2006. p. 1119–29.

64. PDLA Polymer Supplier and Manufacturer in China [Internet]. [cited 2022 May 12]. Available from: https://polylactide.com/polyd-lactide/

65. Castro-Aguirre E, Iñiguez-Franco F, Samsudin H, Fang X, Auras R. Poly(lactic acid)—Mass production, processing, industrial applications, and end of life. Adv Drug Deliv Rev. 2016 Dec 15;107:333–66.

66. Inkinen S, Hakkarainen M, Albertsson AC, Södergård A. From lactic acid to poly(lactic acid) (PLA): Characterization and analysis of PLA and Its precursors. Vol. 12, Biomacromolecules. 2011. p. 523–32.

67. Chen G, Steinbuchel A, editors. Plastics From Bacteria. Munster, Germany: Springer; 2010.

68. Faraj H, Follain N, Sollogoub C, Almeida G, Chappey C, Marais S, et al. Gas barrier properties of polylactide/cellulose nanocrystals nanocomposites. Polym Test [Internet]. 2022 Sep;113:107683. Available from: https://linkinghub.elsevier.com/retrieve/pii/S0142941822002069

69. Singha S, Hedenqvist MS. A review on barrier properties of poly(lactic Acid)/clay nanocomposites. Vol. 12, Polymers. MDPI AG; 2020.

70. Halász K, Hosakun Y, Csóka L. Reducing water vapor permeability of poly(lactic acid) film and bottle through layer-by-layer deposition of green-processed cellulose nanocrystals and chitosan. Int J Polym Sci. 2015;2015.

71. Liu JH, Huang ML, Tao JR, Weng YX, Wang M. Fabrication of recyclable nucleating agent and its effect on crystallization, gas barrier, thermal, and mechanical performance of Poly(-lactide). Polymer (Guildf). 2021 Sep;231:124121.

72. Polyvinyl Alcohol (PVOH). [cited 2022 Jun 14]; Available from: https://www.bpf.co.uk/plastipedia/polymers/polyvinyl-alcohol-pvoh.aspx

73. Basic Physical Properties of PVOH Resin Brochure [Internet]. Tokyo; 2022 Jun [cited 2022 Jun 15]. Available from: https://www.kuraray.eu/fileadmin/product_groups/polyvinylalcohol/downloads/kuraray_poval_basic_physical_properties_web.pdf

74. Barrier Films & Kuraray Poval™ _ Food Packaging_ Kuraray Poval™ – Polyvinyl alcohol _ PVA _ PVOH _ PVA powder. [cited 2022 Jul 13]; Available from: https://www.kuraray-poval.com/applications/barrier-films

75. Idris A, Muntean A, Mesic B, Lestelius M, Javed A. Oxygen barrier performance of poly(Vinyl alcohol) coating films with different induced crystallinity and model predictions. Coatings. 2021 Oct 1;11(10).

76. Poval K. Exceval™ – Attractive protection for your food [Internet]. [cited 2022 Jun 15]. Available from: https://www.kuraray-poval.com/fileadmin/technical_information/brochures/poval/Kuraray_Exceval_attractive_protection_for_your_food_engl.pdf

77. Is EVOH Recyclable_ 10 Things You Should Know (Quick Answers). [cited 2022 Aug 1]; Available from: https://citizensustainable.com/evoh-recyclable/

78. FAQ - T I P A. [cited 2022 Aug 2]; Available from: https://tipa-corp.com/faq/

79. Yael Vodovotz. Why isn't plastic biodegradable_ [Internet]. 2022 [cited 2022 Oct 19]. Available from: https://news.osu.edu/why-isnt-plastic-biodegradable/

80. Ikada Y, Jamshidi K, Tsuji H, Hyon SH. Stereocomplex Formation between Enantiomeric Poly(lactides). Macromolecules. 1987;20(4):904–6.

81. Su X, Feng L, Yu D. Formation of stereocomplex crystal and its effect on the morphology and property of PDLA/PLLA blends. Polymers (Basel). 2020 Nov 1;12(11):1–14.

82. Tsuji H. Poly(lactide) stereocomplexes: Formation, structure, properties, degradation, and applications. Vol. 5, Macromolecular Bioscience. Wiley-VCH Verlag; 2005. p. 569–97.

83. Luo F, Fortenberry A, Ren J, Qiang Z. Recent Progress in Enhancing Poly(Lactic Acid) Stereocomplex Formation for Material Property Improvement. Vol. 8, Frontiers in Chemistry. Frontiers Media S.A.; 2020.

84. Tsuji H, Tsuruno T. Water Vapor Permeability of Poly(L-lactide)/Poly(D-lactide) Stereocomplexes. Macromol Mater Eng. 2010 Aug 11;295(8):709–15.

85. Cao J, Li W, Yun, Jiang L, Dan Y. Design and Synthesis of Stereoblock Polylactic Acid with High Oxygen and Water Vapor Barrier Performances. Ind Eng Chem Res. 2023;62(44):18822–33.

86. About_ PHBV [Internet]. [cited 2024 Jun 8]. Available from: https://dbpedia.org/page/PHBV

87. Chiellini E, Gil H, Braunegg G, Buchert J, Gatenholm P, van der Zee M, editors. Biorelated Polymers Sustainable Polymer Science and Technology. 1st ed. New York: Springer Science + Business Media; 2001.

88. Rudnik E. Compostable Polymer Materials. 1st ed. Elsevier Science; 2007.

89. Selke SEM, Culter JD, Auras RA, Rabnawaz M. Plastics Packaging Properties, Processing, Applications, and Regulations. 4th ed. Munich: Carl Hanser Verlag; 2021.

90. Zembouai I, Kaci M, Bruzaud S, Benhamida A, Corre YM, Grohens Y. A study of morphological, thermal, rheological and barrier properties of Poly(3-hydroxybutyrate-Co-3-Hydroxyvalerate)/polylactide blends prepared by melt mixing. Polym Test. 2013;32(5):842–51.

91. Lo Faro E, Menozzi C, Licciardello F, Fava P. Improvement of paper resistance against moisture and oil by means coatings with poly(-3-hydroxybutyrate-co-3-hydroxyvalerate) (phbv) and polycaprolactone (pcl). Applied Sciences (Switzerland). 2021 Sep 1;11(17).

92. Pilla S, editor. Handbook of Bioplastics and Biocomposites. Polymedia Publisher GmbH; 2011. 373–396 p.

93. Gupta P. Fundamentals of Nanotoxicology Concepts and Applications. Elsevier, Inc.; 2022.

94. Yue S, Wang S, Han D, Huang S, Sun L, Xiao M, et al. Polyvinyl Alcohol/Montmorillonite Nanocomposite Coated Biodegradable Films with Outstanding Barrier Properties. ES Materials and Manufacturing. 2023 Jun 1;20.

95. Plastic Extrusions,Plastic Extrusion Process,Plastic Extrusion Machinery Manufacturers,Exporters,India [Internet]. [cited 2022 Aug 6]. Available from: http://www.industrialextrusionmachinery.com/plastic_extrusion.html

96. Rauwendaal C. Polymer extrusion. 5th edition. Hanser Publications; 2014. 934 p.

97. The Extrusion Process _ Plastics Technology. [cited 2022 Jul 13]; Available from: https://www.ptonline.com/knowledgecenter/profile-extrusion/profile-extrusion-fundamentals/history-and-fundamentals-of-extrusion

98. Crawford RJ, Martin PJ. Processing of plastics. Plastics Engineering. 2020 Jan 1;279–409.

99. Mikeeg55. Extrusion. (2022, October 7). In Wikipedia. https://en.wikipedia.org/wiki/Extrusion [Internet]. 2006 [cited 2022 Jul 14]. Available from: https://en.wikipedia.org/wiki/Extrusion#/media/File:Extruder_section.jpg

100. Crawford RJ, Martin PJ. Processing of plastics. Plastics Engineering. 2020 Jan 1;279–409.

101. Difference Between Single Screw and Twin Screw Extruder - Ainuok Machinery. [cited 2022 Jun 13]; Available from: https://ainuokmachinery.com/difference-between-single-screw-and-twin-screw-extruder/

102. Luker K. Hot Melt Extrusion: pharmaceutical application. 1st ed. Douroumis D, editor. John Wiley and Sons; 2012. 1–21 p.

103. Fundamentals of Cast Film Extrusion - Technology Macro Engineering and Technology [Internet]. [cited 2022 Jun 7]. Available from: http://www.macroeng.com/fundamentals-of-cast-film-extrusion-technology.php

104. Cast vs Blown Stretch Wrap_ The Differences and Benefits of Each [Internet]. [cited 2022 Jun 7]. Available from: https://www.aaapolymer.com/cast-vs-blown-stretch-wrap/

105. Sun Q, Mekonnen T, Misra M, Mohanty AK. Novel Biodegradable Cast Film from Carbon Dioxide Based Copolymer and Poly(Lactic Acid). J Polym Environ. 2016 Mar 1;24(1):23–36.

106. Wang K, Jiao T, Wang Y, Li M, Li Q, Shen C. The microstructures of extrusion cast biodegradable poly(butylene succinate) films investigated by X-ray diffraction. Mater Lett. 2013 Feb 1;92:334–7.

107. Shao J, Sun J, Bian X, Cui Y, Zhou Y, Li G, et al. Modified PLA homochiral crystallites facilitated by the confinement of PLA stereocomplexes. Macromolecules. 2013 Sep 10;46(17):6963–71.

108. Mohammadi M, Heuzey MC, Carreau PJ, Taguet A. Morphological and rheological properties of PLA, PBAT, and PLA/PBAT blend nanocomposites containing CNCs. Nanomaterials. 2021 Apr 1;11(4).

109. Zhu X, Zhong T, Huang R, Wan A. Preparation of hydrophilic poly(lactic acid) tissue engineering scaffold via (PLA)-(PLA-b-PEG)-(PEG) solution casting and thermal-induced surface structural transformation. J Biomater Sci Polym Ed. 2015 Nov 22;26(17):1286–96.

110. Meyer Rod Coating_ Fundamentals and Major Applications [Internet]. [cited 2022 Aug 6]. Available from: https://conversiontechnologies.com/meyer-rod-coating-fundamentals/

111. Coating Rods - Paper, Film & Foil Converter. [cited 2022 Jun 13]; Available from: https://www.pffc-online.com/coat-lam/2840-paper-coating-rods

112. McKeen LW. Production of Films. In: Film Properties of Plastics and Elastomers. Elsevier; 2012. p. 57–71.

113. Wire-Wound metering rod coating technology - Course Notes. [cited 2022 Jun 7]; Available from: https://www.yumpu.com/en/document/view/42480880/wire-wound-metering-rod-coating-technology-course-notes

114. Apicella A, Barbato A, Garofalo E, Scarfato P. Effect of PVOH/PLA + Wax Coatings on Physical and Functional Properties of Biodegradable Food Packaging Films. 2022; Available from: https://doi.org/10.3390/polym14050935

115. Kumar S, Bhatt K, Kumar P, Sharma S, Kumar A, Tripathi CC. Laser patterned, high-power graphene paper resistor with dual temperature coefficient of resistance. RSC Adv. 2019;9(15):8262–70.

116. Lavoine N, Desloges I, Bras J. Microfibrillated cellulose coatings as new release systems for active packaging. Carbohydr Polym. 2014 Mar 15;103(1):528–37.

117. Lilien OM. History of industrial gravure printing up to1920. 1st ed. London: Lund Humphries; 1972.

118. Shim E. Coating and laminating processes and techniques for textiles. Smart Textile Coatings and Laminates [Internet]. 2019 Jan 1 [cited 2022 Jun 5];11–45. Available from: https://www.sciencedirect.com/science/article/pii/B978008102428700002X

119. What is Gravure_. [cited 2022 Jun 8]; Available from: https://www.ohiogt.com/company/gravure_about.html

120. Huang L, Wang ZP, Pu JL, Shen L, Zhang JK. Graphene pattern by gravure printing for wireless strain sensor. In: Proceedings of the International Conference on Sensing Technology, ICST. 2013. p. 387–9.

121. Lee A. Ostness. Coating Technology for Flexible Packaging. In Cincinnati; 2006 [cited 2022 May 27]. Available from: https://www.tappi.org/content/enewsletters/eplace/2006/06PLA50.pdf

122. Pudas M, Hagberg J, Leppävuori S. Gravure offset printing of polymer inks for conductors. Prog Org Coat. 2004 May 1;49(4):324–35.

123. Laminating - Laminating process _ BOBST [Internet]. [cited 2022 Jun 3]. Available from: https://www.bobst.com/usen/products/laminating-flexible-materials/process/

124. Conservation of the South Carolina Constitutions. [cited 2022 Jun 9]; Available from: https://www.nedcc.org/about/nedcc-stories/sc1

125. Chapter 5 Sources in Library and Archival Conservation [Internet]. [cited 2022 Aug 6]. Available from: https://cool.culturalheritage.org/byauth/roggia/barrow/chap05.html

126. Laminating Adhesives Market Global Forecast to 2026_MarketsandMarkets [Internet]. [cited 2022 Jun 9]. Available from: https://www.marketsandmarkets.com/Market-Reports/laminating-adhesives-market-129921733.html

127. Macnamara JF, editor. Film Extrusion Manual Third Edition Process, Materials, Properties. 3rd ed. Peachtree Corners: TAPPI Press; 2020.

128. The Root of the Problem. [cited 2022 Aug 3]; Available from: https://www.packagingimpressions.com/article/the-root-problem-14444/all/

129. Solvent-less laminating troubleshooting guide contents [Internet]. [cited 2022 Aug 3]. Available from: https://1j3ll5vumyt3vhdzq3jw75t9-wpengine.netdna-ssl.com/wp-content/uploads/2020/12/Laminating-Troubleshooting-Final.pdf

130. Wolf R. A Technology Decision-Adhesive Lamination or Extrusion Coating/Lamination? In: TAPPI PLACE Conference. Albuquerque; 2010.

131. Flexible Packaging Film_ What is Solventless Lamination Technology_ [Internet]. [cited 2022 Aug 6]. Available from: https://www.lpsind.com/flexible-packaging-film/

132. Making the Case for Solventless Adhesives _ Adhesives & Sealants Industry. [cited 2022 Aug 4]; Available from: https://www.adhesivesmag.com/articles/87732-making-the-case-for-solventless-adhesives?

133. 3 Reasons Why Going Solvent-Free Improves Sustainability - AWT. [cited 2022 Aug 4]; Available from: https://awtlabelpack.com/2018/05/07/3-reasons-going-solvent-free-improves-sustainability/

134. Advantages and Development Trend Of Solventless Adhesives _ Sinstar. [cited 2022 Aug 4]; Available from: https://www.sinstarsl.com/articles/detail/an-article-to-learn-the-advantages-problems-and-development-trend-of-solventless-adhesives.html

135. BOPP, Nylon & PET Laminating film for paper and packaging [Internet]. [cited 2022 Aug 10]. Available from: https://www.adhesiveplatform.com/laminating-film-for-paper-and-packaging/

136. Manufacturing Capabilities_ Printpack [Internet]. [cited 2022 Aug 10]. Available from: https://www.printpack.com/manufacturing-capabilities/

137. Extrusion and Lamination _ ProAmpac [Internet]. [cited 2022 Aug 10]. Available from: https://www.proampac.com/en-us/extrusion-and-lamination/

138. Manufacturing Capabilities _ Amcor [Internet]. [cited 2022 Aug 10]. Available from: https://www.amcor.com/products/services/manufacturing-capabilities

139. Capabilities & Services _ Winpak [Internet]. [cited 2022 Aug 10]. Available from: https://www.winpak.com/capabilities-and-services

140. HB Fuller Flextra Compost(TM) SF1000 XR2000 Technical Data Sheet [Internet]. St Paul, MN; 2018 [cited 2022 Mar 11]. Available from: Data sheet supplier by the vendor.

141. H.B. Fuller Launches Game-Changing Compostable Adhesives for Flexible Packaging _ Business Wire. Business Wire [Internet]. 2021 Apr 6 [cited 2022 Jul 13]; Available from: https://www.businesswire.com/news/home/20210406005131/en/H.B.-Fuller-Launches-Game-Changing-Compostable-Adhesives-for-Flexible-Packaging

142. Compostable Adhesives for Flexible Packaging [Internet]. [cited 2022 Aug 10]. Available from: https://www.flexpackmag.com/articles/91163-hb-fuller-launches-compostable-adhesives-for-flexible-packaging

143. Compostable Adhesives for Flexible Packaging [Internet]. [cited 2022 Aug 10]. Available from: https://www.hbfuller.com/en/north-america/products-and-technologies/markets-and-applications/packaging/sustainable-packaging-solutions/compostable-adhesives-for-flexible-packaging

144. Tabasi RY, Najarzadeh Z, Ajji A. Development of high performance sealable films based on biodegradable/compostable blends. Ind Crops Prod. 2015 Oct 15;72:206–13.

145. Motru S, Adithyakrishna VH, Bharath J, Guruprasad R. Development and Evaluation of Mechanical Properties of Biodegradable PLA/Flax Fiber Green Composite Laminates. Mater Today Proc. 2020 Jan 1;24:641–9.

146. Memon A, Ithisoponakul S, Pramoonmak S, Lawsuriyonta M, Leenoi D, Passadee N. A Development of Laminating Mulberry Paper by Biodegradable Films. Energy Procedia. 2011 Jan 1;9:598–604.

147. He H, Fu Y, Zhao Y, Liu S, Zuo G, Guo P, et al. Applied properties and life cycle assessment of flexible packaging lamination processes: a comparative study. International Journal of Life Cycle Assessment. 2021 Mar 1;26(3):561–74.

148. Biopolymers industry hampered by production costs _ Resource Magazine [Internet]. [cited 2022 Aug 6]. Available from: https://resource.co/article/Futurevision/Biopolymers_industry_hampered_production_costs-3680

149. Market Update Resin pricing. Winpak June 2022. 2022 Jun.

150. Dictionary of Flexible Packaging Terms _ Catty Corporation [Internet]. [cited 2022 Aug 2]. Available from: https://www.cattycorp.com/2017/04/15/dictionary-flexible-packaging-terms/

151. Yield and Unit Weight - Poly Print. [cited 2022 Aug 3]; Available from: https://www.polyprint.com/understanding-film-properties/flexographic-yield/

152. Muralikrishna I v., Manickam V. Life Cycle Assessment. In: Environmental Management [Internet]. Elsevier; 2017. p. 57–75. Available from: https://linkinghub.elsevier.com/retrieve/pii/B9780128119891000051

153. ISO14040 - 2006 - Environmental management - Life Cycle assessment - Principles and framework.

154. Mathew HS, Hendrickson CT, Mathews D. Life Cycle Assessment: Quantitative Approaches for Decisions That Matter-lcatextbook.com 2 [Internet]. 2014. Available from: https://www.lcatextbook.com/

155. Guinee JB, Heijungs R, Huppes G, Zamagna A, Masoni P, Buonamici R, et al. Life Cycle Assessment: Past, Present, and Future †. Environ Sci Technol. 2011;45:90–6.

156. Auras R, Lim L, Selke S, Tsuji H, editors. Poly(Lactic Acid): Synthesis, Structures, Properties, Processing, and Applications. 2nd ed. Wiley and Sons, incorporated, John; 2022.

157. Selvol Life Cycle Analysis Brochure. 2018 Jul.

158. Kliaugaité D, Stakiškis JK. Comparative Life Cycle Assessment of High Barrier Polymer Packaging for Selecting Resource Efficient and Environmentally Low-Impact Materials. World Academy of Science, Engineering and Technology International Journal of Environmental and Ecological Engineering. 2013;7(11):742–50.

159. Cossutta M, McKechnie J, Pickering SJ. A comparative LCA of different graphene production routes. Green Chemistry. 2017;19(24):5874–84.

160. Jinlong Wang M. The Environmental Footprint of Semi-Fabricated Aluminum Products in North America. 2022 Jan.

161. Vendries J, Sauer B, Hawkins TR, Allaway D, Canepa P, Rivin J, et al. The Significance of Environmental Attributes as Indicators of the Life Cycle Environmental Impacts of Packaging and Food Service Ware. Environ Sci Technol. 2020 May 5;54(9):5356–64.

162. Bauer AS, Tacker M, Uysal-Unalan I, Cruz RMS, Varzakas T, Krauter V. Recyclability and redesign challenges in multilayer flexible food packaging—a review. Vol. 10, Foods. MDPI; 2021.

163. Overview - T I P A. [cited 2022 Aug 2]; Available from: https://tipa-corp.com/about/overview/

164. TIPA 303 Printable and Sealable Home Compostable Films [Internet]. 2022 [cited 2022 Aug 2]. Available from: www.tipa-corp.com

165. T.LAM 106 High Barrier Metallized Compostable Laminate [Internet]. 2022 [cited 2022 Aug 2]. Available from: www.tipa-corp.com

166. Compostable Packaging Solutions _ Eco-Friendly Packaging - TIPA. [cited 2022 Aug 2]; Available from: https://tipa-corp.com/

167. Futamura - Compostable and renewable flexible packaging films. [cited 2022 Aug 2]; Available from: https://www.futamuragroup.com/en/about-us/history/

168. NatureFlex^{TM} NKR Data Features-Transparent High Barrier Heat-sealable Compostable Film [Internet]. [cited 2021 Jun 13]. Available from: www.futamuragroup.com

169. NatureFlex^{TM} NK White Data Features-White High Barrier Heat-sealable Compostable Film [Internet]. [cited 2021 Jun 13]. Available from: www.futamuragroup.com

170. NatureFlex(TM) NE Technical Properties (Typical Values) [Internet]. [cited 2022 Aug 2]. Available from: www.innoviafilms.com

171. Cellophane POO Technical Properties (Typical Values) [Internet]. [cited 2022 Aug 2]. Available from: www.innoviafilms.com

172. Itscompostable - compostable packaging-main. [cited 2022 Aug 5]; Available from: https://www.itscompostable.com/en/

173. Itscompostable - Compostable packaging. [cited 2022 Aug 2]; Available from: https://www.itscompostable.com/en/ima-flx-hub/

174. Novamont Group leader in bioplastics and bioproducts. [cited 2022 Aug 2]; Available from: https://www.itscompostable.com/en/novamont/

175. TicinoPlast leader in extrusion of polyethylene films. [cited 2022 Aug 2]; Available from: https://www.itscompostable.com/en/ticinoplast/

176. Solutions for recyclable or compostable packaging. [cited 2022 Aug 2]; Available from: https://www.itscompostable.com/en/saes-coated-films/

177. Itscompostable Data Sheet. 2021 Feb.

178. Sacchital Group produces new generation packaging. [cited 2022 Aug 2]; Available from: https://www.itscompostable.com/en/sacchital-group/

179. IMA FLX Hub cutting-edge sustainable technologies. [cited 2022 Aug 2]; Available from: https://www.itscompostable.com/en/ima-flx-hub/

180. About Us _ Plastic Suppliers, Inc. [cited 2022 Aug 3]; Available from: https://earthfirstfilms.com/about-us

181. WUL EarthFirst UL 80 - 120 data sheet (UPDATED DRAFT 2018-07-09) [Internet]. 2018 [cited 2022 Aug 2]. Available from: Data sheet supplier by the vendor.

182. 80 AUL EarthFirst Ultralight Data Sheet US [Internet]. 2020 [cited 2022 Aug 2]. Available from: Data sheet supplier by the vendor.

183. MLT_3003_Metallized Barrier Sealant_120g_TDS_May'22 [Internet]. [cited 2024 Jun 8]. Available from: Data sheet supplied by the vendor.

184. 80 AUL EarthFirst Ultralight Data Sheet US (1).

185. Celplast PLA-summary Data Sheet [Internet]. Toronto; [cited 2024 Jun 3]. Available from: https://www.celplast.com/wp-content/uploads/2023/

CHAPTER 3: UNLOCKING THE SECRETS OF HIGH-WATER BARRIER STEREOCOMPLEX POLYLACTIDE BLEND EXTRUSION FILMS

A version of this chapter was published as:

Macnamara, J., Rubino, M., Daum, M., Kathuria, A., Auras, R. Unlocking the secrets of high-water barrier stereocomplex polylactide blend extrusion films, *Green Chemistry*, 26, (2024), 2248-2257, *RSC*.

3.1 Abstract

Consumers, companies, and governments are becoming more interested in compostable materials as the amount of waste generated from single-use petrochemical-based and non-biodegradable plastics has grown exponentially since 1960. A drawback to compostable flexible option films is the lack of equivalent moisture barrier performance to maintain a comparable shelf life of food products compared with traditional petrochemical-based versions. Stereocomplex PLA (sc-PLA), a combination of the stereoisomers l-PLA (PLLA) and d-PLA (PDLA), offers a potential solution to this problem. This study presents a viable and novel method to cast extrude sc-PLA films without using a masterbatch. For comparison, several blend compositions were produced, including 85/15, 70/30, 50/50, and 30/70 PLLA/PDLA and homocomplex PLLA and PDLA films. The samples were then annealed at 160°C for 5, 15, and 30 min to understand their effect on the crystallinity (Xc), moisture vapor permeability coefficient (MVPC), and functional and mechanical performance. As expected, the Xc increased for all the samples upon annealing. We observed increased crystallization kinetics in the blended samples, which crystallized in 5 minutes, which can be ascribed to the nucleation effect, while the PLLA and PDLA started crystallizing between 15 and 30 minutes. PDLA acted as a nucleating agent at levels as low as 15% to induce crystallization in ≤5 minutes in the blended samples. We observed a correlation between the crystallization trend of various compositions and MVPC, with the blended annealed films having a significantly better moisture barrier than all the non-annealed films. The increased Xc reduces the strength properties due to higher brittleness associated with the higher Xc. Further optimization is needed to produce fully viable films for commercial applications; however, this work shows pathways to unlock the creation of PLA films with high barriers to water.

3.2 Introduction

The global flexible packaging industry is expected to grow from approximately USD 129 billion in 2020 to roughly USD 178 billion by 2027. The growth is attributed to the increased demand in the food, beverage, cosmetic, personal care, and pharmaceutical industries (1). By 2030, the demand is expected to reach an estimated USD 272 billion (2). Along with the growth of plastic usage comes the issue of disposal. According to the U.S. EPA, in 2018, 35.7 million tons of plastic waste were generated only in the U.S., representing 12.2 % of the total municipal solid waste (MSW). Of the 35.7 million tons, only c. 8 % were recycled, 16 % were incinerated, and 76 % were sent to landfills (3). This lack of recycling has concerned consumers, businesses, and governments and led to an interest in developing industrial compostable polymers that can potentially replace non-biodegradable and fossil-based plastics since they can be disposed of with organic waste when contaminated (4).

Poly (lactic acid) (PLA) is considered one of the leading candidates to replace fossil-fuel-based polymers since it has the most significant commercial production capacity, with increasing market growth (5,6). It is used in several industrial applications, including biodegradable thermoplastics and food and agricultural packaging (7–9). However, there are a few issues with its widespread usage and potentially increased commercialization, including low heat distortion temperature (10), brittleness (11), poor thermal and hydrolytic stability (12), and moderate barrier properties (13,14).

One potential solution to overcome some of the issues is to combine the two enantiomeric forms of PLA, namely l-PLA (PLLA) and d-PLA (PDLA), to produce stereocomplex PLA (sc-PLA) (15). For a well-blended PLLA and PDLA mixture, multicenter hydrogen bonding leads to a potential alternative arrangement of helical chains between l-lactyl and d-lactyl portions with

opposing chiral confirmation for PLA stereocomplex formation (16,17). The stereocomplex formed from the PLLA/PDLA enantiomers allows for improved intermolecular interactions via dipole-dipole interaction and hydrogen bonding. A more tightly packed chain conformation results side-by-side within the stereocomplex crystal structure, allowing for improved thermal stability and mechanical properties (18,19). sc-PLA has a melting temperature (Tm) of approximately 220 °C, while homocrystallite PLA (hc-PLA) melts around 180 °C, exhibiting a 50 °C variance between them (18). Tensile strength, Young's modulus, and elongation at break of sc-PLA are all reported to improve over hc-PLA (20). Annealed films, after extrusion, increase crystallinity. So, annealing is a common technique in processing polymers to alter their physical and chemical properties (21). Producing sc-PLA within the PLA matrix and increasing their crystallinity through annealing can improve barrier properties (22). The moisture vapor transmission rate (MVTR) of solvent-cast sc-PLA films is 14─23% better than that of hc-PLA, opening new markets in industrial applications such as packaging (23). The higher the crystallinity of sc-PLA, the better the water barrier properties may be if the rigid amorphous fraction (RAF) ─ the phase between the crystalline fraction (CF) and the mobile amorphous fraction (MAF) ─ is fully controlled (22).

This work aimed to determine the optimal conditions for producing sc-PLA by cast film extrusion and explore potential mechanical and barrier properties enhancements. Others have reported on injection molding and twin-screw extrusion of sc-PLA. Luo et al. described the melt processing of PLLA/PDLA to form sc-PLA via an injection molding process (24). Alhaj and Narayan reported a scalable process of sc-PLA by twin-screw extrusion formation of pellets for injection (25). However, cast extrusion films of sc-PLA have yet to be reported and produced. This work focuses on producing sc-PLA films on a single screw extruder without first making a

masterbatch. Blends of 85/15, 70/30, 50/50, and 30/70 PLLA/PDLA, along with PLLA and PDLA, were produced for comparison. Maximizing the amount of PLLA is logical, given its widespread presence in the market, as it is expected to offer advantages in supply chain efficiency and cost (26). PDLA is currently mainly used for the nucleation of PLLA and for producing sc-PLA but is still in much lower demand in the market (27). The role of sc-PLA content on the properties of these blends, such as thermal, mechanical, and moisture barrier measurements, was measured and reported.

3.3 Experimental

3.3.1 Materials

PLLA (Luminy® L175, ≥ 99%(L-isomer)), PLLA (Luminy® L130, ≥ 99%(L-isomer)), PDLA (Luminy® D070, ≥ 99%(D-isomer)), and PDLA (Luminy® D120, ≥ 99%(D-isomer)) were supplied by TotalEnergies Corbion (Gorinchem, Netherlands). All homopolymers were crystalline white pellets in appearance, with a reported weight average molecular weight (Mw) of 175 kDa for L175, 130 kDa for L130, 70 kDa for D070, and 120 kDa for D120 (28–31). The resins were used as received. Tetrahydrofuran (THF), HPLC grade and stabilized with butylated hydroxytoluene, was procured from Pharmco (Brookfield, CT).

3.3.2 Film processing

The PLLA and PDLA resins were dried in a vacuum oven (VWR International, USA) overnight (minimum 12 h) at 60 °C and 24 in-Hg before processing to prevent hydrolytic degradation during processing (28,29).

Dried PLLA and PDLA resins were processed separately to produce respective cast films. Then, the two isomers in a weight ratio of 85/15, 70/30, 50/50, and 30/70 PLLA/PDLA were weighed and thoroughly mixed in a plastic bag before being introduced into the extruder.

Each mix was extruded with a microextruder (Randcastle Extrusion Systems, Cedar Grove, NJ, USA) and made into a cast film as a monolayer film. The extruder has a 1.5875 cm diameter screw, 34 cm^3 volume, and a 24/1 L/D ratio. The processing temperature and the extrusion conditions are provided in **Table A3.1**, Appendix 3A.

The machine was allowed to stabilize at a chill roll speed of 10 RPM, and the first film sample was collected. The nip roller speed was increased to 15 RPM and then 20 RPM to obtain samples with the desired film thickness.

3.3.3 Thermal annealing

Each film sample of approximately 25.4 x 16.5 cm was annealed in a QL438-C hydraulic press (PHI, USA) at 160 °C. Samples were placed between 25.4 x 25.4 cm plates lined with non-stick aluminum foil. The annealing was conducted below the T_m of the hc-PLA, and 160 °C was determined to be the optimal temperature for maximum crystallization without destroying the film's integrity. All the samples were annealed for 5, 15, and 30 min; after annealing in the press, the samples were allowed to cool at ambient temperatures. The annealed samples were stored in a freezer at −20 °C until further analysis.

3.3.4 Size exclusion chromatography (SEC)

The M_w and the number average molecular number (M_n) of the PLLA and PDLA resins were measured using an SEC system from Waters (Milford, MA, USA) equipped with an isocratic pump, an autosampler, a refractive index detector, and a series of Styragel® columns (Styragel® HR-4, HR-3, HR-2), with a controlled temperature of 35 °C and flow rate of 1 mL/min. Approximately 20 mg of each resin was dispersed in 10 mL of THF and stored overnight to dissolve. Each sample was filtered, transferred to a 2-mL glass vial, and capped.

The M_w, M_n, and the polydispersity index, Đ, were analyzed using the Waters Breeze2 software. Six replicates of each resin were measured.

3.3.5 Melt flow rate (MFR)

The MFR of each resin was measured using a Ray Ran (New Castle, DE, USA) Melt Flow Indexer MK II Digital Model 2A. MFR was evaluated at 190 °C with a 2.16 kg weight as per procedure A of the ASTM D1238-20 test standard (32). At least 8 specimens, each of PLLA and PDLA, were evaluated to obtain a low dispersion on the results.

3.3.6 Thermogravimetric analysis (TGA)

PLLA and PDLA resin samples were characterized using a Q50 thermogravimetric analyzer (TA Instruments, USA) from 100 to 600 °C at 10 °C /min, under 50 mL/min nitrogen gas flow. Three samples (5-10 mg) of each resin were evaluated.

3.3.7 Differential scanning calorimetry (DSC)

Thermal analysis was conducted using a Q100 differential scanning colorimeter (TA Instruments) with a refrigerated cooling system under a 70 mL/min nitrogen flow. Resin and film samples, each weighing between 5 and 10 mg, were packed and sealed in a standard aluminum pan and lid. The samples were equilibrated to 20 °C, ramped to 0 °C at 10 °C/min, ramped to 260 °C at 10 °C/min, held isothermal for 1 min, ramped to 0 °C at 10 °C/min, and then to 260 °C at 10 °C/min for a total of two cycles. The heat of fusion (ΔH) of 100% hc-PLA used for the Xc calculation was 139 J/g (18). The ΔH of 100% sc-PLA used for the analysis was 142 J/g (18). Three replicates of each resin and film were tested.

3.3.8 Wide angle X-ray diffraction (WAXD)

The wide-angle x-ray diffraction was analyzed on an AXS D8 Advance X-ray diffractometer (Bruker Co., USA) equipped with a global mirror filter Cu Kα radiation source at

40 kV 100 mA. The diffraction pattern was recorded between a 2θ range from 10° and 40° at a rate of 0.24°/min and an increment of 0.01°. The instrument worked in combination with DIFFRAC. MEASUREMENT CENTER version 7.5.0 software (Bruker Co.) to collect the data. One replicate each of PLLA, PDLA, and produced blend compositions, with each annealing time was studied.

3.3.9 Thickness

Caliper measurements of each film (n=3) were recorded with a TMI digital micrometer (model 49-70-01-0001; USA).

3.3.10 Barrier properties

Moisture vapor transmission rate (MVTR) was evaluated for PLLA, PDLA, and the produced blended films on a Permatran-W® 3/34 instrument (MOCON, USA) at 38 °C and 90% RH according to ASTM F1249-20 (33). Six or more replicates were evaluated for each film.

3.3.11 Tensile strength

Tensile testing was conducted on a Universal Testing System Model #5565 (Instron, USA) and measured according to ASTM D882-18 (34). The samples were evaluated in the machine direction (MD) and cross direction (CD). The initial strain rate was 0.1 mm/mm·min. The grip separation was 12.7 cm for the MD samples and 7.62 cm for the CD samples. The annealed samples were not wide enough in the CD to achieve a 12.7 cm grip separation, as recommended by the standard. All non-annealed samples and the 85/15 and 70/30 PLLA/PDLA samples annealed at 5 and 15 minutes were also tested for comparison. All samples were conditioned at 23 °C and 50% RH for over 40 h before testing. Bluehill version 4.25 software (Instron) is integrated with the Universal Testing System to record and calculate the data. Eight replicates of each variable were evaluated.

3.3.12 Data analysis

Universal Analysis 2000 software version 4.5A (TA Instruments) was used for analyzing and compiling the DSC and TGA data. DIFFRAC.EVA version 5.1.0.5 (Bruker Co.) was used to evaluate the data generated from the DIFFRAC.MEASUREMENT CENTER software for the WAXD. Fityk 1.3.1 was used to deconvolute the XRD data for analysis.

MATLAB® (Mathworks®, USA) and Microsoft Excel (Microsoft®, USA) were used to compile the data and create the graphs. SAS® (Cary, NC, USA) was used for the statistical analysis of the data. An analysis of variance (ANOVA) calculation was completed on the tensile strength and permeability measurements.

3.4 Results and Discussion

Making a blended PLA film via cast extrusion was initially challenging. At first, only one version of each high Mw PLLA and PDLA were obtained, PLLA (L175) and PDLA (D070), and several trials were conducted to establish the best method to produce sc-PLA films. Due to the markedly different MFRs of PLLA (L175) and PDLA (D070), we tried to produce masterbatches in a twin extruder and use the resulting masterbatches to produce sc-PLA. However, due to sc-PLA formation during masterbatch production, we could not cast the films in a single extruder from the masterbatches since the films crystallized in the die. Multiple temperature settings were attempted without success.

Another attempt was to vigorously mix PLLA (L175) and PLLA (D070) in a plastic bag and then cast them in a single extruder. The T_m measured was 176.5 ± 1.3 °C and 177.4 ± 0.5 °C for PLLA and PDLA, respectively, and reported as 175 °C for both resins according to the manufacturer (30,31). However, due to the different MFRs of PLLA (L175) and PDLA (D070), 3.5 ± 0.3 and 10.0 ± 0.9 g/10 min (190 °C/2.16kg), respectively, a good mixing was not

achieved, and the films could not be cast. We tried to extrude it at a lower temperature closer to the T_m of the two resins and then at a higher temperature closer to the T_m of SC-PLA. Still, the MFR was a major issue, regardless of the extrusion temperature. Additional attempts were made, but they were futile.

We then obtained two alternative resins, PLLA (L130) and PDLA (D120), which had similar measured MFRs of 12.1 ± 1.5 and 12.2 ± 1.8 g/10 min (190 °C/2.16kg), respectively, potentially facilitating the extrusion mixing. The data sheet reported the MFR as 10 g/10 min for both resins (190 °C/2.16kg) (28,29). The Tm measured was 176.2 ± 0.5 °C and 179.4 ± 1.2 °C for PLLA and PDLA, respectively, and reported as 175 °C for both resins according to the manufacturer (28,29). **Table A3.1**, Appendix 3A summarizes the MFR data of the four resins, and **Table A3.2** and **Figure A3.1**, Appendix 3A, provide a full characterization of all four resins.

The PLLA (L130) and PDLA (D120) resins with comparable MFR at a similar Tm were crucial for obtaining a homogeneous mixture and optimizing the temperature profile for SC-PLA to be formed during the extrusion process while extruding and casting it into a film in one process. Several trials were needed to optimize the temperature profile: at too low of a temperature, only HC-PLA was achieved, while at high temperatures, the mixture flowed too rapidly and did not form a film.

3.4.1 Cast film production of PLLA/PDLA blend ratios

SC-PLA film has previously been made by solvent casting (19) into a masterbatch for injection molding (25,35) and for additive manufacturing (24).

To the authors' knowledge, no published reports are available on producing SC-PLA film directly using cast film extrusion in a single screw extruder. This is likely due to a combination

of differences in the flow characteristics of two enantiomeric resins and/or sub-optimal temperature profiles of the extruder. In this study, several blends of PLLA/PDLA resins with similar MFR, Tm, and similar M_n were combined and directly extruded in a single-screw extruder without the assistance of a master batch under the processing conditions indicated in **Table A3.3,** Appendix 3B. The film combinations included 85/15, 70/30, 50/50, and 30/70 PLLA/PDLA and homopolymer PLLA and PDLA films for comparison purposes. **Figure 3.1a** shows images of the final films produced and the accompanying UV transmission values at 600 nm, indicating their transparency (36), which were similar for all the films. **Figure A3.2,** Appendix C in the SI presents all the films' transmission rates versus wavelength. **Figure 3.1b** shows the stress versus strain characteristics of all the films in the MD. **Figure A3.3,** Appendix C in the SI shows the film's tensile strength in the CD. No significant differences were observed between the hc-PLA and the various blends. All the samples exhibited fragile behavior with low elongation at break. **Table A3.4,** Appendix 3C in the SI presents the entire tensile characterization of the films. Improvement in tensile strength characteristics has been reported by others when SC-PLA samples were annealed or injection molded (19,25). The extruded homopolymer films and the blends were extruded at about 230 °C. The resulting films were fully amorphous due to the low residence time. The process could not induce crystallinity as it cooled too quickly during the casting/chill process to allow crystallization to take place, as confirmed by DSC and WAXD (discussed in section 3.3). **Figure 3.1c** shows the thermograms of PLLA, PDLA, and PLLA/PDLA blends as extruded, verifying minimal to no crystallization. As reported, the melting point of HC-PLA can be observed at around 175 °C and that of SC-PLA between 220 and 230 °C (18). The PLLA and PDLA thermograms do not show melting peaks at about 220 °C since they are only HC-PLA. All the blends have the characteristic peak, with

the 50/50 PLLA/PDLA blend having the most significant enthalpy depression due to the equimolar composition of L and D-PLA, maximizing the sc-PLA formation. The other four blends have an excess of either PLLA or PDLA and can only form the stereo-complex until one of them is fully consumed. Crystallization of sc-PLA in excess of PLLA or PDLA has been explored and reported. Brochu et al. studied a blend of 100L/80D, which allowed easier crystallization of the HC-PLA and, at the same time, potentially improved the formation of SC-PLA by isothermal crystallization (37). Park and Hong reported that SC-PLA formation significantly promoted crystallinity and that the amount of PDLA dictated the crystallization of the PLLA/PDLA blend; as the amount of PDLA increased, the SC-X_c increased, with the equimolar blend having the highest amount of formed sc-PLA (38). Schmidt and Hillmyer studied blends of PLLA with 0.25 to 15 weight percent optically pure PDLA and determined the blend ratio and the thermal treatment significantly modified the capability of the stereocomplex to nucleate the excess PLLA homopolymer. Also, the stereocomplex influenced the ensuing HC-PLLA crystallization. The amount of HC-PLA crystallization was lower than anticipated compared with the value of the pure homopolymer, attributed to the hindered mobility of the PLLA chains bound to the stereocomplex (39).

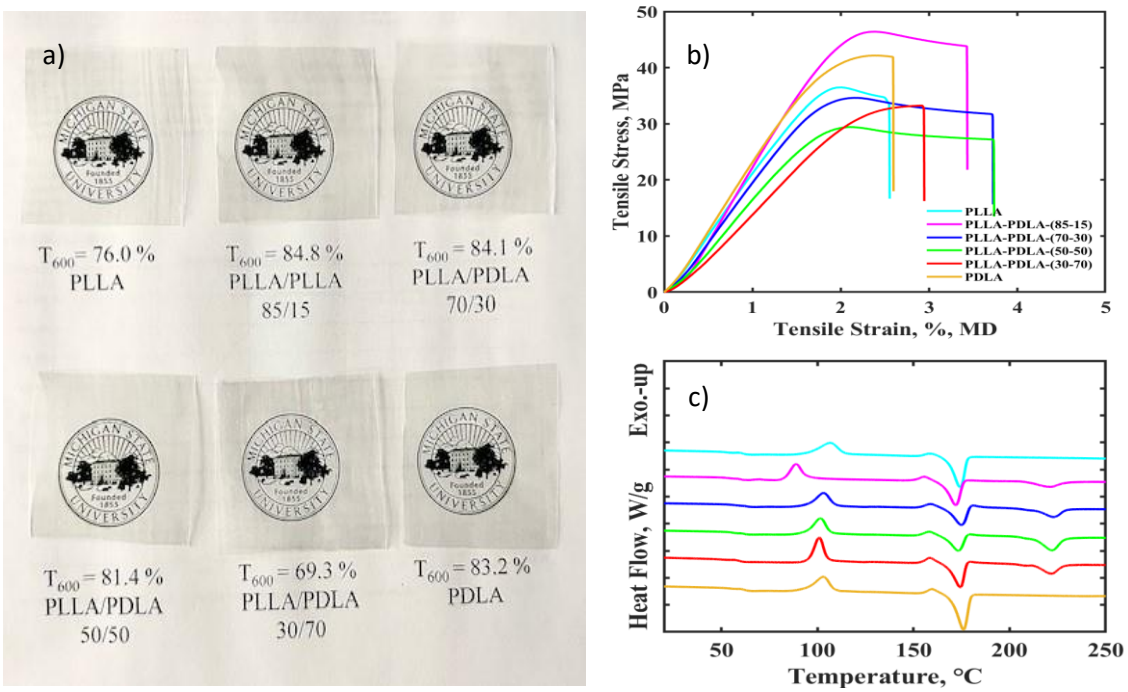

Figure 3.1. **a)** PLLA, PLLA/PDLA 85/15, 70/30, 50/50, 30/70, and PDLA films along with %T at 600 nm; **b)** **t**ensile **s**trength of PLLA, blends, and PDLA in the machine direction (MD**)**; **c)** DSC of PLLA, blends, and PDLA. The identification legend in Figure 1b carries over to Figure 1c (e.g., PLLA – light blue color in the online version of the manuscript).

3.4.2 Annealing the cast film

After the films were successfully produced, the effect of annealing was evaluated. The optimal annealing temperature was determined by running trials at 100, 140, 160, and 180 °C (data not shown). Annealing at temperatures higher than 160 °C made the film unusable since the HC-portion of the material melted. After reviewing the X_c data from the trials, it was established to use 160 °C as the annealing temperature. **Figure 3.2** shows the DSC thermograms and WAXD patterns of PLLA, blends of 70/30 and 50/50 PLLA/PDLA, and PDLA obtained for 30, 15, 5, and 0 min at 160 °C. **Figure A3.4**, Appendix 3C in the SI shows the DSC thermograms and WAXD patterns obtained for the other blends, 85/15 and 30/70 PLLA/PDLA. **Figure 3.2b** and **Figure 3.2h** show that at 15 min, crystallization started in the PLLA and PDLA films, but full crystallization was not obtained until 30 minutes. All blends exhibited almost full crystallization

at 5 min, and complete saturation in crystal growth was observed at 15 min. The crystallization peaks at about 100 °C are absent at ≥5 min of annealing in **Figures 3.2c** and **3.2e**, indicating that complete crystallization is obtained for the blends with just 5 min of annealing or even less (data not shown). The WAXD patterns in **Figure 3.2d** and **3.2f** show distinct peaks corresponding to α-crystals (2Θ at 14.9°, 16.8°, and 19.2° associated with the 010, 110/220, and 203 crystal planes) and sc-crystals (2Θ at 12.0°, 20.8°, and 24.1° associated with the 110, 300/030 and 200 crystal planes) not present in the non-annealed samples (40,41). Brochu et al. (37) reported the nucleating effect of PDLA on PLLA; they looked at PLLA/PDLA blends produced by solvent casting and showed that racemic crystallites formed with as little as 10% PDLA. This finding is consistent with the findings of Tsuji and Ikada [19], indicating that a 50/50 PLLA/PDLA blend produced via solvent casting had complete crystallization at 5 min, while PLLA and PDLA did not show appreciable crystallization until 10 min. Our work shows that complete crystallization can be achieved in cast films with a 50/50 PLLA/PDLA blend and the other blends (85/15, 70/30, and 30/70 PLLA/PDLA) at even 5 min, and maybe even less.

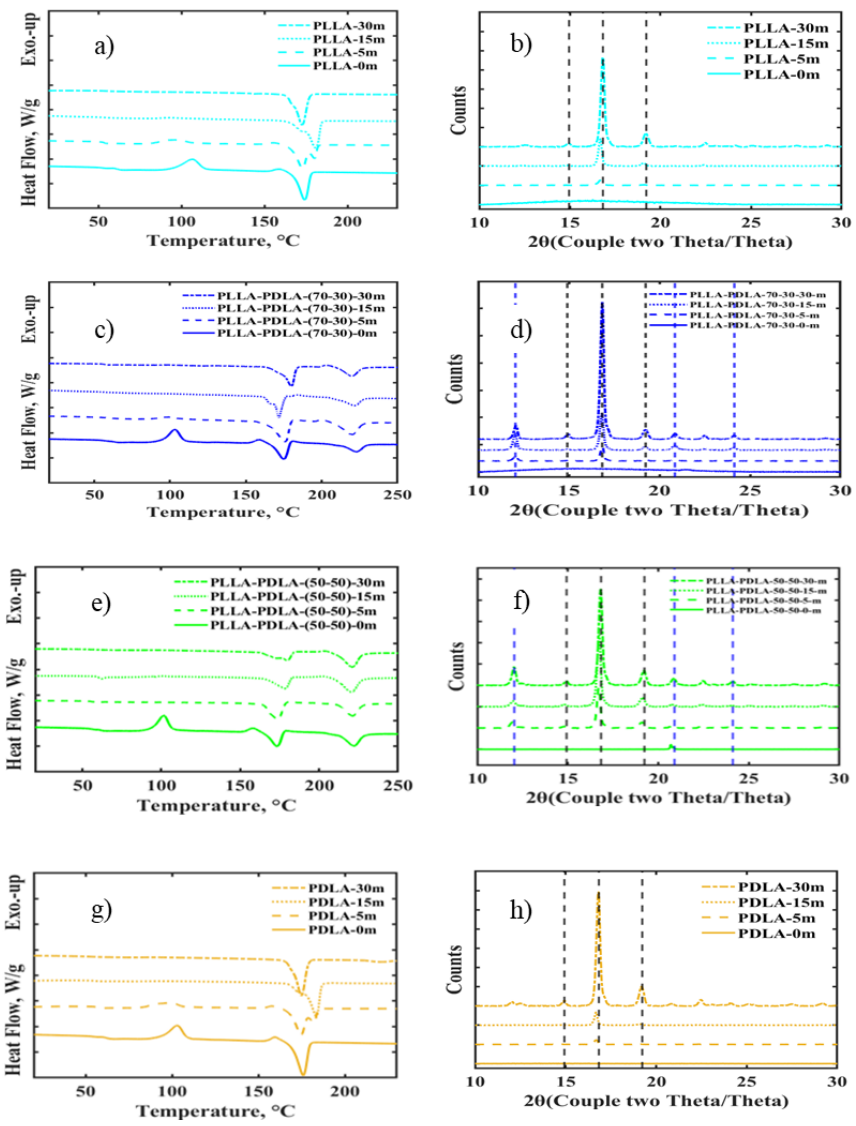

Figure 3.2. **a)** DSC thermograms of annealed PLLA-A-0,5,15,30 min; **b)** WAXD patterns of annealed PLLA-A-0,5,15,30 min; **c)** DSC thermograms of annealed PLLA-PDLA (70/30)-A-0,5,15,30 min; **d)** WAXD patterns of annealed PLLA-PDLA (70/30)-A-0,5,15,30 min; **e)** DSC thermograms of annealed PLLA-PDLA (50/50)-A-0,5,15,30 min; **f)** WAXD patterns of annealed PLLA-PDLA (50/50)-A-0,5,15,30 min; **g)** DSC thermograms of annealed PDLA-A-0,5,15,30 min; **h)** WAXD patterns of annealed PDLA-A-0,5,15,30 min. Note: All DSC samples were annealed at 160 °C. In the WAXD patterns, the dashed black lines represent α-crystals, and the dashed blue lines represent sc-crystals.

Figure 3.3 shows the tensile stress versus strain for the 70/30 and 85/15 PLLA/PDLA blends after annealing at different times. The film strength dropped dramatically in the MD and CD at 5 and 15 min due to increased brittleness. The tensile stress and strain of the two blends

were no better than those of the HC-PLA samples after extruding (data not shown). **Table A3.4** in Appendix 3C summarizes non-annealed tensile stress and strain for all the films. By annealing the samples, the crystallinity was increased to 16%─47%, depending on the annealing time, analyzed via WAXD. Park and Hong also reported tensile curves of PLLA/PDLA blended films, indicating a brittle material with no yield point or plastic deformation (38); samples annealed at 30 min could not be measured due to their brittleness. **Table 3.1** summarizes the tensile stress and strain results for the two blends and shows that all the annealed samples had significantly lower tensile stress and tensile strain than the non-annealed samples; most annealed samples were not significantly different ($P>0.05$). Suder et al. reported that the tensile strength of PLA increased with increasing annealing temperature, with a maximum increase at 100 °C; however, as the annealing temperature went above 100 °C, the tensile strength decreased and was even lower compared with the non-annealed samples (42). The samples in this study were all annealed at 160 °C to maximize crystallization and nucleation of SC. The data collected from the trials mentioned above supported the annealing temperature chosen. The process of annealing the samples had a beneficial effect on inducing crystallinity but had a detrimental impact on the film's overall strength. However, samples with 5 min of annealing time provide sufficient crystallization to tailor other properties, such as moisture vapor transmission rate, discussed in the next section.

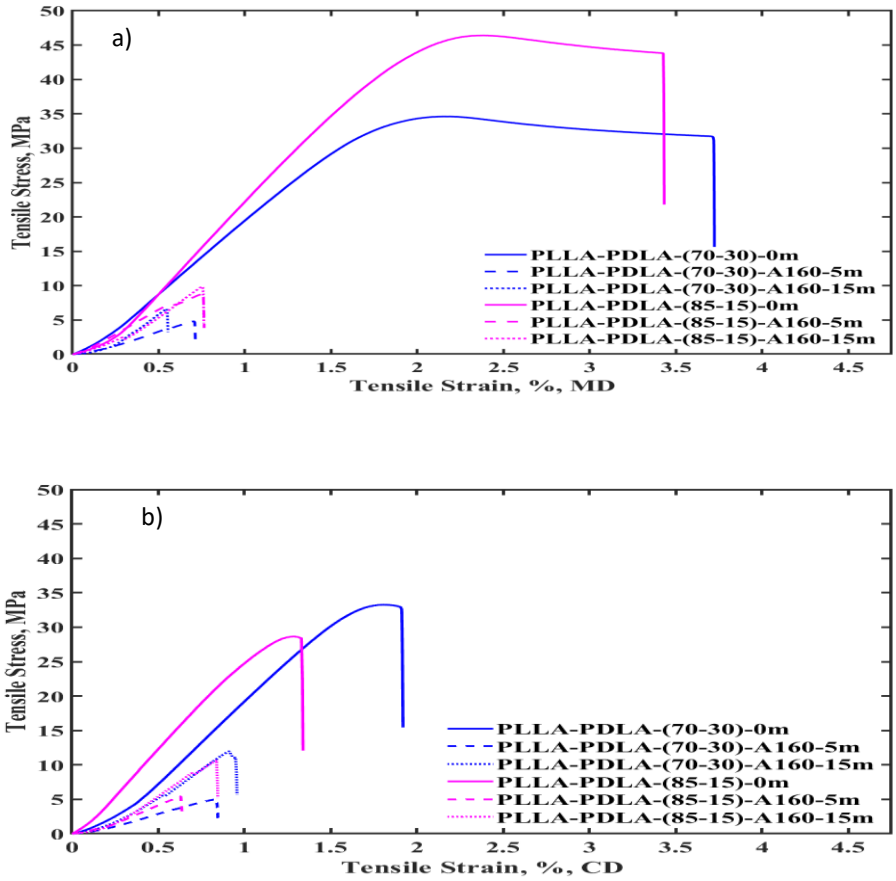

Figure 3.3. Stress versus strain at 160 °C and various annealing times for a) PLLA/PDLA (70/30) and PLLA/PDLA (85/15)─ machine direction(MD), and b) PLLA/PDLA (70/30) and PLLA/PDLA (85/15) ─ cross direction (CD).

Table 3.1. Summary of tensile stress and stain for PLLA/PDLA (70/30) and PLLA/PDLA (85/15) at varying annealing times.

	Tensile stress at Maximum load		Tensile strain at tensile strength	
	MD	CD	MD	CD
Material	MPa	MPa	%	%
PLLA/PDLA(70/30) - 0 minutes	35.49 ± 2.66[a]	30.19 ± 3.93[d]	2.34 ± 0.14[f]	1.82 ± 0.16[h]
PLLA/PDLA(70/30) A160 - 5 minutes	5.15 ± 1.25[b]	5.49 ± 2.23[e]	0.74 ± 0.14[g]	0.86 ± 0.14[i]
PLLA/PDLA(70/30) A160 - 15 minutes	5.37 ± 1.36[b]	8.21 ± 2.38[e]	0.6 ± 0.06[g]	0.93 ± 0.10[i]
PLLA/PDLA(85/15) - 0 minutes	43.97 ± 4.94[c]	28.77 ± 1.15[d]	2.42 ± 0.22[f]	1.33 ± 0.10[j]
PLLA/PDLA(85/15) A160 - 5 minutes	8.80 ± 3.54[b]	5.63 ± 1.82[e]	0.73 ± 0.10[g]	0.63 ± 0.11[k]
PLLA/PDLA(85/15) A160 - 15 minutes	5.70 ± 2.91[b]	8.10 ± 1.22[e]	0.73 ± 0.19[g]	0.86 ± 0.22[i]

Note: Values are means ± SD (n=8); within columns, means with different letters are significantly different at $P \leq 0.05$ (Tukey-Kramer test). Values at 30 min could not be obtained.

3.4.3 Moisture vapor barrier characteristics

Annealed and non-annealed samples were evaluated for moisture vapor transmission to confirm the benefit of the increased crystallinity. The moisture vapor permeability coefficient (MVPC) for PLLA, PDLA, and all the blends annealed at 30 min was compared. **Figure 3.4** summarizes the results and shows that all the annealed samples had significantly better (lower) MVPCs than the non-annealed samples; however, there was no difference among any of the annealed samples. Increasing the crystallinity generally reduces a polymer's solubility, diffusion, and permeability (43). In this case, the increase of crystallinity directly affected the reduction in MVPC. In addition, the intermediate blends of PLLA/PDLA (85/15, 70/30, 50/50, and 30/70) also resulted in significantly improved barriers. Shogren reported the MVTR of a solvent-casted PLLA film to be more than double that of an annealed film at 54 °C for 10 min (44), consistent with the results in **Figure 3.4 .** Siparsky et al. reported on the barrier of solvent-casted PLLA and PLLA/PDLA blends ranging in Xc from 0 to 46%; the permeability coefficients of the three annealed samples measured at 38 °C/90% RH were lower than the non-annealed ones (45), indicating a similar trend as we observed in this study.

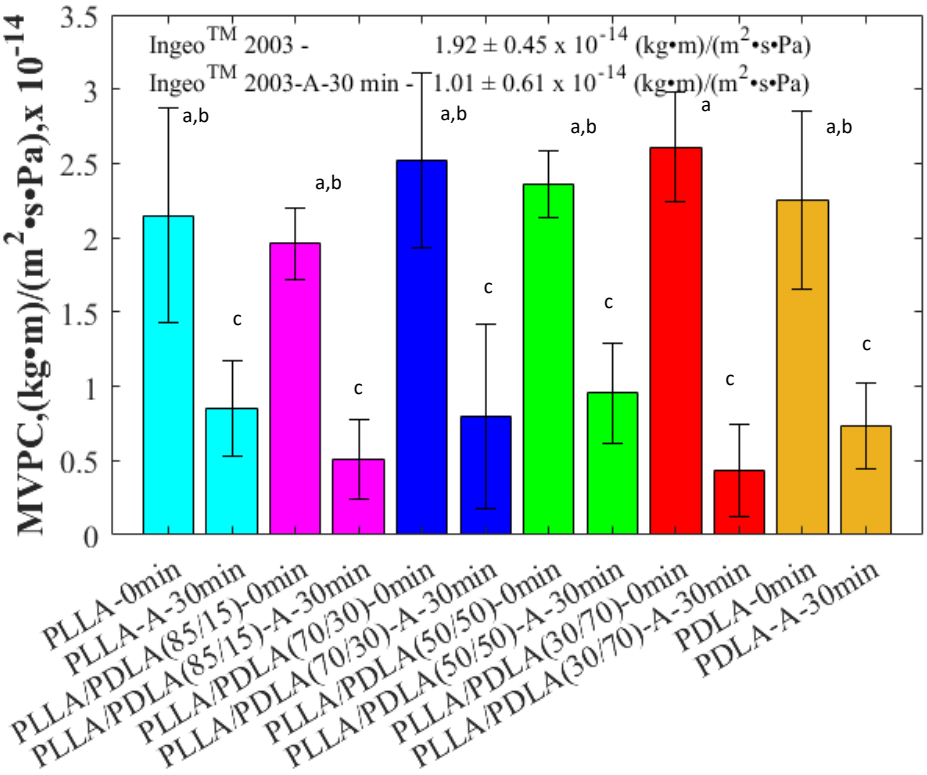

Figure 3.4. Moisture vapor permeability coefficients for all blends evaluated annealed at 0 and 30 minutes. *Note:* Values followed by a different letter are significantly different at $P \leq 0.05$ (Tukey-Kramer test).

The effect of annealing time was explored as it relates to the MVPC and X_c. **Figure 3.5** shows the MVPC for each treatment and indicates whether the sample is amorphous (A) and the HC-PLA and SC-PLA crystalline ratio, where applicable.

Table 3.2 summarizes the MVPC for each treatment and includes the Xc obtained by DSC and WAXD for each annealing time. There was a direct correlation between the improved barrier and the overall percentage of crystallinity. The same trend discussed earlier concerning crystallinity at the various annealing times also appears valid for the MVPC. The blended non-annealed samples significantly differ from the annealed blend composition for all annealing times, i.e., 5, 15, and 30 min. The PLLA samples do not vary considerably from the non-annealed sample until 15 min of annealing time. The 15-min and 30-min annealed PDLA

samples show a significant difference from the non-annealed sample; however, the 5-min PDLA sample does not differ significantly from the other PDLA samples. Tsuji et al. reported that the MVPC of PLLA films decreased monotonically as the Xc increased from 0 to 20% but leveled off at Xc greater than 30%. The finding was attributed to the elevated production of RAF regions to moisture permeation compared with the MAF regions (46). All our annealed samples had an Xc greater than 30%, with no significant difference. Tsuji and Tsuruno reported the MVPC for PLLA, PDLA, and a blend of (50/50) PDLA/PLLA for solvent-cast film and observed a similar trend where all three films markedly improved with annealing; the values reported ranged from 1.00 to 2.29 ((kg·m)/ (m2·s·Pa)) x 10-14 (23), like our reported values. Our work further demonstrated that the intermediate blends of PLLA/PDLA (85/15, 70/30, and 30/70) also resulted in significantly improved barriers. This finding means that improvement is obtained with as low as 15% PDLA, which should be commercially beneficial since PLLA is more economical and commercially available than PDLA at present.

The WAXD crystallinity was decoupled between the α-crystal and the sc-crystal by looking at the various peaks. The peaks at 2θ = 14.9, 16.8, and 19.2 correspond to the α-crystal. The peaks at 2θ = 12.0, 20.8, and 24.1 correspond to the sc-crystal (41,47). As shown in Figure 3.5, the α-crystal dominates in all the blends except the 50/50 PLLA/PDLA blend. In the PLLA/PDLA 50/50 scenario, equal amounts of PLLA and PDLA can maximize the interactivity between the two enantiomeric materials, increasing the amount of sc-PLA formed. Hence, the 50/50 blend has the highest SC-PLA amount of all the samples. In all other combinations, PLLA or PDLA is present at different levels, limiting the reaction between the two and leaving an abundance of unreacted PLLA or PDLA, depending on the blend ratio. This does not stop the remaining PLLA or PDLA from forming α-crystal at the annealing temperature/time combination.

The overall WAXD $X_{c,t}$ for all the annealed materials ranges from 16% to 47%, depending on the annealing time. The MVPC is also about the same for all the annealed samples since there is no significant difference between the annealed blended samples or the HC-PLA annealed samples at 15 min of annealing or more. Chen et al. reported similar findings on SC-PLA and the distribution between the formation of α-crystals and SC-crystals; they reported that at 140 °C, the α-crystals formed in a much higher abundance than SC-crystals (41). This study was conducted at 160 °C but yielded similar findings, which means the overall X_C improves the barrier more than the individual X_{HC} or X_{SC} formed. Additional studies could be conducted to decouple the role of the α-crystals and the SC-crystals. Maybe selective film manipulation could further improve the properties of final films.

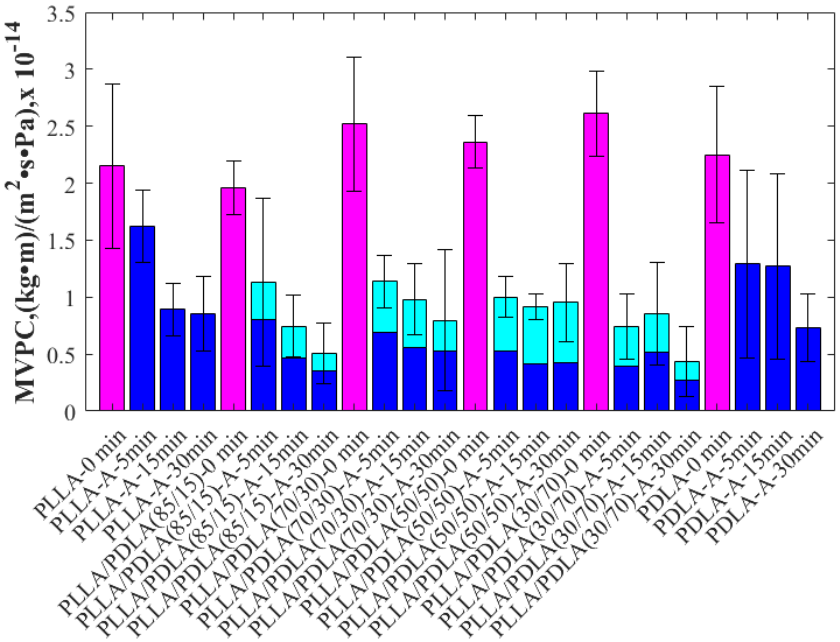

Figure 3.5. Moisture vapor permeability coefficients for all blends evaluated annealed at 0,5, 15, and 30 min. The magenta bars represent amorphous samples, the blue bars represent the hc-PLA crystalline portion, and the cyan bars represent the sc-PLA crystalline portion.

3.5 Conclusion

sc-PLA was produced using cast film extrusion directly in a single-screw extruder without first producing a masterbatch. This is an excellent first step in producing commercial sc-PLA film in one process. We annealed the sc-PLA film with a hydraulic press at a lab-scale level, but the same results could be obtained by orienting in line on a commercial scale while casting the film due to the fast conversion times. The barrier properties were improved from 2.5 to 6 times with annealing, depending on the film, including PLLA and PDLA, indicating that annealing alone can improve MVPC. This is a superior MVPC compared to other compostable options and is a good first step for a high moisture barrier film compared to its petrochemical-based counterparts. However, stereocomplexation decreases the annealing time needed to induce crystallization and subsequent MVPC improvement. Improvement of MVPC characteristics can be achieved with as little as 15% PDLA, which is highly beneficial since PLLA is the more commercially available of the two stereoisomers, helping with the economics due to the price and availability of PDLA compared to PLLA in the marketplace. The total formed crystallinity dictates the improved MVPC and not the contribution of either the homo or stereocomplex crystals. Even though the increased crystallinity improved the MVPC, it had a detrimental effect on the strength characteristics. Future work should be conducted to tailor the brittleness while maintaining the improved MVPC values.

Table 3.2. Moisture vapor permeability coefficients for PDLA, PLLA, various blends, and DSC and WAXD crystallinity values.

	MVPC				DSC				WAXD			
Material	n	((kg·m)/(m²·s·Pa)) x 10^{-14}			$X_{c,HC}$	$X_{c,SC}$	$X_{c,t}$	% SC	Xc-α	$X_{c,SC}$	$X_{c,t}$	% SC
PLLA-A160-30 min	12	0.853	±	0.324[e,f]	41	-	41	-	31	-	31	-
PLLA-A160-15 min	12	0.892	±	0.233[e,f]	42	-	42	-	26	-	26	-
PLLA-A160-5 min	9	1.62	±	0.320[a,c,d]	27	-	27	-	16	-	16	-
PLLA-A160-0 min	14	2.15	±	0.720[a,b]	0	-	0	-	0	-	0	-
PLLA/PDLA(85/15)-A160-30 min	10	0.508	±	0.269[f]	31	14	44	31	34	8	42	19
PLLA/PDLA(85/15)-A160-15 min	12	0.744	±	0.3260[e,f]	26	15	41	38	29	13	42	30
PLLA/PDLA(85/15)-A160-5 min	14	1.130	±	0.590[d,e,f]	29	12	41	28	23	5	28	18
PLLA/PDLA(85/15)-A160-0 min	8	1.960	±	0.240[a,b,c,d]	0	0	0	-	0	0	0	-
PLLA/PDLA(70/30)-A160-30 min	23	0.798	±	0.617[e,f]	28	15	42	35	24	12	36	34
PLLA/PDLA(70/30)-A160-15 min	7	0.981	±	0.312[e,f]	22	17	39	44	20	13	33	40
PLLA/PDLA(70/30)-A160-5 min	10	1.140	±	0.230[d,e,f]	30	19	49	39	29	5	34	14
PLLA/PDLA(70/30)-A160-0min	8	2.520	±	0.590[b]	0	0	0	-	0	0	0	-
PLLA/PDLA(50/50)-A160-30 min	21	0.953	±	0.341[e,f]	19	24	42	56	15	22	37	59
PLLA/PDLA(50/50)-A160-15 min	8	0.918	±	0.113[e,f]	21	25	47	54	40	7	47	15
PLLA/PDLA(50/50)-A160-5 min	10	0.998	±	0.179[e,f]	26	22	48	47	38	7	45	16
PLLA/PDLA(50/50)-A160-0 min	9	2.36	±	0.230[a,b]	0	0	0	-	0	0	0	-
PLLA/PDLA(30/70)-A160-30 min	8	0.433	±	0.310[f]	29	17	46	37	25	7	32	21
PLLA/PDLA(30/70)-A160-15 min	8	0.856	±	0.450[e,f]	26	17	43	40	22	13	35	37
PLLA/PDLA(30/70)-A160-5 min	10	0.741	±	0.287[e,f]	18	16	34	47	11	12	23	51
PLLA/PDLA(30/70)-A160-0 min	15	2.61	±	0.370[b]	0	0	0	-	0	0	0	-
PDLA-A160-30min	8	0.732	±	0.293[e,f]	43	-	43	-	37	-	37	-
PDLA-A160-15min	6	1.270	±	1.530d,[e,f]	48	-	48	-	21	-	21	-
PDLA-A160-5min	6	1.290	±	0.820[c,d,e,f]	34	-	34	-	22	-	22	-
PDLA-A160-0min	7	2.250	±	0.600[a,b,c]	0	-	0	-	0	-	0	-

Note: MVPC values are means ± SD; means followed by a different letter are significantly different at $P \leq 0.05$ (Tukey-Kramer test). DSC and WAXD measured crystallinity. WAXD is the ratio of the crystalline peaks' area to the diffraction pattern's total size. The crystalline peak areas were obtained by subtracting the amorphous halo from the entire peak areas.

3.6 Acknowledgments

J.F.M. would like to thank Michigan State University, College of Natural Resources, Office of Academic and Student Affairs for summer fellowship support for the financial support for a Ph.D. fellowship for the Summers of 2022 and 2023. The authors thank TotalEnergies Corbion for providing the PLLA and PDLA resins.

REFERENCES

1. Global Packaging Film Market Report 2020: Analysis & Forecasts 2012-2019 & 2020-2027 by LDPE, HDPE, BOPP, Polyester, PVC, Polyamide, EVOH - ResearchAndMarkets.com [Internet]. [cited 2022 Aug 1]. Available from: https://www.businesswire.com/news/home/20210211005672/en/Global-Packaging-Film-Market-Report-2020-Analysis-Forecasts-2012-2019-2020-2027-by-LDPE-HDPE-BOPP-Polyester-PVC-Polyamide-EVOH---ResearchAndMarkets.com

2. Flexible Packaging Market Size Worth $373.3 Billion By 2030 [Internet]. [cited 2023 Nov 12]. Available from: https://www.grandviewresearch.com/press-release/flexible-packaging-market

3. Plastics_ Material-Specific Data _ US EPA [Internet]. 2022 [cited 2022 Oct 18]. Available from: https://www.epa.gov/facts-and-figures-about-materials-waste-and-recycling/plastics-material-specific-data

4. Design for sustainability_ understanding compostable plastic packaging [Internet]. [cited 2022 Aug 17]. Available from: https://nutraceuticalbusinessreview.com/news/article_page/Design_for_sustainability_understanding_compostable_plastic_packaging/202066

5. Murariu M, Dubois P. PLA composites: From production to properties. Vol. 107, Advanced Drug Delivery Reviews. Elsevier B.V.; 2016. p. 17–46.

6. One word, bioplastics: Investments pour into biodegradable plastic [Internet]. 2022 [cited 2023 Jun 19]. Available from: https://www.csmonitor.com/Environment/2022/0810/One-word-bioplastics-Investments-pour-into-biodegradable-plastic

7. Li Y, Qiang Z, Chen X, Ren J. Understanding thermal decomposition kinetics of flame-retardant thermoset polylactic acid. RSC Adv. 2019;9(6):3128–39.

8. Bai H, Huang C, Xiu H, Zhang Q, Deng H, Wang K, et al. Significantly Improving Oxygen Barrier Properties of Polylactide via Constructing Parallel-Aligned Shish-Kebab-Like Crystals with Well-Interlocked Boundaries. Biomacromolecules. 2014 Apr 14;15(4):1507–14.

9. Tawakkal ISMA, Cran MJ, Miltz J, Bigger SW. A Review of Poly(Lactic Acid)-Based Materials for Antimicrobial Packaging. J Food Sci. 2014;79(8):1477–90.

10. Deng L, Xu C, Wang X, Wang Z. Supertoughened Polylactide Binary Blend with High Heat Deflection Temperature Achieved by Thermal Annealing above the Glass Transition Temperature. ACS Sustain Chem Eng. 2018 Jan 2;6(1):480–90.

11. Wang M, Wu Y, Li YD, Zeng JB. Progress in Toughening Poly(Lactic Acid) with Renewable Polymers. Vol. 57, Polymer Reviews. Taylor and Francis Inc.; 2017. p. 557–93.

12. Speranza V, De Meo A, Pantani R. Thermal and hydrolytic degradation kinetics of PLA in the molten state. Polym Degrad Stab. 2014 Feb;100(1):37–41.

13. Rasal RM, Janorkar A v., Hirt DE. Poly(lactic acid) modifications. Vol. 35, Progress in Polymer Science (Oxford). 2010. p. 338–56.

14. Singha S, Hedenqvist MS. A review on barrier properties of poly(lactic Acid)/clay nanocomposites. Vol. 12, Polymers. MDPI AG; 2020.

15. Ikada Y, Jamshidi K, Tsuji H, Hyon SH. Stereocomplex Formation between Enantiomeric Poly(lactides). Macromolecules. 1987;20(4):904–6.

16. Okihara T, Tsuji M, Kawaguchi A, Katayama KI, Tsuji H, Hyon SH, et al. Crystal structure of stereocomplex of poly(L-lactide) and poly(D-lactide). Journal of Macromolecular Science, Part B: Physics [Internet]. 1991;30:119–40. Available from: https://www.tandfonline.com/action/journalInformation?journalCode=lmsb20

17. Wan ZQ, Longo JM, Liang LX, Chen HY, Hou GJ, Yang S, et al. Comprehensive Understanding of Polyester Stereocomplexation. J Am Chem Soc. 2019 Sep 18;141(37):14780–7.

18. Tsuji H. Poly(lactide) stereocomplexes: Formation, structure, properties, degradation, and applications. Vol. 5, Macromolecular Bioscience. Wiley-VCH Verlag; 2005. p. 569–97.

19. Tsuji H, Ikada Y. Stereocomplex formation between enantiomeric poly(lactic acid)s. XI. Mechanical properties and morphology of solution-cast films. Polymer (Guildf). 1999;40:6699–708.

20. Shirahama H, Ichimaru A, Tsutsumi C, Nakayama Y, Yasuda H. Characteristics of the Biodegradability and Physical Properties of Stereocomplexes between Poly(L-lactide) and Poly(d-lactide) Copolymers. J Polym Sci A Polym Chem. 2005 Jan 15;43(2):438–54.

21. Materials Part 1_ What Annealing Can Do for Your Process _ Plastics Technology [Internet]. [cited 2022 Aug 25]. Available from: https://www.ptonline.com/blog/post/materials-part-1-what-annealing-can-do-for-your-process

22. Guinault A, Sollogoub C, Domenek S, Grandmontagne A, Ducruet V. Influence of Crystallinity on Gas Barrier and Mechanical Properties of PLA Food Packaging Films. International Journal of Material Forming. 2010;3(SUPPL. 1):603–6.

23. Tsuji H, Tsuruno T. Water Vapor Permeability of Poly(L-lactide)/Poly(D-lactide) Stereocomplexes. Macromol Mater Eng. 2010 Aug 11;295(8):709–15.

24. Luo F, Fortenberry A, Ren J, Qiang Z. Recent Progress in Enhancing Poly(Lactic Acid) Stereocomplex Formation for Material Property Improvement. Vol. 8, Frontiers in Chemistry. Frontiers Media S.A.; 2020.

25. Alhaj M, Narayan R. Scalable Continuous Manufacturing Process of Stereocomplex PLA by Twin-Screw Extrusion. Polymers (Basel). 2023 Feb 1;15(4):922.

26. PDLA Polymer Supplier and Manufacturer in China [Internet]. [cited 2022 May 12]. Available from: https://polylactide.com/polyd-lactide/

27. Lee HS, Kim EH, Kim JD. Effect of Stereocomplex Crystallite as a Nucleating Agent on the Isothermal Crystallization Behavior of Poly(L-Lactic Acid). Plastics Engineering. 2013 Oct;

28. Product data sheet Luminy ® L130 [Internet]. 2022 [cited 2022 Jun 12]. Available from: https://www.totalenergies-corbion.com/media/yvmdsjgr/pds-luminy-l130-190507.pdf

29. Product Data Sheet Luminy® D120 [Internet]. 2019 [cited 2022 Jun 11]. Available from: https://www.totalenergies-corbion.com/media/0mxj0y1o/pds-luminy-d120-190507.pdf

30. Product Data Sheet Luminy® L175 [Internet]. 2019 May [cited 2022 Oct 12]. Available from: www.total-corbion.com

31. Product Data Sheet Luminy® D070 [Internet]. 2019 May [cited 2022 Oct 12]. Available from: www.total-corbion.com

32. ASTM D1238-20 Standard Test Method for Melt Flow Rates of Thermoplastics by Extrusion Plastometer 1 [Internet]. West Conshohocken; 2020. Available from: http://www.ansi.org.

33. ASTM F1249-20 Standard Test Method for Water Vapor Transmission Rate Through Plastic Film and Sheeting Using a Modulated Infrared Sensor [Internet]. West Conshohocken; 2020. Available from: www.astm.org,

34. Standard Test Method for Tensile Properties of Thin Plastic Sheeting 1. Available from: http://www.ansi.org.

35. Bai H, Deng S, Bai D, Zhang Q, Fu Q, Bai HW, et al. REVIEW 1700454 (1 of 12) Recent Advances in Processing of Stereocomplex-Type Polylactide. 2017; Available from: www.advancedsciencenews.com

36. Standard Test Method for Transparency of Plastic Sheeting [Internet]. 2023. Available from: www.astm.org,

37. Brochu S, Prud'homme RE, Barakat I, Jerome R. Stereocomplexation and Morphology of Polylactides. Macromolecules. 1995;28(15):5230–9.

38. Park HS, Hong CK. Relationship between the Stereocomplex Crystallization Behavior and Mechanical Properties of PLLA/PDLA Blends. Polymers (Basel). 2021 Jun 1;13(11):1851.

39. Schmidt SC, Hillmyer MA. Polylactide Stereocomplex Crystallites as Nucleating Agents for Isotactic Polylactide. J Polym Sci B: Polym Phys. 2001;39:300–13.

40. Pan P, Han L, Bao J, Xie Q, Shan G, Bao Y. Competitive Stereocomplexation, Homocrystallization, and Polymorphic Crystalline Transition in Poly(L-lactic acid)/Poly(D-lactic acid) Racemic blends: Molecular Weight Effects. Journal of Physical Chemistry B. 2015 May 28;119(21):6462–70.

41. Chen Q, Auras R, Kirkensgaard. J. K., Uysal-Unalan I. Modulating Barrier Properties of stereocomplex Polylactide: The Polymorphism Mechanism and its Relationship with Rigid Amorphous Fraction. ACS Appl Mater Interfaces. 2023;

42. Suder J, Bobovsky Z, Zeman Z, Mlotek J, Vocetka M. The Influence of Annealing Temperature on Tensile Strength of Polylactic Acid. MM Science Journal. 2020 Nov 1;2020(November):4132–7.

43. Rogers CE. Polymer Permeability [Internet]. 1st ed. Comyn J, editor. London: Chapman and Hall; 1985. Available from: http://link.springer.com/10.1007/978-94-009-4858-7

44. Shogren R. Water Vapor Permeability of Biodegradable Polymers. J Environ Polym Degrad. 1997;5(2):91–5.

45. Siparsky GL, Voorhees KJ, Dorgan JR, Schilling K. Water Transport in Polylactic Acid (PLA), PLA/ Polycaprolactone Copolymers, and PLA/Polyethylene Glycol Blends. J Environ Polym Degrad. 1997;5(3):125–36.

46. Tsuji H, Okino R, Daimon H, Fujie K. Water Vapor Permeability of Poly(lactide)s: Effects of Molecular Characteristics and Crystallinity. J Appl Polym Sci. 2006 Feb 5;99(5):2245–52.

47. Ma B, Zhang H, Wang K, Xu H, He Y, Wang X. Influence of scPLA microsphere on the crystallization behavior of PLLA/PDLA composites. Composites Communications. 2020 Oct 1;21:100380.

APPENDIX 3A: RESIN CHARACTERIZATION

Table A3.1 shows the melt flow rate (MFR) of all four resins used in the study.

Table A3.1. MFR of PLLA and PDLA resins.

	Weight (g/30 sec)	MFR (g/10 min)
PLLA - L130	0.653	13.06
	0.629	12.59
	0.609	12.19
	0.754	15.09
	0.584	11.69
	0.753	15.06
	0.610	12.21
	0.595	11.89
	0.582	11.64
	0.565	11.30
	0.554	11.08
	0.507	10.14
	0.487	9.74
Average	**0.606**	**12.13**
St. Dev.	**0.064**	**1.53**

*190° C and 2.16 kg weight

	Weight (g/30 sec)	MFR (g/10 min)
PDLA - D120	0.619	12.38
	0.512	10.24
	0.483	9.66
	0.736	14.72
	0.661	13.22
	0.570	11.39
	0.507	10.13
	0.626	12.52
	0.494	9.89
	0.738	14.76
	0.751	15.01
	0.604	12.09
	0.598	11.96
Average	**0.608**	**12.15**
St. Dev.	**0.090**	**1.81**

*190° C and 2.16 kg weight

	Weight (g/30 sec)	MFR (g/10 min)
PLLA - L175	0.170	3.40
	0.182	3.64
	0.150	3.00
	0.181	3.62
	0.191	3.82
	0.157	3.13
	0.191	3.81
	0.181	3.61
Average	**0.175**	**3.50**
St. Dev.	**0.014**	**0.28**

*190° C and 2.16 kg weight

	Weight (g/30 sec)	MFR (g/10 min)
PDLA - D070	0.485	9.69
	0.472	9.43
	0.495	9.89
	0.413	8.26
	0.520	10.40
	0.576	11.52
	0.546	10.92
	0.483	9.65
Average	**0.499**	**9.97**
St. Dev.	**0.046**	**0.93**

*190° C and 2.16 kg weight

Table A3.2 shows the study's thermal and physical properties of all four resins.

Table A3.2. Physical properties of PLLA and PDLA resins used in the study.

Thermal Properties	PLLA (L175)			n	PDLA (D070)			n
$T_{d,1\%}$, °C	318	±	5	3	314	±	1	3
T_g, °C	78	±	1	3	75	±	0	3
T_m, °C	177	±	1	3	177	±	1	3
X_c, %	37	±	8	3	56	±	19	3
Melt Flow Rate, g/10 min	3.5	±	0.3	8	10.0	±	0.9	8
Physical Properties								
Density, g/cm^3	1.25	±	0.0	9	1.24	±	0.0	9
M_w, kDa	157	±	6	6	38	±	3	6
M_n, kDa	87	±	7	6	22	±	2	6
$Đ$	1.7	±	0	6	1.8	±	0.1	6

Note: n indicates the number of samples

Thermal Properties	PLLA (L130)			n	PDLA (D120)			n
$T_{d,1\%}$, °C	303	±	5	3	319	±	5	3
T_g, °C	74	±	1	3	72	±	7	3
T_m, °C	176	±	1	3	179	±	1	3
X_c, %	30	±	1	3	30	±	5	3
Melt Flow Rate, g/10 min	12.1	±	1.5	13	12.1	±	1.8	13
Physical Properties								
Density, g/cm^3	1.25	±	0	19	1.25	±	0	12
M_w, kDa	120	±	0	6	101	±	0	6
M_n, kDa	70	±	1	6	59	±	1	6
$Đ$	1.7	±	0.0	6	1.7	±	0.0	6

Note: n indicates the number of samples

Figure A3.1 is the thermograms of the PLLA(L130) and PDLA(D120) resins used in the study.

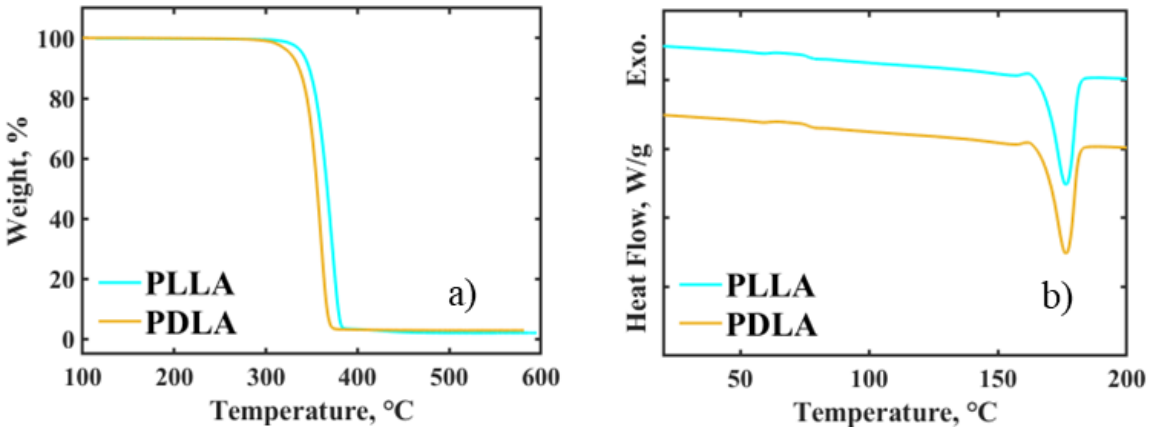

Figure A3.1. **a)** TGA of PLLA (L130) and PDLA (D210) resin; **b)** DSC of PLLA (L130) and PDLA (D120) resin.

APPENDIX 3B: PROCESSING CONDITIONS

Table A3.3 shows the processing conditions in which the film was extruded.

Table A3.3. Cast film extrusion parameters for processing.

Processing temperatures	**Temperature (°C)**
Zone 1	210
Zone 2	220
Zone 3	230
Transfer tube	230
Adapter	230
Feedblock	220
Die	215
Chill Roll	22

Extrusion Settings	**Speed (RPM)**
Screw	25
Chill roll speed	10 to 20

APPENDIX 3C: FILM CHARACTERIZATION

Figure A3.2 is the UV transmission rate versus the wavelength for all the films produced.

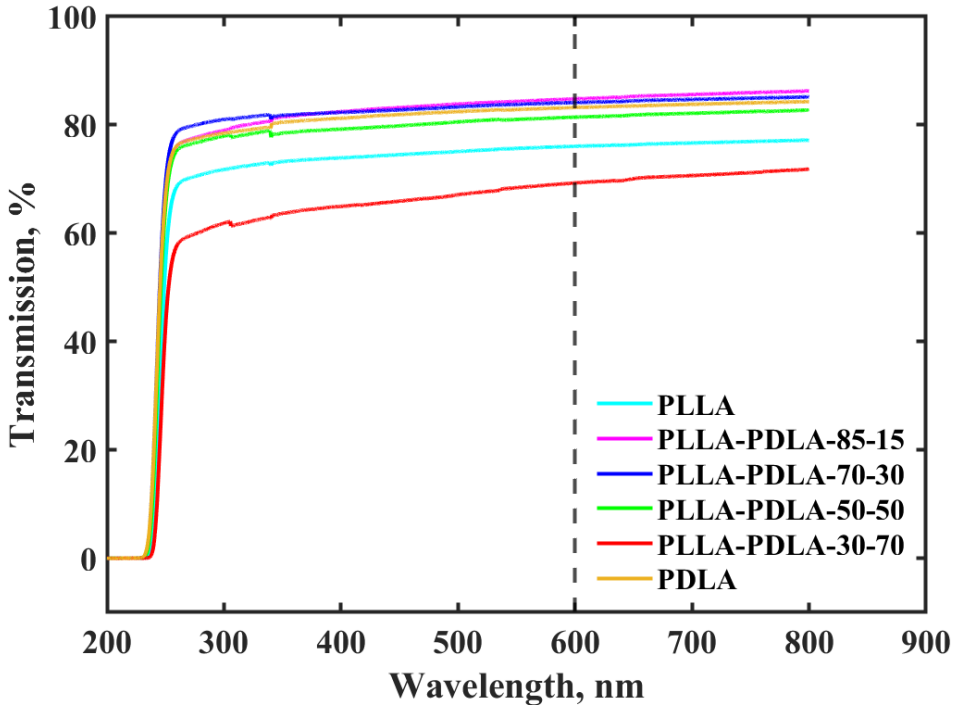

Figure A3.2. UV transmission rate versus wavelength for the various films at a wavelength of 600 nm.

Figure A3.3 shows the Tensile Strength of PLLA, blends, and PDLA in CD.

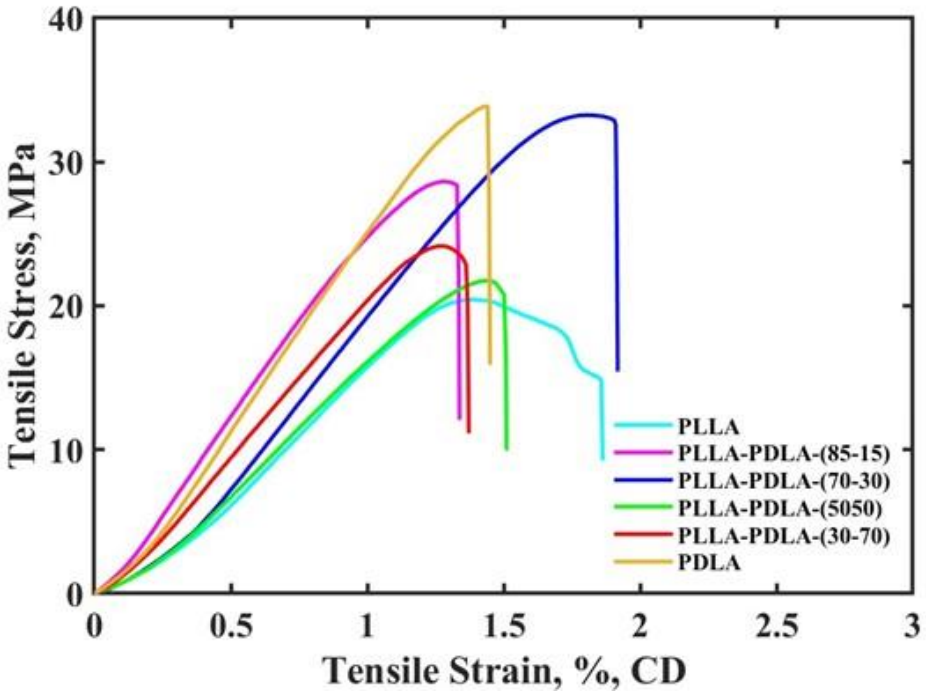

Figure A3.3. Tensile Strength of PLLA, blends, and PDLA in CD.

Table A3.4 summarizes all the films' non-annealed tensile stress and strain.

Table A3.4. Tensile Stress and Strain of PLLA, PDLA and blends, MD, and CD, non-annealed. Values followed by a different letter are significantly different at $P \leq 0.05$ (Tukey test).

	Tensile stress at Maximum load		Tensile strain at tensile strength	
	MD	CD	MD	CD
Material	MPa	MPa	%	%
PLLA - L130-A160 - 0 minutes	36.18 ± 4.36^{b}	19.82 ± 1.96^{e}	2.33 ± 0.11^{f}	1.45 ± 0.14^{g,h}
PLLA/PDLA(85/15)-A160 - 0 minutes	43.97 ± 4.94^{a}	28.77 ± 1.15^{c,d}	2.42 ± 0.22^{f}	1.33 ± 0.10^{g}
PLLA/PDLA(70/30)-A160 - 0 minutes	35.49 ± 2.66^{b}	30.19 ± 3.93^{c}	2.34 ± 0.14^{f}	1.82 ± 0.16^{i}
PLLA/PDLA(50/50)-A160 - 0 minutes	33.43 ± 1.39^{b}	20.61 ± 1.70^{e}	2.25 ± 0.07^{f}	1.56 ± 0.10^{h}
PLLA/PDLA(30/70)-A160 - 0 minutes	33.19 ± 2.74^{b}	24.04 ± 1.47^{d,e}	2.08 ± 0.35^{f}	1.33 ± 0.12^{g}
PDLA - D120-A160 - 0 minutes	41.77 ± 3.05^{a}	32.65 ± 6.00^{c}	2.48 ± 0.24^{f}	1.44 ± 0.23^{g,h}

Figure A3.4 shows the DSC and WAXD of the other blends, (85/15) and (30/70) PLLA/PDLA.

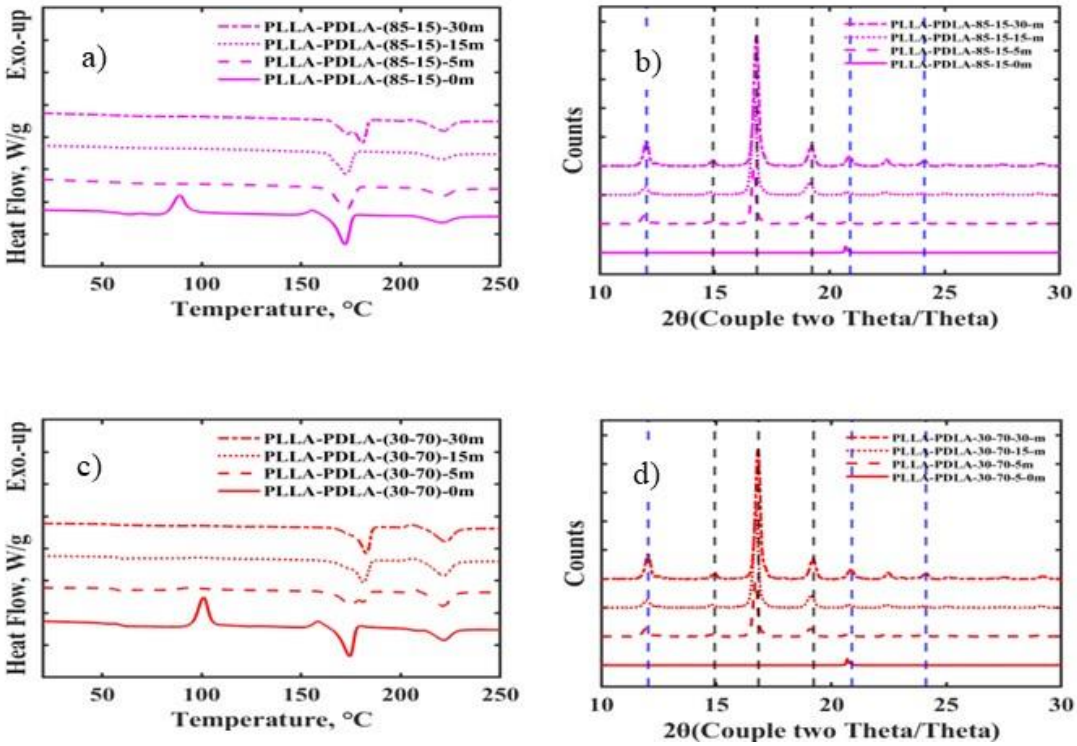

Figure A3.4. a) DSC of annealed PLLA-PDLA (85/15)-A-0,5,15,30 minutes; b) WAXD of annealed PLLA-PDLA 85/15)-A-0,5,15,30 minutes; c) DSC of annealed PLLA-PDLA (30/70)-A-0,5,15,30 minutes; d) WAXD of annealed PLLA-PDLA (30/70)-A-0,5,15,30 minutes. Note: In the WAXD figures, the dashed black lines represent α-crystals. The dashed blue lines represent SC-crystals.

CHAPTER 4: DENSITY AND CRYSTALLINITY CORRELATIONS: ENHANCING MOISTURE BARRIER PROPERTIES IN POLY(L-LACTIC), POLY(D-LACTIC ACID) AND STEREOCOMPLEX-POLY(L,D-LACTIC ACID) FILMS

A version of this chapter was submitted on 7/08/24 as:

Macnamara, J., Vallery, R., Gidley, D., Auras, R. Density and Crystallinity Correlations: Enhancing Moisture Barrier Properties in Poly(L-lactic acid), Poly(D-lactic acid) and Stereocomplex-Poly(L,D-lactic acid) Films, *Macromolecular Rapid Communications.*

4.1 Abstract

Reducing waste from plastic packaging is vital for sustainable development, with the bioplastics sector at the forefront of this effort. Among its notable advancements, stereocomplex poly(lactic acid) is distinguished by its compostability and promising barrier properties, positioning it as a promising material. This study examines the relationship among the density, crystallinity, and moisture barrier properties of poly(L-lactic acid) - PLLA, poly(D-lactic acid) films - PDLA, and their PLLA/PDLA blends (85/15,70/30, 50/50, and 30/70), specifically observing changes when these films are annealed for durations ranging from 0 and 30 minutes. Amorphous film samples displayed densities between 1,230 ± 6 and 1,243 ± 2 kg/m^3, while semi-crystalline samples showed higher densities of 1,250 ± 8 to 1,257 ± 9 kg/m^3. A notable finding is an inverse relationship between density and moisture barrier performance, 2.308 ± 0.207 to 0.713 ± 0.128 x 10^{-14} (kg·m)/(m^2·s·Pa) as density increased. The analysis confirmed a strong correlation between increased density and crystallinity, with fully crystalline PLLA and a 50/50 PLLA/PDLA blend achieving densities of 1,270 and 1,285 kg/m^3, respectively. The impact of annealing time on 50/50 PLLA/PDLA blends was explored, demonstrating that as annealing time increased, so did the stereocomplex-PLA crystallinity and rigid amorphous fraction, impacting the overall density. However, higher densities were observed at shorter annealing times (5 and 15 minutes) when homocomplex structures dominated over stereocomplex structures. In contrast, longer annealing times (30 and 60 minutes) favored stereocomplex structures and exhibited lower densities. This infers that homocomplex crystals are denser than stereocomplex crystals. Despite similar moisture barriers across most annealed samples, those annealed for 60 minutes showed the lowest permeability, suggesting that improvements in barrier properties are more closely tied to overall crystallinity rather than the

proportion of specific crystal types. This study provides crucial insights and experimental data on stereocomplex PLA, supporting its further development for commercial use, particularly in sustainable packaging solutions.

4.2 Introduction

The global flexible packaging market was estimated at USD 271 billion in 2023 and is expected to grow to USD 373 billion by 2030 (1). The demand is driven by consumer convenience and the cost-effectiveness of flexible packaging in the packaged food, beverage, and healthcare sectors (1).

As the plastic packaging market grows, so does the amount of plastic reaching the municipal solid waste (MSW). Plastic solid waste has grown considerably since synthetic polymers started being produced on an industrial scale in the 1940s (2). In the US, plastic waste production surged significantly from 2.9 million metric tons in 1970 to 35.8 million metric tons in 2018 (3). This dramatic rise led to an expected boom in the bioplastic material sector, primarily due to stringent government regulations in North America and Europe to promote materials with lower environmental impact. These policies are set to drive substantial growth in this segment (1).

The pursuit of sustainable solutions has intensified in light of the escalating plastic waste attributed to packaging, which constitutes a significant portion of MSW and heightens environmental concerns. This urgency has catalyzed research into developing materials with reduced environmental impact (4). Among these innovations, compostable materials mainly derived from biobased resources are emerging as a promising alternative to conventional petrochemical-based plastics, offering a solution to mitigate waste generation. These compostable materials break down much faster than their non-biodegradable counterparts and

present the advantage of being disposed of along with organic waste, even when contaminated, thus aligning with the growing environmental regulatory pressures and market demands for sustainable packaging solutions (7, 8).

Poly (lactic acid) - PLA - is an environmentally friendly biopolymer produced from renewable resources and compostable under industrial composting conditions (7). PLA is a potential solution to replace petrochemical-based plastics and decrease the amount of packaging waste sent to landfills, as it can be recycled and fully recovered with organic waste (8). However, PLA lacks good heat resistance and barrier properties (9,10).

Stereocomplex PLA (SC-PLA), a blend of L-PLA (PLLA) and D-PLA (PDLA), has some enhanced properties over PLA, including increased heat resistance and supposedly improved moisture vapor barrier properties, resulting in a lower moisture vapor transmission rate (MVTR) (11). However, fundamental properties such as the density of PLLA, PDLA, and SC-PLA still need to be comprehensively reported, especially as an extruded film, which is crucial to understanding the final packaging structure of this polymer. Several authors have reported the density using various measurement methodologies but have had conflicting results. Cartier *et al*. reported on the density of a 50/50 PLLA/PDLA solvent cast film 1270 kg/m^3 (12). Sawai *et al*. also studied the density of 50/50 PLLA/PDLA solvent cast films and reported the crystal density via wide-angle X-ray diffraction (WAXD) estimation of solely SC-crystals at 1342 ± 2 kg/m^3 (13). Okihara *et al.* reported on the solvent-cast crystal structure of 50/50 PLLA/PDLA based on electron diffraction patterns at 1270 kg/m^3 (14). Brizzolara *et al.* built upon Okihara e*t al*.'s work and proposed an alternative configuration based on WAXD of a 50/50 PLLA/PDLA solvent cast film at 1210 kg/m^3 (15). All the reported data were only completed on a 50/50 PLLA/PDLA solvent cast film with reported dissimilar density values.

This study quantified the density of PLLA, several SC-PLA blends, and PDLA, examining their relationship with crystallinity (X_c) and MVTR. Differential scanning calorimetry (DSC), modulated DSC, and wide-angle X-ray diffraction (WAXD) techniques were employed to assess crystallinity accurately. The specific compositions of the blends evaluated included ratios of 85/15, 70/30, 50/50, and 30/70 PLLA to PDLA, providing a comprehensive overview of how varying PLLA and PDLA proportions impact density, X_c, and MVTR properties. In the stereo complex 50/50 system, positronium annihilation lifetime spectroscopy (PALS - a well-known probe of polymer-free volume) was used to assess how pore size and relative porosity correlate with the crystallinity, density, and permeability changes from increasing the film's annealing time.

4.3 Experimental Section

4.3.1 Materials

The PLLA (Luminy® L130 (≥ 99%(L-isomer)) and PDLA (Luminy® D120 (≥ 99%(D-isomer)) resin were supplied by TotalEnergies Corbion (Gorinchem, Netherlands). The data sheet lists the target molecular weight as 130 kDa for L130 and 120 kDa for D120 (16,17). The resins were not altered with any additives. The density column gradient was made of 99% calcium nitrate tetrahydrate (Beantown Chemical, USA) and HPLC-grade water (Beantown Chemical, USA).

4.3.2 Film Processing

The two resins were dried in a vacuum oven (VWR International, USA) for a minimum of 12 h at 80 °C and 24 in-Hg before processing to minimize the potential of chain-scission reactions due to moisture during processing (16,17).

PLLA and PDLA film were produced individually first from the two dried resins. Next, the two resins were mixed by weight in ratios of 85/15, 70/30, 50/50, and 30/70 PLLA/PDLA in a plastic bag before being added to the extruder. A pilot scale microextruder (Randcastle Extrusion Systems, Cedar Grove, NJ, USA) was used to extrude the material and make it into a cast film. The exact processing conditions are detailed elsewhere (18). A digital micrometer model # 49-70-01-0001 (TMI, USA) was used to measure the caliper of the film ($n \geq 3$), which, among all the samples measured, ranges in thickness from 26 to 120 microns.

4.3.3 Thermal Annealing

A hydraulic press model number QL438-C (PHI, USA) heated to 160 °C was used for annealing each film sample of approximately 25.4 x 16.5 cm^2. The annealing temperature was previously optimized (19). The samples were sandwiched between 25.4 x 25.4 cm^2 plates lined with non-stick aluminum foil. All the samples were annealed for 30 min, while the 50/50 PLLA/PDLA samples were also annealed for 5, 15, and 60 min. Ambient temperature was used to cool the samples after annealing in the press. After cooling, the samples were stored at -20 °C to be analyzed later.

4.3.4 Differential Scanning Calorimetry (DSC) and Modulated DSC (MDSC)

A Q100 DSC (TA Instruments, USA) with a refrigerated cooling system under a 70 mL/min nitrogen flow was used for thermal analysis. Standard aluminum pans and lids were used, and samples weighing 5 to 10 mg were packed and sealed in each pan. The DSC thermogram collection procedure was adapted from Macnamara *et al.* (18). The MDSC procedure used was adapted from Limsukon *et al*. to quantify the mobile amorphous faction (MAF) and rigid amorphous fraction (RAF) (20). Two or more replicates of each sample were tested on the resin and films produced for DSC. Each PLLA/PDLA 50-50-annealed sample was

tested for MDSC. For the X_c calculation, 139 J/g and 142 J/g (21) were used for the heat of fusion (ΔH) of 100% HC-PLA and SC-PLA, respectively. Universal Analysis 2000 software version 4.5A (TA Instruments, USA) was used to analyze and compile the thermograms.

4.3.5 Wide Angle X-ray Diffraction (WAXD)

An AXS D8 Advance X-ray diffractometer (Bruker Co., USA) with a global mirror filter Cu Kα radiation source at 40 kV 100 mA was used to collect WAXD patterns. The data was collected between a 2θ range from 10° and 40° at a rate of 0.24°/min and an increment of 0.01°. DIFFRAC. MEASUREMENT CENTER version 7.5.0 software (Bruker Co.) was used to collect the data. DIFFRAC.EVA version 5.1.0.5 (Bruker Co., USA) was used to evaluate the data generated from the DIFFRAC. MEASUREMENT CENTER software for the WAXD patterns. Fityk 1.3.1 was used to deconvolute the XRD data for analysis. A minimum of one sample of each film sample was tested.

4.3.6 Density gradient column

An auto-density gradient column (Ray Ran, USA) was used to measure density, which was connected to a 200F refrigerated/heating circulator (Julabo, USA) to control the water temperature in the density column. A microprocessor-controlled Density Gradient Column filler (H&D Fitzgerlad Ltd., St. Asaph, UK) was used to fill the column. A solution of water-calcium nitrate ($CaNO_3$) with a density range of 1,050 kg/m3 to 1,320 kg/m^3 was used in the column. Tests were conducted according to ASTM D1505-18 (22). Ten or more replicates were evaluated for each resin or film. The column was calibrated using five beads ranging in density from 1,100.1 to 1,300.0 kg/m^3 (H&D Fitzgerlad Ltd., St. Asaph, UK) with certified calibration of ± 0.15 kg/m^3 per bead (23). A calibration curve was constructed with an $r^2 \geq 0.998$. The samples were allowed to equilibrate in the column for thirty minutes before the measurements were

taken. After each test, the column was swept with a basket to remove as many sample pieces as possible. Techni-Test software version 2.3.3 9 (Ray Ran, USA) was used to compile the density gradient column data.

4.3.7 Barrier properties

Both annealed and non-annealed PLLA, PDLA, and the blended films were measured on a Permatran-W® 3/34 instrument (Mocon, USA) at 38 °C and 90% RH. The MVTR was measured according to ASTM F1249-20 (24). Eight or more replicates were evaluated per sample. Moisture vapor permeability coefficients (MVPC) were estimated by dividing the MVTR by the water partial pressure at 38 °C and 90% RH and multiplying by the sample thickness (25).

4.3.8 Positronium annihilation lifetimes (PALS) analysis

PALS measurements were conducted using a positron source of Na-22 sealed in thin Kapton film sandwiched between about 1 mm of the target sample (by stacking ~20 sheets on either side of the source). Positrons are emitted during the β-decay of Na-22 concomitantly with a 1270 keV nuclear γ-ray which is detected in a fast plastic scintillator attached to a photomultiplier tube and provides the start signal to a Time-to-Analog converter (TAC). Eventually, the positrons annihilate into gamma rays, which are similarly detected and provide the stop signal to the TAC. At least 8 million events were recorded in a time histogram, with a resolution of 0.1210 ns/channel. More details on PALS can be found elsewhere (26). The time histograms were analyzed using PositronFit (27) by fitting each spectra to four lifetimes and their corresponding intensities (the fraction of all positrons that annihilate in each lifetime component). The two shortest lifetimes, τ_1 and τ_2, around 0.13 ns and 0.37 ns, corresponded to singlet positronium and positron annihilation in the pores, respectively. The longer two lifetimes

(our PALS signal), τ_3 and τ_4, were around 1.6 ns and 2.5 ns, respectively, corresponding to positronium annihilation in the pores with, apparently, a range in pore size requiring at least two lifetimes for adequate fitting. The positronium lifetimes were converted into pore diameters using a well-tested conversion algorithm (28).

4.3.9 Data analysis

MATLAB® (Mathworks, USA) and Microsoft Excel (Microsoft®, USA) were used to collect the data and construct the graphs. Statistical data analysis was completed using SAS® (SAS® Institute Inc., USA). An analysis of variance (ANOVA) was completed on the density and permeability measurements.

4.4 Results and Discussion

4.4.1 DSC and WAXD

DSC and WAXD were used to determine the crystallinity of the films. **Figure 4.1** summarizes the DSC thermograms for PLLA, PLLA/PDLA combinations of 85/15,70/30, 50/50, 30/70, and PDLA at 0 and 30 min annealing times at 160 °C. The melting points of HC-PLA and SC-PLA have been reported to be around 175 °C and 225 °C, respectively (29). All the DSC thermograms show the HC-PLA melting point, while all the blended samples also show the SC-PLA melting point at around 225 °C. The crystallization temperature (T_c) for HC-PLA has been reported to be around 100 °C (30). All the samples at 0 min annealing time have the characteristic crystallization peak at around 100 °C. In comparison, none of the samples have it at 30 min annealing time, confirming that the non-annealed samples were amorphous while the annealed samples were semi-crystalline. Alhaj and Naryan reported a similar thermogram of a 50/50 PLLA/PDLA film (31). As the amount of PDLA increases, the amount of SC-crystals formed increases as well, with the maximum amount of SC-crystallinity occurring at a blend of

50/50 PLLA/PDLA, as can be seen by the ratio to the SC-portion of the HC-portion of the thermograms for the range of annealing times explored. Park and Hong reported similar results with a 50/50 blend showing the maximum amount of SC-PLA formed (32). All the blend samples showed double melting temperatures for the HC-fusion range, indicating that the proportion of the L or D isomers may be responsible for the dual melting points when the HC crystallizes. Guo *et al*. saw the same double melting points in a study of the SC and HC formation mechanism in symmetric and asymmetric PLA enantiomers (33), and Limsukon *et al.* also observed that the T_m values of PLA shift to a lower temperature range with increasing D-lactide content (20).

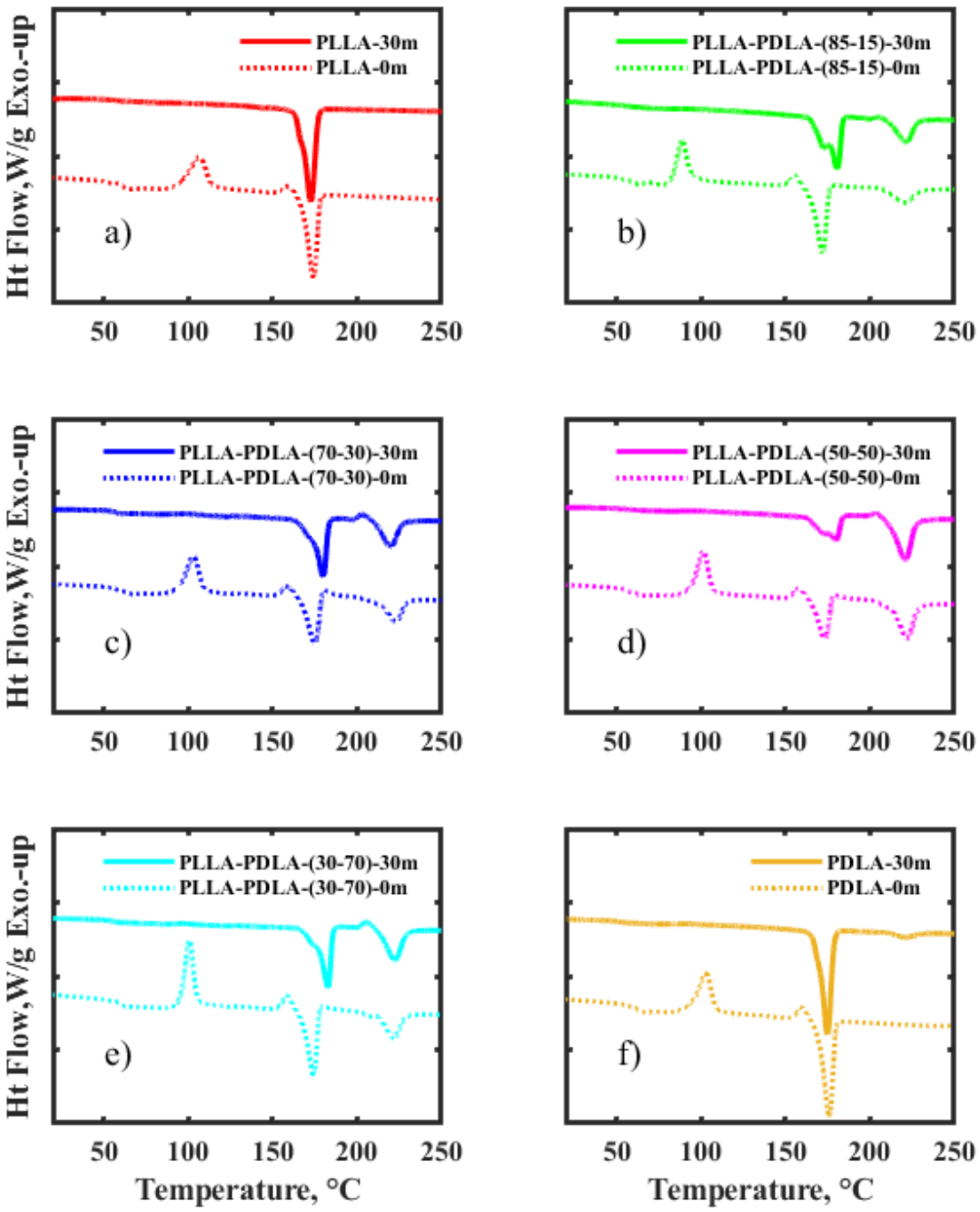

Figure 4.1. DSC thermograms of annealed **a)** PLLA-A-0,30 min; **b)** PLLA-PDLA (85/15)-A-0,30 min; **c)** PLLA-PDLA (70/30)-A-0,30 min; **d)** PLLA-PDLA (50/50)-A-0,30 min; **e)** PLLA-PDLA (30/70)-A-0,30 min; **f)** PDLA-A-0,30 min.

Figure 4.2 shows the WAXD patterns for PLLA, PLLA/PDLA combinations of 85/15, 70/30. 50/50, 30/70, and PDLA at 0 and 30 min annealing times. There are no peaks at 0 min

annealing time, confirming it was fully amorphous off the extruder with no annealing. PLLA crystallized on a 10_7 helix chain formation (orthorhombic) (13), PDLA crystallized on a 10_3 helix chain formation (orthorhombic) (15); SC-PLA crystallized on a chain conformation 3_2 (PLLA) and 3_1 (PDLA) helices (triclinic) (12,14). Zhang *et al*. showed, using calorimetry, how the 10_3 crystals transformed into the 3_1 crystal configuration with time and heat (34). All the annealed films show peaks that correspond to α-crystals at around 2Θ = 14.9°, 16.8°, and 19.2° corresponding to the 010, 110/220 and 203 crystal planes. All the blended film also shows peaks that correspond to the SC-crystals at around 2Θ = 12.0°, 20.8°, and 24.1° associated with 110, 300/030, and 200 crystal planes (35,36). This is in line with the DSC thermograms of the amorphous non-annealed films and the annealed films being crystalline and higher in density. The annealed SC-PLA peak patterns are similar to those reported by Sawai *et al.* of 50/50 PLLA/PDLA samples (13). The difference is that the samples by Sawai *et al.* were fully crystalline, prepared by removing the non-crystalized poly(lactide) in solution with a syringe after crystallization for 3-5 days, so only the SC-peaks were present (13). Chen *et al*. reported similar peaks on a 50/50 PLLA/PDLA sample exhibiting both the SC-PLA and HC-PLA portions (36).

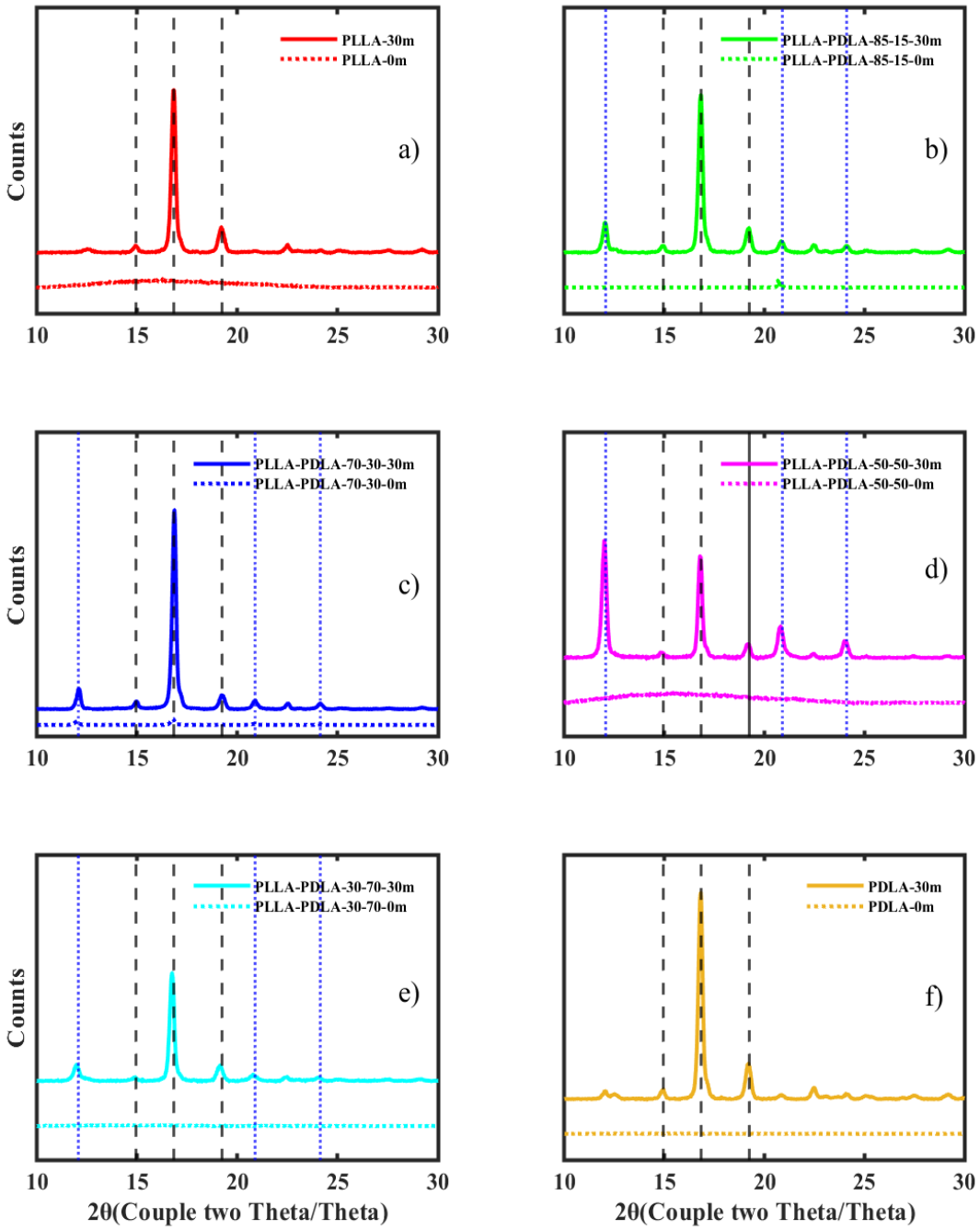

Figure 4.2. WAXD patterns of annealed **a)** PLLA-A-0,30 min; **b)** PLLA-PDLA (85/15)-A-0,30 min; **c)** PLLA-PDLA (70/30)-A-0,30 min; **d)** PLLA-PDLA (50/50)-A-0,30 min; **e)** PLLA-PDLA (30/70)-A-0,30 min; **f)** PDLA-A-0,30 min Note: The dashed black lines represent α-crystal planes, and the dotted blue lines represent SC-crystal planes.

4.4.2 Density

Density measurements were obtained using an auto-density gradient column of all the films produced and the two resins. **Table 4.1** summarizes the density, specific volume (V_s), X_c, by DSC and WAXD, and MVPC data for PLLA, blends of PLLA/PDLA, and PDLA. There is a direct correlation between the annealing time and the density. All the annealed samples have a higher density, correlating to a higher X_c (37). The non-annealed samples were amorphous, while the annealed samples were semi-crystalline with a range between 41 and 46 % total crystallinity measured by DSC. The specific volume ranges from 0.796 to 0.813 cm^3/g. **Figure 4.3a** shows the density of the film samples, non-annealed and annealed at 30 min. For the annealed samples, the density of the 50/50 PLLA/PDLA blend has the lowest density and the highest amount of formed SC-PLA. This would infer that SC-PLA has a lower density than HC-PLA since 50/50 has the largest amount of SC. **Figure 4.3b** shows the X_c measured by DSC versus density for the PLLA, 50/50 PLLA/PDLA, and PDLA samples. The non-annealed samples were amorphous, while the annealed samples were semi-crystalline. Sawai *et al.* measured the density of amorphous PLLA and 50/50 PLLA/PDLA as 1,245 and 1,244 kg/m^3 (13). Our results were similar at 1,236 and 1,240 kg/m^3. Several papers have reported the calculated density of fully crystallized SC-PLA based on unit cell constants measured by various techniques (12–15). Through the annealing process in the compression molder, we achieved between 44 and 46% X_c, and the corresponding density ranged from 1,250 to 1,257 kg/m^3. Okihara *et al.* and Cartier *et al.* reported a theoretical density of 1,270 kg/m3 for a fully 100% crystallized 50/50 blend of PLLA/PDLA (12,14). Brizzolara *et al.* and Sawai *et al.* reported a theoretical density of 1,210 and 1,340 kg/m^3, respectively (13,15). Plotting a line using the two measured points and the reported values for fully crystallized 50/50 PLLA/PDLA ($r^2 = 0.9904$) using the Okihara *et al.*

and Cartier *et al.* value of 1,270 kg/m^3 shows a good correlation. The Sawai *et al.* value of 1,340 kg/m^3 (r^2 =0.8872) shows a lower correlation. The Brizzolara *et al*. value of 1,210 kg/m^3 (r^2 = 0.6104) did not correlate well. Our measurements correlated well with the theoretical values obtained by Okihara *et al.* and Cartier *et al*. (**Figure 4.3b**). Fully crystalline PLLA was calculated to be 1,285 kg/m^3 by Hoogsteen *et al*. (38). Using the same methodology and plotting a line using the two measured points and the reported values for fully crystallized PLLA (r^2 = 1.00) shows an excellent correlation (**Figure 4.3b)**. We could not find a published density for fully crystalline PDLA, so we used the PLLA value of 1,285 kg/m^3 as a proxy since none was available. The line plotted using the two measured values and the assumed density at full crystallinity (r^2 = 0.99) also shows a good correlation, indicating that our experimental values correlate well with published data, and we should expect a fully crystalline PDLA to have a density very close to PLLA although it has a 10_3 helix chain formation. Although these values were derived from three measurements—two experimental and one theoretical — they provide a preliminary basis for calculating the density of PLLA, 50/50 PLLA/PDLA, or PDLA films produced via cast extrusion at any given crystallinity (X_c) until more comprehensive experimental data becomes available.

Table 4.1. Density, crystallinity by DSC and WAXD, and MVPC for PLLA resin, PLLA, various blends, and PDLA resin and PDLA.

						DSC			WAXD				MVPC ((kg·m)/(m²·s·Pa)) x 10^{-14}		
	n	Density Kg/m³			V_s cm³/g	$X_{c,HC}$	$X_{c,SC}$	$X_{c,t}$	X_{c-a}	X_{c-SC}	$X_{c,t}$	n			
PLLA resin	21	1253	±	3[a]	0.798	30	-	30	-	-	-	-	-	-	-
PLLA-0m	20	1236	±	9[c,d]	0.809	0	-	0	0	-	0	14	2.150	±	0.720[a]
PLLA-A160-30m	17	1257	±	2[a]	0.796	41	-	41	31	-	31	12	0.853	±	0.324[b]
PLLA-PDLA-85-15-0m	16	1241	±	4[c]	0.806	0	0	0	0	0	0	8	1.960	±	0.240[a]
PLLA-PDLA-85-15-A160-30m	19	1253	±	12[a]	0.798	31	14	44	34	8	42	10	0.508	±	0.269[b]
PLLA-PDLA-70-30-0m	13	1243	±	2[a,b]	0.805	0	0	0	0	0	0	8	2.520	±	0.590[a]
PLLA-PDLA-70-30-A160-30m	13	1256	±	7[a]	0.796	28	15	42	24	12	36	23	0.798	±	0.617[b]
PLLA-PDLA-50-50-0m	17	1240	±	5[c]	0.806	0	0	0	0	0	0	9	2.360	±	0.230[a]
PLLA-PDLA-50-50-A160-30m	17	1250	±	8[a,b]	0.800	19	24	42	15	22	37	21	0.953	±	0.341[b]
PLLA-PDLA-30-70-0m	13	1230	±	6[d]	0.813	0	0	0	0	0	0	15	2.610	±	0.370[a]
PLLA-PDLA-30-70-A160-30m	11	1257	±	9[a]	0.796	29	17	46	25	7	32	8	0.433	±	0.310[b]
PDLA-0m	10	1241	±	5[b,c]	0.806	0	-	0	0	-	0	7	2.250	±	0.600[a]
PDLA-A160-30m	11	1256	±	5[a]	0.796	43	-	43	37	-	37	8	0.732	±	0.293[b]
PDLA resin	14	1254	±	7[a]	0.797	33	-	33	-	-	-	-	-	-	-

Note: Density and MVPC values are means ± SD; means followed by a different letter are significantly different at P ≤ 0.05(Tukey-Kramer test)

Figure 4.3c shows the MVPC for all the samples grouped into two sets. All the annealed samples are statistically different from the non-annealed ones due to the semi-crystalline structure. Since permeability will not occur in the polymer's crystalline regions, a semi-crystalline film should have a better moisture barrier than an amorphous film as long as the RAF can be controlled (39,40). The RAF results from the restrictions of amorphous chain mobility due to the fixation to the basal plane of the crystalline lamellae. The RAF has specific properties which affect the mechanical and barrier properties of PLA (20,41). It also aligns with the idea that the higher the density, the lower the MVPC since higher density correlates with a higher X_c (42). Tsuji and Tsuruno reported decreasing permeability in a 50/50 PLLA/PDLA film that was solvent-cast as the X_c increased (11). We observe a near-linear decrease between X_c and MVPC. However, the slope may differ depending on the sample and the ratio of D to L-LA. The variability between amorphous and crystalline samples is pronounced, underscoring the need for additional research to thoroughly elucidate the impact of annealing on these variations.

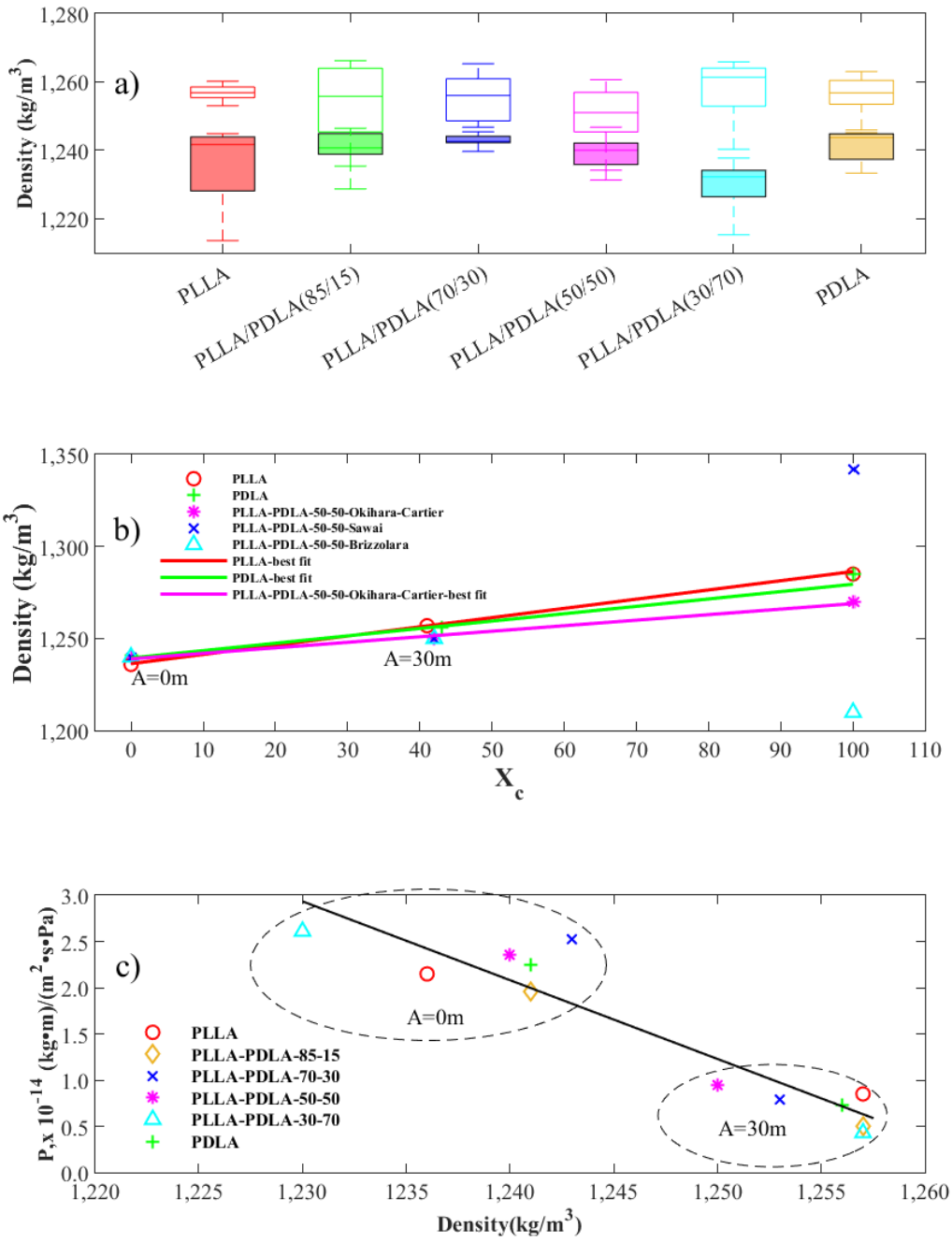

Figure 4.3. **a)** PLLA, various blends of PLLA/PDLA, and PDLA at 0 and 30m annealing times versus density. The solids bars are 0m annealing time. The translucent bars have a 30m annealing time.; **b)** % Crystallinity vs Density of PLLA, 50/50 blend of PLLA/PDLA, and PDLA at 0, 30m annealing times and fully crystallized.; **c)** Density of PLLA, blends of PLLA/PDLA, and PDLA at 0 and 30m annealing times vs. Permeability. The dashed ellipses line groups the values at different annealing times. The line is a first-order linear fitted equation across all the values.

4.4.3 Effect of annealing time on density

The effect of annealing time on density was further explored on the 50/50 PLLA/PDLA samples. **Figure 4.4** shows the DSC thermogram and XRD pattern for the blends annealed at varying times. Looking at the HC melting peak at around 175 °C, we can see the HC decreasing as time increases, as you compare the areas under the peaks. At around 225°C, corresponding to the SC melting point, the SC component increases while the amount of HC decreases, as shown in **Figure 4.4a.** The WAXD pattern in **Figure 4.4b** matches the DSC data. As the annealing time increases, the amount of SC crystallinity increases, evidenced by the peaks at around 2Θ = 12.0°, 20.8°, and 24.1° associated with 110, 300/030, and 200 crystal planes (35,36).

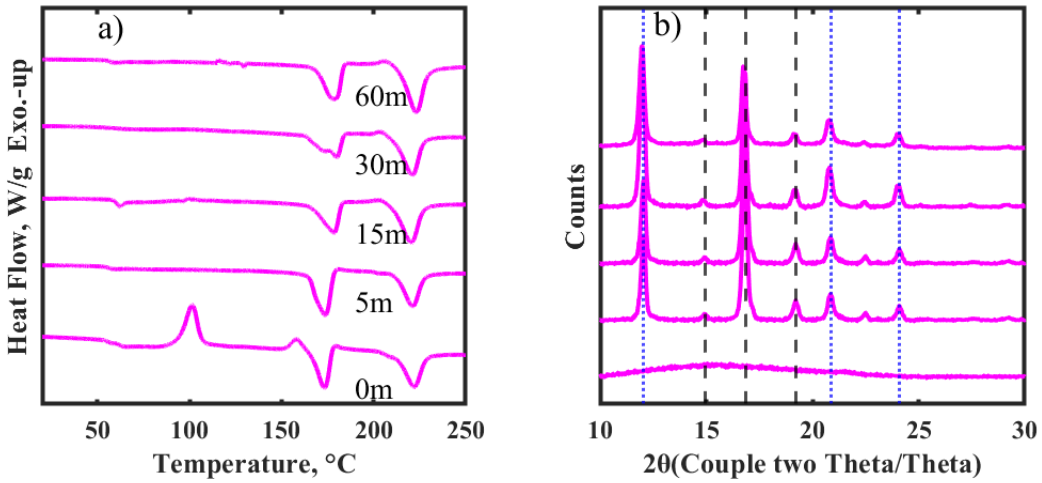

Figure 4.4. **a)** Thermogram of 50/50 PLLA/PDLA at 60,30,15,5,0 min annealing times. **b)** WAXD pattern of 50/50 PLLA/PDLA at 60,30,15,5,0 min annealing times. The identification legend for a) carries over to b). Note: In the WAXD figures, the dashed black lines represent α-crystals, and the dotted blue lines represent SC-crystals.

Table 4.2 summarizes the density, V_s, X_c by DSC and WAXD, and MVPC of the 50/50 PLLA/PDLA data at various annealing times. At 5 min and 15 min annealing times, the amount of α-crystallinity is more significant than the SC crystalline portion in the WAXD patterns, resulting in a higher density. At 30 and 60 min annealing times, the SC portion overtakes the α-

portion, decreasing the density indicated in the DSC and WAXD determinations. The MVPC of all the annealed samples between 5 and 30 min is not significantly different, suggesting that the overall amount of crystallinity dictates the improved/reduced MVPC in the early times and not the distribution between the HC and SC portions. A similar finding was reported by Chen *et al*. that the overall X_c determines the MVPC and not just the presence of SC-PLA (36).

Table 4.2. Density, Crystallinity, and MVPC for PLLA/PDLA 50/50 at various annealing times. DSC and WAXD measured crystallinity.

						DSC			WAXD				MVPC		
Annealing Time, min	n_1	**Density kg/m^3**			**V_s cm^3/g**	**$X_{c,HC}$**	**$X_{c,SC}$**	**$X_{c,t}$**	**$X_{c-\alpha}$**	**X_{c-SC}**	**$X_{c,t}$**	n_2	**((kg·m)/(m^2·s·Pa)) x 10^{-14}**		
0	**39**	**1240**	**±**	**4[a]**	**0.807**	**0**	**0**	**0**	**0**	**0**	**0**	**15**	**2.194**	**±**	**0.294[a]**
5	**28**	**1258**	**±**	**2[b]**	**0.795**	**26**	**22**	**48**	**38**	**7**	**45**	**12**	**1.005**	**±**	**0.167[b]**
15	**29**	**1258**	**±**	**1[b]**	**0.795**	**22**	**25**	**47**	**40**	**7**	**47**	**14**	**0.937**	**±**	**0.141[b]**
30	**27**	**1250**	**±**	**8[c]**	**0.800**	**19**	**24**	**43**	**15**	**21**	**36**	**21**	**0.953**	**±**	**0.341[b]**
60	**13**	**1252**	**±**	**1[c]**	**0.799**	**21**	**26**	**47**	**15**	**27**	**42**	**14**	**0.587**	**±**	**0.191[c]**

Note: Density and MVPC values are means ± SD; means followed by a different letter are significantly different at P ≤ 0.05(Tukey-Kramer test). For DSC, at least duplicate measurements were taken. For the WAXD, one measurement was taken per annealing time. WAXD is the ratio of the crystalline peaks' area to the diffraction pattern's total size. The crystalline peak areas were obtained by subtracting the amorphous halo from the entire peak areas. n_1 and n_2 are the number of films tested for density and MVPC, respectively.

Figure 4.5a shows the density of 50/50 PLLA/PDLA at 5 and 15 min annealing times were higher than at 0, 30, and 60 min. At 0 min, the films were amorphous. The 30 and 60 min values were lower, but the 30 min values have a much higher dispersity than the 60 min values. We believe dispersity values change as the material is annealed as conversion from HC to SC proceeds **(Table 4.2**). Further insights are provided below. The 30 and 60 min annealing times have the highest SC present. This may indicate that SC-PLA has a lower density than α-PLA. This reinforces the findings by Cartier *et al*. and Hoogsteen *et al*. that a fully crystalized 50/50 PLLA/PDLA film has a lower density than fully crystalized PLLA, which were reported as 1,270 kg/m^3 and 1285 kg/m^3, respectively (12,38). This may explain why the 50/50 PLLA/PDLA density and X_c at 5 and 15 min annealing times were higher than the density at 30 and 60 min

since there is more HC present in those samples than the ones at 30 and 60-min annealing times, as can be seen in the thermograms in **Figure 4.4a.** The MVPCs were not significantly different among the 5,15 and 30-min annealed samples. The non-annealed and 60-min annealed samples were significantly different, with the non-annealed sample having a higher MVPC and the 60-min annealed sample having a lower MVPC **(Figure 4.5c**).

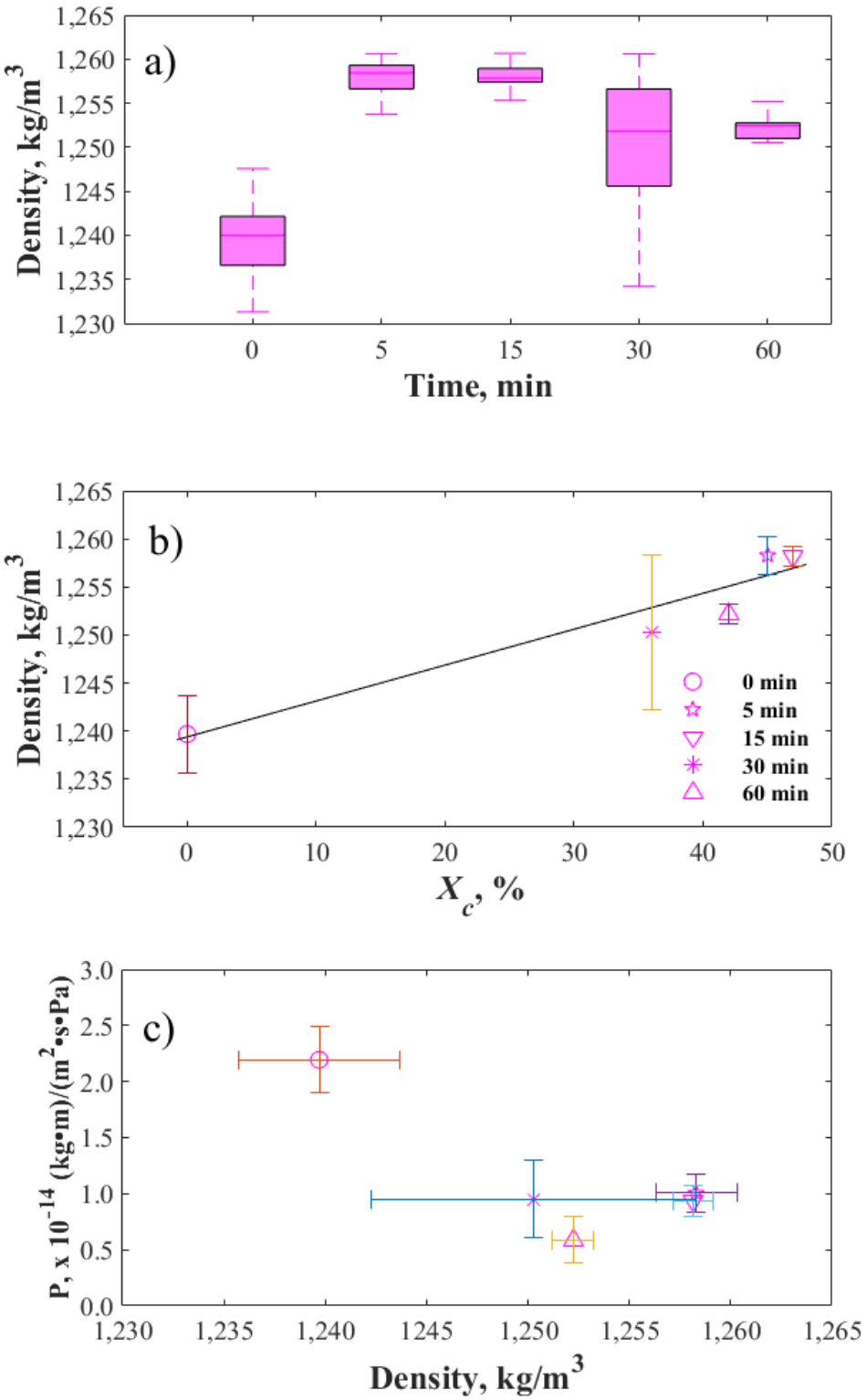

Figure 4.5. **a)** PLLA/PDLA 50/50 at varying annealing times versus density; **b)** X_c vs Density of PLLA/PDLA 50/50 at varying annealing times; **c)** Density of PLLA/PDLA 50/50 vs. Permeability at varying annealing times. The identification legend for b) carries over to c).

The lower density for SC at 30 and 60 min may also correlate with the polymer's RAF and free volume (F_v) evolution. F_v in a polymer can be visualized as the volume fraction of the sample mass not occupied by polymer chains. F_v is the gap or pores occupied between the chains of polymers (43). Hence, diffusing molecules can be located there during their permeation path, increasing permeance solubility. Sangroniz *et al*. reported on the F_v of PLLA and a 50/50 blend of PLLA/PDLA at varying annealing times using PALS. For PLLA at 0, 2, 4, and 60 min, they saw an increase in density at 2 min but a decrease at 4 and 60 min. Corresponding to the density, they saw a reduction in the F_v at 2 min but an increase at 4 and 60 min (44). The annealing times did not align with our work, but we saw the increase in density and corresponding X_c at 30 min annealing time for PLLA. They reported a decrease in F_v for the 50/50 blend of PLLA/PDLA at 30, 60, and 480 min, while the corresponding density increased starting at 30 min (44). Our study examined 0, 5, 15, 30, and 60 min annealing times, reflecting more feasible industrial applications. Furthermore, the balance of HC to SC switches between the 15 and 30-min samples, with the SC being dominant at some point after 15 min. The 30 and 60-min density increased to the initial amorphous samples, but the 5 and 15-min samples were denser.

In this study, PALS analyses were conducted on the PLLA/PDLA 50/50 samples annealed at different times to further characterize the density and crystallinity changes in terms of pore size and relative porosity (free volume fraction). PALS is a robust probe of internal porosity (26), with sensitivity to pore diameters ranging from 3 – 30 nm, and it has been used extensively to characterize polymers (45). PALS measures a material's lifetime of positrons and positronium (*P*s, the bound state of a positron and an electron). Fitting the PALS lifetime spectrum can be quite volatile when analyzing samples with two closely spaced *Ps* lifetimes and two positron lifetimes. The lifetimes and their corresponding intensities can be highly correlated,

leading to an extensive range in the individual fitted lifetimes and intensities. To reduce volatility and enhance the precision of the comparison of the PALS results between different sample annealing times, we have taken the intensity-weighted average *Ps* lifetime (thus corresponding to the single Ps lifetime fitting used by Sangroniz *et al.* (44) and converted that into pore diameter and, hence, average pore volume (using a spherical pore volume). This average pore volume and the corresponding total *Ps* intensity are plotted in **Figure 4.6a**. Pore diameters and their respective intensities are included in the electronic supplementary information (ESI) **Table A4.1**, Appendix 4A, with the error bars in parentheses.

The dependence of these two properties (i.e., pore volume and *Ps* intensity) on annealing time in **Figure 4.6a** is quite complex. Still, the underlying crystallinity evolution of the samples and the ratio between HC and SC are quite complex. The PALS data seems grouped according to the sample crystallinity and the nominal trend of increasing density observed in **Table 4.2**. The unannealed, amorphous sample has a moderate intensity of very large pores, indicating the highest porosity of the samples and, hence, the lowest density. The next grouping of samples, 5 and 15 min annealing and dominated by HC crystals, as seen in **Figure 4.6b**, presents about 10% higher intensity of pores that are about 20% lower in average volume and hence lower in overall porosity (higher density). The third grouping is distinguished by SC crystal dominance, as seen in **Figure 4.6b**. It has comparable total intensity to the amorphous film but about 14% smaller average pore volume, suggesting lower porosity by 14%. Typically, one calculates the relative porosity (and hence free volume fraction) to be proportional to the product of IV since *Ps* intensity I is usually taken to be proportional to the number density of pores (44). However, here, we hesitate in such a complex amorphous/crystalline system to rigorously assert this proportionality of IV to relative porosity. We have presented this IV graph in the ESI, but further

PALS work on HC and SC systems is required to untangle the crystals' changing size and geometry and the possible changing shape of the voids as the sample evolves with annealing time and the presence of HC and SC crystals. Hence, we also try to elucidate the effect of annealing time on the Xc of the 50/50 PLLA/PDLA samples by using MDSC and quantifying the proportion of MAF and RAF, shown in **Figure 4.6b** secondary y-axis. The results indicate that the MAF decreased as the annealing time increased while the overall X_c remained relatively constant. Consequently, the RAF increases over time. The RAF free volume can increase as the MAF free volume decreases, which appears to affect the density, as it decreases with increasing annealing time, as seen in **Figure 4.5a**. The numerical RAF data is included in **Table A4.2**, Appendix 4B. Further work could be conducted, which may differentiate the porosity from MAF and RAF, by acquiring PALS data over a temperature range down to cryogenic temperatures.

Regarding the observed variability in density at 30 minutes of annealing, the movement within the structure is constrained due to the presence of HC content and SC increases. The interphase between HC and SC is frozen and hard to move, inducing a larger amount of RAF as the structure rearranges. Consequently, the dispersity increases, tending to lower density and larger RAF. By 60 minutes, all the HC to SC is completed, and the structure becomes dominated by SC, as can be seen in **Figure 4.6b**. The dispersity decreases back to the levels it was in the 5 and 15 min samples, as seen in **Figure 4.5a**. **Figure 4.6b** shows a big difference between HC and SC, which occurs between 15 and 30 min, and the accompanying increase in RAF.

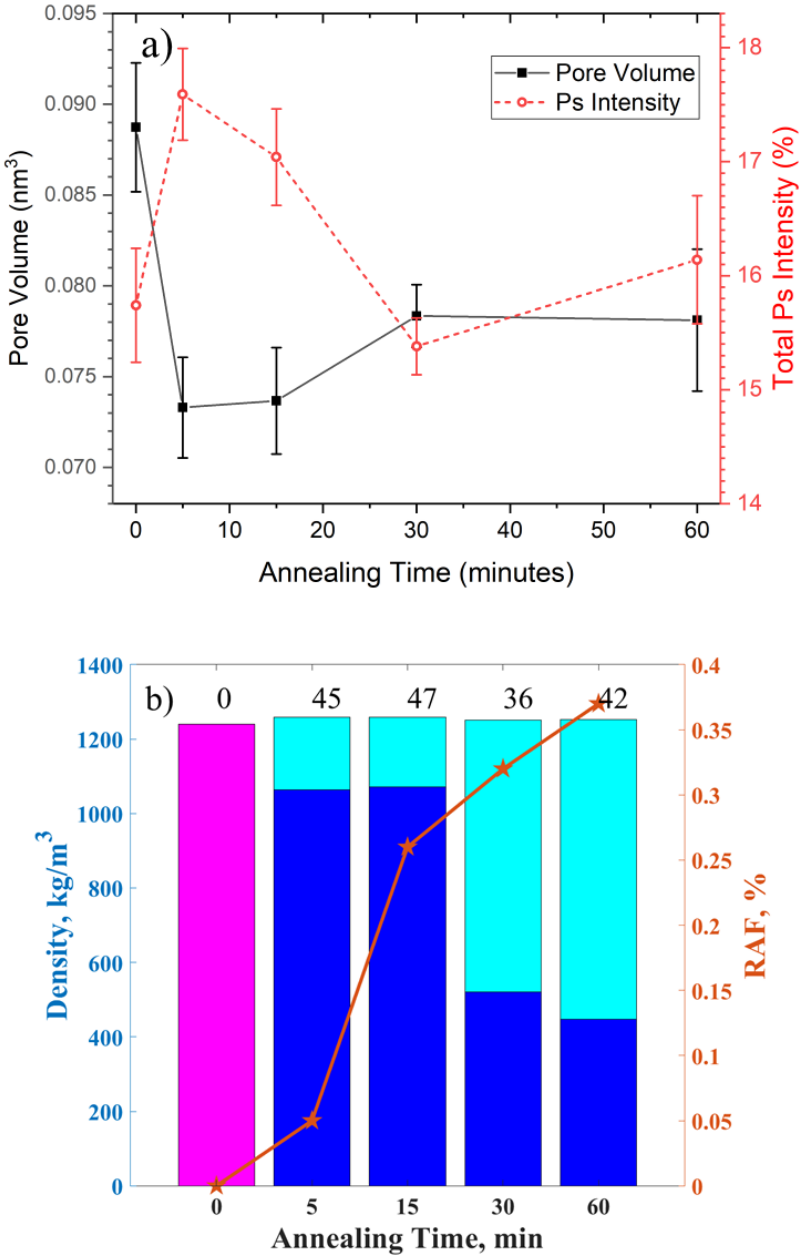

Figure 4.6. **a)** Average pore volume and total Ps intensity versus Annealing time for PLLA/PDLA 50/50 samples at A = 0,5,15, 30, and 60 min.; **b)** Density and RAF versus annealing time for PLLA/PDLA 50/50 samples at annealing times = 0,5,15, 30, and 60 min. The magenta bars represent amorphous samples, the blue bars represent the HC crystalline portion, and the cyan bars represent the SC crystalline portion. The numbers above the bars represent the total X_c.

Our research distinctly demonstrates that as PLLA, PDLA, and their blends undergo annealing, both their density and crystallinity increase, which are directly linked to

improvements in their MVPC. PLLA/PDLA blend films may benefit from an annealing process to enhance their water barrier properties. Additionally, our investigations into the PLLA/PDLA 50/50 films indicate that annealing between 5 and 30 minutes consistently improves the MVPC. However, it is not until the annealing extends to 60 minutes that we observe a further enhancement, likely due to the complete transition from HC to SC crystal dominance within the structure. Additional research utilizing PALS on HC to SC systems is essential to elucidate the dynamics of crystal size, geometry, and the potential transformation of void shapes as the sample progresses through different annealing durations and crystal structures.

4.5 Conclusion

The density, X_c, and permeability of PLLA, various blends of PLLA/PDLA (85/15,70/30, 50/50, 30/70), and PDLA were measured at 0 and 30 min annealing times. All the non-annealed samples at 0 min were lower in density and X_c and higher in permeability. The values at 0 min had a density ranging from 1,236 to 1,243 kg/m^3, with no crystallinity since they were amorphous. The values at 30 min annealing time had a density between 1,250 and 1,257 kg/m^3, with an X_c between 41 to 46%. This, coupled with the fully crystalline values of 50/50 PLLA/PDLA (1,270 kg/m^3) reported by Cartier *et al.* and Okihara *et al.* and PLLA (1,285 kg/m^3) reported by Hoogsteen *et al*. shows a strong correlation. The DSC thermograms and XRD patterns confirmed that the 30 min annealed samples were semi-crystalline with HC and SC crystals. The effect of annealing time shows that as the time increases of a 50/50 PLLA/PDLA blend, the amount of SC crystallinity increases while the amount of HC crystallinity decreases. This infers that SC-PLA is less dense than HC-PLA since the material annealed at 30 min (1,250 kg/m^3) and 60 min (1,252 kg/m^3) is less dense than at 5 or 15 min (1,258 kg/m^3). The X_c measured by DSC correlates to the density since the X_c at 30 min (42 %) is lower than 5 (47 %)

and 15 min (48 %) as well. PALS analysis showed a decrease in pore size with a trend to higher densities with increased crystalline fraction. RAF also increases as the annealing time gets longer, which is also not accounted for in the PALS analysis, making it hard to interpret on PALS alone. Future work would include confirming the density and X_c at the intermediary blends (PLLA/PDLA 85/15, 70/30, and 30/70) follow the same trend as the 50/50 blend, with the density of the 30 min annealed films being higher in SC crystallinity but lower in density. Our research offers deeper insights into the water barrier capabilities of PLLA/PDLA blends, highlighting their potential as bio-based and biodegradable films with moderate water barrier properties.

4.6 Acknowledgments

J.F.M. would like to thank the Michigan State University, College of Natural Resources, Office of Academic and Student Affairs for financial support for a Ph.D. fellowship for the Summers of 2022 and 2023. The authors also thank TotalEnergies Corbion for providing the PLLA and PDLA resins and Wanwarang Limsukon for helping create the density column and interpreting the MSDC results.

REFERENCES

1. Flexible Packaging Market Size Worth $373.3 Billion By 2030 [Internet]. [cited 2023 Nov 12]. Available from: https://www.grandviewresearch.com/press-release/flexible-packaging-market.
2. Al-Salem SM, Lettieri P, Baeyens J. Recycling and recovery routes of plastic solid waste (PSW): A review. Waste Management. 2009 Oct 1;29(10):2625–43.
3. U.S. plastic waste generation 1960-2018 _ Statista [Internet]. [cited 2022 Aug 20]. Available from: https://www.statista.com/statistics/1097290/us-plastic-waste-generation/
4. Song JH, Murphy RJ, Narayan R, Davies GBH. Biodegradable and compostable alternatives to conventional plastics. Phil Trans R Soc, B [Internet]. 2009;364:2127–39. Available from: www.bioplastics24.com.
5. Design for sustainability_ understanding compostable plastic packaging [Internet]. [cited 2022 Aug 17]. Available from: https://nutraceuticalbusinessreview.com/news/article_page/Design_for_sustainability_understanding_compostable_plastic_packaging/202066.
6. Breaking Down Compostable Packaging and Bioplastics _ Jabil. [cited 2022 Aug 3]; Available from: https://www.jabil.com/blog/compostable-packaging.html.
7. Kale G, Kijchavengkul T, Auras R, Rubino M, Selke SE, Singh SP. Compostability of bioplastic packaging materials: An overview. Vol. 7, Macromolecular Bioscience. 2007. p. 255–77.
8. Lim LT, Auras R, Rubino M. Processing technologies for poly(lactic acid). Vol. 33, Progress in Polymer Science (Oxford). 2008. p. 820–52.
9. Jin FL, Hu RR, Park SJ. Improvement of thermal behaviors of biodegradable poly(lactic acid) polymer: A review. Vol. 164, Composites Part B: Engineering. Elsevier Ltd; 2019. p. 287–96.
10. Ahmed J, Bher A, Auras R, Al-Zuwayed SA, Joseph A, Mulla MF, et al. Morphological, thermo-mechanical, and barrier properties of coextruded multilayer polylactide composite films reinforced with graphene nanoplatelets and encapsulated thyme essential oil. Food Packag Shelf Life. 2023 Dec 1;40.
11. Tsuji H, Tsuruno T. Water Vapor Permeability of Poly(L-lactide)/Poly(D-lactide) Stereocomplexes. Macromol Mater Eng. 2010 Aug 11;295(8):709–15.
12. Cartier L, Okihara T, Lotz B. Triangular Polymer Single Crystals: Stereocomplexes, Twins, and Frustrated Structures. Macromolecules [Internet]. 1997;30:6313–22. Available from: https://pubs.acs.org/sharingguidelines

13. Sawai D, Tsugane Y, Tamada M, Kanamoto T, Sungil M, Hyon SH. Crystal Density and Heat of Fusion for a Stereo-Complex of Poly(L-lactic acid) and Poly(D-lactic acid). J Polym Sci B Polym Phys. 2007 Sep 15;45(18):2632–9.

14. Okihara T, Tsuji M, Kawaguchi A, Katayama KI, Tsuji H, Hyon SH, et al. Crystal Structure of Stereocomplex of Poly(L-lactide) and Poly(D-lactide). Journal of Macromolecular Science, Part B. 1991 Mar 1;30(1–2):119–40.

15. Brizzolara D, Cantow HJ, Diederichs K, Keller E, Domb AJ. Mechanism of the Stereocomplex Formation between Enantiomeric Poly(lactide)s. Macromolecules [Internet]. 1996;29:191–7. Available from: https://pubs.acs.org/sharingguidelines

16. Product data sheet Luminy ® L130 [Internet]. 2022 [cited 2022 Jun 12]. Available from: https://www.totalenergies-corbion.com/media/yvmdsjgr/pds-luminy-l130-190507.pdf

17. Product Data Sheet Luminy® D120 [Internet]. 2019 [cited 2022 Jun 11]. Available from: https://www.totalenergies-corbion.com/media/0mxj0y1o/pds-luminy-d120-190507.pdf

18. Macnamara Jr JF, Rubino M, Daum M, Kathuria A, Auras R. Unlocking the Secrets of High-Water Barrier Stereocomplex Polylactide Blend Extrusion Films . Green Chemistry. 2024;

19. Macnamara JF, Rubino M, Daum M, Kathuria A, Auras R. Unlocking the secrets of high-water barrier stereocomplex polylactide blend extrusion films. Green Chemistry [Internet]. 2024; Available from: http://xlink.rsc.org/?DOI=D3GC04805E

20. Limsukon W, Auras R, Smith T. Effects of the Three-Phase Crystallization Behavior on the Hydrolysis of Amorphous and Semicrystalline Poly(lactic acid)s. ACS Appl Polym Mater. 2021 Nov 12;3(11):5920–31.

21. Tsuji H. Poly(lactide) stereocomplexes: Formation, structure, properties, degradation, and applications. Vol. 5, Macromolecular Bioscience. Wiley-VCH Verlag; 2005. p. 569–97.

22. ASTM D1505-18 Standard Test Method for Density of Plastics by the Density-Gradient Technique [Internet]. West Conshohocken; 2018. Available from: http://www.ansi.org.

23. Density Gradient Column Floats _ H&D Fitzgerald [Internet]. [cited 2023 Oct 13]. Available from: https://www.density.co.uk/products/gradient-column-floats/

24. ASTM F1249-20 Standard Test Method for Water Vapor Transmission Rate Through Plastic Film and Sheeting Using a Modulated Infrared Sensor [Internet]. West Conshohocken; 2020. Available from: www.astm.org,

25. Selke SEM, Culter JD, Auras RA, Rabnawaz M. Plastics Packaging Properties, Processing, Applications, and Regulations. 4th ed. Munich: Carl Hanser Verlag; 2021.

26. Gidley DW, Peng HG, Vallery RS. Positron annihilation as a method to characterize porous materials. Annu Rev Mater Res. 2006;36:49–79.

27. Kirkegaard P, Eldrup M. POSITRONFIT: A Versatile program for analysing positron lifetime spectra. Computer Physics Communication. 1972 May;3(3):240–55.

28. Dull TL, Frieze WE, Gidley DW, Sun JN, Yee AF. Determination of pore size in mesoporous thin films from the annihilation lifetime of positronium. Journal of Physical Chemistry B. 2001 May 24;105(20):4657–62.

29. Tsuji H. Poly(lactic acid) stereocomplexes: A decade of progress. Adv Drug Deliv Rev. 2016 Dec 15;107:97–135.

30. Zhai W, Ko Y, Zhu W, Wong A, Park CB. A study of the crystallization, melting, and foaming behaviors of polylactic acid in compressed CO2. Int J Mol Sci. 2009 Dec;10(12):5381–97.

31. Alhaj M, Narayan R. Scalable Continuous Manufacturing Process of Stereocomplex PLA by Twin-Screw Extrusion. Polymers (Basel). 2023 Feb 1;15(4):922.

32. Park HS, Hong CK. Relationship between the Stereocomplex Crystallization Behavior and Mechanical Properties of PLLA/PDLA Blends. Polymers (Basel). 2021 Jun 1;13(11):1851.

33. Guo M, Wu W, Wu W, Gao Q. Competitive Mechanism of Stereocomplexes and Homocrystals in High-Performance Symmetric and Asymmetric Poly(lactic acid) Enantiomers: Qualitative Methods. ACS Omega. 2022 Nov 15;7(45):41412–25.

34. Zhang M, Fan X, Guo W, Zhou H, Li Z, Ma Y, et al. Insights into Stereocomplexation of Poly(lactic acid) Materials: Evolution of Interaction between Enantiomeric Chains and Its Role in Conformational Transformation in Racemic Blends. ACS Appl Polym Mater. 2022 Aug 12;4(8):5891–900.

35. Pan P, Han L, Bao J, Xie Q, Shan G, Bao Y. Competitive Stereocomplexation, Homocrystallization, and Polymorphic Crystalline Transition in Poly(L-lactic acid)/Poly(D-lactic acid) Racemic blends: Molecular Weight Effects. Journal of Physical Chemistry B. 2015 May 28;119(21):6462–70.

36. Chen Q, Auras R, Kirkensgaard JJK, Uysal-Unalan I. Modulating Barrier Properties of Stereocomplex Polylactide: The Polymorphism Mechanism and Its Relationship with Rigid Amorphous Fraction. ACS Appl Mater Interfaces. 2023 Oct 25;15(42):49678–88.

37. Li D, Zhou L, Wang X, He L, Yang X. Effect of crystallinity of polyethylene with different densities on breakdown strength and conductance property. Materials. 2019 Jun 1;12(11).

38. Hoogsteen W, Postema AR, Pennings AJ, Ten Brinke G, Zugenmaier P. Crystal Structure, Conformation, and Morphology of Solution-Spun Poly(L-lactide) Fibers. Macromolecules [Internet]. 1990;23:634–42. Available from: https://pubs.acs.org/sharingguidelines

39. Siracusa V. Food packaging permeability behaviour: A report. Int J Polym Sci. 2012;2012:302029.

40. Sonchaeng U, Iñiguez-Franco F, Auras R, Selke S, Rubino M, Lim LT. Poly(lactic acid) mass transfer properties. Prog Polym Sci. 2018 Nov 1;86:85–121.

41. Limsukon W, Rubino M, Rabnawaz M, Lim LT, Auras R. Hydrolytic degradation of poly(lactic acid): Unraveling correlations between temperature and the three phase structures. Polym Degrad Stab. 2023 Nov 1;217.

42. Density of Plastics Material_ Technical Properties Table [Internet]. [cited 2023 Dec 27]. Available from: https://omnexus.specialchem.com/polymer-property/density.

43. Swapna VP, Abhisha VS, Stephen R. Polymer/polyhedral oligomeric silsesquioxane nanocomposite membranes for pervaporation. In: Polymer Nanocomposite Membranes for Pervaporation. Elsevier; 2020. p. 201–29.

44. Sangroniz A, Chaos A, Iriarte M, Del Río J, Sarasua JR, Etxeberria A. Influence of the Rigid Amorphous Fraction and Crystallinity on Polylactide Transport Properties. Macromolecules. 2018 Jun 12;51(11):3923–31.

45. Jean YC, Van Horn JD, Hung WS, Lee KR. Perspective of positron annihilation spectroscopy in polymers. Macromolecules. 2013 Sep 24;46(18):7133–45.

APPENDIX 4A: PALS DATA

Table A4.1 shows the Pore diameters and Relative Porosity for PLLA/PDLA 50-50 samples at varying annealing times

Table A4.1. Average pore diameters and Relative Porosity (product of IV) for PLLA/PDLA 50-50 samples: Left table, at varying annealing times at 160 ºC from 0 to 60 minutes; Right table, five separate runs on 30 minute samples to check reproducibility. The "original" sample was rerun later with 4 times more counts (Long) and then again with the sample stacks flipped over, essentially rendering it as a different sampling of films all cut from the same sheet. New long and short refer to runs on a totally different set of 30 minute films. The 30 minute data in the left table is the average of the five data tuns on that sample.

	D_{ave} (nm)/ I_{total} (%)	IV (%·nm^3)
0 min	0.553 (7) 15.74 (50)	1.40 (2)
5 min	0.519 (7) 17.59 (40)	1.29 (2)
15 min	0.520 (7) 17.04 (42)	1.26 (2)
30 min	0.537 (4) 15.38 (18)	1.20 (1)
60 min	0.530 (9) 16.14 (56)	1.26 (2.5)

30 min runs	D_{ave} (nm)/ I_{total} (%)	IV (%·nm^3)
Original	0.537 (8) 14.82 (50)	1.20 (2)
Original (Long)	0.526 (4) 15.77 (25)	1.20 (1)
Flipped	0.533 (7) 14.98 (41)	1.19 (2)
New (Long)	0.536 (5) 15.08 (33)	1.21 (1.2)
New (short)	0.527 (8) 15.67 (51)	1.20 (2)

Figure A4.1 shows the plot of PALS data, intensity times average specific pore volume as a measure of relative porosity. The 30 min data point is the average of the five data runs on those samples. This IV product can also be thought of as being proportional to the fractional free volume of the sample.

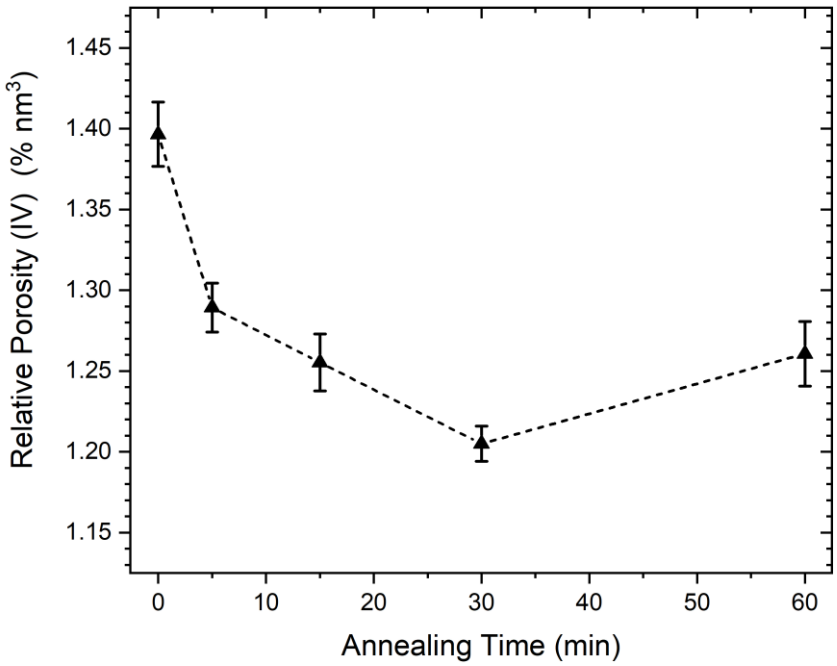

Figure A4.1. Plot of PALS data, intensity times average specific pore volume as a measure of relative porosity. The 30 min data point is the average of the five data runs on those samples. This IV product can also be thought of as being proportional to the fractional free volume of the sample.

APPENDIX 4B: MDSC DATA

Table A4.2 shows the MDSC data for the PLLA/PDLA 50-50-A samples.

Table A4.2. MDSC data for the PLLA/PDLA 50-50-A samples.

	C_p	T_g, °C	MAF, %	$T_{m\text{-}HC}$, °C	$T_{m\text{-}SC}$, °C	$X_{c\text{-}HC}$	$X_{c\text{-}SC}$	RAF,%
PLLA/PDLA-50-50-A160-5-mod-a	0.3140	52.60	0.57	174.04	223.82	0.17	0.22	0.05
PLLA/PDLA-50-50-A160-15m-mod-a	0.2010	60.07	0.36	178.85	224.02	0.16	0.20	0.28
PLLA/PDLA-50-50-A160-15m-mod-b	0.2222	59.88	0.40	177.36	224.66	0.17	0.19	0.23
PLLA/PDLA50-50-A160-30m-mod-a	0.1761	61.07	0.32	176.23	224.63	0.17	0.20	0.32
PLLA/PDLA-50-50-A160-60m-mod-a	0.1450	59.87	0.26	180.01	225.42	0.19	0.18	0.37

CHAPTER 5: BIODEGRADABLE AND TRANSPARENT WATER AND OXYGEN BARRIER MULTILAYER FILM

A version of this chapter was submitted on 6/26/24 as:

Macnamara, J., Rubino, M., Daum, M., Kathuria, A., Auras, R. Biodegradable and transparent water and oxygen barrier multilayer film, *Applied Polymer Materials*, *ACS*.

5.1 Abstract

Plastic waste remains a critical environmental challenge, with 14.5 million tons generated in 2018 alone, 85% of which ended up in landfills in the US. A key contributor to this issue is the non-recyclability of multilayer laminations; when different materials are fused, they cannot be easily separated for recycling, thereby exacerbating municipal solid waste problems. This study explores an innovative approach by laminating base layers of poly (3-hydroxybutyrate-*co*-3-hydroxyvalerate) or stereocomplex-polylactic acid with a biodegradable coating of polyvinyl alcohol and nanoclay to PLA. Since all the materials are biodegradable, the final structure is also anticipated to be biodegradable in compost environments opening an additional regenerative end-of-life scenario. The effectiveness of these biodegradable layers was assessed by measuring the moisture vapor transmission rate (MVTR) and oxygen transmission rates (OTR), which ranged from 20 to 30 g/(m^2·d) and 54 to 69 cc/(m^2·d), respectively. Through optimizing, theoretical rates were estimated at an MVTR of 10 g/(m^2·d) at 38° and 90% RH and an OTR of 60 cc/(m^2·d) at 23 °C and 50% RH, showcasing low permeability for several biodegradable products. Additionally, barrier activation energy was measured across four selected structures, ranging from 41 to 58 kJ/mol, indicating that the developed material can potentially package several types of food products in a biodegradable format—a significant advancement from previous plastic and packaging industry capabilities.

5.2 Introduction

Flexible single-use plastic (FSUP) films, composed of single or multilayer plastic sourced from fossil-based materials, present significant recycling challenges. Predominantly, they contribute to landfill waste in the US and environmental pollution in areas lacking robust waste management systems. In 2018, the US generated an alarming 292 million tons of municipal solid waste (MSW), a significant rise from 150 million tons in 1980 (1). Containers and packaging, including plastic, constituted roughly one-quarter of this total, amounting to 82 million tons. Plastic waste comprised 18% of this packaging waste, equivalent to 14.5 million tons (2). By 2022, half of the plastic produced in the US was for single-use purposes, leading to its immediate disposal. Shockingly, only 5% of this single-use plastic was recycled, 10% was incinerated, and a staggering 85% ended up in landfills (3,4). With the global market for plastic packaging projected to soar from USD 265 billion in 2022 to USD 385.5 billion by 2028, the implications for future MSW generation are profoundly concerning (5).

Among the plastic packaging applications, the global market for flexible packaging laminations is projected to surge from USD 6.3M in 2024 to USD 9.7M in 2034 (6). Laminations enhance flexible packaging by merging the properties of individual layers, boosting physical durability, aesthetic appeal, and barrier effectiveness beyond what single layers can achieve (7). However, this innovation has a significant environmental drawback: the fused layers in these FSUP films complicate recycling processes, rendering the films inseparable and frequently consigned to landfills, exacerbating the MSW crisis (8).

Significant research efforts are underway to develop multilayer structures that are either fully biodegradable or recyclable (9,10). A key to recycling such structures is consistency in material composition across all layers, with only a minimal presence of ancillary components

(11). Achieving the necessary barrier properties using uniform materials remains a formidable challenge. For instance, while polyethylene (PE) offers excellent moisture resistance, it falls short of providing an adequate oxygen barrier. An alternative approach involves engineering multilayer structures where every layer is biodegradable, thus enabling the entire structure to break down naturally and avoid contributing to landfill accumulation.

There are various biodegradable options in the marketplace now. Among the companies producing these multi-layer biodegradable structures are several Asian, North American, and European companies. Futamura is a Japanese company that makes cellophane, but to have a barrier or be heat sealable, it must be coated with a nitrocellulose polyvinylidene chloride (PVDC) coating. PVDC is banned in Europe and certain states within the US (12). The nitrocellulose-coated options do not have a good barrier, which limits their applications. Celplast Metallized Products, a Canadian company, offers two grades of metallized polylactic acid (PLA), Duramet® PLA and Enviromet® PLA. The moisture vapor transmission rate (MVTR) and oxygen transmission rate (OTR) barriers range from 1 to 8 g/(m^2·d) and 4.6 cc/(m^2·d), respectively, but the conditions are not specified (13). According to Celplast Metallized Products, the company purchases PLA on the open market and metallizes the film with aluminum to increase the barrier; the product inside the package cannot be seen due to the metallization. Plastic Suppliers Incorporated, an American company, makes Earthfirst® biopolymer films and offers a variety of PLA films, also metallized or coated, with MVTR and OTR barriers ranging from 3.9 to 232 g/(m^2·d) (38°C/90% RH) and 7.8 to 400 cc/(m^2·d) (23 °C /0% RH), respectively, depending on the thickness and configuration (14–16). A European consortium, BIO4MAP, developed a biodegradable coextruded coated structure of PLA/tie/polyvinyl alcohol (PVOH)/tie/PLA/wax-based coating to package fresh pasta and

different types of cheese (17). Barrier levels have not been reported, but cheese and fresh pasta require oxygen barrier levels as low as 1 cc/(m^2·d) (23 °C/90% RH) and moisture barrier levels as low as 5 g/(m^2·d) (38 °C /0% RH). ProAmpac, also an American company, has a line of commercial products called Proactive Compostable®, with moisture and oxygen barriers of 7 g/(m^2·d) and 0.8 cc/(m^2·d), respectively, but the conditions are not specified (18). These products are laminations of either paper or PLA to a metallized film to obtain the barrier levels. Other structures are available but proprietary, and public information about their components is lacking.

Since laminations involve multiple layers, it is advantageous to examine individual biodegradable materials that maximize moisture or oxygen barrier properties. By strategically combining these materials, we can effectively harness the enhanced properties of both barriers in the final product.

Poly (3-hydroxybutyrate-*co*-3-hydroxyvalerate) (PHBV) is a biodegradable thermoplastic produced naturally by bacteria (19). It exhibits a reasonable moisture barrier similar to non-biodegradable films, such as polyethylene terephthalate (PET) and polyvinyl chloride (PVC) (20). PHBV, part of the polyhydroxyalkanoates (PHA) family, is reported to have better moisture barrier properties than most biodegradable plastics (21); however, its oxygen barrier properties are not as reasonable. Zembouai *et al.* reported the MVTR of PHBV at 103 g/(m^2·d) normalized to 1 mil at 23 °C 50% RH (22). Crétois *et al.* incorporated up to 10 % nanoclay (Nc) into PHBV via twin screw extruding pellets and then compression molded a film to examine the barrier properties. The oxygen barrier properties remained unchanged while the moisture barrier decreased. The authors suggested that the effects of tortuosity and degradation, in combination, contributed to the oxygen barrier remaining the same. They also claimed that the increase in

moisture was due to the hydrophilic nature of the nanofiller, inducing a rise in water solubility in the Nc, thus increasing the permeability (23).

PLA exists in two enantiomeric forms, L-PLA (PLLA) and D-PLA (PDLA). When combined, these forms make stereocomplex PLA (SC-PLA), which has some enhanced properties over PLA, namely thermal stability and mechanical properties (24,25). Several studies on SC-PLA have examined the characteristics of moisture barriers. Tsuji and Tsuruno compared PLLA, PDLA, and a 50-50 PLLA/PDLA blend of solvent-cast films; the best results were with the 50-50 PLLA/PDLA annealed films (26). The PLLA/PDLA film was annealed for 5 min at varying temperatures, ranging from 205 to 255 °C; as the crystallinity (X_c) increased, the barrier decreased, with the highest crystallinity and barrier achieved at 205 °C, with an MVTR of 98.1 g/(m^2·d), at 25 °C/90% RH, normalized at 25 microns (26). Macnamara *et al.* produced various blends of PLLA and PDLA by extrusion casting that were annealed from 5 to 30 min, with an MVTR ranging from around 70 to 230 g/(m^2·d) at 25 °C/90%RH, normalized to 25.4 microns, depending on the annealing time and the blend (27).

Polyvinyl alcohol (PVOH) is a biodegradable polymer known for its oxygen barrier and biodegradable properties (28). The hydrogen bonding between the polymer chains and its crystalline structure makes it an ideal oxygen barrier. However, due to its hydrophilic nature, the hydrogen bonding also makes PVOH susceptible to water, so it has to be protected within a structure to prevent water from affecting the absorption and diffusion of other gases and degrading the polymer (29).

Incorporating Nc is an excellent way to improve the oxygen barrier of various polymer structures. Clay is impermeable, and its large aspect ratio increases the tortuosity of a gas molecule through a polymer, thereby increasing the oxygen barrier (30). Yue *et al.* reported

coating cellulose with a PVOH-Nc coating, lowering the OTR from 10.44 to less than 1 cc/(m^2 • d) at 23 °C/0%RH (31). Schiessl *et al.* reported that a PVOH-Nc coating on polypropylene (PP) resulted in a barrier improvement factor of 12 for the permeability coefficient of oxygen (32).

While several alternatives exist for compostable FSUP multilayer films, transparency and non-metallization remain rare. This research innovates by employing PHBV and SC-PLA base films produced through cast extrusion and enhancing them with a PVOH-Nc coating to improve the oxygen barrier. Subsequently, these coated films are laminated to PLLA with a compostable adhesive to form a sealant layer. All components are biodegradable (33–36), suggesting that the entire structure should also be biodegradable, although further testing will be necessary for confirmation. Our approach is pioneering because it maintains complete biodegradability, provides adequate oxygen and moisture barriers, and avoids the previously stated issues with metallization or using PVDC. The moisture barrier properties were examined under conditions of 37.8 °C/90% RH, 23 °C/85% RH, and 11 °C/85% RH, enabling the calculation of barrier activation energy. Additionally, the oxygen barrier properties were assessed at 23 °C/50% RH, underlining the robustness of this novel structure.

5.3 Materials and Methods

5.3.1 Materials

The PLA resins were supplied by TotalEnergies Corbion (Netherlands), PLLA (Luminy® L130(≥ 99%(L-isomer)) and PDLA (Luminy® D120 (≥ 99%(D-isomer)) (37,38). The PHBV resin was purchased from TianAn Biopolymer (China), grade Y1000P (39). Kuraray (Japan) provided the PVOH, Exceval™ HR3010, a white powder with a degree of hydrolysis of 99.2 mol % (40). The adhesive, Flextra® SF-1000CP/XR-2000XP, is a two-part polyurethane, 100% solids compostable adhesive supplied by H.B. Fuller (USA) (41). Organomodified

montmorillonite (OMMT), Nanomer® 1.34 TCN was obtained from Nanocor (USA) (42), consisting of 80% montmorillonite (MMT) and 20% of surfactant. Dimethyl sulfoxide (DMSO), a spectrophotometric grade of 99.9+%, was purchased from Alfa Aesar (USA).

5.3.2 Film Processing

PLLA and PDLA were dried in a vacuum oven (VWR International, USA) at 80 °C and 24 in-Hg for at least 12 h before processing to minimize hydrolytic degradation due to moisture during processing (37,38).

PLLA and PDLA films were produced. Then, the two resins were mixed, by weight, in ratios of 50-50 and 85-15 for PLLA/PDLA before being introduced to the extruder. Each film was extruded on a pilot-scale microextruder (Randcastle Extrusion Systems, USA). The processing conditions are detailed elsewhere (27).

PHBV was run in the same microextruder to produce cast films, and the processing conditions are summarized in the electronic supplementary information (**ESI**) in **Table A5.1**, Appendix 5A.

5.3.3 Thermal Annealing

The PHBV and the 50-50 and 85-15 PLLA/PDLA film samples were annealed in a hydraulic press (model number QL438-C, PHI, USA) heated to 160 °C. Each sample was approximately 25.4 × 16.5 cm^2. Two 25.4 × 25.4 cm^2 plates lined with non-stick aluminum foil were used, and the samples were placed between the two plates of the press. The samples were annealed for 3, 5, or 30 min and then cooled at room temperature. After cooling, the samples were stored at -20 °C to reduce polymeric chain mobility and any possible morphological changes associated with it so they could be analyzed later.

5.3.4 Plasma Treatment

A PE-25 Series Plasma system (Plasma-Etch, USA) treated the films to increase the surface tension above 44 dynes/cm before applying the coating. Treating the film increases surface tension, allowing the coating to wet out effectively on the film's surface (43). Before treating the film, the surface tension was less than 34 dynes/cm, which was too low for the coating to wet out on the substrate. The coated barrier and sealant layers were treated before coating or laminating. The plasma treatment time was set to 8 seconds [43].

5.3.5 Coating Preparation

The coating was prepared stepwise. PVOH and OMMT Nc were added to DMSO at 5% and 2.5%, respectively, while stirring at room temperature. The solution was heated to 95 °C, stirred for 2 hours, and then slowly cooled to room temperature. It was used at room temperature to coat the films; it was continually stirred between coating applications.

5.3.6 Coating and Laminating

A K303 Multicoater (RK Printing Instruments, UK), with various size Mayer rods, was used for coating the film substrates with a coating or adhesive, depending on the step in the process. The speed setting was 1 m/min. A #3 Mayer rod was used for the coating process. The coating was applied onto the barrier film, either SC-PLA or PHBV film, in multiple layers, allowing each layer to dry for a minimum of 6 hours before applying the next layer; four layers of the coating were used for each substrate. The coated substrates were dried in a PT-1 Peltier effect temperature-controlled portable cabinet with a Pelt-5 Temperature Controller (Sable Systems, USA) set to 45 °C.

The coating combination was PVOH and OMMT dispersed in DMSO for lab testing simplicity, but other greener solvents, such as deionized water, could be explored in future

works. Chandio *et al.* were able to disperse MMT and PVOH in water but mentioned that dispersion was challenging at levels above 5 % MMT (44). Initially, we attempted to use deionized water to coat the films; however, despite plasma treatment, the films did not exhibit satisfactory wettability. This led us to switch to a solvent with lower surface tension. Specifically, water has a surface tension of 72 dynes/cm, whereas DMSO offers a significantly lower surface tension of 43.5 dynes/cm, improving the coating application (45). After the coating was applied and subsequently dried, the adhesive was applied, and the layer of PLLA was placed on top. The structure was then placed into the compression molder at 55° C for 5 min to simulate a heated nip roller. A #2 Mayer rod was used for the adhesive application. The samples were then stored under pressure for 3 days to cure.

5.3.7 UV/VIS Measurement

A UV/VIS spectrophotometer (model 1800, Shimadzu, Japan) measured film transparency(%T) from 200 to 800 nm. Three samples of each film, including the base and laminated samples, were tested.

5.3.8 Barrier Properties

The barrier properties of each structure were measured with a Permatran-W® 3/34 (Mocon, USA) for WVTR, determined at 37.8 °C/90% RH, 23 °C/85% RH, 11 °C/85% RH, and an Ox-tran® 2/20 at 23 °C/50% RH according to ASTM F1249-20 (46) and ASTM D3985-17 (47) for MVTR and OTR, respectively. A foil mask was used, with a sample size of 3.14 in^2 exposed to the sensor. Six or more replicates were evaluated for each film sample.

5.3.9 Differential Scanning Calorimetry (DSC)

Thermal analysis was conducted on the base films chosen as the likely candidates to determine the X_c and the split between the HC and SC crystalline portions for the SC-PLA samples.

The DSC thermogram procedure was adapted from Macnamara *et al.* (48). Three replicates were tested for each film produced. For the X_c calculation of the SC-PLA samples, 139 J/g and 142 J/g (49) were used for the heat of fusion (ΔH) of 100% HC-PLA and SC-PLA, respectively. For the X_c calculation of PHBV samples, 143 J/g (50) was used for the ΔH of 100 % crystalline HPBV.

5.3.10 Scanning Electron Microscope (SEM)

Cross-sectional scans of the four laminated structures were captured using a scanning electron microscope model JSM 6610LV (Jeol USA Inc., USA). The operating conditions were 12 kV accelerated voltage and vacuum pressure of 1.33 x 10-5 Pa with a magnification of about 330x. The samples were sputtered with gold using a current of 20 mA for 3 min.

5.3.11 Data Analysis

MATLAB® (Mathworks, USA) and Microsoft Excel (Microsoft®, USA) were used to collect the data and construct the graphs. Statistical Analysis was conducted using SAS® version 9.4 (SAS® Institute Inc., USA). An analysis of variance (ANOVA) was completed on the permeability measurements to compare the OTR and MVTR barrier values at a significance level of $P \leq 0.05$ using the Tukey-Kramer test.

5.4 Results and Discussion

An extensive initial screening was done on several base substrates to determine which substrates had the lowest oxygen and moisture barrier levels before applying the coating. Several variables were considered. First, it had to be a compostable material. The actual oxygen and moisture barrier was measured for each deemed viable candidate. The biodegradable polymer had to be a commercially viable material to process on conventional converting equipment. Cost was also considered, but it was not a variable for which a potential candidate was eliminated. Most films were extruded on the cast film pilot line and annealed on the hydraulic press at the

Michigan State University School of Packaging. A few of the screened biodegradable films were commercial products, including Poly-butylene succinate (PBS), Poly(butylene-co-adipate terephthalate) (PBAT), and Polycaprolactone (PCL).

Figure 5.1 shows the candidate films that stood out as the lead contenders used from the evaluation. **Figure 5.1a** summarizes the moisture barrier levels, and **Figure 5.1b** summarizes the oxygen barrier levels. The split between HC and SC X_c in the films is reflected in the bars in the figures. The HC is in blue, and the SC is in cyan. **Table A5.2,** Appendix 5B summarizes the actual X_c values for the films. **Figure A5.1**, Appendix 5B shows the MVTR of all the screened candidate films, and **Tables A5.3** and **A5.4**, Appendix 5B provide the MVTR and OTR for all the screened candidates. PHBV performed the best in the MVTR screening exercise with a normalized MVTR of 48.04 g/(m^2·d) at 38°C and 90% RH, so it was selected as one of the base films. Corre *et al.* reported PBHV having an MVTR barrier of 54 g/(m^2·d) at 23 °C and 50% RH, similar to our values (51). PHBV film annealed for 5 min did not have a better barrier than the non-annealed PHBV film, so the non-annealed sample was selected. The MVTR data for the PHBV annealed sample (PHBV-A5min) is included in **Table A5.3**, Appendix 5B. The X_c was measured to be 59% for the as-cast PHBV and 66% for the annealed PHBV, so there was no appreciable difference between the two films, which is likely why there was no improvement in the MVTR. The X_c values for the films are included in **Table A5.2,** Appendix B. Zhou *et al.* reported the X_c of solution-cast PHBV at 56.8%, similar to what we determined (52). Most of the annealed SC-PLA structures were similar in moisture barrier values, so we selected PLLA/PDLA 50-50 - A160 base film at both 3 min and 30 min annealing times. We also selected 85-15 PLLA/PDLA-A3 min as an alternate film due to its lower proportion of PDLA and to reduce the annealing time to make production more commercially viable. PDLA is more costly than PLLA

and less commonly used in production. We expected the base film to add a moisture barrier to the structure. None of the candidates had a low oxygen barrier, so we coated the base film with a PVOH-Nc coating to add an oxygen barrier to the structure. The variability observed in the OTR measurements seemed related to the low number of measurable samples and sample conditions. Chandio *et al.* coated PVOH-Nc onto PET but used montmorillonite (MMT) clay instead of the OMMT clay used in this study (44). The authors evaluated clarity and moisture barrier characteristics but not the oxygen barrier. The presence of the clay did not affect transparency; all samples had a transparency of around 92% in the white light region. The MVTR of the coated structure improved by up to 86% over pristine PVOH, but the authors reported that films with 6 wt.% clay, where they saw the maximum benefit, were difficult to process. Li *et al.* reported up to a 40% improvement in the oxygen barrier of a PLA/OMMT film produced by mixing the PLA and OMMT and then compression molding the film (53).

PLLA served as our sealant layer, which is why it is included in **Figure 5.7**. PLLA is commonly used as a sealant layer, and Plastic Suppliers, Inc. manufactures grade 3002 in 20 microns for such an application (54). Hence, we decided to produce a three-layered structure.

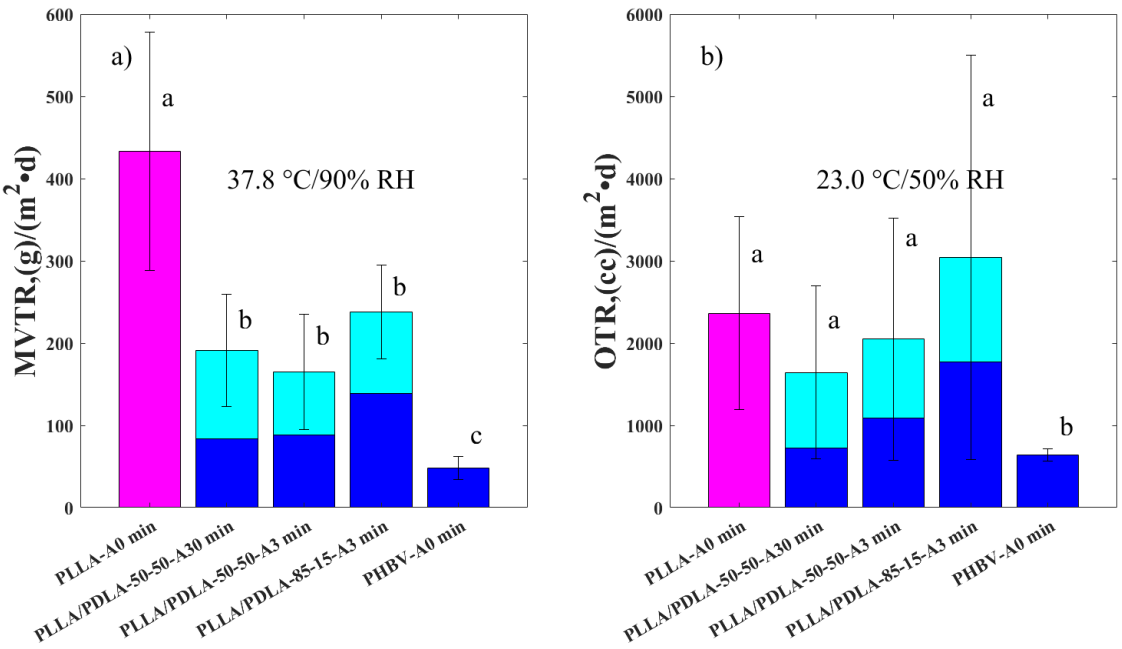

Figure 5.1. **(a)** MVTR values of potential candidate films normalized at 25.4 microns, and **(b)** OTR values of potential candidate films normalized at 25.4 microns. The magenta bars represent amorphous samples, the blue bars represent the HC crystalline portion, and the cyan bars represent the SC crystalline portion. Note: values followed by a different letter are significantly different at $P \leq 0.05$ (Tukey-Kramer test).

Once the base substrates were selected, the films were plasma treated, and the coating was applied via Mayer rod to the film in multiple stages. After coating, it was laminated to PLLA. The final structures assembled are summarized below:

1-55-micron PLLA/PDLA-50-50-A30 min/29-micron PVOH-Nc/Adh/49-micron PLLA
2- 67-micron PLLA/PDLA-50-50-A3 min/24-micron PVOH-Nc/Adh/63-micron PLLA
3-81-micron PLLA/PDLA-85-15-A3 min/25-micron PVOH-Nc/Adh/63-micron PLLA
4-48-micron PHBV/20-micron PVOH-Nc/Adh/63-micron PLLA

After 3 days of curing, the 4 main structures were tested for UV/VIS transmission and oxygen and moisture barrier levels. **Figure 5.2** shows samples of the four completed structures and their % transmission values at 600 nm, indicating their transparency (55). Film 4 was hazier than the other three structures, indicated by the lowest transmission value (22%). **Figure A5.2** shows all the films' transmission rates versus wavelength, including the base films. The base

films had slightly higher transmission values at 600 nm than the laminated structures. **Table A5.5**, Appendix 5C summarizes the % T values at 600 nm for various candidate films. **Figure A5.3,** Appendix 5C shows SEM pictures of the four structures where the three layers can be distinctly seen.

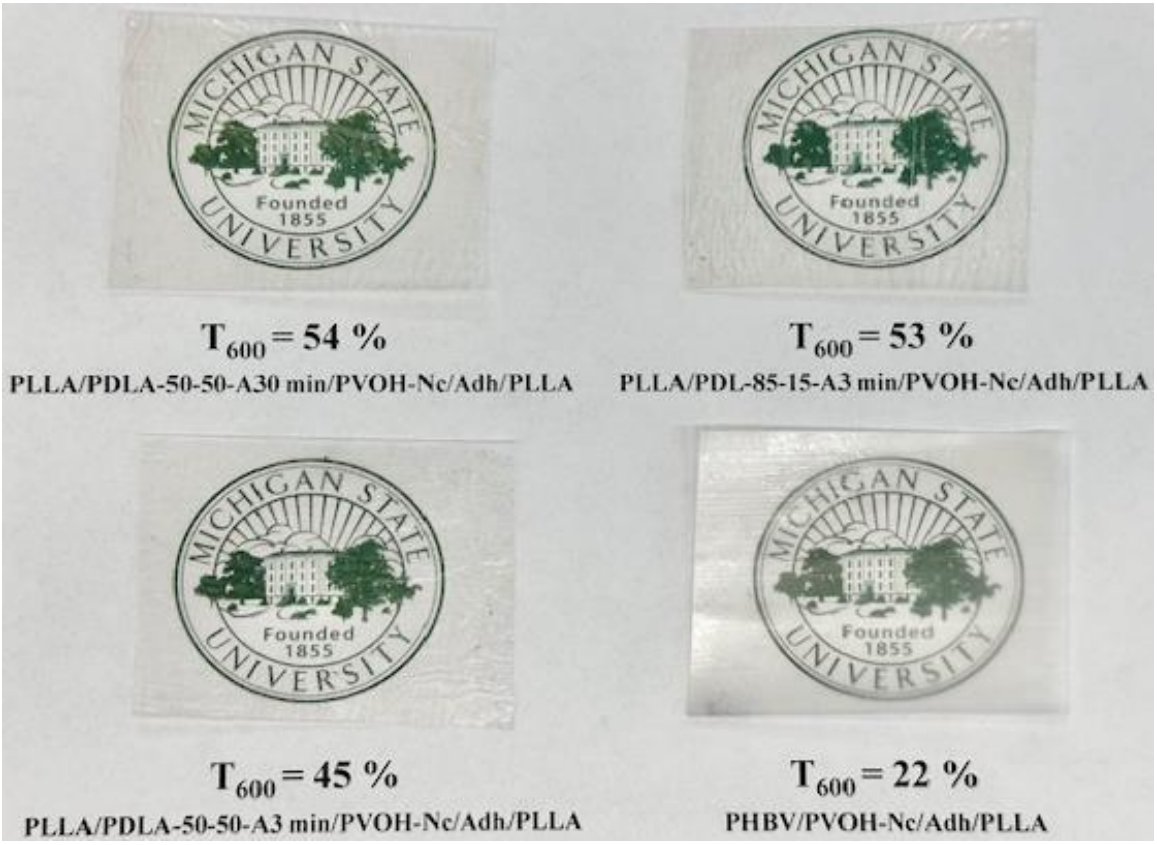

Figure 5.2. PLLA/PDLA 50-50-A30/PVOH-Nc/PLLA, PLLA/PDLA 85-15-A3/PVOH-Nc/PLLA, PLLA/PDLA 50-50-A3/PVOH-Nc/PLLA, PHBV/PVOH-Nc/PLLA films along with %T at 600 nm.

Figure 5.3 shows the MVTR and OTR values obtained for the four laminated structures at three testing conditions. All MVTR values were similar, but there was a statistical difference at 37.8 °C/90% RH between the structure with PLLA/PDLA 85-15 and those with PHBV and PLLA/PDLA 50-50. This finding aligns with the fact that the PLLA/PDLA 85-15 base layer was the thickest of the four materials, at 81 microns, and most of the moisture barrier comes

from the base film layer. Comparing the MVTR of the base layers of the four materials shows no significant difference between any of the four materials, which reinforces the fact that the moisture barrier is all related to the base layer (i.e., PLLA/PDLA 85-15, PLLA/PDLA 50-50, and PHBV). The OTR of the four structures were not statistically different, which is unsurprising since the coating layer is similar in all of them, and the oxygen barrier is mainly provided by the PVOH-Nc layer. A statistical difference between the OTR of the base films and the final structures reinforces that the coating layer adds the oxygen barrier to the structures.

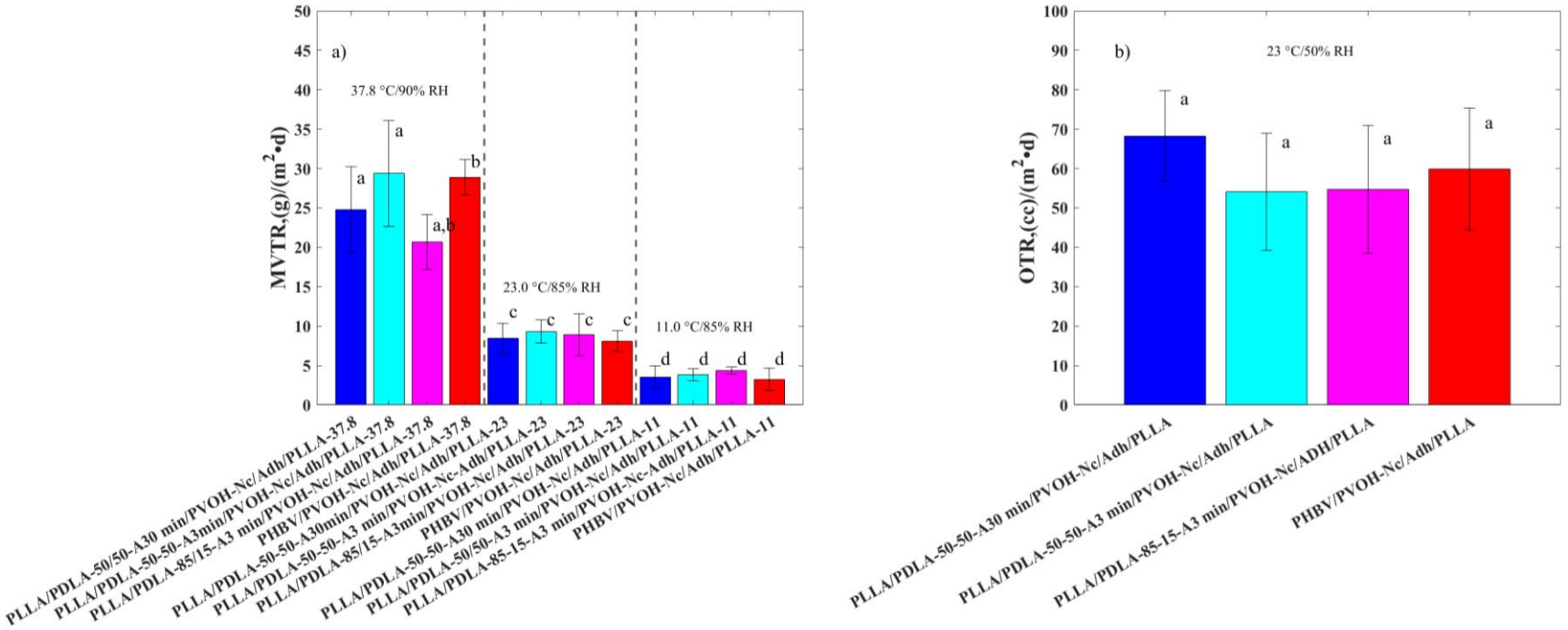

Figure 5.3. **a)** MVTR values of the four laminated structures at 37.8 °C/90%RH, 23.0 °C/85%RH, and 11.0 °C/85%RH; **b)** OTR of the four laminated structures at 23.0 °C/50%RH. Note: values followed by a different letter are significantly different at $P \leq 0.05$ (Tukey-Kramer test).

The contribution to the barrier layers can be estimated using **Equation 5.1** for multilayer structures, and individual barrier contributions can be calculated.

$$\frac{l_t}{P_t} = \frac{l_1}{P_1} + \frac{l_2}{P_2} + \frac{l_3}{P_3} \qquad \textbf{(5.1)}$$

where l_t is the total thickness of the material l_1, l_2, and l_3 are the thicknesses of layers 1, 2, and 3, respectively; P_t is the permeability coefficient of the overall structure; and P_1, P_2, and P_3 are the permeability coefficients of layers 1, 2, and 3, respectively.

We can optimize the PHBV structure using the equation above and the measured barrier values, leading to practical applications in the food industry. In the screening experiments, the normalized MVTR of 25.4-micron PLLA and PHBV films were 432.97 and 48.04 g/(m^2·d), respectively, at 38 °C/90% RH. The sealant layer of PLLA can also be decreased to 20 microns since it is already a commercial-grade film. Negating the coating layer, since it has a negligible contribution to the MVTR, if we reduce the thickness of the sealant layer to 20 microns and increase the thickness of the PHBV base layer to 127 microns, the MVTR would decrease to 10.23 g/(m^2·d) 38 °C/90% RH, with an OTR of 59.87 cc/(m^2·d) at 23 °C/50% RH. The final structure would be 127 microns PHBV/(20 microns PVOH-Nc)/20 microns PLLA, for a total thickness of 167 microns. This is an acceptable MVTR level in food packaging applications for products like oatmeal, certain spices, or cheeses, and the structure thickness is in the commercialized acceptable range. Otherwise, we can optimize the OTR if we reduce the thickness of the sealant layer to 20 microns and increase the thickness of the PVOH/Nc layer to 99 microns. The OTR would decrease to 14.61 cc/(m^2·d) at 23 °C/50 % RH, with an MVTR of 24.28 g/(m^2·d) at 38 °C/90% RH. The final structure would be 48 microns PHBV/(99 microns PVOH-Nc)/20 microns PLLA, for a total thickness of 167 microns. This structure would suit other food packaging applications, like pretzels and refrigerated meats. The optimized values

were calculated at 37.8 °C/90% RH. The MVTR was also measured at 23 °C/85% RH and 11 °C/85% RH; a downward trend in the MVTR was observed as the temperature decreased, down to <5 ($g/m^2 \cdot d$) for all the structures at 11 °C/85% RH. The OTR was not measured at the lower temperatures due to equipment constraints, but we would expect a similar decrease. This would open the door for using the structures to pack additional refrigerated products. **Figure 5.4** shows the MVTR versus OTR for the four multi-layer structures and the optimized versions. The area within the triangle (indicated by the dashed lines) represents the barrier levels we can theoretically produce by altering either the base film or the coating thickness while maintaining the overall thickness at 167 microns. Several food product groups are included in the figure to show where the structures fit the food group packaging requirements. Rocca-Smith *et al.* evaluated a 3-layered structure of PLA/wheat gluten (WG)/PLA, altering how the WG was produced and comparing the effect to corona treating the PLLA film. A hot press was used for the lamination, which increased the PLA film's crystallinity during processing and achieved a 20% improvement in the MVTR and a 55% improvement in the OTR. The authors attributed the MVTR decrease to the PLA layer and the OTR decrease to the WG layer (56). We had similar findings that the annealing process induced the crystallization of the SC-PLA films and that all the layers served a specific purpose in the structure. Chen *et al.* reported on a PLA/Cellulose nanocrystals (CNC)/PLA three-layered structure and saw a 70-fold improvement in the OTR compared to that of pure PLA and a 7-fold improvement in the MVTR compared to that of pure CNC film. Our values were lower since our base film layer was already semi-crystalline, but we saw the same trend: a synergistic effect between the layers to improve both the MVTR and OTR (57).

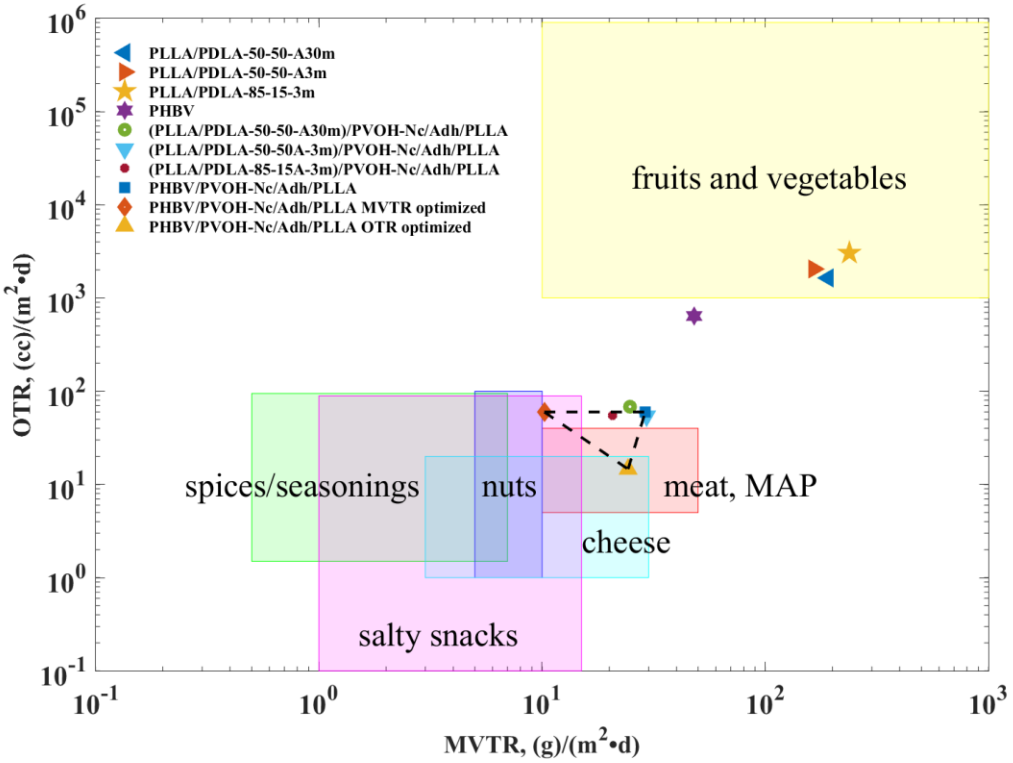

Figure 5.4. MVTR versus OTR of the various structures plus their base films. Typical food products and their respective required barrier ranges for packaging are included in the colored rectangles. The area within the dashed-line triangle includes the possible barrier levels obtainable with the optimization of either the MVTR or OTR. Note: MVTR at 38 °C/90% RH; OTR at 23 °C/50 % RH.

Obtaining the MVTR values at three different temperatures allows the estimation of the permeability activation energy of the structures using the Arrhenius equation (**Equation 5.2)**:

$$P = P_0 exp\,(-\frac{E_p}{RT}) \qquad \textbf{(5.2)}$$

where P_0 is the pre-exponential term, E_p is the permeability activation energy, and R is the universal gas constant. The water vapor permeability coefficient (WVPC) was calculated using **Equation 5.3**.

$$MVPC = \frac{MVTR\ x\ l}{\Delta P} \qquad \textbf{(5.3)}$$

where MVTR is the moisture vapor transmission rate at g/(m^2·d), l is the thickness in mm, and ΔP is the difference in the water vapor pressure across the film. Since the MVTR is mainly due to the base barrier layer, we assumed that the average thickness of just that layer was used to calculate the MVPC. **Figure 5.5** is a plot of 1/T versus the semilog of MVPC. The slope is $-E_p/R$, which can be used to calculate the E_p. There is a good correlation between the two variables, which can be seen by the R^2 in **Table 5.1**. Also included in **Table 5.1** is the activation energy of the four structures. Shogren reported the permeability activation energy of PHBV-6, 12, and 18 % valerate as 30, 30, and 31 kJ/mol, respectively (58). For the PHBV we used, 3% valerate had a permeability activation energy of 58.11 kJ/mol, a little higher. Shogren also reported a permeability activation energy for crystallized PLA of -0.1 kJ/mol (58). We have not found a reported moisture barrier activation energy for SC-PLA.

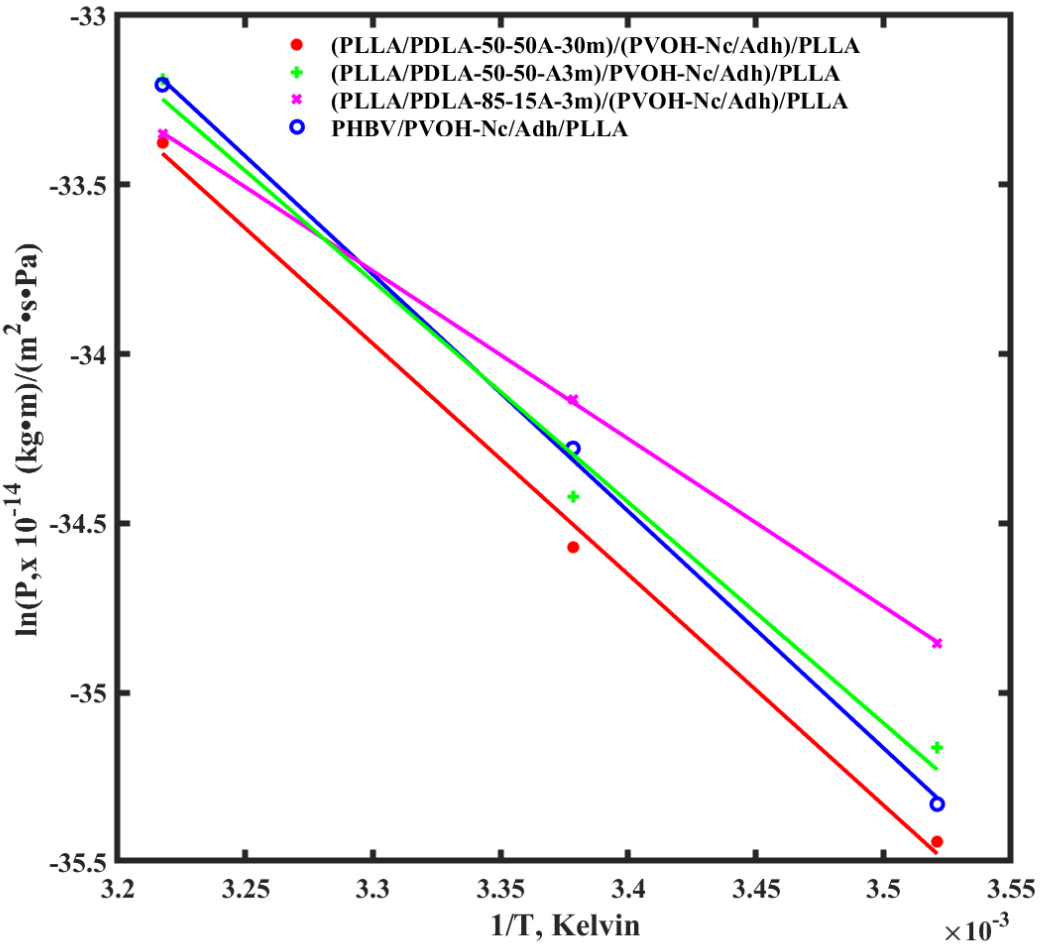

Figure 5.5. MVPC (kg·m)/(m^2·s·Pa) versus 1/T, *K* of the four structures. The lines represent the best fit between the three data points per structure.

Table 5.1. Activation energy and correlation coefficient of the structures

Structure	E_p (kJ/mol)	R^2
1-55-micron PLLA/PDLA (50-50)-A30min/29-micron PVOH-Nc/Adh/49-micron PLLA	56.63	0.9968
2- 67-micron PLLA/PDLA (50-50)-A3min/24-micron PVOH-Nc/Adh/63-micron PLLA	54.23	0.9883
3-81-micron PLLA/PDLA (85-15)-A3min/25-micron PVOH-Nc/Adh/63-micron PLLA	41.19	0.9999
4-48-micron PHBV/20-micron PVOH-Nc/Adh/63-micron PLLA	58.11	0.9992

This work began with selecting base biodegradable structures that showed the most promise for creating transparent, biodegradable, flexible films with adequate water and oxygen

barriers. We identified PHBV and two variations of PLLA/PDLA blends (50-50-A3m and 50-50-A30m) as optimal candidates. To reduce the amount of PDLA due to cost, we incorporated a PLLA/PDLA 85-15-A3 blend. To enhance the oxygen barrier, which was insufficient in the base substrates, we applied a PVOH/Nc coating to these structures. They were then laminated to PLLA as the sealant layer, achieving exceptional moisture and oxygen barrier properties for a non-metallized, PVDC-free, and biodegradable structure. Further customization of the MVTR and OTR barriers could be achieved by biaxially orienting the based barrier film (59,60)The MVTR was meticulously analyzed at three different temperatures, enabling us to calculate the moisture barrier activation energy—a parameter not previously reported for multiple blends of sc-PLA in relation to MVTR. Depending on the specific optimization of MVTR or OTR, the optimized structure is suitable for packaging various food products, including oatmeal, spices, cheese, pretzels, and meats.

5.5 Conclusions

An extensive screening was done on several variables to determine the best base layer of a laminated structure to optimize the MVTR and OTR. PHBV and three different SC-PLA ratios were determined to be the best options. Four different structures were produced utilizing SC-PLA or PHBV as the base layer of a three-layered structure. The middle layer was a PVOH-Nc coating, and the sealant layer was PLLA for all four structures. The MVTR values ranged from 20.69 to 29.38 g/(m^2·d) at 38 °C/90% RH, and the OTR values ranged from 54.10 to 68.24 cc/(m^2·d) at 23 °C/50% RH. All the materials used are biodegradable, so it is reasonable to assume the final structure is also biodegradable. We were able to optimize the structure utilizing the permeability equation and calculate a theoretical MVTR of 10.23 g/(m^2·d) at 38 °C/90% RH, with an OTR of 59.87 cc/(m^2·d) at 23 °C/50% RH, or an OTR of 14.61 cc/(m^2·d) at 23 °C/50%

RH, with an MVTR of 24.28 g/(m^2·d) at 38 °C/90% RH. This is a low barrier level for a biodegradable structure compared to other structures that do not incorporate metallization or PVDC. The permeability activation energy was also calculated since the MVTR was measured at three different temperatures. The E_p ranged from 41.19 to 54.23 kJ/mol. The novelty of the research included taking a base layer of a cast extruded biodegradable film with good moisture barrier characteristics, incorporating a layer of PVOH-Nc for added oxygen characteristics and adding a layer of PLLA for heat seal properties. We showed that optimizing the structure could obtain either a maximized MVTR of 10.23 g m^2/day at 38 °C/90% RH or a maximized OTR of 14.46 cc/(m^2·d) at 23 °C/50% RH, both exceptional for a clear biodegradable structure that does not incorporate PVDC. The novel-produced biodegradable and multilayer structure not only advances the functionality of biodegradable packaging materials but also enhances their application in preserving food quality and extending shelf life.

5.6 Acknowledgements

J.F.M. would like to thank the Michigan State University, College of Natural Resources, Office of Academic and Student Affairs for financial support for a Ph.D. fellowship in the Summers of 2022, 2023, and 2024. The authors thank TotalEnergies Corbion for providing the PLLA and PDLA resins and Anibal Bher for extruding the PHBV.

REFERENCES

1. Environmental Protection Agency U, of Land O, Management E, of Resource Conservation O. Advancing Sustainable Materials Management: 2018 Fact Sheet Assessing Trends in Materials Generation and Management in the United States. 2020.
2. Containers and Packaging_ Product-Specific Data _ US EPA [Internet]. 2023 [cited 2024 Mar 19]. Available from: https://www.epa.gov/facts-and-figures-about-materials-waste-and-recycling/containers-and-packaging-product-specific.
3. Packaging waste 101: the problem [Internet]. [cited 2022 Aug 17]. Available from: https://supplychain.edf.org/resources/sustainability-101-packaging-waste-the-problem/
4. At Least 85 Percent of U.S. Plastic Waste Went to Landfills in 2021 _ Smart News_ Smithsonian Magazine [Internet]. [cited 2022 Aug 16]. Available from: https://www.smithsonianmag.com/smart-news/the-us-recycled-just-5-percent-of-its-plastic-in-2021-180980052/
5. Global plastic packaging market size 2022 to 2028 [Internet]. 2024 [cited 2024 Mar 19]. Available from: https://www.statista.com/statistics/1343145/global-plastic-films-packaging-market-size
6. Packaging Laminate Market Opportunities and Forecast to 2034 [Internet]. 2022 [cited 2024 May 22]. Available from: https://www.futuremarketinsights.com/reports/packaging-laminates-market
7. The Role of Laminating in Flexible Packaging [Internet]. 2020 [cited 2024 May 22]. Available from: https://www.kymc.com/msg/role-of-laminating-in-flexible-packaging.html
8. Bizongo [Internet]. 2023 [cited 2024 Mar 19]. Available from: https://www.bizongo.com/blog/increasing-demand-for-recyclable-laminates
9. Recycling Multi-Layer Packaging_ Yes, It Can Be Done - Lubrizol [Internet]. 2022 [cited 2024 Jun 1]. Available from: https://www.lubrizol.com/Coatings/Blog/2022/05/Recycling-Multi-Layer-Packaging
10. Narancic T, Cerrone F, Beagan N, O'Connor KE. Recent advances in bioplastics: Application and biodegradation. Polymers (Basel). 2020 Apr 1;12(4).
11. Plastics Technology [Internet]. 2019 [cited 2024 Mar 23]. Recyclable All-PE Pouches_ Sustainable Opportunity for Film Extruders _ Plastics Technology. Available from: https://www.ptonline.com/articles/recyclable-all-pe-pouches-sustainable-opportunity-for-film-extruders
12. Sustainable Alternatives to Polyvinylidene Chloride-coated Films Create New Growth Opportunities and Transform the Food Packaging Markets in Western Europe and North America [Internet]. 2016 [cited 2024 Mar 21]. Available from:

https://www.prnewswire.com/news-releases/sustainable-alternatives-to-polyvinylidene-chloride-coated-films-create-new-growth-opportunities-and-transform-the-food-packaging-markets-in-western-europe-and-north-america-300371315.html

13. ENVIROMET-2309 Technical Data Sheet. [Internet]. [cited 2024 Jun 3]. Available from: https://www.celplast.com/wp-content/uploads/2023/09/ENVIROMET-2309.pdf

14. 80 AUL EarthFirst Ultralight Data Sheet US [Internet]. 2020 [cited 2022 Aug 2]. Available from: Data sheet supplier by the vendor.

15. EarthFirst® High Performance Sealant Films - Barrier _ Plastic Suppliers, Inc. [Internet]. [cited 2022 Aug 2]. Available from: Data sheet supplier by the vendor.

16. WUL EarthFirst UL 80 - 120 data sheet (UPDATED DRAFT 2018-07-09) [Internet]. 2018 [cited 2022 Aug 2]. Available from: Data sheet supplier by the vendor.

17. Transparent and high barrier biodegradable film and sheet for customized Modified Atmosphere food Packaging _ BIO4MAP _ Project _ Fact sheet _ FP7 _ CORDIS _ European Commission [Internet]. 2017 [cited 2024 May 27]. Available from: https://cordis.europa.eu/project/id/606144

18. ProActive Compostable Technical data sheet. [Internet]. 2023 [cited 2024 Jun 1]. Available from: https://www.proampac.com/en-us/proactive-compostable/

19. Rodríguez-Cendal AI, Gómez-Seoane I, de Toro-Santos FJ, Fuentes-Boquete IM, Señarís-Rodríguez J, Díaz-Prado SM. Biomedical Applications of the Biopolymer Poly(3-hydroxybutyrate-co-3-hydroxyvalerate) (PHBV): Drug Encapsulation and Scaffold Fabrication. Int J Mol Sci. 2023 Jul 1;24(14).

20. Miguel O, Iruin JJ. Water transport properties in poly(3-hydroxybutyrate) and poly(3-hydroxybutyrate-co-3-hydroxyvalerate) biopolymers. J Appl Polym Sci. 1999;73(4):455–68.

21. Selke SEM, Culter JD, Auras RA, Rabnawaz M. Plastics Packaging Properties, Processing, Applications, and Regulations. 4th ed. Munich: Carl Hanser Verlag; 2021.

22. Zembouai I, Kaci M, Bruzaud S, Benhamida A, Corre YM, Grohens Y. A study of morphological, thermal, rheological and barrier properties of Poly(3-hydroxybutyrate-Co-3-Hydroxyvalerate)/polylactide blends prepared by melt mixing. Polym Test. 2013;32(5):842–51.

23. Crétois R, Follain N, Dargent E, Soulestin J, Bourbigot S, Marais S, et al. Microstructure and barrier properties of PHBV/organoclays bionanocomposites. J Memb Sci. 2014 Oct 1;467:56–66.

24. Tsuji H. Poly(lactide) stereocomplexes: Formation, structure, properties, degradation, and applications. Vol. 5, Macromolecular Bioscience. Wiley-VCH Verlag; 2005. p. 569–97.

25. Tsuji H, Ikada Y. Stereocomplex formation between enantiomeric poly(lactic acid)s. XI. Mechanical properties and morphology of solution-cast films. Polymer (Guildf). 1999;40:6699–708.

26. Tsuji H, Tsuruno T. Water Vapor Permeability of Poly(L-lactide)/Poly(D-lactide) Stereocomplexes. Macromol Mater Eng. 2010 Aug 11;295(8):709–15.

27. Macnamara JF, Rubino M, Daum M, Kathuria A, Auras R. Unlocking the secrets of high-water barrier stereocomplex polylactide blend extrusion films. Green Chemistry [Internet]. 2024; Available from: http://xlink.rsc.org/?DOI=D3GC04805E

28. Idris A, Muntean A, Mesic B, Lestelius M, Javed A. Oxygen barrier performance of poly(Vinyl alcohol) coating films with different induced crystallinity and model predictions. Coatings. 2021 Oct 1;11(10).

29. Barbato A, Apicella A, Malvano F, Scarfato P, Incarnato L. High-Barrier, Biodegradable Films with Polyvinyl Alcohol/Polylactic Acid + Wax Double Coatings: Influence of Relative Humidity on Transport Properties and Suitability for Modified Atmosphere Packaging Applications. Polymers (Basel). 2023 Oct 15;

30. Ben Dhieb F, Dil EJ, Tabatabaei SH, Mighri F, Ajji A. Effect of nanoclay orientation on oxygen barrier properties of LbL nanocomposite coated films. RSC Adv. 2019;9(3):1632–41.

31. Yue S, Wang S, Han D, Huang S, Sun L, Xiao M, et al. Polyvinyl Alcohol/Montmorillonite Nanocomposite Coated Biodegradable Films with Outstanding Barrier Properties. ES Materials and Manufacturing. 2023 Jun 1;20.

32. Schiessl S, Kucukpinar E, Cros S, Miesbauer O, Langowski HC, Eisner P. Nanocomposite Coatings Based on Polyvinyl Alcohol and Montmorillonite for High-Barrier Food Packaging. Front Nutr. 2022 Mar 7;9.

33. Itavaara M, Karjomaa S, Selin JF. Biodegradation of polylactide in aerobic and anaerobic thermophilic conditions. Chemosphere [Internet]. 2002 Jun 22;46:879–85. Available from: www.elsevier.com/locate/chemosphere

34. Tomita K, Tsuji H, Nakajima T, Kikuchi Y, Ikarashi K, Ikeda N. Degradation of poly(D-lactic acid) by a thermophile. Polym Degrad Stab. 2003;81(1):167–71.

35. Betty Lucy López O, Amanda Inés Mejía G, Ligia Sierra G. Biodegradability of poly(vinyl alcohol). Polym Eng Sci. 1999;39(8):1346–52.

36. Lyshtva P, Voronova V, Barbir J, Leal Filho W, Kröger SD, Witt G, et al. Degradation of a poly(3-hydroxybutyrate-co-3-hydroxyvalerate) (PHBV) compound in different environments. Heliyon. 2024 Feb 15;10(3).

37. Product data sheet Luminy ® L130 [Internet]. 2022 [cited 2022 Jun 12]. Available from: https://www.totalenergies-corbion.com/media/yvmdsjgr/pds-luminy-l130-190507.pdf

38. Product Data Sheet Luminy® D120 [Internet]. 2019 [cited 2022 Jun 11]. Available from: https://www.totalenergies-corbion.com/media/0mxj0y1o/pds-luminy-d120-190507.pdf

39. Technical Data Sheet & Processing Guide and ENMAT PHBV resin [Internet]. 2021 [cited 2024 Mar 3]. Available from: https://api.atomler.com/file/110457086

40. EXCEVAL TM Characteristics Specifications EXCEVAL TM Grades [Internet]. [cited 2022 Jun 21]. Available from: https://www.kuraray-poval.com/fileadmin/user_upload/KURARAY_POVAL/technical_information/grades_by_region/grades_exceval_asia/TDS-English-KRC-Exceval_English.pdf

41. HB Fuller Flextra Compost(TM) SF1000 XR2000 Technical Data Sheet [Internet]. St Paul, MN; 2018 [cited 2022 Mar 11]. Available from: Data sheet supplier by the vendor.

42. Nanomer® 1.34TCN Technical Data Sheet. [Internet]. 2023 [cited 2024 Mar 27]. Available from: https://polymer-additives.specialchem.com/product/a-nanocor-nanomer-1-34tcn

43. Wetting Tension and Contact Angle - Poly Print [Internet]. 2024 [cited 2024 May 22]. Available from: https://www.polyprint.com/understanding-film-properties/wetting-tension-and-contact-angle/

44. Chandio AD, Channa IA, Rizwan M, Akram S, Javed MS, Siyal SH, et al. Polyvinyl alcohol and nano-clay based solution processed packaging coatings. Coatings. 2021 Aug 1;11(8).

45. Vargaftik BN, Volkov BN, Voljak LD. International Table of the Surface Tension of Water. J Phys Chem. 1983;12(3):817–20.

46. ASTM F1249-20 Standard Test Method for Water Vapor Transmission Rate Through Plastic Film and Sheeting Using a Modulated Infrared Sensor [Internet]. West Conshohocken; 2020. Available from: www.astm.org,

47. ASTM D3985-17 Standard Test Method for Oxygen Gas Transmission Rate Through Plastic Film and Sheeting Using a Coulometric Sensor [Internet]. West Conshohocken; 2017. Available from: www.astm.org.

48. Macnamara Jr JF, Rubino M, Daum M, Kathuria A, Auras R. Unlocking the Secrets of High-Water Barrier Stereocomplex Polylactide Blend Extrusion Films . Green Chemistry. 2024;

49. Tsuji H. Poly(lactide) stereocomplexes: Formation, structure, properties, degradation, and applications. Vol. 5, Macromolecular Bioscience. Wiley-VCH Verlag; 2005. p. 569–97.

50. Righetti MC, Cinelli P, Mallegni N, Stäbler A, Lazzeri A. Thermal and mechanical properties of biocomposites made of poly(3-hydroxybutyrate-co-3- hydroxyvalerate) and potato pulp powder. Polymers (Basel). 2019 Feb 12;11(2).

51. Corre YM, Bruzaud S, Audic JL, Grohens Y. Morphology and functional properties of commercial polyhydroxyalkanoates: A comprehensive and comparative study. Polym Test. 2012 Apr;31(2):226–35.

52. Zhou Y, Zhao M, Guo H, Li Y, Liu Q, Deng B. Morphology and crystallization behavior of poly(3-hydroxybutyrate-: Co -3-hydroxyvalerate)/polyhedral oligomeric silsesquioxane hybrids. RSC Adv. 2019;9(15):8146–58.

53. Liu B, Zhang J, Guo H. Research Progress of Polyvinyl Alcohol Water-Resistant Film Materials. Membranes (Basel). 2022 Mar 20;12(3):347.

54. 3002 Technical Data Sheet US 80ga Plastic Suppliers, Inc. [Internet]. Columbus; 2020 [cited 2024 Aug 2]. Available from: Data sheet supplier by the vendor.

55. Standard Test Method for Transparency of Plastic Sheeting [Internet]. 2023. Available from: www.astm.org,

56. Rocca-Smith JR, Pasquarelli R, Lagorce-Tachon A, Rousseau J, Fontaine S, Aguié-Béghin V, et al. Toward Sustainable PLA-Based Multilayer Complexes with Improved Barrier Properties. ACS Sustain Chem Eng. 2019 Feb 18;7(4):3759–71.

57. Chen C, Wang L, Shams Es-haghi S, Tajvidi M, Wang J, Gardner DJ. Biodegradable and recyclable bio-based laminated films of poly (lactic acid) and cellulose nanocrystals for food barrier packaging. Food Packag Shelf Life. 2024 Mar 1;42.

58. Shogren R. Water Vapor Permeability of Biodegradable Polymers. J Environ Polym Degrad. 1997;5(2):91–5.

59. Marano S, Laudadio E, Minnelli C, Stipa P. Tailoring the Barrier Properties of PLA: A State-of-the-Art Review for Food Packaging Applications. Polymers (Basel). 2022 Apr 1;14(8).

60. Liu X, Mo Z, Cui L, Yu C, Zou Z, Liu Y, et al. Effect of biaxial stretching on the microstructure evolution, optical, mechanical and oxygen barrier properties of biodegradable poly(lactic acid) (PLA)/poly(butylene adipate-co-terephthalate) (PBAT) films. Int J Biol Macromol. 2023 Dec 31;253.

APPENDIX 5A: PROCESSING CONDITIONS

Table A5.1 includes the processing conditions for cast extruding PHBV on the microextruder.

Table A5.1. Processing conditions for PHBV on the microextruder.

Processing temperatures	**Temperature (°C)**
Zone 1	166
Zone 2	166
Zone 3	166
Transfer tube	166
Adapter	168
Feedblock	168
Die	166
Chill Roll	70

Extrusion Settings	**Speed (RPM)**
Screw	35
Chill roll speed	20

APPENDIX 5B: FILM CHARACTERIZATION

Figure A5.1 is the MVTR of all the screen candidates normalized to 25.4 microns.

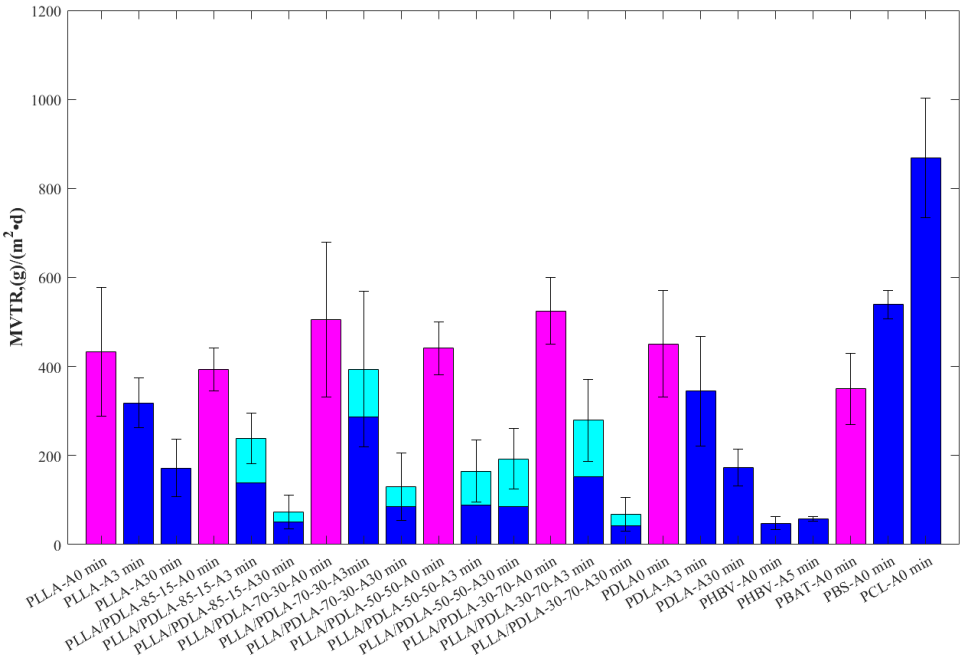

Figure A5.1. MVTR values of all candidates screened. The magenta bars represent amorphous samples, the blue bars represent the HC crystalline portion, and the cyan bars represent the SC crystalline portion.

Table A5.2 shows the X_c values for the potential candidates used for the study, reflecting the split between SC and HC for the sc PLA films.

Table A5.2. X_c values for the potential candidates used for the study.

Material	**X_{HC}, %**	**X_{SC}, %**	**X_t, %**
PLLA/PDLA-50-50-A30 min	19	24	42
PLLA/PDLA-50-50-A3 min	25	22	47
PLLA/PDLA-85-15-A3 min	23	17	40
PHBV	59	-	59
PHBV-A5 min	66	-	66
PLLA-A0 min	0	-	-

Table A5.3 shows the moisture permeation and MVTR values for all the films screened normalized to 25.4 microns.

Table A5.3. Permeation and MVPC values for all variables screened. Note: values followed by a different letter are significantly different at $P \leq 0.05$ (Tukey-Kramer test).

Structure - Film	*n*	RH, %	Temp, ºC	Permeation, g-mm/m2/day	Std dev	MVPC (kg-m)/(m2-s-Pa)	Std dev	MVTR (1mil Normalized)g /m2/day
PLLA - A0 min[b]	14	90	37.8	11.00	3.68	2.15E-14	7.20E-15	432.97
PLLA - A3 min[b,c,d,e]	11	90	37.8	8.09	1.43	1.59E-14	3.25E-15	318.45
PLLA - A30 min[e,f,g,h]	12	90	37.8	4.36	1.65	8.53E-15	3.24E-15	171.66
PLLA/PDLA 85-15 - A0 min[b,c]	8	90	37.8	10.01	1.23	1.96E-14	2.40E-15	394.18
PLLA/PDLA 85-15 - A3 min[d,e,f]	10	90	37.8	6.05	1.44	1.19E-14	2.82E-15	238.16
PLLA/PDLA 85-15 - A30 min[e,f,g,h]	10	90	37.8	2.59	1.37	5.08E-15	2.69E-15	101.98
PLLA/PDLA 70-30 - A0 min[b]	8	90	37.8	12.83	4.42	2.52E-14	5.90E-15	505.04
PLLA/PDLA 70-30 - A3 min[b,c,d]	6	90	37.8	9.99	4.45	1.96E-14	8.71E-15	393.49
PLLA/PDLA 70-30 - A30 min[e,f,g,h]	21	90	37.8	3.30	1.91	6.46E-15	3.73E-15	129.93
PLLA/PDLA 50-50 - A0 min[b]	15	90	37.8	11.19	1.49	2.19E-14	2.94E-15	440.56
PLLA/PDLA 50-50 - A3 min[e,f,g,h]	18	90	37.8	4.19	1.78	8.22E-15	3.48E-15	165.08
PLLA/PDLA 50-50 - A30 min[e,f,g]	21	90	37.8	4.86	1.74	9.53E-15	3.41E-15	191.36
PLLA/PDLA 30-70 - A0 min[b]	9	90	37.8	13.34	1.90	2.61E-14	3.71E-15	525.04
PLLA/PDLA 30-70 - A3 min[c,d,e]	11	90	37.8	7.09	2.35	1.39E-14	4.60E-15	278.94
PLLA/PDLA 30-70 - A30 min[f,g,h]	7	90	37.8	1.75	0.96	3.43E-15	1.90E-15	68.81
PDLA - A0 min[b]	7	90	37.8	11.47	3.06	2.25E-14	6.00E-15	451.48
PDLA - A3 min[b,c,d,e]	6	90	37.8	8.76	2.42	1.72E-14	4.78E-15	344.89
PDLA - A30 min[e,f,g,h]	7	90	37.8	4.38	1.07	8.59E-15	2.08E-15	172.54
PHBV[h]	7	90	37.8	1.22	0.36	2.39E-15	7.15E-16	48.04

Table A5.3 (cont'd)

PHBV - A5 min[g,h]	5	90	37.8	1.45	0.14	2.85E-15	2.63E-16	57.26
PBAT[b,c,d,e]	2	90	37.8	8.89	2.02	1.74E-14	4.02E-15	350.11
PBS[b]	2	90	37.8	13.68	0.82	2.68E-14	1.63E-15	538.70
PCL[a]	4	90	37.8	22.06	3.40	4.32E-14	6.67E-15	868.64

Table A5.4 shows the oxygen permeation and OTR values for all the films screened normalized to 25.4 microns.

Table A5.4. Permeation and OPC values for all variables screened. Note: values followed by a different letter are significantly different at $P \leq 0.05$ (Tukey-Kramer test).

Structure - Film	n	RH, %	Temp, ºC	Permeation, cc-mm/m²/day	Std dev	OTR (cc-m)/(m²-s-Pa)	Std dev	OTR (1mil Normalized) cc/m²/day
PLLA - A0 min[a,b,c]	12	50	23	59.98	29.74	6.85E-14	3.40E-14	2361.54
PLLA/PDLA-85-15 -A0 min[c,d]	12	50	23	15.67	14.89	1.79E-14	1.70E-14	616.76
PLLA/PDLA-85-15 -A3 min[a,b,c]	4	50	23	77.24	62.43	8.82E-14	7.13E-14	3040.99
PLLA/PDLA-85-15 -A15 min[d]	8	50	23	15.67	14.89	1.79E-14	1.70E-14	616.76
PLLA/PDLA-70-30 - A0 min[a,b,c,d]	7	50	23	52.03	8.81	5.94E-14	1.01E-14	2048.40
PLLA/PDLA-70-30 - A3 min[c,d]	5	50	23	20.49	5.00	2.34E-14	5.71E-15	806.60
PLLA/PDLA-70-30 - A15 min[b,c,d]	5	50	23	38.41	22.37	4.39E-14	2.56E-14	1512.19
PLLA/PDLA-70-30 - A30 min[a,b]	3	50	23	46.81	5.32	5.35E-14	6.08E-15	1843.08
PLLA/PDLA-50-50 - A0 min[a,b,c,d]	8	50	23	52.67	17.91	6.02E-14	2.05E-14	2073.71
PLLA/PDLA-50-50-3 min[a,b,c,d]	3	50	23	52.02	37.30	5.94E-14	4.26E-14	2048.06
PLLA/PDLA-50-50 - A30 min[a,b,c,d]	3	50	23	41.72	26.71	4.77E-14	3.05E-14	1642.68
PLLA/PDLA-30-70 - A0 min[b,c,d]	10	50	23	38.70	11.35	4.42E-14	1.30E-14	1523.80
PDLA - A0 min[c,d]	9	50	23	33.95	13.45	3.88E-14	1.54E-14	1336.69
PHBV-A0 min[c,d]	3	50	23	16.28	1.93	1.86E-14	2.21E-15	641.12
PBS-A0 min[b,c,d]	4	50	23	35.65	25.66	4.07E-14	2.93E-14	1403.46
PCL-A0 min[a]	4	50	23	109.70	29.28	1.25E-13	3.34E-14	4318.76

APPENDIX 5C: STRUCTURE CHARACTERIZATION

Figure A5.2 shows the UV transmission rate versus the wavelength for all the films produced, including the base and laminated structures.

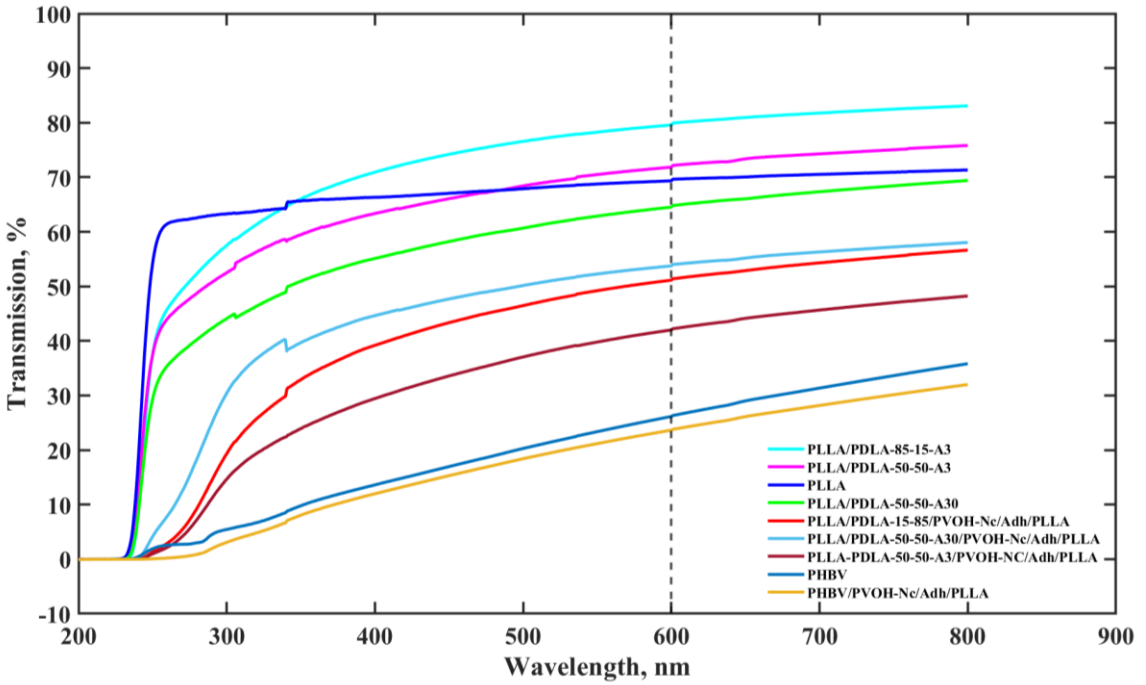

Figure A5.2. UV transmission rate versus wavelength for the various films at a wavelength of 600 nm.

Table A5.5 shows the UV/VIS % data value for all the base and laminated films.

Table A5.5. UV/VIS % Data value for the various samples at 600 nm.

Sample	a, %	b, %	c, %	Average	Std Dev.
PLLA/PDLA-85-15-A3 min	80	75	65	73	8
PLLA/PDLA-50-50-A3 min	72	69	65	68	4
PLLA	69	66	68	68	2
PLLA/PDLA-50-50-A30 min	58	53	61	57	4
PLLA/PDLA-85-15-A3/PVOH-Nc/Adh/PLLA	51	53	54	53	2
PLLA/PDLA-50-50-A30/PVOH-Nc/PLLA	54	48	56	53	4
PLLA/PDLA-50-50-A3/PVOH-Nc/PLLA	42	45	45	44	2
PHBV	27	26	21	25	3
PHBV/PVOH-Nc/PLLA	24	27	17	22	5

Figure A5.3 is SEM micrographs of the four laminated structures.

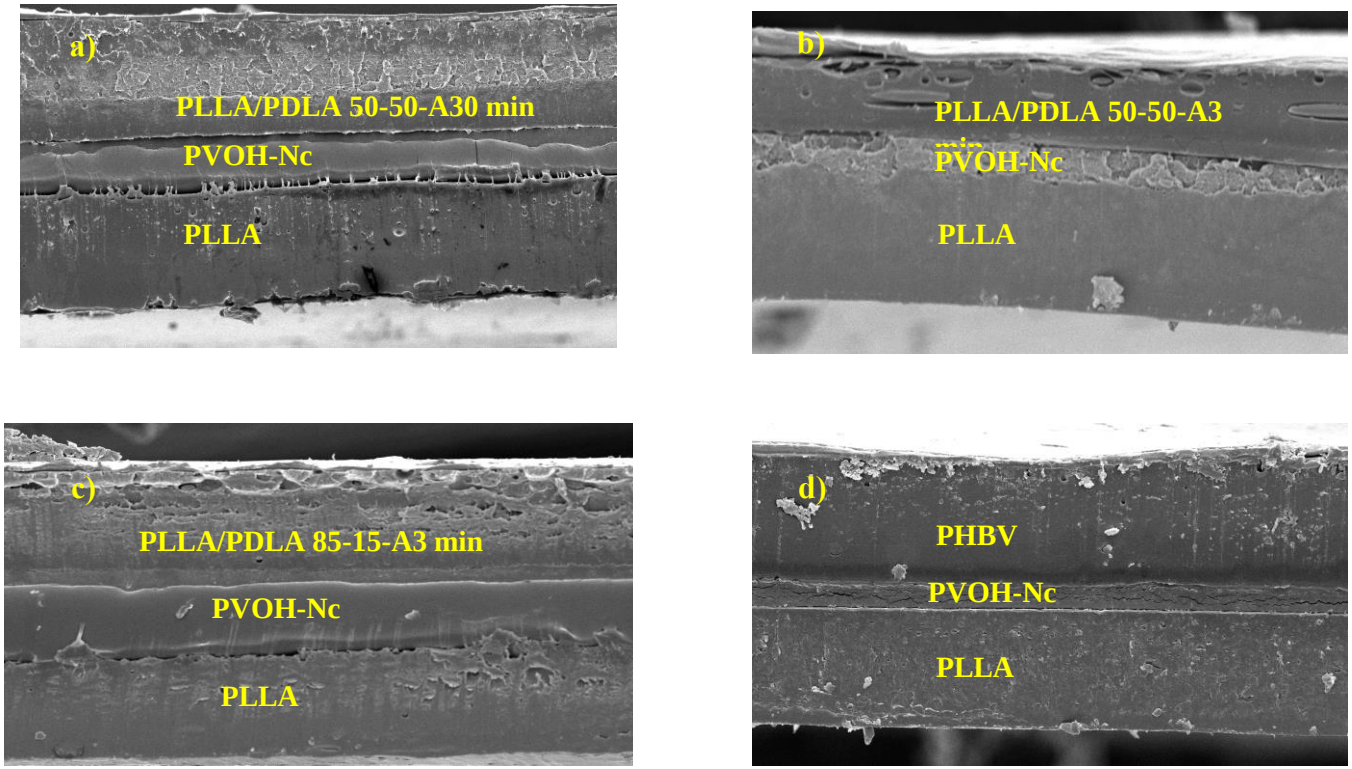

Figure A5.3. SEM micrographs showing the cross-section of the four laminated structures a) PLLA/PDLA-50-50-A30 min/PVOH-Nc/Adh/PLLA; b) PLLA/PDLA-50-50-A3 min/PVOH-Nc/Adh/PLLA; PLLA/PDLA-85-15-A3 min/PVOH-Nc/Adh/PLLA; d) PHBV/PVOH-Nc/Adh/PLLA. Note: Thicknesses in layers may be different in areas due to squeezing the structure during the cutting of the cross-section.

CHAPTER 6: COMPOSTING PERFORMANCE OF POLY(L-LACTIC ACID), POLY(D-LACTIC ACID), AND THEIR STEREOCOMPLEX BLEND FILMS

A version of this chapter was submitted on 7/18/24 as:

Macnamara, J., Bher, A., Auras, R. Composting Performance of Poly(L-lactic acid), Poly(D-lactic acid), and Their Stereocomplex Blend Films., *ACS Omega*.

6.1 Abstract

Plastic waste due to single-use plastics is an ongoing issue. However, there is hope in the form of biodegradable plastics, with polylactic acid being a promising example. This study examined the biodegradation of L-polylactic acid, D-polylactic, and various blends of SC-polylactic acid, as well as a sample of SC-polylactic acid-50-50-Annealed for 30 minutes to induce crystallization. A simulated study in a lab-scale direct measurement respirometer was conducted in compost to compare the abiotic and biotic degradation of the various films. The crystallinity was shown to increase quickly at the beginning before plateauing. The molecular weight decreased first due to hydrolysis to about day 45 to 60, depending on the film, and then due to biodegradation when the microorganisms were able to assimilate the film after it was broken down enough by hydrolysis. The SC-polylactic acid-50-50 annealed film biodegraded the most at the end of the 120 days at 97%, with the SC-polylactic acid -50-50 film close behind at 86%. D-polylactic acid biodegraded the least at only 40% after 120 days, with the other films in between. Scanning electron microscope micrographs visually show the films' erosion over the experiment's progression. These findings, showcasing the potential of stereocomplex polylactic acid as a biodegradable plastic alternative, will support the pursuit of replacing traditional petrochemical-based plastics.

6.2 Introduction

Crafting biodegradable, sustainable polymers requires a nuanced balance between functionality, performance, and environmental impact at end-of-life (1). There is a growing demand for materials that offer superior water barrier properties and enhanced thermal resistance. However, to promote both abiotic and biotic degradation at the end of their life cycle, these polymers must also be engineered for water susceptibility and increased chain mobility, heightening degradation potential (2). Thus, developing these innovative, sustainable polymers is a strategic endeavor to optimize performance while ensuring effective recovery and environmental stewardship at the end of their lifecycle.

Biodegradation involves microorganisms decomposing organic materials into water, biomass, and CO_2 (3). As global efforts to mitigate the environmental impact of single-use plastics (SUP) intensify, biodegradable materials are gaining prominence across various sectors, including plastics, packaging, and disposable service ware. Recognizing the potential to reduce the environmental impact of SUP, governments worldwide are prioritizing the expansion of the biodegradable plastics market. A report by Allied Market Research projects a significant growth trajectory for the global bioplastics and biodegradable market, forecasting an increase from USD 1.6 billion in 2019 to USD 4.2 billion by 2026 (4).

Compostable plastics are a subset of biodegradable polymers, which can be derived from fossil or renewable sources (2). It refers to biodegradation under specific conditions, within a particular time frame, without leaving any toxic residue or chemicals (5). Various ASTM and ISO standards dictate the criteria upon which material must conform to be claimed compostable. The primary standards are ASTM D6400-21 (6), ASTM D6868-21 (7), and ISO14855 Parts 1 and 2 (8,9). They have similar basic requirements: a) disintegration during composting; b)

biodegradation in a set time frame compared with a readily biodegradable control such as cellulose; and c) no adverse effects on the ability of the compost to support plant growth (7).

The composting environment presents an ideal solution for the disposal of materials unsuitable for recycling due to contamination that could disrupt the recycling process. This particularly applies to items like food packaging, which should not be landfilled (10). Such materials often include various types of single-use packaging and service ware typically contaminated with food and beverages, making composting a practical and environmentally responsible end-of-life option.

Poly(lactic acid) (PLA) is a biodegradable polymer derived from renewable resources, designed to decompose under industrial composting conditions (11). The most commercially prevalent form of PLA, primarily consisting of L-PLA (PLLA), represents a promising alternative to fossil-based plastics, aiming to reduce the volume of non-biodegradable packaging waste in landfills (12). However, despite its environmental benefits, PLLA faces challenges such as a lower moisture barrier (13), low heat distortion temperature (14), and inferior hydrolytic and thermal stability (15) compared to traditional fossil-based plastics.

Combining PLLA with the other enantiomer of PLA, D-PLA (PDLA), under specific processing conditions can produce stereocomplex PLA (SC-PLA), which has improved properties over homocomplex PLA (HC-PLA), namely enhanced moisture vapor transmission rate (MVTR) (16) increased heat resistance (17,18), and hydrolytic stability (19); desired properties for single-use packaging and food/beverage contact applications. Much of the research on SC-PLA films has utilized solvent casting, which is impractical for commercial-scale production. Additionally, it has been reported that the annealing process of SC-PLA films can enhance the moisture barrier properties of these films by promoting crystallization (18).

PDLA has not been extensively studied in most areas, including hydrolysis or biodegradation. Mbarki *et al*. compared PDLA and PDLA/cellulose microfibers biodegradation with a specific strain at mesophilic temperatures. They determined that crystallinity was the principal factor. During the biodegradation process, the PDLA/cellulose microfibers swelled less by water, hence having a slower breakdown rate (20). However, it only compared PDLA to PDLA/cellulose microfibers. Tomita *et al.* reported on the degradation of PDLA by the strain *Bacillus stearothermophilus #73* (21). They ran a biodegradation study on PDLA with and without the strain and reported that the sample with strain 73 proved biodegradable. Similar changes were seen in the sample without the strain, but they were inferior to those seen in the run with the strain. They did not include PLLA or any other material for comparison.

Our work uniquely addresses the interplay between polymers' enhanced properties during their useful life and their subsequent end-of-life performance. We evaluate the biodegradation performance of previously developed SC-PLA films across various blends of PLLA/PDLA and PDLA produced via cast extrusion, both with and without annealing (18). This research meticulously analyzes the degradation process's impact on molecular weight, crystallinity, and thermal performance. Our approach is innovative in examining multiple PLLA/PDLA blends, including an annealed version, over 120 days to assess abiotic and biotic biodegradation. We also include controls of PLLA and cellulose—both well-documented materials—to provide a comparative baseline. Notably, our study also introduces PDLA tested at thermophilic temperatures, a comparison previously unexplored.

6.3 Experimental Section

6.3.1 Materials

PLLA and PDLA resin were supplied by TotalEnergies Corbion (Netherlands). The specific grades used were Luminy® L130 (≥ 99%(L-isomer)) and Luminy® D120 (≥ 99%(D-isomer)). The resins were processed as received. Tetrahydrofuran (THF), used as the mobile solvent to dissolve the materials to determine the molecular weight, was procured from Pharmco by Greenfield Global (USA). Cellulose powder was procured from Sigma-Aldrich (USA). Mature compost was obtained from the Michigan State University (MSU) composting facility (East Lansing, MI, USA).

6.3.2 Film Processing

All the films were produced on a pilot-scale cast film microextruder (Randcastle Extrusion Systems, Cedar Grove, USA). PLLA and PDLA films were extruded separately from the two dried resins. Then, the two resins were blended by weight in ratios of 70/30, 50/50, and 30/70 PLLA/PDLA before being introduced to the extruder. The exact processing conditions are detailed elsewhere (18).

6.3.3 Thermal Annealing

The 50/50 PLLA/PDLA sample was annealed at 160 °C for 30 min to induce crystallization in a hydraulic press model number QL438-C (PHI, City of Industry, CA, USA). The size of the samples was approximately 25.4 x 16.5 cm^2. The samples were placed between 25.4 x 25.4 cm plates lined with non-stick aluminum foil. After annealing, the samples were cooled at ambient temperature and stored in a freezer at -20 °C before being prepared for the biodegradation experiment.

6.3.4 CHN analysis

The samples' carbon, hydrogen, and nitrogen amounts were analyzed using a CHNS/O Elemental Analyzer, 2400 Series II (Perkin Elmer, Waltham, MA, USA). About 2 mg of each sample was weighed in a small tin capsule and analyzed. Triplicate measurements of each sample were taken. **Table A6.1**, Appendix A shows the carbon content values of the films used in the study.

6.3.5 Sample Preparation for Biodegradation

After processing, the samples were stored in a freezer at -20 °C, and before the biodegradation test, the samples were ground into a powder using a Single Speed Mini Cutting Mill model # E3300.00 (Eberbach Corporation, Van Buren Township, MI, USA). A 20-mesh screen was used in the mill to allow only pieces with lower dimensions than that to pass through it. The samples to be removed for differential scanning calorimetry (DSC) and size exclusion chromatography (SEC) testing were cut into 1 x 1 cm squares since the powder could not be easily separated from the compost during biodegradation. At least 24 g of each powder and 8 g of each square per variable were collected to test 3 bioreactors for biodegradation and one for sampling. They were then placed back into the freezer until the biodegradation test started.

6.3.6 Biodegradation Test in Compost

The biodegradation of PLLA, PDLA, and several blends of SC-PLA was evaluated under aerobic conditions using a direct measurement respirometric (DMR) system at the MSU School of Packaging (SoP). The system has a non-dispersive infrared gas analyzer (Li-Cor®, USA), which measures the CO_2 that evolved throughout the experiment. The chamber's temperature and relative humidity (RH) were maintained at 58 ± 2 °C and 50 ± 5 % RH. The airflow rate was regulated at 40 ± 2 cm^3min^{-1}. More information on the DMR system is detailed elsewhere (22).

Manure compost was procured from the MSU composting facility and sifted in a 10-mm screen to remove large chunks of debris. The laboratory analysis of the compost is included in T**able A6.2**, Appendix A. The compost was adjusted to 50 ± 5 % RH using deionized water. The screenings were then conditioned to 58 ± 2 °C. Each bioreactor was filled with 400 g of compost, and then 8 g of each test variable was introduced to each bioreactor individually for testing in triplicate. A blank (only compost) and positive control (cellulose) were included in the test.

During the test, deionized water was injected into the bioreactors weekly to maintain the moisture content at the optimal level. Air without CO_2 was introduced to each bioreactor, and the amount of CO_2 liberated was measured over a finite period. The system was purged after each measurement to eliminate any CO_2 left over from the previous measurement and to maintain a clean baseline. The percent biodegradation, which is the amount of carbon transformed to CO_2, was calculated from **Equation 6.1** (22):

$$\% \text{ of Biodegradation} = \frac{(CO_2)_t - (CO_2)_b}{M_t \times C_t \times \frac{44}{12}} \times 100 \qquad \textbf{(6.1)}$$

$(CO_2)_t$ – average total CO_2 evolved from the bioreactor containing the sample

$(CO_2)_b$ – average total CO_2 evolved from the blank

M_t – total mass of the sample in the bioreactor

C_t – total carbon content of the sample as measured by CHN analysis

44 is the molecular weight of CO_2, and 12 is the atomic weight of carbon.

6.3.7 Differential Scanning Calorimetry (DSC)

Samples of all the films from 0, 7, 14, 21, 28, and 45 days were tested using a Q100 differential scanning colorimeter (TA Instruments, New Castle, DE, USA). PLLA and PDLA were also tested at 60 days. The DSC has a cooling system using 70 mL/min nitrogen flow.

Samples weighing 5 to 10 mg were packed and tested in standard aluminum pans and lids. The thermograms were collected from 20 °C to 260 °C at 10 °C min^{-1} for two cycles. In between cycles, it was held isothermally for 1 min at 260 °C. One or more replicates of each sample were tested on each film in the study at each period. The heat of fusion (ΔH) of 100 % HC-PLA and SC-PLA used was 139 J/g and 142 J/g (17), respectively, to calculate the X_c. The analysis was run on the Universal Analysis 2000 software version 4.5A (TA Instruments, USA) to collect the DSC thermograms.

6.3.8 Size Exclusion Chromatography (SEC)

The number average molecular weight (M_n), weight average molecular weight (M_w), and molecular weight distribution (*MWD*) of the PLLA and PDLA samples at 0, 7, 14, 21, 28, 45, and 60 days were measured using an SEC system from Waters (Waters, New Castle, DE, USA). The SEC has an autosampler, a refractive index detector, and an isocratic pump with a series of Styragel® columns (Styragel® HR-4, HR-3, HR-2). Approximately 20 mg of each sample was dispersed in 10 mL of THF and stored overnight to dissolve. After sitting overnight, the samples were put into an oven at 80 °C to dissolve the samples thoroughly. The samples were filtered, transferred to a 2 mL glass vial, and capped. The test was run at a temperature of 35 °C at a flow rate of 1 mL/min for 50 min for each sample. To determine the samples' *Mn, Mw, and MWD*, the Mark-Houwink constants used for PLA were K = 0.000174 dL/g and α = 0.736 (23). Waters Breeze2™ software was used to analyze the data. At least three replicates of each sample were measured. We could not test the PLLA/PDLA blended samples since they do not dissolve in THF, and our SEC exclusively runs THF.

6.3.9 Scanning Electron Microscope (SEM)

Surface scans of various films at day 0 and retrieved from biodegradation were captured using a scanning electron microscope model JSM 6610LV (Jeol USA Inc., USA) to track the samples' surface deterioration throughout the study. The operating conditions were 12 kV accelerated voltage, spot size 30, and vacuum pressure of 1.33×10^{-5} Pa, with a magnification of 330x and 5000x, depending on the sample. The samples were sputtered with gold using a current of 20 mA for 3 min.

6.3.10 Data analysis

The data and graphs were compiled and analyzed using Microsoft Excel (Microsoft®, Redmond, WA, USA) and MATLAB® 2024a (Mathworks, Natick, MA, USA).

6.4 Results and Discussion

The biodegradation samples were prepared, placed into the bioreactors, and mixed with compost before being put into the DMR. The test was conducted for 120 days, with sampling at 7, 14, 21, 28, 45, and 60 days. After day 60, it was no longer possible to collect samples, so only CO_2 measurements were collected. CO_2 measurements were continually collected throughout the test to calculate the % biodegradation. **Figure A6.1,** Appendix B includes pictures of the bioreactors at each sampling point. Below are the results and discussion for thermal, crystallinity, and M_w evolution for samples at day 0, and samples retrieved during biodegradation.

6.4.1 Thermal Evolution

DSC was used to determine the crystallinity of the samples in the study from day 0 to day 60 when samples could still be collected. We collected samples for PLLA and PDLA up to day 60, but the others could only be collected up to day 45. **Figure 6.1** summarizes the main results for the samples' thermal evolution. All the thermograms show the HC-melting point at around

175 °C. All the blended thermograms also show the SC-melting point at around 225 °C (24). On day 0, all the non-annealed films were amorphous, as can be seen by the thermograms in **Figure A6.2**, Appendix B. As time progressed, the amount of HC-crystallinity decreased while the amount of SC-crystallinity increased. By day 21, all the blended films had more sc-crystals than HC-crystals. This aligned with the idea that the SC crystalline content exhibited higher resistance to hydrolysis than the HC portion. This is in line with the findings by Kara *et al.* that the HC regions are more susceptible to hydrolysis than the SC areas, which they believe was due to inherently higher crystallinity, higher thermal and mechanical stability, and strong stereocomplex interactions. (25). It can also be seen that the T_m decreases as the degradation time increases. This signifies the reduced thickness of the crystalline lamellae regions due to hydrolytic degradation, with the most significant decrease occurring on day 45. Tsuji and Tsuruno reported similar findings in a study on hydrolytic degradation of PLLA, PDLA, and a PLLA/PDLA 50-50 mix prepared by solvent casting (19).

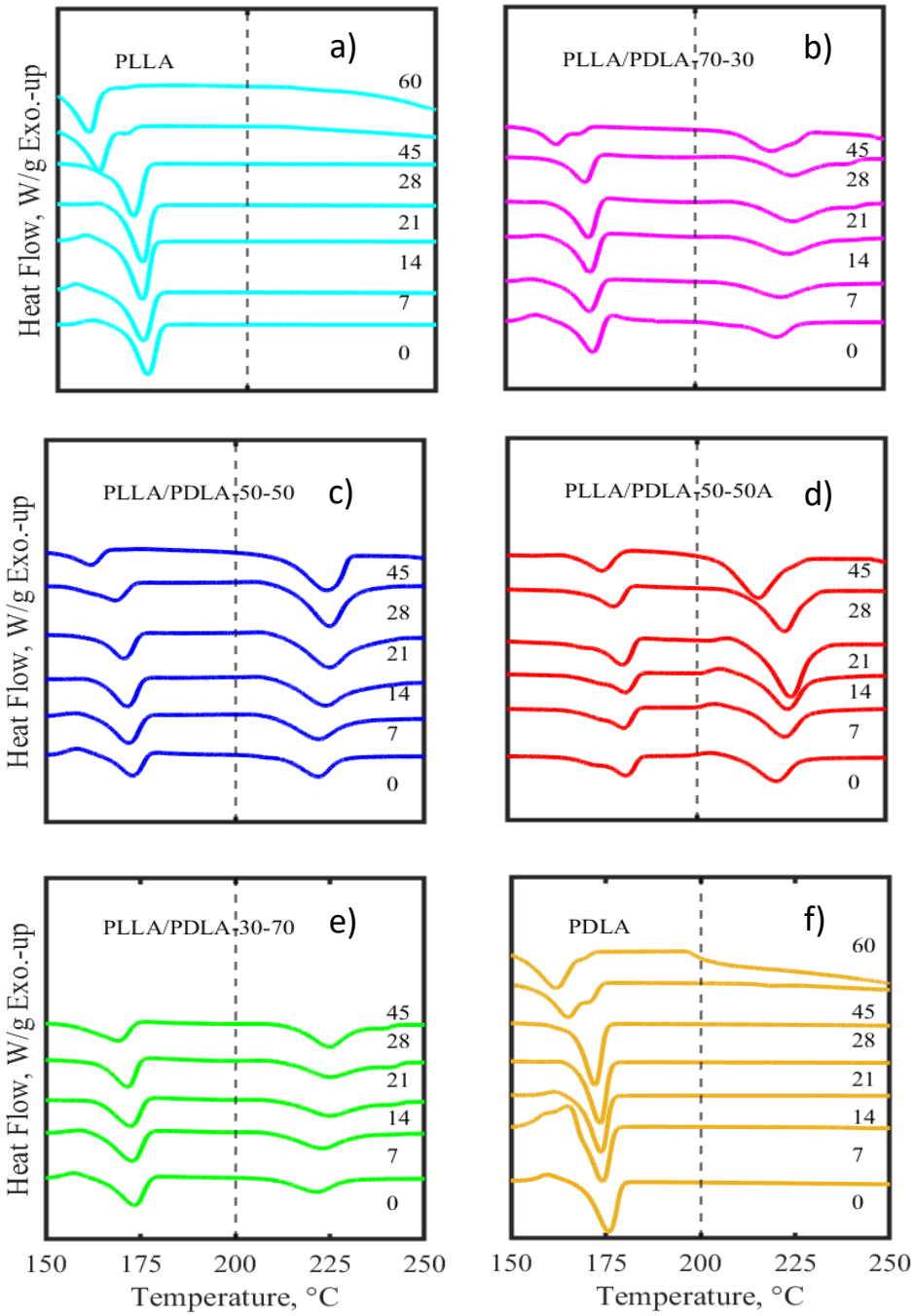

Figure 6.1. DSC thermograms of various films from 150 to 250 °C measured from biodegradation samples collected at each sampling time; **a)** PLLA; **b)** PLLA/PDLA-70-30; **c)** PLLA/PDLA-50-50; **d)** PLLA/PDLA-50-50-A; **e)** PLLA/PDLA-30-70; **f)** PDLA.

Figure 6.2 shows the progression of crystallinity for the various films over time and the split between HC and SC-crystallinity. A significant increase occurred from day 0 to day 7 in the

non-annealed films when they were amorphous, indicating hydrolysis's unflinching effect on PLA L and D amorphous regions. As time progressed, the amount of SC increased for the blended samples while the amount of HC either remained the same or decreased. For the PLLA and PDLA films, after day 7, the amount of HC crystallinity gradually increases over time, which makes sense as the amorphous regions are broken down. Tsuji *et al.* reported similar findings in a study on the hydrolysis of PLLA in a phosphate-buffered solution (26).

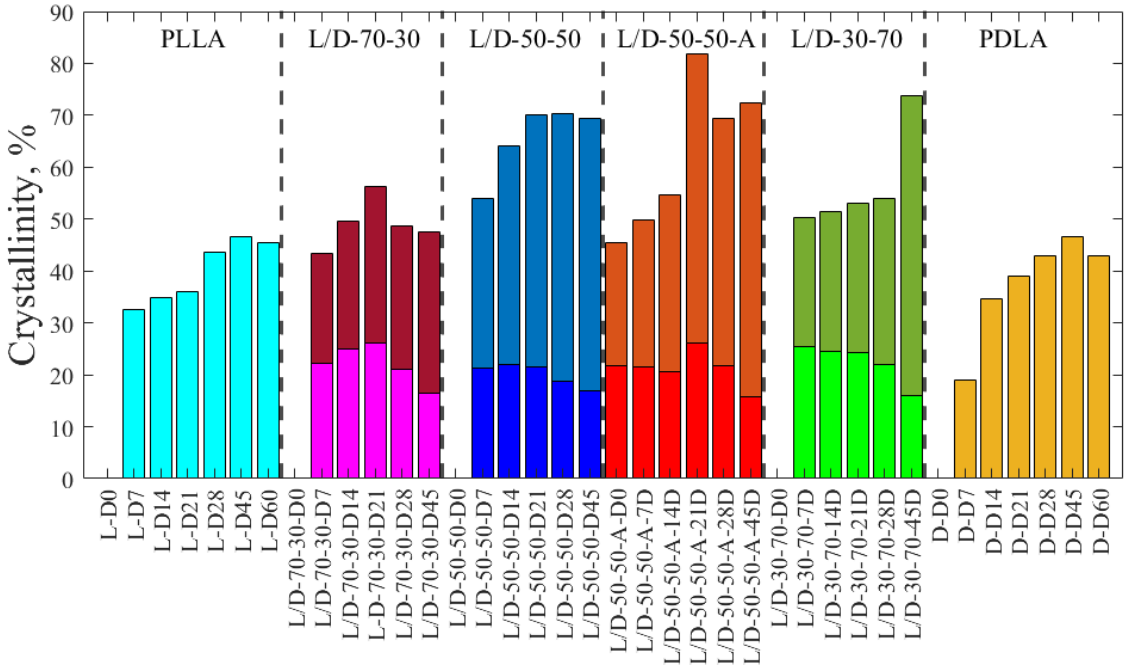

Figure 6.2. The HC- and SC-crystallinity percentages of the various films over time measured from biodegradation samples collected at each sampling time. The bottom bars represent the HC-crystalline portion, and the top bars represent the SC-crystalline portion.

6.4.2 Molecular Weight Evolution

Figure 6.3 depicts the normalized M_n reduction as a function of time for PLLA and PDLA in compost media. The experimental data was fitted using a first-order equation of $M_n/M_{n0} = e^{(-kt)}$ where M_{n0} is the M_n at day 0, k is the rate constant in d^{-1}, and t is time in days (27,28). There was no significant difference between the k values between PLLA and PDLA at $P \leq 0.05$

using a Tukey-Kramer test. The PLLA and PDLA M_n dropped below 10 kDa around day 45, as can be seen in **Table A6.3**, Appendix B**.** Castro-Aguirre *et al.* showed that looking at M_n may not be the best approach for looking at the evolution of PLA samples with different M_w. However, looking at the changes in the *MWD* may be a better indicator of degradation behavior during the lag phase (29).

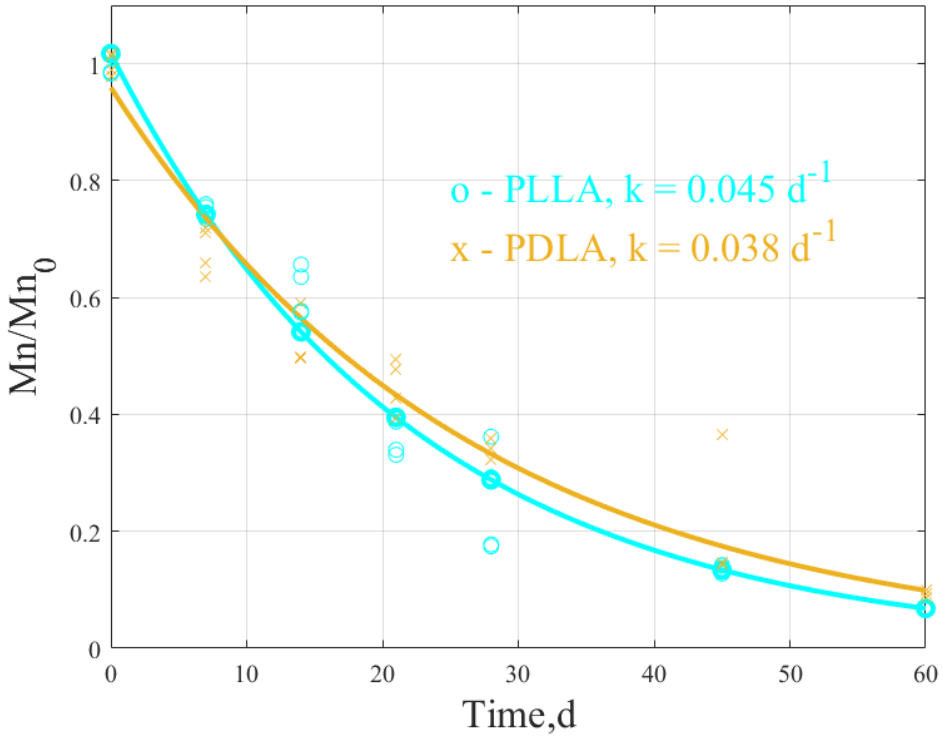

Figure 6.3. Normalized M_n reduction as a function of time for PLLA and PDLA was measured from biodegradation samples collected at each sampling time.

Figure 6.4 depicts the *MWD* as a function of time for PLLA and PDLA samples evaluated during biodegradation until day 60. A shift in the *MWD* peak to the left signifies a decrease in the M_w due to hydrolysis, while the broadening of the peak is related to an increase in the polydispersity (Đ) due to chain scission (30). Both exhibited multimodal distribution starting at day 45. At the beginning of hydrolysis, the molecular weight decreases because of ester bond breakdown, resulting in a shift in *MWD* to a lower M_w. As time progresses, the *MWD* widens

because of an increased number of varying chain lengths within the polymer. By day 45, the bimodal distribution occurs due to differences in the chain lengths within the polymer as it degrades (31,32). Castro-Aguirre *et al.* and Limsukon *et al.* reported similar findings on the multimodal distribution of PLA during hydrolytic degradation (33,34). After day 60, we could no longer collect samples since they were too brittle and small. A summary of the average M_w and M_n is included in **Table A6.4**.

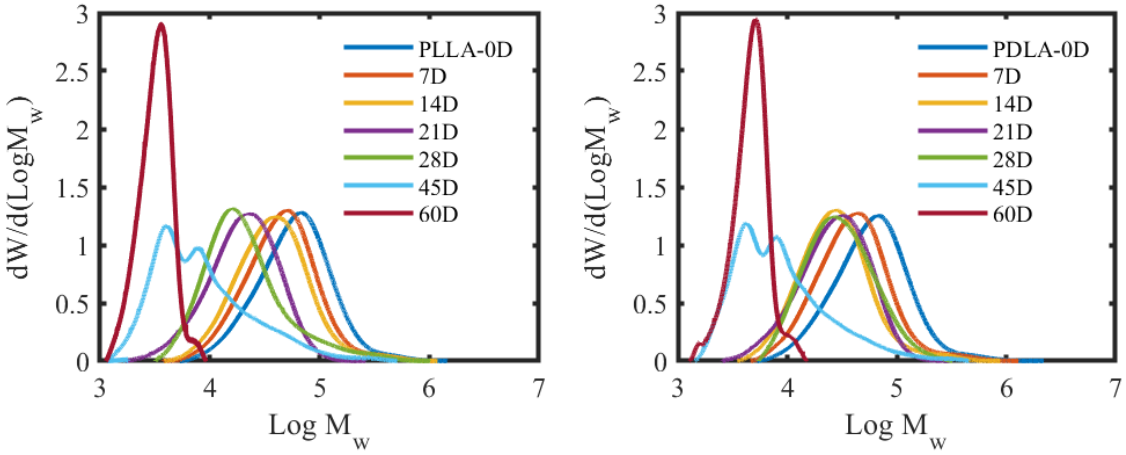

Figure 6.4. The MWD of PLLA and PDLA at 58 ± 2 °C from days 0 to 60 was measured from biodegradation samples collected at each sampling time. This specific temperature was chosen to simulate the conditions of a composting environment, allowing us to observe the polymer's behavior under these circumstances.

6.4.3 Biodegradation in simulated composting conditions

CO_2 evolution and biodegradation results until 120 days of testing are presented in **Figure 6.5. Figure 6.5a** and **Figure 6.5b** shows the results for the Blank, Cellulose, PLLA, PLLA/PDLA 70-30, 50-50, 30-70, and PDLA. **Figure 6.5c** and **Figure 6.5d** show the results for the Blank, Cellulose, PLLA/PDLA 50-50, and 50-50-A. **Table A6.4**, Appendix B summarizes the % biodegradation data for each sample on days 0, 45, 60, 90, and 120. The three phases of biodegradation—lag, biodegradation, and plateau—can be seen in **Figure 6.5b** and **Figure 6.5d**. Cellulose reached almost 95% biodegradation by day 30. Cellulose's hydrophilic nature, along

with the activity of naturally occurring enzymes, breaks it down so that it can be transferred through the cell wall of microorganisms to be easily assimilated by metabolic pathways (35). Cellulose powder has a very short lag phase, with biodegradation starting almost immediately after the experiment begins.

In the case of PLA, all the film samples had an extended lag time of around 40 to 60 days, depending on the sample. There was not a big difference in the lag or hydrolysis phase of the amorphous films, as seen in **Figure 6.5b**. This is in contrast to what has been reported by Tsuji and Tsuruno, who reported that PLLA/PDLA blended films have higher hydrolysis resistance compared to the α-form of the PLLA crystalline regions in solvent-cast films (19). Tsuji, in another paper, reported that the hydrolysis resistance of PLA materials can be increased by stereocomplexation of PLLA and PDLA, with the rate being altered by the mixing ratio in solvent-cast films (36). Karst and Yang also reported that a PLLA/PDLA-50-50 blend had greater resistance to hydrolysis than PLLA or PDLA due to stronger hydrogen bonding and dipole-dipole interactions than pure PLLA or PDLA based on modeling scenarios from data collected by Tsuji (37). Since all the data collected previously has been based on solvent-cast films, we believe the cast extrusion process affects hydrolysis, making all our samples similar in breakdown due to hydrolysis since we had both HC and SC portions present in the films. Hydrolysis is initially needed to break down the largest M_n chains so the microorganisms can digest the material.

After the lag phase, biodegradation starts, where microorganisms assimilate the broken-down oligomers, producing CO_2 and water (38). Castro-Aguirre *et al.* determined that the M_n needed to drop below 10 kDa before assimilation could occur by the microorganisms after hydrolysis had been completed (35). This is evident in our samples as the M_n dropped below that

level for PLLA and PDLA around day 45 when there was a transition from hydrolysis dominant degradation to the biodegradation phase. Until day 45, no significant difference existed between the films in the lag phase. As the test progressed, though, the PDLA film showed a lower CO_2 evolution than the other films. Research on the biodegradation of PDLA is limited, with only a few studies, such as one by Mbarki *et al.*, focused on the biodegradation of PDLA/cellulose microfibers biocomposites (20). This study, conducted at mesophilic temperatures, did not include comparisons with PLLA or other materials. It concluded that crystallinity significantly influenced the rate of biodegradation. The higher the crystallinity, the slower the biodegradation rate. Looking at **Figure 6.5b**, they all started progressing upward at different rates as they crossed over into the biotic biodegradation phase. The PLLA/PDLA-50-50 sample had the steepest increase, followed by PLLA/PDLA-70-30, PLLA, PLLA/PDLA-30-70, and PDLA. PDLA got out of the lag phase between 45 and 60 days. Since the PLLA/PDLA-30-70 sample is predominately PDLA, it is not surprising that it is closer to the PDLA sample. Once it converted from hydrolysis to biodegradation, the synergistic effect of PLLA coupled with minor amounts of PDLA accelerated the degradation process. As the amount of PDLA increased the degradation rate slowed down.

We then looked at the effect of annealing the PLLA/PDLA-50-50 sample. In **Figure 6.5d**, the crystallinity in the PLLA/PDLA50-50-A film slowed down the hydrolytic degradation compared to the PLLA/PDLA-50-50 sample. Loo *et al.* reported on the hydrolysis of annealed poly(lactide-*co*-glycolide) that the degree of crystallinity is believed to slow down hydrolytic degradation but only to a degree, after which the formation of voids due to annealing increases the rate of hydrolytic degradation (39). Pantani *et al.* reported on the influence of crystallinity on the biodegradation rate of injection-molded PLA samples in controlled composting conditions.

They compared an amorphous sample to an injection-molded annealed sample and found that crystallinity slowed the degradation rate initially. Still, it only affected it partially in the early stages of hydrolysis, while it significantly affected the final swelling of the material and the subsequent biodegradation rate. It was concluded that the more compact structure of the annealed sample was less permeable to the enzymatic attach and breakdown of the oligomer diffusion; once the crystalline sample was broken down, the degradation rate became faster and closer to the amorphous sample (40). We saw similar results: the PLLA/PDLA-50-50-A sample started slowly but eventually was comparable in degradation to the PLLA/PDLA-50-50 sample, which began as fully amorphous as seen in **Figure 6.5d**.

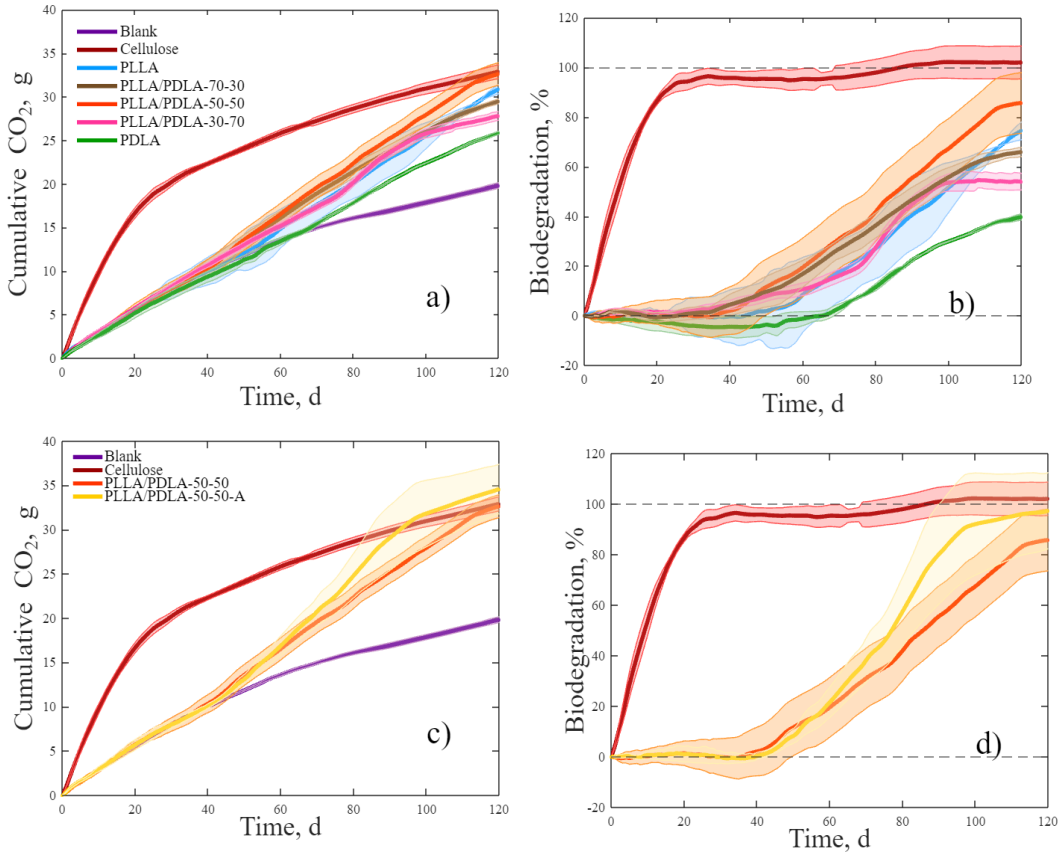

Figure 6.5. **a)** CO_2 results of Blank, Cellulose, PLLA, PLLA/PDLA-70-30, PLLA/PDLA-50/50, and PLLA/PDLA-30-70 and PDLA; **b)** Biodegradation results of Cellulose, PLLA, PLLA/PDLA-70-30, PLLA/PDLA-50-50, PLLA/PDLA-30/70, and PDLA; **c)** CO_2 results of Blank, Cellulose, PLLA/PDLA-50/50, and PLLA/PDLA-50-50-A; **d)** Biodegradation results of Cellulose, PLLA/PDLA-50-50, and PLLA/PDLA-50-50-A.

6.4.4 Surface evolution

Figure 6.6 shows SEM micrographs of the films at 330x magnification. It shows micrographs of each film at each sample stage: days 0, 7, 14, 21, 28, 45, and 60. The films are progressively broken down as time evolves. There is minimal disturbance on day 0, except for the PLLA/PDLA-50-50-A sample, which had crystallization present at day 0. By day 7, you can already see crystals forming on the sample surfaces, especially on the PLLA/PDLA-50-50-A sample, where you can see tiny crystals. By days 45 and 60, depending on the sample, the surface was very rough and broken down due to the degradation that occurred, eroded mainly by hydrolysis at the early stages. Enzymatic degradation did not appear to begin until after samples were no longer able to be collected, as can be seen in **Figure 6.5b**. **Figure A6.3,** Appendix B shows the micrographs of each film magnified at 5000x and 330x in the same area on the sample. They all show biofilm formation with voids or holes on the surface of the samples at 5000x magnification, which shows the effect of the hydrolysis having taken place. They all have a rough, uneven surface corresponding to what occurs at that later stage, as seen in **Figure 6.5b**. Kijchavengkul *et al.* and Mbarki *et al.* showed similar results on SEM surface scans of PBAT and PDLA, respectively, where there was a progressive erosive change in the film surface from the beginning to the end of the experiment (20,41).

Our research shows how PLLA, PDLA, several blends, and an annealed blended sample perform in a simulated biodegradation test. Most of the films were amorphous on day 0, except for the annealed one, but by day 7, the blended films had already caught up to the PLLA/PDLA-50-50-A film concerning overall crystallinity. Annealing appears to slow the initial hydrolysis, but once it reaches the biodegradation phase, it recovers as the outer crystalline layers are broken down. PDLA, which biodegradation in a simulated compost environment had not been

previously reported, degraded the slowest, only reaching 40% degradation by the end of the experiment at 120 days. Additionally, the presence of D-LA made the blend more resistant to hydrolysis. The results provide a unique opportunity to tailor the degradation of PLLA/PDLA blends in pursuing PLA or any of its blended versions as more benign alternatives at end-of-life.

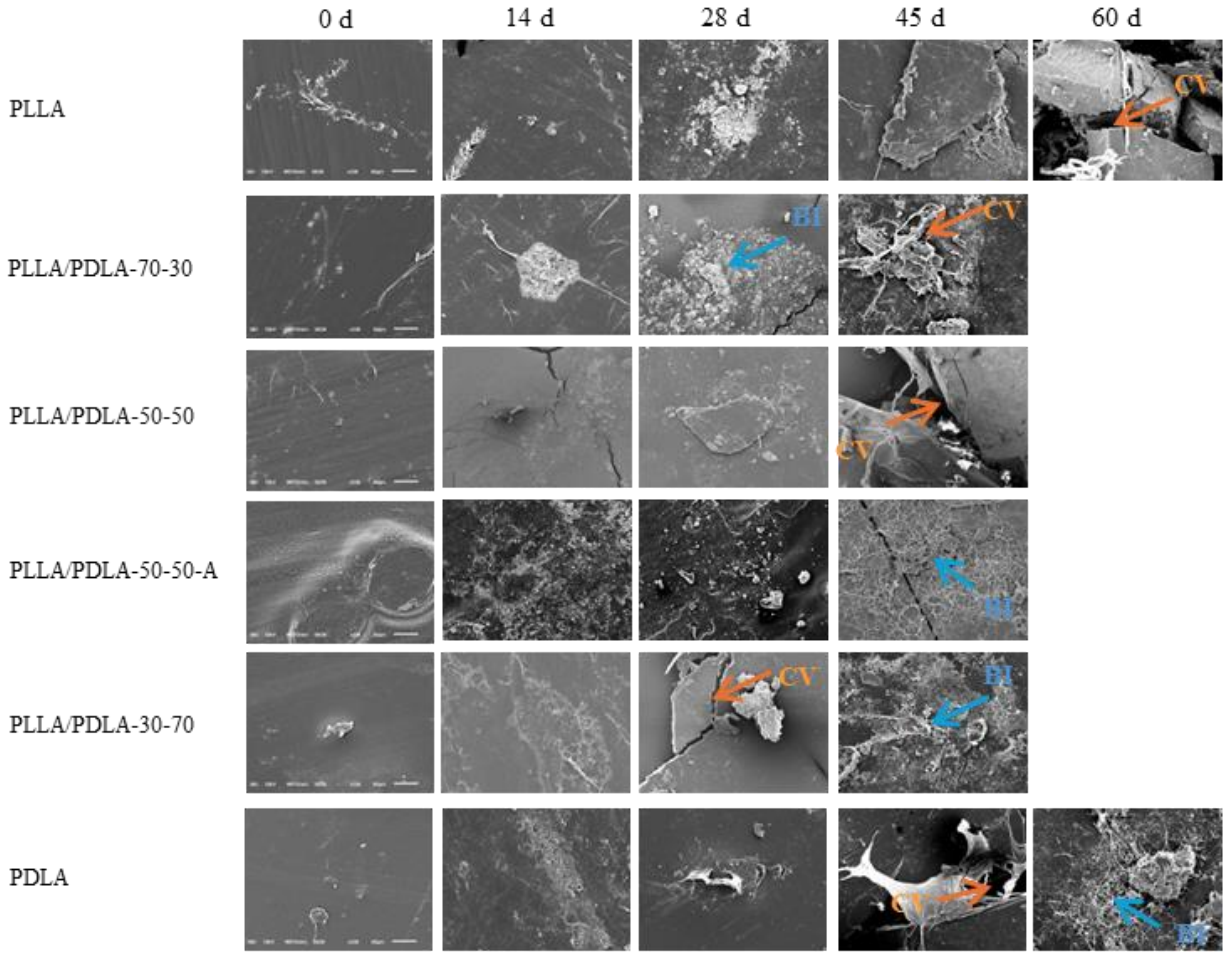

Figure 6.6. SEM micrographs of all the films at various experiment stages: days 0, 7, 14, 28, 45, and 60. All of the pictures are 330x magnification. The bar on day 0 stands for 50 microns and applies to all the micrographs. CV stands for cavity, and BI stands for biofilm.

6.5 Conclusion

This study explored the biodegradation of several PLLA/PDLA films produced via cast extrusion, including multiple blends of PLLA/PDLA and an annealed PLLA/PDLA-50-50 sample. The results show that at the beginning of the experiment, in the lag phase, all the films performed similarly until about day 45. The X_c of the films jumped between days 0 and 7 but progressed slowly after the initial jump. In the blended films, the fraction of HC-crystals broke down faster than the SC-crystals, which showed that HC is more susceptible to hydrolysis than SC-crystals. We also saw a progressive decrease in the M_w as time progressed for both PLLA and PDLA, with a bimodal distribution occurring at day 45 due to differences in the chain lengths within the polymer as it degrades. The results of the % biodegradation from the DMR show that all the films were in the lag phase until between days 45 and 60, then they all increased between days 60 and 120, with the annealed sample progressing the quickest, followed closely by the PLLA/PDLA-50-50 and PLLA samples. The biodegradation performance of the other PLLA/PDLA blends varies, mainly depending on the PDLA content, with pure PDLA reaching only about 40% degradation by the end of our testing period. Given the limited existing research on PDLA, our findings offer new insights into the behavior of various blended films compared to pure PLLA. This study is novel in its comprehensive examination of the biodegradation of cast extruded PLLA, PDLA, and their blends under identical conditions. It provides a deeper understanding of the biodegradation mechanisms, enhancing the potential for using PLA in commercial applications as a more sustainable alternative. Future research could explore the effects of annealing on different PLLA/PDLA blends to assess consistency in performance.

6.6 Acknowledgments

J.F.M. would like to thank the Michigan State University, College of Natural Resources, Office of Academic and Student Affairs for funding a Ph.D. fellowship for the Summers of 2022, 2023, and 2024. The authors also thank TotalEnergies Corbion for providing the PLLA and PDLA resins.

REFERENCES

1. Epps TH, Korley LTJ, Yan T, Beers KL, Burt TM. Sustainability of Synthetic Plastics: Considerations in Materials Life-Cycle Management. JACS Au. 2022 Jan 24;2(1):3–11.
2. Bher A, Mayekar PC, Auras RA, Schvezov CE. Biodegradation of Biodegradable Polymers in Mesophilic Aerobic Environments. Vol. 23, International Journal of Molecular Sciences. MDPI; 2022.
3. Mazumder MAR, Jubayer MF, Ranganathan T V. Biodegradation of Plastics by Microorganisms. In: Hussain CM, Kadeppagari RK, editors. Biotechnology for Zero Waste: Emerging Waste Management Techniques. Wiley; 2022. p. 123–41.
4. Biodegradable Plastic Market Size, Share _ Industry Forecast, 2027 [Internet]. [cited 2024 Mar 17]. Available from: https://www.alliedmarketresearch.com/biodegradable-plastic-market
5. Compostable Plastics_ The Next Generation Of Plastics [Internet]. 2019 [cited 2022 Jun 9]. Available from: https://www.worldcentric.com/journal/compostable-plastics-the-next-generation-of-plastics
6. ASTM D6400 − 21 Standard Specification for Labeling of Plastics Designed to be Aerobically Composted in Municipal or Industrial Facilities 1 [Internet]. West Conshohocken; 2021. Available from: http://www.ansi.org.
7. ISO 14855-1:2012, Determination of the ultimate aerobic biodegradability of plastic materials under controlled composting conditions - Method of analysis of evolved carbon dioxide, Part 1: General Method. 2nd ed. 2012.
8. ISO 14855-2:2018, Determination of the ultimate aerobic biodegradability of plastic materials under controlled composting conditions — Method by analysis of evolved carbon dioxide. 2nd ed. 2018.
9. ASTM D6868 − 21 Standard Specification for Labeling of End Items that Incorporate Plastics and Polymers as Coatings or Additives with Paper and Other Substrates Designed to be Aerobically Composted in Municipal or Industrial Facilities 1 [Internet]. West Conshohocken; 2021. Available from: www.oecd.org.
10. Composting At Home _ US EPA [Internet]. 2923 [cited 2024 Jun 18]. Available from: https://www.epa.gov/recycle/composting-home
11. Kale G, Kijchavengkul T, Auras R, Rubino M, Selke SE, Singh SP. Compostability of bioplastic packaging materials: An overview. Vol. 7, Macromolecular Bioscience. 2007. p. 255–77.
12. Lim LT, Auras R, Rubino M. Processing technologies for poly(lactic acid). Vol. 33, Progress in Polymer Science (Oxford). 2008. p. 820–52.

13. Singha S, Hedenqvist MS. A review on barrier properties of poly(lactic Acid)/clay nanocomposites. Vol. 12, Polymers. MDPI AG; 2020.

14. Deng L, Xu C, Wang X, Wang Z. Supertoughened Polylactide Binary Blend with High Heat Deflection Temperature Achieved by Thermal Annealing above the Glass Transition Temperature. ACS Sustain Chem Eng. 2018 Jan 2;6(1):480–90.

15. Speranza V, De Meo A, Pantani R. Thermal and hydrolytic degradation kinetics of PLA in the molten state. Polym Degrad Stab. 2014 Feb;100(1):37–41.

16. Tsuji H, Tsuruno T. Water Vapor Permeability of Poly(L-lactide)/Poly(D-lactide) Stereocomplexes. Macromol Mater Eng. 2010 Aug 11;295(8):709–15.

17. Tsuji H. Poly(lactide) stereocomplexes: Formation, structure, properties, degradation, and applications. Vol. 5, Macromolecular Bioscience. Wiley-VCH Verlag; 2005. p. 569–97.

18. Macnamara JF, Rubino M, Daum M, Kathuria A, Auras R. Unlocking the secrets of high-water barrier stereocomplex polylactide blend extrusion films. Green Chemistry [Internet]. 2024; Available from: http://xlink.rsc.org/?DOI=D3GC04805E

19. Tsuji H, Tsuruno T. Accelerated hydrolytic degradation of Poly(L-lactide)/Poly(D-lactide) stereocomplex up to late stage. Polym Degrad Stab. 2010 Apr;95(4):477–84.

20. Mbarki K, Fersi M, Louati I, Elleuch B, Sayari A. Biodegradation study of PDLA cellulose microfibres biocomposites by Pseudomonas aeruginosa. Environ Technol. 2021;42(5):731–42.

21. Tomita K, Tsuji H, Nakajima T, Kikuchi Y, Ikarashi K, Ikeda N. Degradation of poly(D-lactic acid) by a thermophile. Polym Degrad Stab. 2003;81(1):167–71.

22. Castro-Aguirre E. MS Thesis: Design and construction of a medium-scale automated direct measurement respirometric system to assess aerobic biodegradation of polymers. [East Lansing]: Michigan State University; 2013.

23. Dorgan JR, Janzen J, Knauss DM, Hait SB, Limoges BR, Hutchinson MH. Fundamental solution and single-chain properties of polylactides. J Polym Sci B Polym Phys. 2005 Nov 1;43(21):3100–11.

24. Iñiguez-Franco F, Auras R, Ahmed J, Selke S, Rubino M, Dolan K, et al. Control of hydrolytic degradation of Poly(lactic acid) by incorporation of chain extender: From bulk to surface erosion. Polym Test. 2018 May 1;67:190–6.

25. Iñiguez-Franco F, Auras R, Dolan K, Selke S, Holmes D, Rubino M, et al. Chemical recycling of poly(lactic acid) by water-ethanol solutions. Polym Degrad Stab. 2018 Mar 1;149:28–38.

26. Tsuji H. Poly(lactide) stereocomplexes: Formation, structure, properties, degradation, and applications. Vol. 5, Macromolecular Bioscience. Wiley-VCH Verlag; 2005. p. 569–97.

27. Kara Y, Molnár K. Decomposition Behavior of Stereocomplex PLA Melt-Blown Fine Fiber. J Polym Environ. 2023 Nov;31:1398–414.

28. Tsuji H, Ikarashi K, Fukuda N. Poly(L-lactide): XII. Formation, growth, and morphology of crystalline residues as extended-chain crystallites through hydrolysis of poly(L-lactide) films in phosphate-buffered solution. Polym Degrad Stab. 2004 Jun;84(3):515–23.

29. Castro-Aguirre E, Auras R, Selke S, Rubino M, Marsh T. Enhancing the biodegradation rate of poly(lactic acid) films and PLA bio-nanocomposites in simulated composting through bioaugmentation. Polym Degrad Stab. 2018 Aug 1;154:46–54.

30. Tsuji H, Ikada Y. Blends of Crystalline and Amorphous Poly(lactide). III. Hydrolysis of Solution-cast Blend Films. Appl Poly Sci . 1997;63:855–63.

31. Li S, Garreau H, Vert M. Structure-property relationships in the case of the degradation of massive poly(-hydroxy acids) in aqueous media Part 3 Influence of the morphology of poly(L-/actic acid). Journal of Materials Science: Materials in Medicine . 1990 Nov;1:198–206.

32. Rodriguez E, Shahbikain S, Marcos B, Huneault MA. Hydrolytic stability of polylactide and poly(methyl methacrylate) blends. J Appl Polym Sci. 2018 Mar;135(11):45991.

33. Limsukon W, Sakkaplangkul P, Rubino M, Rabnawaz M, Lim LT, Auras R. Population Balance Modeling for Simulating Molecular Weight Distribution in Hydrolytic Degradation. In: 24th IAPRI World Packaging Conference. Valencia, Spain; 2024.

34. Castro-Aguirre E, Auras R, Selke S, Rubino M, Marsh T. Insights on the aerobic biodegradation of polymers by analysis of evolved carbon dioxide in simulated composting conditions. Polym Degrad Stab. 2017 Mar 1;137:251–71.

35. Tsuji H. In vitro hydrolysis of blends from enantiomeric poly(lactide)s Part 1. Well-stereo-complexed blend and non-blended films. Polymer (Guildf). 2000;41:3621–30.

36. Karst D, Yang Y. Molecular modeling study of the resistance of PLA to hydrolysis based on the blending of PLLA and PDLA. Polymer (Guildf). 2006 Jun 14;47(13):4845–50.

37. Limsukon W, Auras R, Selke S. Hydrolytic degradation and lifetime prediction of poly(lactic acid) modified with a multifunctional epoxy-based chain extender. Polym Test. 2019 Dec 1;80.

38. Chye Joachim Loo S, Ooi CP, Hong Elyna Wee S, Boey YCF. Effect of isothermal annealing on the hydrolytic degradation rate of poly(lactide-co-glycolide) (PLGA). Biomaterials. 2005 Jun 1;26(16):2827–33.

39. Pantani R, Sorrentino A. Influence of crystallinity on the biodegradation rate of injection-moulded poly(lactic acid) samples in controlled composting conditions. Polym Degrad Stab. 2013 May;98(5):1089–96.

40. Kijchavengkul T, Auras R, Rubino M, Ngouajio M, Fernandez RT. Assessment of aliphatic-aromatic copolyester biodegradable mulch films. Part II: Laboratory simulated conditions. Chemosphere. 2008 Apr;71(9):1607–16.

APPENDIX 6A: RAW MATERIAL CHARACTERIZATION

Table A6.1 shows the average carbon content of the films measured by CHN.

Table A6.1. Average carbon content measured by CHN.

Sample	Average Carbon content (%)		Standard Deviation (%)
Cellulose	42.50	±	0.08
PLLA	50.59	±	0.14
PLLA/PDLA-70-30	50.43	±	0.13
PLLA/PDLA-50-50	50.88	±	0.24
PLLA/PDLA-50-50-A	51.51	±	0.38
PLLA/PDLA-30-70	49.87	±	0.84
PDLA	51.56	±	0.22

Table A6.2 shows the laboratory analysis of the compost used in the experiment.

Table A6.2. Laboratory analysis of manure compost used for the biodegradation test.

Compost				
Tests	**Units**	**Desired Range**	**Results**	**Interpretation Low Desired High**
pH		6.0 – 8.0	7.22	**X**
E. C. - Saturation Paste	mmho/cm	< 4	13.8	**X**
Nitrate-N (NO_3-N)*	ppm	40 – 99		
Ammonium-N (NH_4-N)*	ppm			
Total Dry Solid	%		55.7	**X**
Total Volatile Solid	%		44.4	
C/N Ratio		<25	10.3	**X**
Tests	**Units**		**Wet Weight Basis**	
Total Nitrogen (N)	%		2.27	
Total Phosphorus (P)	%		1.36	
Total Potassium (K)	%		1.46	
Total Calcium (Ca)	%		6.11	
Total Magnesium (Mg)	%		1.57	
Total Zinc (Zn)	ppm		380	
Total Iron (Fe)	ppm		7033	
Total Manganese (Mn)	ppm		294	
Total Copper (Cu)	ppm		126	
Total Carbon (C)	%		23.3	
Total Sodium (Na)	%		0.347	
Total Aluminum (Al)	%		0.198	
Total Sulfur (S)	%		0.505	
Total Boron (B)	ppm		39	

***Interpretation for nitrate-N is for growing media only. If this material is to be used as soil amendment, the interpretation for nitrate-N is not applicable.

APPENDIX 6B: EXPERIMENTAL FILM DATA

Figure A6.1 shows the bioreactors at the time of sampling.

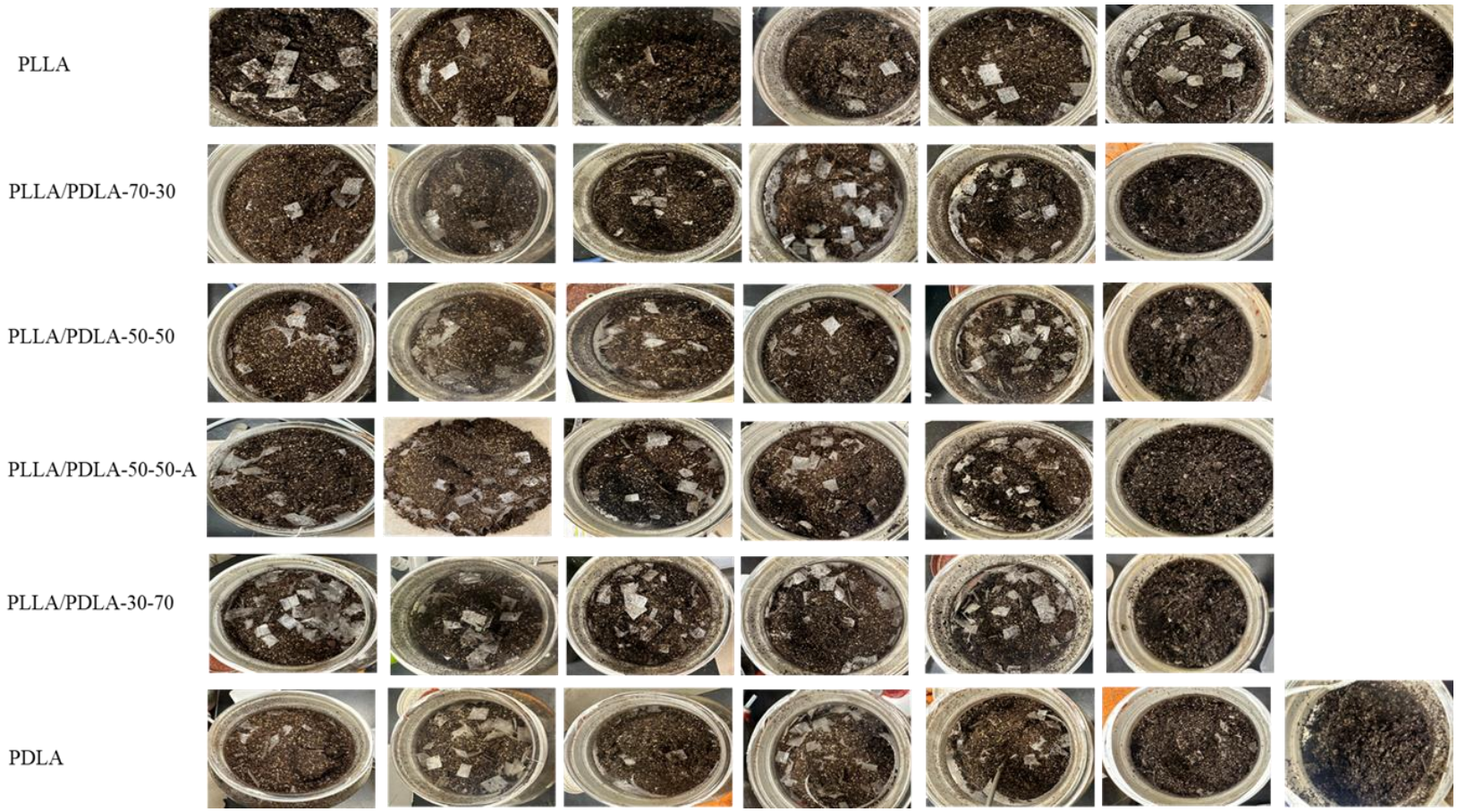

Figure A6.1. Pictures of bioreactors at sampling days 7,14,21,28,45,60, and 90 for the various films. By day 60, the blended films were barely discernible. The same holds for PLLA and PLDA by day 90.

Figure A6.2 shows the DSC thermograms on day 0.

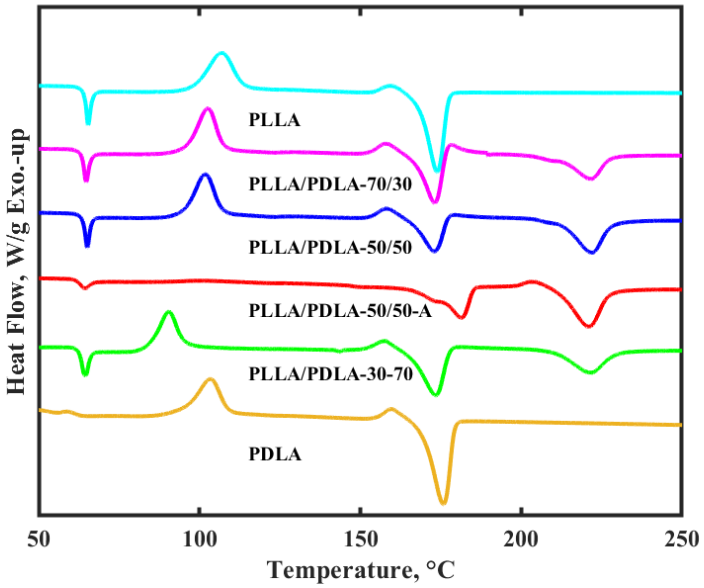

Figure A6.2. DSC thermograms of all the films at day 0 from 50 to 250 °C.

Table A6.3 shows the Mw and Mn of the films at the time of sampling.

Table A6.3. M_w and M_n for the films at times of sampling.

	***Mn* (kDa)**				***Mw* (kDa)**			
	PLLA		**PDLA**		**PLLA**		**PDLA**	
Day	Average	St Dev.	Average	St Dev.	Average	St Dev.	Average	St Dev.
0	44951	798	42882	787	82641	2313	79999	2313
7	33535	593	29218	1739	60952	2393	54113	5630
14	27458	1858	23618	2008	51098	4537	43494	6245
21	17542	1437	19217	1956	31219	3360	31936	3244
28	11489	3161	14841	752	25932	1422	25372	1954
45	6084	315	7492	1636	16300	1837	20777	8038
60	3002	12	4011	256	3491	29	4782	157

Table A6.4 shows the biodegradation % at various stages of the experiment.

Table A6.4. Biodegradation, % for each film at days 0, 45, 60, 90, and 120.

	% Biodegradation - Day											
Film	**0**	**45**			**60**			**90**			**120**		
Cellulose	0	95	±	3	95	±	4	101	±	6	102	±	7
PLLA	0	0	±	2	9	±	15	41	±	14	75	±	4
PLLA/PDLA-70-30	0	7	±	5	17	±	5	47	±	5	66	±	2
PLLA/PDLA-50-50	0	6	±	11	20	±	12	56	±	12	86	±	12
PLLA/PDLA-50-50-A	0	3	±	2	21	±	6	80	±	20	97	±	15
PLLA/PDLA-30-70	0	6	±	2	11	±	3	45	±	3	54	±	3
PDLA	0	-5	±	4	-1	±	3	22	±	1	40	±	1

Figure A6.3 shows SEM micrographs of the films on the last day of sampling at 330x and 5000x magnification.

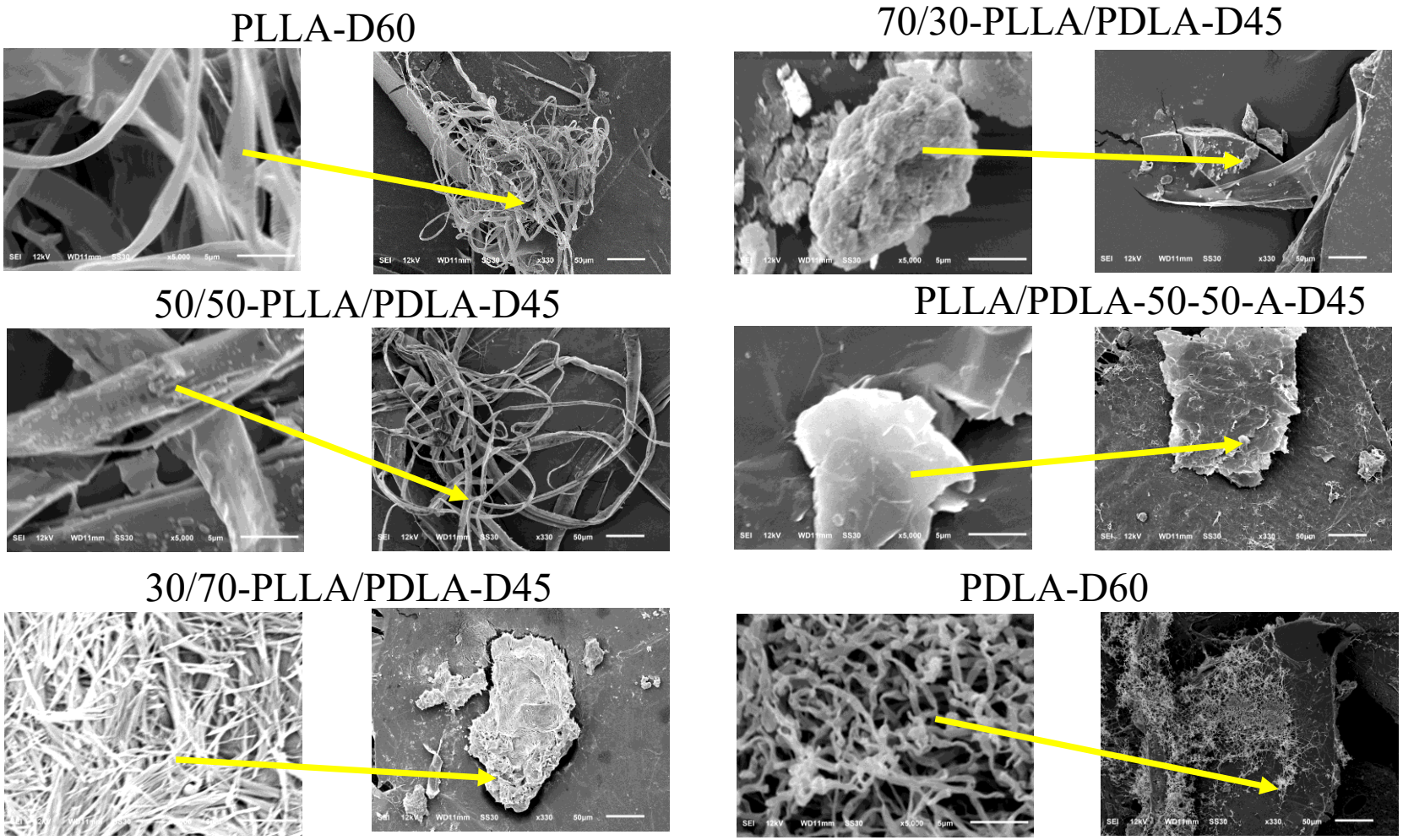

Figure A6.3. SEM micrographs of all the films at various experiment stages at 5000x and 330x magnification on the last sampling day. The micrograph on the right is magnified at 5000x, and the one on the right is 330x. The bar in each micrograph signifies the scale. The bar on the micrographs at 5000 equals 5 microns. The bar on the micrographs at 330x equals 50 microns. The arrows represent the area that is being magnified between the two micrographs.

CHAPTER 7: OVERALL CONCLUSION AND RECOMMENDATIONS FOR FUTURE WORK

7.1 Overall Conclusion

Plastic waste is a growing issue, and single-use plastic packaging is one of the biggest reasons. As of 2017, 8.3 billion metric tons of plastic had been produced since it was invented in the 1950s (1). 79% of that amount still exists in landfills or the natural environment (2). In 2017, packaging production accounted for 146 million tons of plastic being used, which was the highest demand that year (3). The plastic in the landfills breaks down into tiny toxic particles that contaminate the soil and waterways, entering the food chain when animals inadvertently ingest them (4). Terrestrial microplastic pollution is 4 to 23 times higher than marine microplastic pollution, depending on the environment. Ultimately, this could have harmful health effects on humans and animals (5). Biodegradable plastics are one desirable alternative that is growing (6). The market for sustainable plastic is expected to grow from USD 80 billion in 2020 to USD 127.50 billion by 2028 (7). A drawback to biodegradable flexible options is the lack of equivalent moisture and oxygen barrier performance to maintain a comparable shelf life of food products compared with accepted petrochemical-based options.

The primary goal of this dissertation was to develop a compostable film structure with high oxygen and water barrier properties. To achieve this, we explored stereocomplex polylactic acid (SC-PLA), a biobased and biodegradable plastic known for its adequate moisture barrier. We enhanced its properties by adding a polyvinyl alcohol/nanoclay (PVOH-Nc) coating for an improved oxygen barrier. We laminated it with L-polylactic acid (PLLA) as a heat seal layer. Our research began by detailing the production of SC-PLA films through cast extrusion, a process that has yet to be documented. Subsequently, we designed an assembly for the structure that achieves high oxygen and water barrier properties, maintains full transparency, and remains industrially

compostable. Lastly, we assessed the biodegradation of the SC-PLA films, rounding out our comprehensive study of their environmental impact and performance.

Chapter 3 presented the optimal conditions for producing SC-PLA by cast extrusion and explored potential mechanical and barrier properties enhancements. This work focused on producing SC-PLA films on a single screw extruder without first making a masterbatch. Blends of 85/15, 70/30, 50/50, and 30/70 PLLA/PDLA, along with PLLA and PDLA, were produced for comparison, and the processing conditions were reported. The samples were also annealed to induce crystallinity and improve the moisture vapor transmission rate (MVTR). The role of SC-PLA content on the properties of these blends, such as thermal, mechanical, and moisture barrier measurements, was measured and reported. All the SC-blends showed improved heat resistance and, once annealed, also showed enhanced MVTR values. Still, the annealing process also made the material brittle, severely decreasing its overall stress and strain. This chapter presents the first SC-PLA films produced using cast extrusion technology.

Chapter 4 quantified the density of PLLA, several SC-PLA blends, and PDLA, examining their relationship with crystallinity (X_c) and MVTR, which had not been reported previously. Differential scanning calorimetry (DSC), modulated DSC, and wide-angle X-ray diffraction (WAXD) techniques were employed to assess crystallinity accurately. The specific compositions of the blends evaluated included ratios of 85/15, 70/30, 50/50, and 30/70 PLLA to PDLA, providing a comprehensive overview of how varying PLLA and PDLA proportions impact density, *Xc*, and MVTR properties. In the SC- PLA 50/50 system, positronium annihilation lifetime spectroscopy (PALS- a well-known probe of polymer-free volume) was used to assess how pore size and relative porosity correlate with the crystallinity, density, and permeability changes from increasing the film's annealing time. All the blended SC-PLA films annealed for 30

min showed higher density and increased X_c, which resulted in improved MVTR barriers. We also explored the effect of annealing time on a PLLA/PDLA-50-50 film annealed at 0, 5, 15, 30, and 60 min. Interestingly, the 5 and 15 min samples were higher in density than the 30 and 60 min annealed samples. There was also a switch from HC to SC crystal dominance between 15 and 30 min, which may provide insights and make us infer that SC-crystals are less dense than HC-crystals. PALS analysis conducted on the PLLA/PDLA-50-50 samples showed a decrease in pore size with a trend to higher densities with increased crystalline fraction due to annealing. Rigid amorphous fraction (RAF) also increases as the annealing time gets longer, which is also not accounted for in the PALS analysis, making it hard to interpret on PALS alone.

Chapter 5 innovates by employing PHBV and SC-PLA base films produced through cast extrusion and enhancing them with a PVOH-Nc coating to improve the oxygen barrier. Subsequently, these coated films were laminated to PLLA with a compostable adhesive to form a sealant layer. Our original approach maintained complete biodegradability and provided adequate oxygen and moisture barriers. We avoided using metallization or polyvinylidene chloride. The moisture barrier properties were examined under conditions of 37.8 °C/90% RH, 23 °C/85% RH, and 11 °C/85% RH, enabling the calculation of barrier activation energy. Additionally, the oxygen barrier properties were assessed at 23 °C/50% RH, underlining the robustness of this novel structure. The MVTR values ranged from 21 to 29 g/(m^2·d) at 38 °C/90% RH, and the OTR values ranged from 54 to 68 cc/(m^2·d) at 23 °C/50% RH. All the materials used were biodegradable, so it is reasonable to assume the final structure is also biodegradable. We were able to optimize the structure utilizing the permeability equation and calculate a theoretical MVTR of 10 g/(m^2·d) at 38 °C/90% RH, with an OTR of 60 cc/(m^2·d) at 23 °C/50% RH, or an OTR of 14 cc/(m^2·d) at 23 °C/50% RH, with an MVTR of 24 g/(m^2·d) at

38 °C/90% RH. This is a low barrier level for a biodegradable structure compared to other structures that do not incorporate metallization or PVDC. The permeability activation energy was also calculated for all the structures since the MVTR was measured at three different temperatures. The E_p ranged from 41.19 to 54.23 kJ/mol. The novelty of the research included taking a base layer of a cast extruded biodegradable film with good moisture barrier characteristics, incorporating a layer of PVOH-Nc for added oxygen characteristics and adding a layer of PLLA for heat seal properties. We showed that optimizing the structure could obtain either a maximized MVTR of 10 g m^2/day at 38 °C/90% RH or a maximized OTR of 14 cc/(m^2·d) at 23 °C/50% RH, both exceptional for a clear biodegradable structure that does not incorporate PVDC or metallization. The novel-produced biodegradable and multilayer structure not only advances the functionality of biodegradable packaging materials but also enhances their application in preserving food quality and extending shelf life.

Chapter 6 evaluates the biodegradation performance of SC-PLA of several different blends of PLLA/PDLA and PDLA produced using cast extrusion with and without annealing and the effect of the degradation process on molecular weight, crystallinity, and thermal performance. In addition to cellulose, PLLA was also included as a control against which to compare during the biodegradation process. This chapter explores multiple blends of PLLA/PDLA, one of them annealed, to track the abiotic and biotic biodegradation over 120 days and see how they compare, including controls of PLLA and cellulose, which have been extensively studied. Biodegradation of PDLA was not previously published at thermophilic temperatures and compared to other materials in the same study. All the films performed similarly in the hydrolysis phase up to about day 45, but the PLLA/PDLA-50-50-A-30m film performed best overall at 97 % biodegraded at the end of the 120 days, while the PLDA

performed the lowest at 40 % biodegraded, with the others falling in between. This work provides insights into the biodegradation mechanism of PLLA/PDLA blends, which can be leveraged to support commercial applications using PLA as a more environmentally friendly alternative.

7.2 Recommendations for future work

Several areas should be investigated further after exploring SC-PLA for oxygen and moisture barrier improvement. For the cast extruded SC-PLA film, additional studies could be conducted to dissociate the role of the α-crystal and the SC-crystals. Selective film manipulation could enhance the properties of the final films. Future work should be performed to decrease the brittleness while preserving the improved moisture vapor barrier. The biaxial orientation of the film should be explored as well as opposed to annealing to induce crystallization, which is a more conventional converting technology since annealing is not always commercially feasible.

Exploring a three-layer-coextruded structure is another exciting area for further research. The outer two layers of the structure are PLLA, sandwiched between them by PDLA. The idea is to form SC-PLA at the interfaces between the PLLA and PDLA. We tried this approach but failed to obtain adhesion between the PLLA and PDLA layers to induce sc-PLA formation.

While reporting on the density of SC-PLA was new and novel, additional research utilizing PALS on HC to SC systems is needed to clarify the dynamics of crystal size, geometry, and potential transformation of void shapes as the sample progresses through the different annealing durations and crystal structures. More specifically, the role of the mobile amorphous fraction (MAF) and rigid amorphous fraction (RAF) in PALS must be understood better to understand how it can be interpreted. A polymer's RAF and MAF region and free volumes can be measured using PALS. More work on other blends at varying annealing times should also be conducted to see how they compare to the PLLA/PDLA-50-50 blend explored in this work.

An alternative, greener solvent to dimethyl sulfoxide (DMSO), such as deionized water, should be explored to produce a biodegradable structure. Corona treatment of the film should also be considered as opposed to plasma treatment since corona treatment is a more conventional commercial technique of increasing the surface energy of the films. Calculating the oxygen activation energy of the four structures would be another area that should be explored to complement the moisture activation energy by measuring the OTR at 11 °C/50% RH and 38 °C/50% RH.

Finally, additional research on the effect of annealing other blends of PLLA/PDLA at varying annealing times should be explored to see if they perform similarly to the ones we reported concerning biodegradation. The biodegradable structures should be tested as complete structures to confirm that even though the components are biodegradable, the overall structure is also biodegradable, as suspected.

REFERENCES

1. Cohen J. 8.3 billion metric tons of plastic ... and counting _ University of California [Internet]. 2017 [cited 2024 Jun 22]. Available from: https://www.universityofcalifornia.edu/news/83-billion-metric-tons-plastic-and-counting
2. Geyer R, Jambeck JR, Law KL. Production, use, and fate of all plastics ever made. Sci Adv [Internet]. 2017 Jul 19; Available from: https://www.science.org
3. Garside M. Plastic planet_ How tiny plastic particles are polluting our soil [Internet]. 2024 [cited 2024 Jun 22]. Available from: https://www.statista.com/statistics/1134796/plastic-production-by-industrial-sector-worldwide/
4. Jacobsen S. Plastic Bag Pollution [Internet]. [cited 2024 Jun 22]. Available from: https://dpw.lacounty.gov/epd/plasticbags/articles/googobits_07-21-05.pdf
5. Plastic planet_ How tiny plastic particles are polluting our soil [Internet]. 2021 [cited 2024 Jun 22]. Available from: https://www.unep.org/news-and-stories/story/plastic-planet-how-tiny-plastic-particles-are-polluting-our-soil
6. Trifol J, van Drongelen M, Clegg F, Plackett D, Szabo P, Daugaard AE. Impact of thermal processing or solvent casting upon crystallization of PLA nanocellulose and/or nanoclay composites. J Appl Polym Sci. 2019 May 20;136(20).
7. Sustainable Plastic Packaging Market Size Worth USD 127.50 [Internet]. 2021 [cited 2024 Jun 11]. Available from: https://www.globenewswire.com/en/news-release/2021/03/10/2190583/0/en/Sustainable-Plastic-Packaging-Market-Size-Worth-USD-127-50-Billion-By-2028-CAGR-of-6-0-Reports-And-Data.html